UNIWERSYTET
PRZYRODNICZY
WE WROCŁAWIU
WYDZIAŁ PRZYRODNICZO-TECHNOLOGICZNY

mgr inż. Aleksandra Loba

Erozja i rozwój gleb w krajobrazie lessowym Wzgórz Trzebnickich w ujęciu badań izotopowych (^{10}Be, $^{239+240}$Pu) i datowań OSL

Soil erosion and development in the loess landscape of the Trzebnica Hills reflected in isotopic analyses (^{10}Be, $^{239+240}$Pu) and OSL dating

Praca doktorska wykonana pod kierunkiem
Promotora **dr. hab. inż. Jarosława Waroszewskiego**
w Instytucie Nauk o Glebie, Żywienia Roślin
i Ochrony Środowiska

Wrocław, 2022

Szczególne podziękowania składam mojemu Promotorowi, który zachęcił mnie do kontunuowania kariery naukowej,
dr. hab. inż. Jarosławowi Waroszewskiemu,
za poświęcony czas, wiedzę, bezcenne rady, cierpliwość i życzliwość oraz za pomoc merytoryczną udzieloną podczas pisania niniejszej pracy doktorskiej.

Pragnę podziękować
prof. dr hab. inż. Cezaremu Kabale,
za możliwość realizacji doktoratu w Instytucie Nauk o Glebie, Żywienia roślin i Ochrony Środowiska oraz za wsparcie podczas procesu publikacyjnego.

Dziękuję Marcinowi Sykule za wsparcie, wyrozumiałość i motywację na każdym etapie realizacji doktoratu.

Dziękuję Rodzicom, którzy dali mi możliwość rozwoju w kierunku, jaki sobie wybrałam.

Wykaz publikacji

Autoreferat został przygotowany na podstawie cyklu trzech oryginalnych, powiązanych ze sobą artykułów naukowych. Prace zostały opublikowane w latach 2021-2022, w czasopismach znajdujących się z wykazie czasopism naukowych i recenzowanych materiałów z konferencji międzynarodowych Ministerstwa Edukacji i Nauki oraz posiadających wskaźnik cytowań *Impact Factor* (IF). Łączna liczba punktów zgodnie z punktacja MEiN wynosi **340**, a sumaryczny wskaźnik IF jest równy **12,721**. Cykl publikacji składa się z następujących prac:

- **Aleksandra Loba**, Jarosław Waroszewski, Dmitry Tikhomirov, Francesca Calitri, Marcus Christl, Marcin Sykuła, Markus Egli, 2021. *Tracing erosion rates in loess landscape of the Trzebnica Hills (Poland) over time using fallout and cosmogenic nuclides.* Journal of Soils and Sediments 21, 2952 – 2968, doi:10.1007/s11368-021-02996-x, (**IF$_{2021}$: 3,536; MEiN: 100 pkt.**),

- **Aleksandra Loba,** Jarosław Waroszewski, Marcin Sykuła, Cezary Kabała, Markus Egli, 2022. *Meteoric ^{10}Be, ^{137}Cs and $^{239+240}Pu$ as tracers of long- and medium-term soil erosion — A review.* Minerals, 12, 359, doi:10.3390/min12030359, (**IF$_{2022}$: 2,818**, **MEiN: 100 pkt.**),

- **Aleksandra Loba,** Junjie Zhang, Sumiko Tsukamoto, Marek Kasprzak, Joanna Beata Kowalska, Manfred Frechen, Jarosław Waroszewski, 2023. *Multiproxy approach to the reconstruction of soil denudation events and the disappearance of Luvisols in the loess landscape of south-western Poland.* CATENA 220, 106724, doi:10.1016/j.catena.2022.106724, (**IF$_{2022}$: 6,367, MEiN: 140 pkt.**).

Powyższe publikacje są ściśle związane z głównym celem niniejszych badań, którym było szczegółowe zbadanie procesów erozji w krajobrazie lessowym z uwzględnieniem:

1) określenia tempa erozji gleb z użyciem metod izotopowych ^{10}Be in-situ oraz $^{239+240}$Pu;

2) transformacji gleb w warunkach zachodzących procesów erozyjnych;

3) rekonstrukcji przedziałów czasowych procesów denudacyjnych z wykorzystaniem datowań optycznie stymulowanej luminescencji.

Spis treści

Streszczenie w języku polskim

Krajobrazy lessowe są bardzo podatne na procesy erozyjne, co wpływa na stabilność, produktywność oraz przekształcenia gleb. Wzgórza Trzebnickie zlokalizowane w południowo-zachodniej Polsce są jednym z takich obszarów.

W niniejszych badaniach zastosowano metody izotopowe jak ^{10}Be in-situ i $^{239+240}$Pu do określenia tempa erozji. ^{10}Be in-situ, który jest bezpośrednio wytwarzany w sieci krystalicznej kwarcu w wyniku oddziaływania promieni kosmogenicznych, umożliwia określenie tempa erozji długoterminowej, czyli zachodzącej od momentu ukształtowania się powierzchni. Natomiast $^{239+240}$Pu, który został globalnie wprowadzony do środowiska głównie w wyniku produkcji i testowania bomb jądrowych w latach 60-tych XX wieku, pozwala określić wielkość erozji krótkoterminowej, która miała miejsce w ciągu ostatnich 60 lat. Ponadto, datowania optycznie stymulowanej luminescencji (OSL) zostały wykorzystane do rekonstrukcji czasowej procesów erozyjno–depozycyjnych. Określono także kierunki rozwoju gleb użytkowanych rolniczo w warunkach intensywnej erozji.

Profile glebowe zlokalizowano i wykonano w toposekwencji stokowej o wyraźnych cechach erozji, w południowej części Wzgórz Trzebnickich. W pobranych próbkach glebowych przeprowadzono podstawowe analizy fizykochemiczne, izotopowe (^{10}Be in–situ, $^{239+240}$Pu) oraz geochemiczne. W wybranych poziomach wykonano datowania OSL oraz analizy mikromorfologiczne.

Tempo erozji długoterminowej wynosiło od 0,44 do 0,85 t/ha/rok, a erozji krótkoterminowej od 1,2 do 10,9 t/ha/rok. Wielkości te mieszczą się w zakresie danych przedstawianych dla innych obszarów lessowych w Europie. Przyczyną znacznie wyższego tempa erozji krótkoterminowej od długoterminowej jest intensyfikacja i mechanizacja rolnictwa w XX wieku, ale również zmiany klimatyczne mogą być dodatkowym czynnikiem intensyfikującym procesy erozyjne. Ponadto, określone tempo erozji krótkoterminowej znacznie przekracza jej dopuszczalne wskaźniki, które wynoszą od 0,5 do 1,0 t/ha/rok, co oznacza, że gleby na badanym obszarze ulegają degradacji. Przejawia się to w spłycaniu poziomów eluwialnych i iluwialnych w glebach płowych (Luvisols), a po pewnym czasie procesy erozyjne prowadzą do całkowitego usunięcia tych poziomów, więc gleba jest przekształcona w kierunku gleb słabo ukształtowanych – regosoli (Regosols). Natomiast, w dolnych częściach stoku, gdzie erodowany materiał był deponowany, występują gleby deluwialne. Datowania OSL wykazały, że pierwsza faza

redepozycji osadów na stokach wystąpiła około 9,1 ± 0,4 tys. lat temu. Kolejne miały miejsce w neolicie (6,4 ± 0,3 tys. lat), epoce brązu (3,8 ± 0,2 tys. lat), średniowieczu (1,5 ± 0,1 tys. lat), i wczesnym okresie nowożytnym (0,4 ± 0,02 tys. lat). Wyniki te są zgodne z wynikami innych badań dotyczących Europy Środkowej, tym samym potwierdzają występowanie dynamicznego systemu denudacji i wielu zdarzeń erozyjno–akumulacyjnych w krajobrazie lessowym południowo-zachodniej Polski.

Słowa kluczowe: krajobraz lessowy, erozja gleb, denudacja, ^{10}Be in-situ, $^{239+240}$Pu, radionuklidy, datowania OSL, gleby płowe.

Streszczenie w języku angielskim

Loess landscapes are very susceptible to erosion processes which affects the stability, productivity, and transformation of soils. The Trzebnica Hills located in south–western Poland are one of such areas.

In present study, isotopic methods such as ^{10}Be in–situ, $^{239+240}$Pu were used to determine soil erosion rates. ^{10}Be in–situ, which is directly produced in the quartz crystal lattice as a result of cosmogenic rays, enables to determine long–term erosion, i.e., occurring since the surface was formed. In contrast, $^{239+240}$Pu, which were globally introduced into the environment mainly as a result of the production and testing of nuclear bombs in the 1960s, give a possibility to calculate short–term erosion rates, which has occurred over the past 60 years. In addition, optically stimulated luminescence (OSL) dating was used to reconstruct temporal erosion–deposition processes. Directions for the development of agriculturally used soils under conditions of intensive erosion were also identified.

Two transects along two slopes with pronounced erosional features were sampled in the southern part of Trzebnica Hills. In collected soil samples basic physico-chemical analyses and isotopic analyses (^{10}Be in–situ, $^{239+240}$Pu) were performed. Moreover, in selected soil horizons OSL dating, and micromorphology analyses were done.

Long–term soil erosion rates ranged from 0.44 to 0.85 t/ha/yr, while short–time erosion rates ranged from 1.2 to 10.9 t/ha/yr. These values lie within the range of data presented for other loess areas in Europe. Short–term erosion rates are significantly higher than long–term due to the intensification and mechanisation of agriculture in the XX century, but also climate change may be an additional factor intensifying erosion processes. Moreover, short–term erosion rates considerably exceed tolerable erosion rates which range from 0.5 to 1.0 t/ha/yr, thus soils in the study area are subject to degradation. It is reflected in the shallowing of the eluvial and argic horizons in soils classified as Luvisols. Progressive erosion processes lead to the complete removal of these horizons, so the soils are transformed into Regosols. However, in the lower parts of slopes eroded material was deposited, soils with solimovic qualifier occurr. OSL dating reveal that the first phase of sediment redeposition on the slopes occurred about 9.1 ka ago. Subsequent ones occurred in the Neolithic (6.4 ± 0.3 ka), Bronze Age (3.8 ± 0.2 ka), Medieval (1.5 ± 0.1 ka) and early Modern Period (0.4 ± 0.02 ka). These results are

consistent with those of other studies in Central Europe, thus confirming the occurrence of a dynamic denudation system and multiple erosion–accumulation events in the loess landscape of south–western Poland.

1. Wstęp

Erozja gleby powoduje rozpad struktury gleby i niszczy jej powierzchnię poprzez mechaniczne przenoszenie cząstek pod wpływem działania sił wody – erozja wodna, lub wiatru – erozja wietrzna (FAO, 2019; Karczewska, 2012; Morgan, 2005). Tempo erozji gleby zależy nie tylko od jej podstawowych właściwości, takich jak uziarnienie, zawartość materii organicznej, struktura, gęstość korzeni, ale również jest związane z użytkowaniem terenu i pokrywą roślinną (Alewell i in., 2014, 2008; Karczewska, 2012; Konz i in., 2012; Święchowicz, 2016). Zagospodarowanie leśne lub w kierunku użytków zielonych minimalizuje erozję poprzez ustabilizowanie powierzchni (Ouyang i in., 2018; Rejman i in., 2014b). Natomiast wzrost tempa erozji jest bezpośrednią konsekwencją nadmiernej i często nieprawidłowej eksploatacji rolniczej (zabiegi uprawowe) i zagraża stabilności, jakości oraz produktywności gleb (Alewell i in., 2017; Guzmán i in., 2015; Rickson, 2014). Erozja powoduje straty materii organicznej, która odgrywa kluczową rolę w sekwestracji węgla i jest niezbędna do tworzenia stabilnej struktury gleby (Gonet, 2007; Šimanský i in., 2019; Zádorová i in., 2011). Ponadto, długotrwała i intensywna erozja usuwa powierzchniową warstwę gleby w górnych częściach stoku, a następnie deponuje zerodowany materiał w jego dolnych częściach generując tworzywo dla rozwoju gleb deluwialnych (Dotterweich, 2008; Kołodyńska-Gawrysiak i in., 2018; Świtoniak i in., 2016; Zádorová i Penížek, 2018). W konsekwencji następują nieodwracalne zmiany w naturalnej strukturze tych gleb i w układzie poziomów glebowych (Drewnik i Żyła, 2019; Kaiser i in., 2021; Klimowicz i Uziak, 2001; Świtoniak, 2014).

Less, definiowany jako osad lądowy powstały w wyniku eolicznej akumulacji frakcji pyłowej, szczególnie podczas plejstoceńskich zimnych faz suchych (Muhs, 2013; Pye, 1995; Waroszewski i in., 2018b), jest jednym z najbardziej podatnych na erozję materiałów (Licznar i in., 1981; Poręba i in., 2019; Rejman i Iglik, 2010; Zhang i in., 2018). W Europie osady lessowe są szeroko rozpowszechnione i występują m.in. na obszarze Francji, Belgii, Niemiec, Polski, Ukrainy, Rosji (Frechen, 2003; Haase i in., 2007; Lehmkuhl i in., 2021). Ich najbardziej intensywna akumulacja zachodziła tuż przed lub po osiągnięciu przez lodowiec maksymalnego zasięgu (LGM) podczas ostatniego zlodowacenia – Vistulianu (Frechen, 2003; Jary, 1996). Produktywne gleby wytworzyły się na lessach, takie jak czarnoziemy czy gleby płowe (Altermann i in., 2005; Drewnik

i Żyła, 2019; Gerlach i in., 2012; Labaz i in., 2018; Smetanová i in., 2017). W konsekwencji już od Neolitu obszary lessowe były wylesiane i przekształcane w grunty orne, co spowodowało intensyfikację procesów erozyjnych (Gerlach i in., 2012; Kołodyńska-Gawrysiak i in., 2017; Poręba i in., 2019). Procesy te powodują sukcesywne zmniejszanie miąższości poziomów próchnicznych, a w konsekwencji, znaczne rozjaśnienie ich barwy poprzez włączanie głębszych, jaśniejszych warstw (Drewnik i Żyła, 2019). W związku z tym kryteria dla poziomu molik nie są spełnione, a gleby należą do jednostki gleb płowych (Kabała i in., 2019; Labaz i in., 2018), które również są produktywne ze względu na wysokie wysycenie kompleksu sorpcyjnego kationami wymiennymi oraz korzystne właściwości hydro-fizyczne (Glina i in., 2014; Rejman i in., 2014a; Turski i Witkowska-Walczak, 2004; Vitharana i in., 2008). Jednakże, gleby płowe są intensywnie użytkowane rolniczo, zatem są narażone na dalszą degradację (Klimowicz i Uziak, 2001).

Dotychczasowe badania empiryczne dotyczące wskaźników erozji gleb prowadzone były głównie z wykorzystaniem pułapek sedymentacyjnych, które zatrzymywały erodowany materiał u podnóża stoków (Alewell i in., 2014; Kaszubkiewicz i in., 2008; Rejman i Usowicz, 2002; Święchowicz, 2016). Jednak zjawiska erozyjne mają charakter okresowy, a nie regularny oraz często nieliniowy. Powoduje to, że wiarygodne dane z pułapek sedymentacyjnych mogą zostać uzyskane dopiero na podstawie wieloletnich cykli pomiarowych, co jest problematyczne, m.in. ze względu na to, iż na powierzchniach doświadczalnych powinno być utrzymywane takie samo pokrycie powierzchni roślinami (Kaszubkiewicz i in., 2008). W związku z tym wielu naukowców rezygnuje z samodzielnego szacowania tempa erozji gleby z wykorzystaniem pułapek sedymentacyjnych i skupia się na doświadczeniach innych naukowców, które zostały podsumowane w modelu strat glebowych RUSLE (Revised Universal Soil Loss Equation). Model ten obejmuje takie parametry jak: erozyjność deszczy i spływów, podatność gleby na erozję, długość i nachylenie zbocza, sposób użytkowania i rodzaj upraw, czy też zabiegi przeciwerozyjne (Kaszubkiewicz. i in., 2011; Wischmeier i Smith, 1978). Model RUSLE jest powszechnie stosowany również w celu uniknięcia nakładów finansowych i możliwości popełnienia błędów związanych ze stosowaniem pułapek osadów stokowych. Jednak RUSLE jest modelowaniem matematycznym, które często nie może zastąpić bezpośrednich badań i pomiarów in-situ. W związku z tym konieczne jest poszukiwanie i aplikowanie nowych narzędzi/metod do badania tempa erozji gleby in-situ.

Taką możliwość dają techniki izotopowe, jak np. ^{10}Be, $^{239+240}$Pu, które były z powodzeniem stosowane w Szwajcarii, Niemczech, Chinach czy Australii (Alewell i in., 2014; Calitri i in., 2020, 2019; Hoo i in., 2011; Lal i in., 2020; Loba i in., 2022; Musso i in., 2020; Xu i in., 2015; Zollinger i in., 2015). Natomiast w Polsce badania tempa erozji z użyciem izotopów były rzadkością, a na obszarach lessowych skupiały się głównie na aplikacji izotopu cezu – ^{137}Cs (Poręba i in., 2019, 2011, 2015). ^{137}Cs jest radionuklidem opadowym (fallout radionuclide; FRN), który został globalnie wprowadzony do środowiska głównie w wyniku produkcji i testowania bomb jądrowych w latach 60-tych XX wieku (Alewell i in., 2017, 2014; Meusburger i in., 2020, 2016; Zollinger i in., 2015). Jednakże, ^{137}Cs charakteryzuje się krótkim okresem połowicznego rozpadu, wynoszącym 30 lat, a ostatnie szacunki wskazują, że ponad 70% ^{137}Cs zniknęło w wyniku jego rozpadu promieniotwórczego (Xu i in., 2015). W związku z tym, na obszarach cechujących się erozją, gdzie powierzchniowa warstwa gleby zasobna w ^{137}Cs jest sukcesywnie usuwana, a pozostała jego zawartość uległa połowicznemu rozpadowi, wykrywalność i pomiar radioaktywnego cezu stają się coraz trudniejsze. Ponadto, awaria elektrowni atomowej w Czarnobylu w 1986 roku spowodowała, że rozkład przestrzenny ^{137}Cs w Europie Środkowej i Zachodniej nie jest już jednorodny, co skutkuje pewnymi ograniczeniami w jego stosowaniu (Alewell i in., 2017; Arata i in., 2016; Loba i in., 2020). W rezultacie izotopy plutonu – $^{239+240}$Pu, które mają takie samo pochodzenie jak ^{137}Cs, są stosowane jako bezpieczniejsza alternatywa, ponieważ nie były zawarte w lotnej frakcji zanieczyszczeń uwolnionych podczas awarii reaktora w Czarnobylu, w związku z czym mają jedno źródło pochodzenia – wyłącznie testy bomb jądrowych (Arata i in., 2016; Zollinger i in., 2015). Wspomniane izotopy $^{239+240}$Pu cechują się również dłuższym czasem połowicznego rozpadu (odpowiednio 24 110 i 6 561 lat), w porównaniu z ^{137}Cs (Alewell i in., 2017). Ponadto, cechują się silnym powinowactwem do materii organicznej, są skutecznie wiązane przez frakcję ilastą gleby i transportowane podczas procesów erozyjnych z przemieszczającymi się cząstkami gleby (Everett i in., 2008; Ketterer i in., 2004b). Zaletą stosowania izotopów plutonu (jak i cezu) jest możliwość określenia tempa erozji krótkoterminowej, która miała miejsce w ciągu ostatnich 60 lat (Alewell i in., 2017; Arata i in., 2016).

Tempo erozji długoterminowej, czyli zachodzącej od momentu ukształtowania się powierzchni, można określić za pomocą nuklidów kosmogenicznych, takich jak ^{10}Be (Calitri i in., 2019; Hidy i in., 2010; Zollinger i in., 2015). Na podstawie pochodzenia

wyróżnia się dwa rodzaje izotopu berylu o liczbie masowej 10: (1) ^{10}Be meteoryczny, który jest wytwarzany w górnej części atmosfery w wyniku spallacji azotu i tlenu przez promienie kosmiczne, a następnie deponowany jest na powierzchni Ziemi z opadami deszczu (Graly i in., 2010; Willenbring i von Blanckenburg, 2010; Wyshnytzky i in., 2015), oraz (2) ^{10}Be in-situ, który jest bezpośrednio wytwarzany w sieci krystalicznej kwarcu w wyniku oddziaływania promieni kosmogenicznych (Hidy i in., 2010; Loba i in., 2022). Dotychczas ^{10}Be meteoryczny był wykorzystywany, m.in. w badaniach zmienności paleoklimatycznej (Gu i in., 1997; Zhou i in., 2015), datowaniu moren glacjalnych (Dahms et al., 2018; Eaves et al., 2018) czy ustalaniu skali czasowych depozycji lessu (Shen Chengde i in., 1992). Natomiast w kontekście krajobrazów lessowych brakuje badań wykorzystujących ^{10}Be meteoryczny lub ^{10}Be in-situ do określenia tempa erozji.

W większości badań, omawiane izotopy cezu (^{137}Cs), plutonu ($^{239+240}$Pu) czy berylu (^{10}Be) były wykorzystywane oddzielnie do określania tempa erozji (Arata i in., 2016; Musso i in., 2020; Waroszewski i in., 2018a). Jednak ostatnio zauważalny jest trend łączenia dwóch rodzajów izotopów, aby porównać krótko- i długoterminowe tempo erozji. Na przykład Calitri i in. (2019), Jelinski i in. (2019) czy Zollinger i in. (2015) zastosowali oba typy izotopów do porównania procesów erozyjnych z ostatnich 60 lat ze wskaźnikami długoterminowymi w celu określenia wpływu antropopresji i zmian klimatu na procesy stokowe i glebowe.

Dane uzyskane na temat tempa erozji gleby mogą być również wspierane przez techniki datowań, jak na przykład optycznie stymulowaną luminescencję (OSL). Metoda ta umożliwia określenie, kiedy ziarna mineralne były po raz ostatni wystawione na działanie światła słonecznego, a tym samym kiedy osady ulegały (re)depozycji (Fuchs i in., 2010; Kołodyńska-Gawrysiak i in., 2017; Poręba i in., 2011; Rahimzadeh i in., 2019). Takie badania umożliwiają rekonstrukcję zdarzeń erozyjno–depozycyjnych, analizę ewolucji rzeźby terenu w plejstocenie i holocenie oraz modelowanie dynamiki środowiska w przeszłości (Döhler i in., 2018; Kołodyńska-Gawrysiak i in., 2018; Malik i in., 2021; Poręba i in., 2019; Rahimzadeh i in., 2019; Scherer i in., 2021).

W związku z powyższym, w niniejszej pracy doktorskiej przedstawiono wyniki badań z pierwszej próby zastosowania ^{10}Be in-situ i $^{239+240}$Pu do oceny tempa erozji na obszarze lessowym, uzupełnione o datowania OSL w celu rekonstrukcji procesów erozyjno-depozycyjnych.

Problem erozji gleb został ostatnio podkreślony w Rezolucji Parlamentu Europejskiego w sprawie ochrony gleb oraz przez Organizację Narodów Zjednoczonych do spraw Wyżywienia i Rolnictwa (European Parliament, 2021; FAO, 2019). W związku z tym szczegółowe badania tempa erozji gleb nowymi, efektywnymi metodami są niezbędne w celu ograniczenia tego zjawiska, poprzez planowanie skutecznych zabiegów przeciwerozyjnych, kluczowych dla zrównoważonego zarządzania zasobami glebowymi na obszarach erodowanych.

2. Cel pracy

Celem niniejszej rozprawy doktorskiej było szczegółowe zbadanie procesów erozyjno–depozycyjnych, ze szczególnym uwzględnieniem:

(1) określenia tempa erozji krótko– i długoterminowej gleb ornych w krajobrazie lessowym Wzgórz Trzebnickich, za pomocą metod izotopowych (^{10}Be in-situ, $^{239+240}$Pu),

(2) rekonstrukcji czasowej procesów erozyjno–depozycyjnych, w krajobrazie lessowym Wzgórz Trzebnickich za pomocą datowań OSL,

(3) określenia kierunków rozwoju gleb użytkowanych rolniczo pozostających pod silną presją procesów erozyjnych, na przykładzie Wzgórz Trzebnickich,

(4) zweryfikowania przydatności i możliwości zastosowania narzędzi izotopowych (^{10}Be, $^{239+240}$Pu, ^{137}Cs) do określenia tempa erozji w różnych środowiskach, w tym lessowych.

3. Charakterystyka obszaru badań

Obszar badań położony jest w południowo–zachodniej Polsce, w brzeżnej części Wzgórz Trzebnickich, nieopodal wsi Wysoki Kościół (Fig. 1; Loba i in., 2021). W geologii obszaru dominują osady czwartorzędowe (lessy, gliny zwałowe, osady fluwioglacjalne), ale lokalnie na niewielkich obszarach występują również osady neogeńskie jak gliny, piaski i żwiry (Dyjor, 1970; Dyjor and Kościówko, 1982; Jary, 1996; Pachucki, 1952). Less, który jest najmłodszym osadem plejstoceńskim, tworzy na obszarze Wzgórz Trzebnickich płytkie pokrywy o zróżnicowanej miąższości, średnio 2-5 m (Jary, 1996; Waroszewski i in., 2021), a odsłonięcie w Zaprężynie stanowi istotny zapis dynamiki lessu oraz procesów glebowych od ostatniego interglacjału (Eemian, MIS 5e) do górnego plenivistulianu (MIS 2) (Jary and Ciszek, 2013).

Gleby Wzgórz Trzebnickich, wykształcone w większości z osadów lessowych, charakteryzują się głównie przemyciem iłu i jego akumulacją w głębszych partiach profilu (gleby płowe), marginalnie w położeniach akumulacyjnych pojawiają się płaty gleb deluwialnych czarnoziemnych czy też gleb szarych (Glina i in., 2014; Kabała and Marzec, 2010; Licznar and Licznar, 2002; Licznar i in., 1988; Zmuda i in., 2009). Od neolitu ulegają one zintensyfikowanym procesom erozyjno–depozycyjnym, na skutek użytkowania rolniczego (Anioł–Kwiatkowska, 1998; Loba i in. 2023).

Rodzima roślinność jest reprezentowana przez lasy dębowo-grabowe, ale większość terenów jest wykorzystywana rolniczo ze względu na produktywność gleb (Anioł-Kwiatkowska, 1998). Głównymi uprawianymi roślinami są: pszenica, buraki cukrowe, kukurydza. Według klasyfikacji klimatów Köppena–Geigera Wzgórza Trzebnickie cechują się ciepłym latem i wilgotnym klimatem kontynentalnym. Średnia roczna temperatura wynosi 8°C, a średnie temperatury w najzimniejszym i najcieplejszym miesiącu wynoszą odpowiednio -3°C (styczeń) oraz 18°C (lipiec) (Bac and Rojek, 2012). Średnia roczna suma opadów wynosi ok. 600 mm (Bac and Rojek, 2012).

4. Metodyka badań

4.1. Prace terenowe

Prace terenowe prowadzono w latach 2018–2019 w południowej części Wzgórz Trzebnickich, w sąsiedztwie miejscowości Wysoki Kościół. W celu prześledzenia wielokierunkowego charakteru erozji gleb, wykonano łącznie 12 profili glebowych zaaranżowanych w dwa transekty badawcze na dwóch stokach wykazujących wyraźne cechy procesów denudacyjnych (Fig. 1 w Loba i in., 2021). Punktem wspólnym dla obu transektów był profil WK1. Zakres nachylenia stoków był podobny dla badanych transektów i osiągał najwyższe wartości (12–13°) w środkowych partiach stoków. Ponadto, w pobliskim, płaskim zalesionym obszarze wykonano profil referencyjny (WK0), będący reperem dla analityki izotopowej.

Wszystkie odkrywki glebowe zostały opisane zgodnie z wytycznymi do opisu gleb (FAO, 2006) oraz sklasyfikowane zgodnie z zasadami międzynarodowej klasyfikacji gleb WRB (IUSS Working Group WRB, 2022) i Systematyki gleb Polski wyd. 6 (SGP, 2019). Ze wszystkich poziomów glebowych pobrano ~1 kg materiału glebowego do analiz fizykochemicznych i geochemicznych, oraz próbki gleby o nienaruszonej strukturze, do stalowych cylinderków o objętości 100 cm^3, w celu wykonania analizy gęstości objętościowej. Aby uzyskać wystarczającą ilość ziaren kwarcu (o średnicy od 0,25 do 0,60 mm) do analizy ^{10}Be in-situ pobrano dodatkowo 8–9 kg materiału glebowego w interwałach co 20 cm, do głębokości 100 cm. Do analizy aktywności $^{239+240}$Pu pobrano próbki gleby co 5 cm od powierzchni do głębokości 40 cm. Jednakże, ze względu na jednorodność poziomów Ap (0–20/0–25 cm) pobrano tylko jedną próbkę z tych warstw. Ponadto, z wybranych poziomów glebowych pobrano 15 próbek do datowań optycznie stymulowanej luminescencji (OSL), 12 próbek do analizy mikromorfologicznej i 3 próbki twardych noduli węglanowych do datowania radiowęglowego (^{14}C).

4.2. Analizy laboratoryjne

Materiał glebowy pobrany podczas prac terenowych został wysuszony w temperaturze pokojowej, a następnie roztarty i przesiany przez sito o średnicy 2 mm, w celu oddzielenia części ziemistych od frakcji szkieletowych.

Analizy fizykochemiczne wykonano w częściach ziemistych (< 2mm). W laboratoriach Instytutu Nauk o Glebie, Żywienia Roślin i Ochrony Środowiska (Uniwersytet Przyrodniczy we Wrocławiu) oznaczono:

- o gęstość objętościową metodą suszarkowo-wagową;
- o skład granulometryczny metodą areometryczno-sitową zgodnie z normą PN-R-04032 (1998);
- o pH metodą potencjometryczną w wodzie destylowanej, w stosunku 1:2,5;
- o całkowitą zawartość węgla organicznego w poziomach mineralnych metodą spalania katalitycznego i pomiaru wydzielonego CO_2 za pomocą detektora spektroskopowego (Ströhlein CS-mat 5500);
- o całkowitą zawartość azotu ogółem w powierzchniowych próbkach mineralnych metodą Kjeldahla;
- o kwasowość hydrolityczną w 1M octanie sodu w próbkach z gleb uprawnych;
- o kwasowość wymienną i glin wymienny w 1M chlorku potasu w proporcji 1:10 w próbkach z gleb leśnych;
- o wymienne kationy zasadowe po ekstrakcji w octanie amonu o pH 7,0, w proporcji 1:10, metodą atomowej spektrofotometrii absorpcyjnej (Mg) i emisyjnej (Ca, K i Na);
- o zawartość węglanu wapnia metodą Scheiblera.

Ponadto w laboratoriach Uniwersytetu w Zurychu oznaczono skład geochemiczny badanych próbek za pomocą fluorescencji rentgenowskiej (XRF), wykonano ekstrakcję i oznaczenie aktywności $^{239+240}$Pu według metody Ketterer i in. (2004) oraz przeprowadzono analizę ekstrakcji ^{10}Be in-situ według zmodyfikowanej metodyki von Blanckenburg i in. (1996), a następnie oznaczono jego zawartość za pomocą akceleratorowego spektrometru masowego (AMS) Tandy na Politechnice Federalnej w Zurychu (ETHZ).

W laboratoriach Instytutu Geofizyki Stosowanej (Leibniz Institute for Applied Geophysics – LIAG) w Hanowerze, w warunkach stłumionego światła czerwonego wykonano datowania OSL oraz oznaczono skład granulometryczny za pomocą analizatora dyfrakcji laserowej na urządzeniu Beckman – Coulter (LS 13320 PIDS), w celu uchwycenia większej rozdzielczości frakcji pyłu.

Szlify mikromorfologiczne zostały wykonane w laboratorium mineralogii i petrografii Uniwersytetu w Ghent (Belgia), a następnie specyficzne cechy były obserwowane

i opisane z użyciem mikroskopu Zeiss Axio Lab A1 i terminologii zaproponowanej przez Stoopsa (2003).

Datowania radiowęglowe (^{14}C) noduli węglanowych zostały wykonane w Poznańskim Laboratorium Radiowęglowym z wykorzystaniem akceleratora masowego (AMS), a skalibrowane daty uzyskano w oparciu o zastosowanie programu OxCal 4.4.

Bardziej szczegółowy opis metodyki analiz laboratoryjnych został przedstawiony w cyklu publikacji stanowiącym niniejszą pracę doktorską (Loba i in. 2023, 2022, 2021).

5. Wyniki

5.1. Morfologia i pozycja systematyczna badanych gleb

Badane gleby wykształciły się głównie w obrębie materiałów lessowych o miąższości do 1,5 m. Jednak niektóre profile glebowe wykazywały w swojej dolnej części osady fluwioglacjalne (profil WK2) i/lub gliny zwałowe (profile WK7, WK8, WK9).

Prawie wszystkie z badanych gleb wykazują wyraźne zróżnicowanie morfologiczne związane z iluwiacją iłu. W pełni wykształcone gleby płowe z poziomami E i Bt występują tylko na szczycie badanego wzgórza (profil WK1) oraz w środkowej części stoku (profile WK4, WK5, WK6). Pozostałe profile wykazywały cechy silnie związane z erozją, takie jak brak poziomu E i worywanie poziomu Bt do poziomu Ap (profile WK2, WK3, WK10, WK11) czy też tworzenie się głębokiego deluwium w dolnej części stoku (WK12). Akumulację wtórnych węglanów w formie twardych konkrecji odnotowano w trzech profilach glebowych (WK7, WK8 i WK9). Szczegółowe informacje dotyczące morfologii gleb zostały przedstawione w Loba i in. (2021), Tabela 2.

Mimo, że większość badanych gleb doświadczyła procesów erozyjnych, prawie wszystkie zostały zaliczone do grupy referencyjnej Luvisols, jedynie profile WK7, WK9 i WK12 zostały zaliczone do grupy Regosols (Loba i in. 2023) (IUSS Working Group WRB, 2022). Według Systematyki gleb Polski (SGP, 2019) badane profile glebowe należy sklasyfikować jako: gleby płowe typowe, gleby płowe zerodowane, gleby deluwialne oraz regosole typowe (Tabela1).

Tab. 1. Pozycja systematyczna badanych gleb

Profil	SGP (2019)	WRB (2015)	WRB (2022)
WK1	Gleba płowa typowa	Albic Luvisol (Aric, Cutanic, Ochric, Siltic)	Albic Luvisol (Pantosiltic, Aric, Cutanic, Ochric)
WK2	Gleba płowa zerodowana	Haplic Luvisol (Aric, Cutanic, Endodensic, Endoloamic, Ochric, Episiltic, Raptic)	Haplic Luvisol (Episiltic, Endoloamic, Aric, Cutanic, Endodensic, Ochric, Raptic)
WK3	Gleba płowa zerodowana	Lamellic Luvisol (Aric, Cutanic, Ochric, Siltic)	Lamellic Luvisol (Pantosiltic, Aric, Cutanic, Ochric)
WK4	Gleba płowa typowa	Stagnic Albic Luvisol (Aric, Cutanic, Ochric, Siltic)	Stagnic Albic Luvisol (Pantosiltic, Aric, Cutanic, Ochric)
WK5	Gleba płowa typowa	Albic Luvisol (Aric, Cutanic, Ochric, Siltic)	Albic Luvisol (Pantosiltic, Aric, Cutanic, Ochric)
WK6	Gleba płowa typowa	Haplic Luvisol (Aric, Colluvic, Cutanic, Endoloamic, Ochric, Episiltic)	Haplic Luvisol (Episiltic, Endoloamic, Aric, Cutanic, Ochric, Solimovic)
WK7	Gleba deluwialna właściwa typowa	Eutric Colluvic Regosol (Aric, Ochric, Raptic, Episiltic)	Eutric Solimovic Regosol (Episiltic Endoloamic, Aric, Ochric,)
WK8	Gleba płowa zerodowana	Calcic Luvisol (Aric, Cutanic, Densic, Endoloamic, Ochric, Episiltic, Raptic)	Haplic Luvisol (Episiltic, Endoloamic, Aric, Cutanic, Ochric, Raptic)
WK9	Regosol typowy	Eutric Regosol (Aric, Densic, Endoloamic, Ochric, Episiltic)	Eutric Regosol (Episiltic , Endoloamic, Aric, Ochric,)
WK10	Gleba płowa zerodowana	Haplic Luvisol (Aric, Cutanic, Endoloamic, Ochric, Episiltic, Raptic)	Haplic Luvisol (Episiltic, Endoloamic, Aric, Cutanic, Ochric, Raptic)
WK11	Gleba płowa zerodowana	Haplic Luvisol (Aric, Cutanic, Ochric, Siltic)	Haplic Luvisol (Pantosiltic , Aric, Cutanic, Ochric)
WK12	Gleba deluwialna właściwa typowa	Endostagnic Colluvic Eutric Regosol (Ochric, Pantosiltic)	Endostagnic Solimovic Eutric Regosol (Pantosiltic, Ochric,)
WK0	Gleba płowa typowa	Albic Luvisol (Ochric, Siltic)	Albic Luvisol (Pantosiltic, Ochric)

5.2. Uziarnienie gleb

Badane gleby cechowały się głównie uziarnieniem pyłu gliniastego i pyłu ilastego, z dominującą frakcją pyłu grubego (w zakresie 45–50 µm), co jest typowe dla osadów lessowych. W glebach charakteryzujących się nieciągłościami litologicznymi, dolne części profilu glebowego cechowały się uziarnieniem pyłu zwykłego i gliny lekkiej, z dominującą frakcją piasku średniego (WK2), lub z zaznaczającymi się frakcjami pyłu średniego, piasku drobnego i średniego (WK8, WK9). Utwory lessowe zdeponowane podczas MIS 2 mają wąski zakres dominującej frakcji, mieszczącej się w zakresie od 44 do 48 µm. Natomiast w osadach redeponowanych między czasami prehistorycznymi a nowożytnością, wyraźnie zaznacza się dominacja frakcji pyłu grubego, w zakresie od 35 do 58 µm (Tab. 2 w Loba i in. 2021; Fig. 6 w Loba i in. 2023).

5.3. Mikromorfologia gleb

Cienkie szlify glebowe wskazywały na obecność struktury gruzełkowej oraz foremnowielościennej–zaokrąglonej (np. WK6, WK12). Wśród najczęściej występujących wtórnych cech glebowych były typowe i agregatowe, słabo i średnio wysycone nodule żelaziste, typu anortycznego (ex-situ) oraz ortycznego (in-situ). Obecność cech wtórnych związanych z procesem iluwiacji była bardzo zróżnicowana. Najlepiej wykształcone i zachowane cechy iluwiacji iłu były widoczne w profilu WK2, a najsłabiej w profilu WK3, WK4, WK8, WK9. Natomiast w profilach WK6, WK11 oraz WK12 poza bardzo szczątkowymi i pofragmentowanymi otoczkami ilastymi, nie stwierdzono cech pedogenicznych typowych dla procesu iluwiacji. Jedynie poziomy Eg i EBgb w profilu WK6 i poziom BC1g w profilu WK12 zawierały fragmenty mikrolaminowanych czerwono-brązowych otoczek iluwialnych. Ich morfologia i rozmiar sugerowały pochodzenie ex-situ, prawdopodobnie jako efekt spływu powierzchniowego, tylko nieliczne z nich miały charakter rezydualny.

5.4. Wybrane właściwości chemiczne i geochemiczne gleb

Badane gleby charakteryzują się głównie lekko kwaśnym i obojętnym odczynem. Jedynie w profilu WK9 oraz poziomie 4Cgk profilu WK7 stwierdzono odczyn zasadowy, ale spowodowane jest to obecnością $CaCO_3$. Zawartości węgla organicznego są niskie

(0,04%–1,22%) i maleją wraz z głębokością (Tab. 2 w Loba i in. 2021). Również całkowita zawartość azotu w badanych glebach jest bardzo niska (0,01%–0,08%). Wartości kwasowości hydrolitycznej są niewielkie, maksymalnie osiągają 2 cmol(+)/kg w profilu WK4. Suma kationów zasadowych wynosi od 4,1 cmol(+)/kg do 87 cmol(+)/kg, a stopień wysycenia kationami zasadowymi waha się od 80,6% w profilu WK12 do 100% w profilu WK7, WK8, WK9.

Zawartość głównych pierwiastków w badanych glebach jest mało zróżnicowana i oscyluje w granicach 61,1–87,0% dla SiO_2, 5,6–11,8% dla Al_2O_3, 1,0–3,7% dla Fe_2O_3 i 1,7–2,8% dla K_2O. Zawartości Zr i Hf, które są wskaźnikami procesów eolicznych (McLennan, 2001) umożliwiają odróżnienie materiałów lessowych od osadów lodowcowych. Dolne warstwy profili WK2, WK7 i WK9 mają znacznie niższe wartości Zr i Hf (maksymalnie 256 i 6,9 mg kg^{-1}, odpowiednio), od średnich zawartości wyznaczonych dla lessów, które wynoszą 302 mg kg^{-1} dla Zr i 8,9 mg kg^{-1} dla Hf (McLennan, 2001). Odzwierciedla to obserwowaną w terenie nieciągłość litologiczną. Zawartości tych pierwiastków wskaźnikowych dla pozostałych profili są takie same bądź wyższe jak wyznaczona średnia dla utworów lessowych (Loba i in., 2021).

5.5. Zawartość ^{10}Be in-situ i tempo erozji długoterminowej

Średnia zawartość ^{10}Be in-situ w badanych glebach wynosi od 0,9 do 1,5 (×10^5) atomów/g. W obu transektach gleby zlokalizowane w górnej części stoku cechują się niższymi zawartościami izotopu berylu (0,9 – 1,0 (×10^5) atomów/g) niż gleby położone w dolnej części stoku (1,2 – 1,5 (×10^5) atomów/g). Obliczone wartości tempa erozji długoterminowej są podobne dla obu transektów. We wspólnym punkcie początkowym – WK1 – erozja wynosi 0,46 t/ha/rok. W środkowej części stoku tempo erozji rośnie, przyjmując wartości między 0,56 a 0,85 t/ha/rok, natomiast w dolnej części stoku erozja maleje, wynosząc od 0,44 do 0,50 t/ha/rok. Największym tempem erozji cechuje się profil WK9, a najmniejszym profil WK6.

5.6. Aktywność $^{239+240}$Pu i tempo erozji krótkoterminowej

Aktywność $^{239+240}$Pu w badanych glebach jest na ogół niska i wynosi od 0,002 do 0,520 Bq/kg. Wskaźniki tempa erozji krótkoterminowej różnią się znacznie w zależności od zastosowanego modelu. PDM (Profile Distribution Model) wskazuje na wyższe tempo

erozji, od 1,4 do 16,9 t/ha/rok, natomiast MODERN (Modelling Deposition and Erosion rates with Falling Radionuclides) niższe, wynoszące od 1,2 do 10,9 t/ha/rok. Różnice te szczegółowo zostały omówione w Loba i in. 2021. Ogólnie gleby znajdujące się w drugim transekcie charakteryzują się wyższymi wskaźnikami tempa erozji niż w pierwszym. Największe wartości erozji skalkulowano w profilu WK9, a najniższe w profilu WK12.

5.7. Datowania OSL

Datowania luminescencyjne badanych gleb pokazują szeroki zakres czasowy. Większość dat koreluje z MIS2 (od 14,5 ± 0,7 do 26,6 ± 1,8 tys. lat), kiedy lessy na badanym obszarze zostały zdeponowane, ale również z mezolitem (9,1 ± 0,4 tys. lat), neolitem (6,4 ± 0,3 tys. lat) i epoką brązu (1,5 ± 0,1 tys. lat). Najmłodsze daty badanych osadów są związane z wczesnym (1,5 ± 0,1 tys. lat) i późnym (0,7 ± 0,03 tys. lat) średniowieczem oraz wczesną nowożytnością (0,4 ± 0,02 tys. lat). Ponadto dwie próbki pobrane z dolnych partii profilu WK2 i WK9 osiągnęły punkt saturacji zarówno dla kwarcu jak i skaleni, ponieważ były znacznie starsze niż ostatnie zlodowacenie, nie było możliwe określenie ich wieku metodą OSL.

Ponadto, uzyskane pomiary luminescencyjne zostały przeanalizowane metodą Murray i in. (2012), co potwierdziło, że sygnał OSL kwarcu został całkowicie zresetowany przed zdeponowaniem próbki, więc uzyskane datowania OSL są wiarygodne.

6. Dyskusja

W artykule Loba i in. 2022 przedstawiono przegląd artykułów naukowych, w których izotopy ^{10}Be, ^{137}Cs i $^{239+240}$Pu były stosowane jako znaczniki tempa erozji gleb w różnych środowiskach, w tym lessowych. Wartości erozji skalkulowane za pomocą modelu RUSLE dla obszarów lessowych były często zgodne z wartościami uzyskanymi w oparciu o analizy izotopowe, co jednoznacznie wykazało, że narzędzia izotopowe stanowią wiarygodną alternatywę dla klasycznych metod.

Przeprowadzone badania rozszerzają bazę danych dotyczącą metod izotopowych jako alternatywy w badaniach tempa erozji gleb, a niniejszy rozdział zawiera skróconą dyskusję na temat uzyskanych wyników badań, która bardziej szczegółowo została przedstawiona w publikacjach Loba i in. 2021, 2023.

6.1. Tempo erozji gleb w krajobrazach lessowych

Tempo erozji długoterminowej badanych gleb, obliczone na podstawie ^{10}Be in-situ, jest zgodne z danymi pochodzącymi z innych badań krajobrazów lessowych z zastosowaniem różnych metod (Loba i in., 2021). W Niemczech, Dreibrodt i in. (2013, 2010) określił erozję we wczesnej epoce brązu (0,3–0,6 t/ha/rok) oraz od późnego neolitu do epoki brązu (0,4–0,5 t/ha/rok) poprzez rekonstrukcję przekrojów stoków i/lub odniesienia się do masy zdeponowanych osadów w zlewni. Gillijns i in. (2005) i Kołodyńska-Gawrysiak i in. (2018) analizowały dane z obniżeń bezodpływowych w Belgii i w Polsce. Oszacowane w ten sposób tempo erozji od 430 r n.e. do czasów obecnych wynosiło 2,1 t/ha/rok dla stanowisk w Belgii (Gillijns i in., 2005), natomiast dla wybranych stanowisk w Polsce wahało się od 0,24 do 0,27 t/ha/rok od późnego Vistulianu (Weichselian) do czasów współczesnych (Kołodyńska-Gawrysiak i in., 2018).

Natomiast tempo erozji krótkoterminowej badanych gleb, określone na podstawie aktywności $^{239+240}$Pu, różni się od dotychczas prezentowanych danych dla krajobrazów lessowych w Polsce, określonych za pomocą pułapek sedymentacyjnych, ^{137}Cs czy USLE (Tab. 6 w Loba i in. 2021). Głównymi przyczynami tych rozbieżności są różnice w podejściu koncepcyjnym stosowanych metod, lokalna zmienność rzeźby terenu oraz modyfikacje zagospodarowania terenu w czasie.

Jednakże, wyznaczone w niniejszych badaniach wielkości erozji krótkoterminowej mieszczą się w zakresie danych z innych obszarów lessowych w Europie (Tab. 6 w Loba

i in. 2021). W Niemczech, przy wykorzystaniu bazy danych CORINE (Cerdan i in., 2010) erozja jest wyznaczona w przedziale od 2 do 10 t/ha/rok. Przy zastosowaniu innych metod, jak rekonstrukcja przekroju zbocza, wskaźniki erozji mieszczą się w przedziale od 3,2 do 13,3 t/ha/rok (Dreibrodt i in., 2013, 2010). W Belgii tempo erozji szacowane za pomocą obniżeń bezodpływowych wynosi od 5,5 do 9,8 t/ha/rok (Gillijns i in., 2005), dane z pułapek sedymentacyjnych to 0,5 do 7,9 t/ha/rok (Evrard i in., 2008; Verstraeten and Poesen, 2001), model SEDEM wyznacza wartości od 2 do 5 t/ha/rok (Van Rompaey i in., 2001), a dane z ^{137}Cs to 3 t/ha/rok (Van Oost i in., 2003).

6.2. Porównanie tempa erozji krótko- i długoterminowej

Zastosowanie izotopów, które obejmują różne zakresy czasowe, umożliwia porównanie tempa erozji krótko- i długoterminowej (Jelinski i in., 2019; Zollinger i in., 2015) oraz zapewnia wgląd w wielokierunkowy przebieg i intensywność procesów erozyjnych.

Na badanym obszarze krótkoterminowe wskaźniki erozji są znacząco wyższe (nawet 10–krotnie) od wskaźników długoterminowych. Tendencja ta bardzo dobrze wpisuje się w wyniki uzyskane przez Kołodyńską-Gawrysiak i in. (2018), które wskazywały, że tempo erozji od czasów prehistorycznych (0,39–0,57 t/ha/rok) wzrosło prawie 10–krotnie, w porównaniu z wartościami określonymi dla okresu między średniowieczem a czasami nowożytnymi (2,7–5,9 t/ha/rok). Ponadto, wyniki analiz ^{10}Be in-situ i $^{239+240}$Pu wskazują na intensywność procesów erozyjnych wzdłuż stoków. W profilach glebowych położonych w środkowej części stoku, generalnie obserwuje się większe tempo erozji. Szczególnie jest to widoczne w drugim transekcie, gdzie morfologia gleby wykazuje cechy silnie związane z erozją, takie jak brak poziomu E i worywanie poziomu Bt do Ap. Natomiast u podnóża stoku erodowany materiał jest zazwyczaj deponowany, a więc spodziewana jest tutaj akumulacja (Henkner i in., 2017). Jednakże na badanym obszarze również u podnóży stoków stwierdzono występowanie procesów erozyjnych (Fig. 2 w Loba i in. 2021), co świadczy o ich intensywności. Podczas ulewnych deszczy materiał był erodowany na całej długości stoku, nawet ze stanowisk, gdzie nachylenie stoku było niewielkie.

Jak wspomniano tempo erozji krótkoterminowej jest znacznie większe niż długoterminowej. Jest to przede wszystkim związane z intensyfikacją i mechanizacją

rolnictwa (Foucher i in., 2014; Kopittke i in., 2019; Poręba i in., 2019). Zmiany klimatyczne mogą być dodatkowym czynnikiem powodującym wzrost tempa erozji w ostatnich dekadach, ponieważ powodują one przesuszenie gleb, a także mniejszą liczbę zdarzeń opadowych, ale za to o dużo większej intensywności (Routschek i in., 2014; Zádorová i Penížek, 2018; Zollinger i in., 2015). Dopuszczalne wskaźniki erozji gleby (z ang. tolerable erosion rates) muszą być mniejsze lub równe wskaźnikom produkcji gleby, w przeciwnym razie gleba zacznie ulegać degradacji (Alewell i in., 2015). Ponieważ wskaźniki produkcji gleby znacznie maleją wraz z jej wiekiem, również dopuszczalne wskaźniki erozji (jako procesu niszczącego glebę) maleją wraz z upływem czasu. Większość gleb europejskich na terenach nizinnych jest starszych niż 10 tys. lat. Dopuszczalne wskaźniki erozji gleb występujących w klimacie górskim i starszych niż 10 tys. lat. wynoszą od 0,5 do 1 t/ha/rok (Alewell i in., 2015). Także Verheijen i in. (2009) wykazali, że dopuszczalne wskaźniki erozji dla gleb europejskich powinny być mniejsze niż 1 t/ha/rok. W związku z tym wykazane wartości dopuszczalnych wskaźników erozji dotyczą również badanego obszaru. Wskaźniki erozji długoterminowej mieszczą się w wyznaczonych przedziałach. Natomiast wskaźniki erozji krótkoterminowej przekraczały dopuszczalne wskaźniki od 10 do 22 razy. W związku z tym obecne straty gleby znacząco przekraczają jej produkcję i będą prowadzić do jej silnego spłycania oraz zmniejszenia jej produktywności (Alewell i in., 2015).

6.3. Zapis zjawisk denudacyjnych na badanym obszarze

Procesy denudacyjne, rozumiane jako obniżenie powierzchni terenu przez erozję i procesy powierzchniowe, prowadzą do znacznych modyfikacji krajobrazu (Karasiewicz i in., 2014; Raab i in., 2021). Zjawisko denudacji jest szczególnie widoczne w krajobrazach rolniczych oraz obszarach górskich (Meij i in., 2019; Raab i in., 2018), a jego rekonstrukcja czasowa możliwa jest z wykorzystaniem datowań OSL (Fuchs i in., 2010; Kołodyńska-Gawrysiak i in., 2017; Poręba i in., 2011; Rahimzadeh i in., 2019).

Na badanym obszarze datowania OSL wskazują, że osady lessowe zostały zdeponowane po osiągnięciu przez lodowiec maksymalnego zasięgu podczas ostatniego zlodowacenia (LGM) – Vistulianu, co jest typowe dla cienkich pokryw lessowych w południowo–zachodniej Polsce (Moska i in., 2019; Waroszewski i in., 2021). Jednakże, daty z poziomów eluwialnych gleb zlokalizowanych w dolnych częściach stoku

wskazywały na redepozycję osadów wzdłuż wyznaczonych transektów w wyniku procesów erozyjnych. Na podstawie uzyskanych wyników datowań OSL stwierdzono, że pierwsza faza redepozycji materiału glebowego miała miejsce w mezolicie (9,1 ± 0,4 tys. lat; profil WK5). Następnie, procesy erozji–depozycji zostały zintensyfikowane nie wcześniej niż w neolicie (6,4 ± 0,3 tys. lat; profil WK6) oraz epoce brązu (3,8 ± 0,2 tys. lat; profil WK4). Późniejsze fazy redepozycji datuje się na wczesne (1,5 ± 0,1 tys. lat) oraz późne (0,7 ± 0,03 tys. lat) średniowiecze (profile WK6, WK7, WK10). Ostatni epizod erozyjno–akumulacyjny datowany jest na wczesny okres nowożytny (0,4 ± 0,02 tys. lat; profil WK12), który odpowiadał małej epoce lodowcowej.

Jednakże, procesy denudacyjne nie przebiegały jednakowo na wypukłych (pierwszy transekt) i wklęsłych (drugi transekt) stokach badanego obszaru. Wiek materiałów deluwialnych był znacznie zróżnicowany w układzie katenowym. Na przykład deluwia tworzące górną warstwę profilu WK4 i WK5 znacznie różniły się wiekiem depozycji, gdzie w pierwszym określono go na 3,8 tys. lat, a w drugim na 9,1 tys. lat. W drugim transekcie deluwium (1,3 tys. lat) w profilu WK10, kontrastuje ze znacznie starszą warstwą (26,6 tys. lat) w pobliskim profilu WK11. To zróżnicowanie w datowaniach OSL wskazuje na dynamikę procesów denudacji i obecność wielu zdarzeń erozyjnych i akumulacyjnych, które miały miejsce w holocenie. Otrzymane wyniki pokazują użyteczność datowań OSL do rekonstrukcji zmian środowiskowych, ponieważ umożliwiają śledzenie procesów denudacyjnych i umożliwiają identyfikację, która warstwa (poziom) była redeponowana/ogłowiona.

6.4. Zanikanie gleb płowych

Na obszarach lessowych, w obrębie których zachodzą aktywne procesy denudacyjne, gleby tworzą mozaikowy układ wzdłuż stoków (Rejman i Iglik, 2010). Na Dolnym Śląsku lessy zostały zdeponowane w postaci miąższach osadów głównie w okresie LGM i według datowań radiowęglowych twardych, wtórnych konkrecji węglanowych, ulegały odwapnieniu w dwóch starszych fazach, tj. ~17 000 BP i 11 000 BP, oraz jednej młodszej, ~5 000 BP. Pod koniec plejstocenu/we wczesnym holocenie najprawdopodobniej czarnoziemy typowe rozwinęły się w utworach lessowych (Altermann i in., 2005; Eckmeier i in., 2007; Kabała i in., 2019; Kołodyńska-Gawrysiak i in., 2017; Labaz i in., 2018). Można postawić hipotezę, że były one zachowane do czasu neolitu (Kabała i in.,

2019), w którym zaczęły ulegać degradacji do czarnoziemów z poziomem argik, a następnie do gleb płowych typowych (Labaz i in., 2018). Ostatni etap przemiany gleb jest dostrzegalny na badanym obszarze, gdzie dominującym typem gleb są właśnie gleby płowe, cechujące się zróżnicowaną morfologią w wyniku wielokrotnych zdarzeń erozyjno–akumulacyjnych, zależnych od dynamiki procesów stokowych. W środkowych i dolnych częściach stoków (profil WK4, WK6 i WK7) materiał deluwialny zredeponowany w epoce neolitu, brązu i średniowieczu stanowił podłoże dla rozwoju głębokich poziomów eluwialnych. Natomiast w wyższych partiach stoków, w których procesy erozyjne osiągnęły swoje maksyma, zaobserwowano postępujące spłycenie pokrywy lessowej, co znacznie wpłynęło na modyfikację morfologii gleby. W ten sposób w pierwszej fazie powstały gleby płowe zerodowane (ogłowione) będące bezpośrednim efektem włączania poziomu eluwialnego (E) do poziomu próchnicznego w wyniku orki, natomiast w drugiej fazie poziomy argik traciły swoją horyzontalną ciągłość i zostały włączone do powierzchniowych poziomów próchnicznych (profile WK2, WK10 i WK11). W takich sytuacjach często w poziomach Ap występowały otoczki ilaste pochodzące z agregatów poziomu argik (Bt), woranych podczas zabiegów agrotechnicznych. Dalsze spłycanie pokrywy lessowej spowodowało odsłonięcie starszych osadów zalegających pod lessami, takich jak gliny zwałowe i materiały fluwioglacjalne (żwiry i piaski) cechującymi się bardzo słabymi przekształceniami pedogenicznymi (WK9) co spowodowało, że gleby te zostały sklasyfikowane są jako regosole typowe. Zerodowany materiał deponowany był najczęściej w jego niższych partiach, tworząc gleby deluwialne (WK7 i WK12), a czasami wypełniał rowy melioracyjne.

Tempo erozji krótkoterminowej określonej ilościowo za pomocą analiz $^{239+240}$Pu daje możliwość określenia przypuszczalnego czasu zaniku poziomów Bt w badanych glebach. Degradacja gleb była najbardziej intensywna w profilach WK2, WK8 i WK10, gdzie erozja osiągała bardzo wysokie wartości, prowadząc do wyraźnego spłycenia pokrywy lessowej. Zanik poziomu Bt, a zarazem zmiana klasyfikacji wspomnianych profili glebowych może już zajść odpowiednio za ~200, 130 i 80 lat. Dla pozostałych gleb zanik poziomu Bt szacowany jest na ponad 300 lat. Należy jednak zwrócić uwagę, że obliczenia te opierają się na wartościach erozji wyznaczonych w roku 2019. Postępujące zmiany klimatyczne i dalsza intensyfikacja rolnictwa mogą prowadzić do zintensyfikowania procesów erozyjnych (Calitri i in., 2019; Routschek i in., 2014; Zollinger i in., 2015). W związku z tym zanikanie gleb płowych może zachodzić jeszcze szybciej niż wskazują na to prognozy.

7. Wnioski

1. Tempo erozji długoterminowej w krajobrazie lessowym Wzgórz Trzebnickich wynosi od 0,45 do 0,85 t/ha/rok, a erozji krótkoterminowej jest do dziesięciu razy wyższe i oscyluje między 1,2, a 10,9 t/ha/rok. Jest to przede wszystkim związane z intensyfikacją i mechanizacją rolnictwa oraz zmianami klimatycznymi.

2. Datowania OSL wykazały, że procesy erozji–depozycji osadów na stoku występowały od mezolitu, a następnie miały swoją kontynuację w neolicie, epoce brązu, średniowieczu i okresie nowożytnym, co potwierdza występowanie dynamicznego systemu denudacji w krajobrazie lessowym południowo–zachodniej Polski.

3. Z metodologicznego punktu widzenia ^{10}Be in-situ oraz $^{239+240}$Pu mogą zapewnić szczegółowy wgląd w dynamikę erozji gleb w krajobrazach lessowych.

4. Gleby płowe (Luvisols) występujące na badanym obszarze ulegają intensywnym procesom erozyjno–depozycyjnym, co powoduje ich przekształcenie w gleby słabo ukształtowane -regosole (Regosols) lub gleby deluwialne.

5. Kluczowe dla zrównoważonego gospodarowania zasobami glebowymi obszarów lessowych jest zapobieganie spłycaniu warstwy lessowej i degradacji poziomów ornych.

8. Literatura

Alewell, C., Egli, M., Meusburger, K., 2015. An attempt to estimate tolerable soil erosion rates by matching soil formation with denudation in Alpine grasslands. J. Soils Sediments 15, 1383–1399. https://doi.org/10.1007/s11368-014-0920-6

Alewell, C., Meusburger, K., Brodbeck, M., Bänninger, D., 2008. Methods to describe and predict soil erosion in mountain regions. Landsc. Urban Plan. 88, 46–53. https://doi.org/https://doi.org/10.1016/j.landurbplan.2008.08.007

Alewell, C., Meusburger, K., Juretzko, G., Mabit, L., Ketterer, M.E., 2014. Suitability of 239+240Pu and 137Cs as tracers for soil erosion assessment in mountain grasslands. Chemosphere 103, 274–280. https://doi.org/10.1016/j.chemosphere.2013.12.016

Alewell, C., Pitois, A., Meusburger, K., Ketterer, M., Mabit, L., 2017. 239+240 Pu from "contaminant" to soil erosion tracer: Where do we stand? Earth-Science Rev. 172, 107–123. https://doi.org/10.1016/j.earscirev.2017.07.009

Altermann, M., Rinklebe, J., Merbach, I., Körschens, M., Langer, U., Hofmann, B., 2005. Chernozem - Soil of the Year 2005. J. Plant Nutr. Soil Sci. 168, 725–740. https://doi.org/10.1002/jpln.200521814

Anioł-Kwiatkowska, J., 1998. Endangered and rare segetal species in the microregion Trzebnica Hills. Acta Univ. Lodz. 13, 169–176.

Arata, L., Alewell, C., Frenkel, E., A'Campo-Neuen, A., Iurian, A.R., Ketterer, M.E., Mabit, L., Meusburger, K., 2016. Modelling Deposition and Erosion rates with RadioNuclides (MODERN) - Part 2: A comparison of different models to convert 239+240Pu inventories into soil redistribution rates at unploughed sites. J. Environ. Radioact. 162–163, 97–106. https://doi.org/10.1016/j.jenvrad.2016.05.009

Bac, S., Rojek, M., 2012. Meteorologia i klimatologia w inżynierii środowiska. Wydawnictwo Uniwersytetu Przyrodniczego we Wrocławiu, Wrocław.

Calitri, F., Sommer, M., Norton, K., Temme, A., Brandová, D., Portes, R., Christl, M., Ketterer, M.E., Egli, M., 2019. Tracing the temporal evolution of soil redistribution rates in an agricultural landscape using 239+240 Pu and 10 Be. Earth Surf. Process. Landforms esp.4612. https://doi.org/10.1002/esp.4612

Calitri, F., Sommer, M., van der Meij, M.W., Egli, M., 2020. Soil erosion along a transect in a forested catchment: Recent or ancient processes? CATENA 194, 104683. https://doi.org/10.1016/j.catena.2020.104683

Cerdan, O., Govers, G., Le Bissonnais, Y., Van Oost, K., Poesen, J., Saby, N., Gobin, A., Vacca, A., Quinton, J., Auerswald, K., Klik, A., Kwaad, F.J.P.M., Raclot, D., Ionita, I., Rejman, J., Rousseva, S., Muxart, T., Roxo, M.J., Dostal, T., 2010. Rates and spatial variations of soil erosion in Europe: A study based on erosion plot data. Geomorphology 122, 167–177. https://doi.org/10.1016/j.geomorph.2010.06.011

Dahms, D., Egli, M., Fabel, D., Harbor, J., Brandová, D., de Castro Portes, R., Christl, M., 2018. Revised Quaternary glacial succession and post-LGM recession, southern Wind River Range, Wyoming, USA. Quat. Sci. Rev. 192, 167–184.

https://doi.org/10.1016/j.quascirev.2018.05.020

Döhler, S., Terhorst, B., Frechen, M., Zhang, J., Damm, B., 2018. Chronostratigraphic interpretation of intermediate layer formation cycles based on OSL-dates from intercalated slope wash sediments. Catena 162, 278–290. https://doi.org/10.1016/j.catena.2017.11.003

Dotterweich, M., 2008. The history of soil erosion and fluvial deposits in small catchments of central Europe: Deciphering the long-term interaction between humans and the environment — A review. Geomorphology 101, 192–208. https://doi.org/10.1016/j.geomorph.2008.05.023

Dotterweich, M., Rodzik, J., Zgłobicki, W., Schmitt, A., Schmidtchen, G., Bork, H.-R., 2012. High resolution gully erosion and sedimentation processes, and land use changes since the Bronze Age and future trajectories in the Kazimierz Dolny area (Nałęczów Plateau, SE-Poland). CATENA 95, 50–62. https://doi.org/10.1016/j.catena.2012.03.001

Dreibrodt, S., Bork, H., 2021. Soil Erosion and Sedimentation in Central Europe From the Neolithic to the Industrial Revolution-The German and Polish Records, in: Reference Module in Earth Systems and Environmental Sciences. Elsevier, pp. 1–15. https://doi.org/10.1016/B978-0-12-818234-5.00061-4

Dreibrodt, S., Jarecki, H., Lubos, C., Khamnueva, S. V., Klamm, M., Bork, H.-R., 2013. Holocene soil formation and soil erosion at a slope beneath the Neolithic earthwork Salzmünde (Saxony-Anhalt, Germany). CATENA 107, 1–14. https://doi.org/10.1016/j.catena.2013.03.002

Dreibrodt, S., Lubos, C., Terhorst, B., Damm, B., Bork, H.-R., 2010. Historical soil erosion by water in Germany: Scales and archives, chronology, research perspectives. Quat. Int. 222, 80–95. https://doi.org/10.1016/j.quaint.2009.06.014

Drewnik, M., Żyła, M., 2019. Properties and classification of heavily eroded post-chernozem soils in Proszowice Plateau (southern Poland). Soil Sci. Annu. 70, 225–233. https://doi.org/10.2478/ssa-2019-0020

Dyjor, S., 1970. Seria poznańska w Polsce Zachodniej. Kwart. Geol. 14, 819–834.

Dyjor, S., Kościówko, H., 1982. Formacja trzeciorzędowa południowo-zachodniej Polski i związane z nią perspektywy wybranych surowców. Biul. Inst. Geol. 341.

Eaves, S.R., Collins, J.A., Jones, R.S., Norton, K.P., Tims, S.G., Mackintosh, A.N., 2018. Further constraint of the in situ cosmogenic10Be production rate in pyroxene and a viability test for late Quaternary exposure dating. Quat. Geochronol. 48, 121–132. https://doi.org/10.1016/j.quageo.2018.09.006

Eckmeier, E., Gerlach, R., Gehrt, E., Schmidt, M.W.I., 2007. Pedogenesis of Chernozems in Central Europe — A review. Geoderma 139, 288–299. https://doi.org/10.1016/j.geoderma.2007.01.009

European Parliament, 2021. Resolution on soil protection (2021/2548(RSP)) [WWW Document]. URL https://www.europarl.europa.eu/doceo/document/TA-9-2021-0143_EN.html

Everett, S.E., Tims, S.G., Hancock, G.J., Bartley, R., Fifield, L.K., 2008. Comparison of Pu and 137Cs as tracers of soil and sediment transport in a terrestrial environment. J. Environ. Radioact. 99, 383–393. https://doi.org/https://doi.org/10.1016/j.jenvrad.2007.10.019

Evrard, O., Vandaele, K., van Wesemael, B., Bielders, C.L., 2008. A grassed waterway and earthen dams to control muddy floods from a cultivated catchment of the Belgian loess belt. Geomorphology 100, 419–428. https://doi.org/10.1016/j.geomorph.2008.01.010

FAO, 2019. Soil erosion: the greatest challenge to sustainble soil management. Rome. https://doi.org/10.1080/00050326.1941.10437468

FAO, 2006. Guidlines for soil description, 4th ed. Rome. https://doi.org/10.1007/978-3-030-33443-7_3

Foucher, A., Salvador-Blanes, S., Evrard, O., Simonneau, A., Chapron, E., Courp, T., Cerdan, O., Lefèvre, I., Adriaensen, H., Lecompte, F., Desmet, M., 2014. Increase in soil erosion after agricultural intensification: Evidence from a lowland basin in France. Anthropocene 7, 30–41. https://doi.org/10.1016/j.ancene.2015.02.001

Frechen, M., 2003. Loess in Europe—mass accumulation rates during the Last Glacial Period. Quat. Sci. Rev. 22, 1835–1857. https://doi.org/10.1016/S0277-3791(03)00183-5

Fuchs, M., Fischer, M., Reverman, R., 2010. Colluvial and alluvial sediment archives temporally resolved by OSL dating: Implications for reconstructing soil erosion. Quat. Geochronol. 5, 269–273. https://doi.org/10.1016/j.quageo.2009.01.006

Gerlach, R., Fischer, P., Eckmeier, E., Hilgers, A., 2012. Buried dark soil horizons and archaeological features in the Neolithic settlement region of the Lower Rhine area, NW Germany: Formation, geochemistry and chronostratigraphy. Quat. Int. 265, 191–204. https://doi.org/10.1016/j.quaint.2011.10.007

Gillijns, K., Poesen, J., Deckers, J., 2005. On the characteristics and origin of closed depressions in loess-derived soils in Europe—a case study from central Belgium. CATENA 60, 43–58. https://doi.org/10.1016/j.catena.2004.10.001

Glina, B., Waroszewski, J., Kabal, C., 2014. Water retention of the loess-derived Luvisols with lamellic illuvial horizon in the Trzebnica Hills (SW Poland). Soil Sci. Annu. 65, 18–24. https://doi.org/10.2478/ssa-2014-0003

Gonet, S.S., 2007. Ochrona zasobów materii organicznej gleb, in: Gonet, Sławomir, S., Markiewicz, M. (Eds.), Rola Materii Organicznej w Środowisku. Polskie Towarzystwo Substancji Humusowych, Wrocław, pp. 7–29.

Graly, J.A., Bierman, P.R., Reusser, L.J., Pavich, M.J., 2010. Meteoric 10Be in soil profiles - A global meta-analysis. Geochim. Cosmochim. Acta 74, 6814–6829. https://doi.org/10.1016/j.gca.2010.08.036

Gu, Z.Y., Lal, D., Liu, T.S., Guo, Z.T., Southon, J., Caffee, M.W., 1997. Weathering histories of Chinese loess deposits based on uranium and thorium series nuclides and cosmogenic 10 Be. Geochim. Cosmochim. Acta 61, 5221–5231. https://doi.org/10.1016/S0016-7037(97)00313-X

Guzmán, G., Laguna, A., Cañasveras, J.C., Boulal, H., Barrón, V., Gómez-Macpherson, H., Giráldez, J.V., Gómez, J.A., 2015. Study of sediment movement in an irrigated maize–cotton system combining rainfall simulations, sediment tracers and soil erosion models. J. Hydrol. 524, 227–242. https://doi.org/10.1016/j.jhydrol.2015.02.033

Haase, D., Fink, J., Haase, G., Ruske, R., Pécsi, M., Richter, H., Altermann, M., Jäger, K.D., 2007. Loess in Europe-its spatial distribution based on a European Loess Map, scale 1:2,500,000. Quat. Sci. Rev. 26, 1301–1312. https://doi.org/10.1016/j.quascirev.2007.02.003

Henkner, J., Ahlrichs, J.J., Downey, S., Fuchs, M., James, B.R., Knopf, T., Scholten, T., Teuber, S., Kühn, P., 2017. Archaeopedology and chronostratigraphy of colluvial deposits as a proxy for regional land use history (Baar, southwest Germany). CATENA 155, 93–113. https://doi.org/10.1016/j.catena.2017.03.005

Hidy, A.J., Gosse, J.C., Pederson, J.L., Mattern, J.P., Finkel, R.C., 2010. A geologically constrained Monte Carlo approach to modeling exposure ages from profiles of cosmogenic nuclides: An example from Lees Ferry, Arizona. Geochemistry Geophys. Geosystems 11, Q0AA10. https://doi.org/10.1029/2010GC003084

Hoo, W.T., Fifield, L.K., Tims, S.G., Fujioka, T., Mueller, N., 2011. Using fallout plutonium as a probe for erosion assessment. J. Environ. Radioact. 102, 937–942. https://doi.org/10.1016/j.jenvrad.2010.06.010

IUSS Working Group WRB, 2022. World Reference Base for Soil Resources. International soil classification system for naming soils and creating legends for maps. 4th edition. FAO, Rome, Vienna, Austria.

Jary, Z., 1996. Chronostratygrafia oraz warunki sedymentacji lessów południowo-zachodniej Polski na przykładzie Płaskowyżu Głubczyckiego i Wzgórz Trzebnickich. Studia Geograficzne LXIII Uniwersytetu Wrocławskiego, Wrocław.pdf.

Jary, Z., Ciszek, D., 2013. Late Pleistocene loess-palaeosol sequences in Poland and western Ukraine. Quat. Int. 296, 37–50. https://doi.org/10.1016/j.quaint.2012.07.009

Jelinski, N.A., Campforts, B., Willenbring, J.K., Schumacher, T.E., Li, S., Lobb, D.A., Papiernik, S.K., Yoo, K., 2019. Meteoric Beryllium-10 as a Tracer of Erosion Due to Postsettlement Land Use in West-Central Minnesota, USA. J. Geophys. Res. Earth Surf. 124, 874–901. https://doi.org/10.1029/2018JF004720

Kabała, C., Marzec, M., 2010. Vertical and spatial diversity of grain-size distribution in Luvisols developed from lorss in south-western Poland. Rocz. Glebozn. LXI, 52–64.

Kabała, C., Przybył, A., Krupski, M., Łabaz, B., Waroszewski, J., 2019. Origin, age and transformation of Chernozems in northern Central Europe – New data from Neolithic earthen barrows in SW Poland. Catena 180, 83–102. https://doi.org/10.1016/j.catena.2019.04.014

Kaiser, K., Tolksdorf, J.F., de Boer, A.M., Herbig, C., Hieke, F., Kasprzak, M., Kočár, P., Petr, L., Schubert, M., Schröder, F., Fülling, A., Hemker, C., 2021. Colluvial sediments originating from past land-use activities in the Erzgebirge Mountains, Central Europe: occurrence, properties, and historic environmental implications. Archaeol. Anthropol. Sci. 13, 220. https://doi.org/10.1007/s12520-021-01469-z

Karasiewicz, M.T., Hulisz, P., Świtoniak, M., 2014. Wpływ procesów denudacji na właściwości osadów wypełniających zagłębienia między krętymi wałami z erozji wód subglacjalnych w okolicy Zbójna (Pojezierze Dobrzyńskie). Landf. Anal. 25, 29–42. https://doi.org/10.12657/landfana.025.004

Karczewska, A., 2012. Ochrona gleb i rekultywacja terenów zdegradowanych, II. ed. Wydawnictwo Uniwersytetu Przyrodniczego we Wrocławiu, Wrocław.

Kaszubkiewicz., J., Tasz, W., Kawałko, D., Serafin, R., 2011. USLE model simplification proposal for application in a small agricultural catchment area. Rocz. Glebozn. LXII, 75–81.

Kaszubkiewicz, J., Tasz, W., Andrzejczak, M., 2008. Zawartość makroelementów w materiale zmywanym i w erodowanych glebach Kotliny Kłodzkiej. Rocz. Glebozn. LIX, 108–114.

Ketterer, M.E., Hafer, K.M., Link, C.L., Kolwaite, D., Wilson, J., Mietelski, J.W., 2004a. Resolving global versus local/regional Pu sources in the environment using sector ICP-MS. J. Anal. At. Spectrom. 19, 241–245. https://doi.org/10.1039/B302903D

Ketterer, M.E., Hafer, K.M., Mietelski, J.W., 2004b. Resolving Chernobyl vs. global fallout contributions in soils from Poland using Plutonium atom ratios measured by inductively coupled plasma mass spectrometry. J. Environ. Radioact. 73, 183–201. https://doi.org/10.1016/j.jenvrad.2003.09.001

Klimowicz, Z., Uziak, S., 2001. The influence of long-term cultivation on soil properties and patterns in an undulating terrain in Poland. Catena 43, 177–189. https://doi.org/10.1016/S0341-8162(00)00162-4

Kołodyńska-Gawrysiak, R., Chodorowski, J., Mroczek, P., Plak, A., Zgłobicki, W., Kiebała, A., Trzciński, J., Standzikowski, K., 2017. The impact of natural and anthropogenic processes on the evolution of closed depressions in loess areas. A multi-proxy case study from Nałęczów Plateau, Eastern Poland. CATENA 149, 1–18. https://doi.org/10.1016/j.catena.2016.07.029

Kołodyńska-Gawrysiak, R., Poesen, J., Gawrysiak, L., 2018. Assessment of long-term Holocene soil erosion rates in Polish loess areas using sedimentary archives from closed depressions. Earth Surf. Process. Landforms 43, 978–1000. https://doi.org/10.1002/esp.4296

Konz, N., Prasuhn, V., Alewell, C., 2012. On the measurement of alpine soil erosion. CATENA 91, 63–71. https://doi.org/https://doi.org/10.1016/j.catena.2011.09.010

Kopittke, P.M., Menzies, N.W., Wang, P., McKenna, B.A., Lombi, E., 2019. Soil and the intensification of agriculture for global food security. Environ. Int. 132, 105078. https://doi.org/10.1016/j.envint.2019.105078

Krzyszkowski, D., 1993. Pleistocene stratigraphy near Trzebnica, Silesian Rampart, Southwestern Poland. Bull. Polish Acad. Sci. Earth Sci. 40.

Labaz, B., Musztyfaga, E., Waroszewski, J., Bogacz, A., Jezierski, P., Kabala, C., 2018. Landscape-related transformation and differentiation of Chernozems – Catenary approach in the Silesian Lowland, SW Poland. Catena 161, 63–76. https://doi.org/10.1016/j.catena.2017.10.003

Lal, R., Fifield, L.K., Tims, S.G., Wasson, R.J., Howe, D., 2020. A study of soil erosion rates using 239Pu, in the wet-dry tropics of Northern Australia. J. Environ. Radioact. 211, 106085. https://doi.org/10.1016/j.jenvrad.2019.106085

Lehmkuhl, F., Nett, J.J., Pötter, S., Schulte, P., Sprafke, T., Jary, Z., Antoine, P., Wacha, L., Wolf, D., Zerboni, A., Hošek, J., Marković, S.B., Obreht, I., Sümegi, P., Veres, D., Zeeden, C., Boemke, B., Schaubert, V., Viehweger, J., Hambach, U., 2021. Loess landscapes of Europe – Mapping, geomorphology, and zonal differentiation. Earth-Science Rev. 215, 103496. https://doi.org/10.1016/j.earscirev.2020.103496

Licznar, M., Kowaliński, S., Drozd, J., 1981. Changes of some physical properties of soils of the głubczyce plateau under the water erosion effect. Rocz. Glebozn. XXXII, 45–52.

Licznar, M., Licznar, P., 2002. Erodibility of Trzebnica Hills loessive soils. Zesz. Probl. postępów Nauk Rol. 487, 129–136.

Licznar, P., Sasik, J., Żmuda, R., 2002. Prognozowanie erozji wodnej w małych zlewniach rolniczych Wzgórz Trzebnickich. Zesz. Probl. postępów Nauk Rol. 487, 137–146.

Licznar, S., Kowaliński, S., Licznar, M.., 1988. Zastosowanie metod mikromorfologicznych i submikromorfologicznych w badaniu gleb erodowanych. Rocz. Glebozn. 39, 21–34.

Loba, A., Sykuła, M., Kierczak, J., Łabaz, B., Bogacz, A., Waroszewski, J., 2020. In situ weathering of rocks or aeolian silt deposition: key parameters for verifying parent material and pedogenesis in the Opawskie Mountains—a case study from SW Poland. J. Soils Sediments 20, 435–451. https://doi.org/10.1007/s11368-019-02377-5

Loba, A., Waroszewski, J., Sykuła, M., Kabala, C., Egli, M., 2022. Meteoric 10Be, 137Cs and 239+240Pu as Tracers of Long- and Medium-Term Soil Erosion—A Review. Minerals 12, 359. https://doi.org/10.3390/min12030359

Loba, A., Waroszewski, J., Tikhomirov, D., Calitri, F., Christl, M., Sykuła, M., Egli, M., 2021. Tracing erosion rates in loess landscape of the Trzebnica Hills (Poland) over time using fallout and cosmogenic nuclides. J. Soils Sediments 21, 2952–2968. https://doi.org/10.1007/s11368-021-02996-x

Loba, A., Zhang, J., Tsukamoto, S., Kasprzak, M., Beata Kowalska, J., Frechen, M., Waroszewski, J., 2023. Multiproxy approach to the reconstruction of soil denudation events and the disappearance of Luvisols in the loess landscape of south-western Poland. CATENA 220, 106724. https://doi.org/10.1016/j.catena.2022.106724

Malik, I., Poręba, G., Wistuba, M., Woskowicz-Ślęzak, B., 2021. Combining 137Cs, 210Pb and dendrochronology for improved reconstruction of erosion–sedimentation events in a loess gully system (southern Poland). L. Degrad. Dev. 32, 2336–2350. https://doi.org/10.1002/ldr.3903

McLennan, S.M., 2001. Relationships between the trace element composition of sedimentary rocks and upper continental crust. Geochemistry, Geophys. Geosystems 2, n/a-n/a. https://doi.org/10.1029/2000GC000109

Meij, W.M., Reimann, T., Vornehm, V.K., Temme, A.J.A.M., Wallinga, J., Beek, R., Sommer, M., 2019. Reconstructing rates and patterns of colluvial soil redistribution in agrarian (hummocky) landscapes. Earth Surf. Process. Landforms 44, 2408–2422. https://doi.org/10.1002/esp.4671

Meusburger, K., Evrard, O., Alewell, C., Borrelli, P., Cinelli, G., Ketterer, M., Mabit, L., Panagos, P., van Oost, K., Ballabio, C., 2020. Plutonium aided reconstruction of caesium atmospheric fallout in European topsoils. Sci. Rep. 10, 11858. https://doi.org/10.1038/s41598-020-68736-2

Meusburger, K., Mabit, L., Ketterer, M., Park, J.H., Sandor, T., Porto, P., Alewell, C., 2016. A multi-radionuclide approach to evaluate the suitability of 239 + 240Pu as soil erosion tracer. Sci. Total Environ. 566–567, 1489–1499. https://doi.org/10.1016/j.scitotenv.2016.06.035

Mietelski, J.W., Was, B., 1995. Plutonium from Chernobyl in Poland. Appl. Radiat. Isot. 46, 1203–1211. https://doi.org/https://doi.org/10.1016/0969-8043(95)00162-7

Morgan, R.P.., 2005. Soil erosion and conservation. Blackwell Science Ltd.

Moska, P., Jary, Z., Adamiec, G., Bluszcz, A., 2019. Chronostratigraphy of a loess-palaeosol sequence in Biały Kościół, Poland using OSL and radiocarbon dating. Quat. Int. 502, 4–17. https://doi.org/10.1016/j.quaint.2018.05.024

Murray, A.S., Thomsen, K.J., Masuda, N., Buylaert, J.P., Jain, M., 2012. Identifying well-bleached quartz using the different bleaching rates of quartz and feldspar luminescence signals. Radiat. Meas. 47, 688–695. https://doi.org/10.1016/j.radmeas.2012.05.006

Muhs, D.R., 2013. The geologic records of dust in the quaternary. Aeolian Res. 9, 3–48. https://doi.org/10.1016/j.aeolia.2012.08.001

Musso, A., Ketterer, M.E., Greinwald, K., Geitner, C., Egli, M., 2020. Rapid decrease of soil erosion rates with soil formation and vegetation development in periglacial areas. Earth Surf. Process. Landforms 45, 2824–2839. https://doi.org/10.1002/esp.4932

Ouyang, W., Wu, Y., Hao, Z., Zhang, Q., Bu, Q., Gao, X., 2018. Combined impacts of land use and soil property changes on soil erosion in a mollisol area under long-term agricultural development. Sci. Total Environ. 613–614, 798–809. https://doi.org/10.1016/j.scitotenv.2017.09.173

Pachucki, C., 1952. Badania geologiczne na arkuszach 1:100 000 Trzebnica i Syców. Biul. Inst. Gelogicznego 66, 355–394.

Poręba, G., Śnieszko, Z., Moska, P., 2011. Some aspects of age assessment of Holocene loess colluvium: OSL and 137Cs dating of sediment from Biała agricultural area, South Poland. Quat. Int. 240, 44–51. https://doi.org/10.1016/j.quaint.2011.02.005

Poręba, G., Śnieszko, Z., Moska, P., Mroczek, P., Malik, I., 2019. Interpretation of soil erosion in a Polish loess area using OSL, 137Cs, 210Pbex, dendrochronology and micromorphology – case study: Biedrzykowice site (s Poland). Geochronometria 46, 57–78. https://doi.org/10.1515/geochr-2015-0109

Poręba, G.J., Śnieszko, Z., Moska, P., 2015. Application of OSL dating and 137Cs

measurements to reconstruct the history of water erosion: A case study of a Holocene colluvium in Świerklany, south Poland. Quat. Int. 374, 189–197. https://doi.org/10.1016/j.quaint.2015.04.004

Pye, K., 1995. The nature, origin and accumulation of loess. Quat. Sci. Rev. 14, 653–667. https://doi.org/10.1016/0277-3791(95)00047-X

Raab, G., Martin, A.P., Norton, K.P., Christl, M., Scarciglia, F., Egli, M., 2021. Complex patterns of schist tor exposure and surface uplift, Otago (New Zealand). Geomorphology 389, 107849. https://doi.org/10.1016/j.geomorph.2021.107849

Raab, G., Scarciglia, F., Norton, K., Dahms, D., Brandová, D., Castro Portes, R., Christl, M., Ketterer, M.E., Ruppli, A., Egli, M., 2018. Denudation variability of the Sila Massif upland (Italy) from decades to millennia using 10Be and 239+240Pu. L. Degrad. Dev. 29, 3736–3752. https://doi.org/10.1002/ldr.3120

Rahimzadeh, N., Khormali, F., Gribenski, N., Tsukamoto, S., Kehl, M., Pint, A., Kiani, F., Frechen, M., 2019. Timing and development of sand dunes in the Golestan Province, northern Iran—Implications for the Late-Pleistocene history of the Caspian Sea. Aeolian Res. 41, 100538. https://doi.org/10.1016/j.aeolia.2019.07.004

Rejman, J., Brodowski, R., Iglik, I., 2008. Annual variations of soil erodibility of silt loam developed from loess based on 10-years runoff plot studies. Ann. Warsaw Univ. Life Sci. - SGGW. L. Reclam. 39, 77–83. https://doi.org/10.2478/v10060-008-0007-4

Rejman, J., Iglik, I., 2010. Topsoil reduction and cereal yields on loess soils of southeast Poland. L. Degrad. Dev. 21, 401–405. https://doi.org/10.1002/ldr.963

Rejman, J., Iglik, I., Paluszek, J., Rodzik, J., 2014a. Soil redistribution and crop productivity in loess areas (Lublin Upland, Poland). Soil Tillage Res. 143, 77–84. https://doi.org/10.1016/j.still.2014.05.011

Rejman, J., Rafalska-Przysucha, A., Rodzik, J., 2014b. The Effect of Land Use Change on Transformation of Relief and Modification of Soils in Undulating Loess Area of East Poland. Sci. World J. 2014, 1–11. https://doi.org/10.1155/2014/341804

Rejman, J., Usowicz, B., 2002. Evaluation of soil-loss contribution areas on loess soils in Southeast Poland. Earth Surf. Process. Landforms 27, 1415–1423. https://doi.org/10.1002/esp.438

Rickson, R.J., 2014. Can control of soil erosion mitigate water pollution by sediments? Sci. Total Environ. 468–469, 1187–1197. https://doi.org/10.1016/j.scitotenv.2013.05.057

Routschek, A., Schmidt, J., Kreienkamp, F., 2014. Impact of climate change on soil erosion - A high-resolution projection on catchment scale until 2100 in Saxony/Germany. Catena 121, 99–109. https://doi.org/10.1016/j.catena.2014.04.019

Scherer, S., Deckers, K., Dietel, J., Fuchs, M., Henkner, J., Höpfer, B., Junge, A., Kandeler, E., Lehndorff, E., Leinweber, P., Lomax, J., Miera, J., Poll, C., Toffolo, M.B., Knopf, T., Scholten, T., Kühn, P., 2021. What's in a colluvial deposit? Perspectives from archaeopedology. Catena 198. https://doi.org/10.1016/j.catena.2020.105040

SGP, 2019. Systematyka Gleb Polski, wyd. 6. Wydawnictwo Uniwersytetu Przyrodniczego we Wrocławiu, Instytut Nauk o Glebie i Ochrony Środowiska

Uniwersytetu Przyrodniczego we Wrocławiu, Polskie Towarzystwo Gleboznawcze, Komisja Genezy, Klasyfikacji i Kartografii Gleb.

Shen Chengde, Beer, J., Liu Tungsheng, Oeschger, H., Bonani, G., Suter, M., Wölfli, W., 1992. 10Be in Chinese loess. Earth Planet. Sci. Lett. 109, 169–177. https://doi.org/10.1016/0012-821X(92)90081-6

Šimanský, V., Juriga, M., Jonczak, J., Uzarowicz, Ł., Stępień, W., 2019. How relationships between soil organic matter parameters and soil structure characteristics are affected by the long-term fertilization of a sandy soil. Geoderma 342, 75–84. https://doi.org/10.1016/j.geoderma.2019.02.020

Smetanová, A., Verstraeten, G., Notebaert, B., Dotterweich, M., Létal, A., 2017. Landform transformation and long-term sediment budget for a Chernozem-dominated lowland agricultural catchment. CATENA 157, 24–34. https://doi.org/10.1016/j.catena.2017.05.007

Starkel, L., 2005. Role of climatic and anthropogenic factors accelerating soil erosion and fluvial activity in Central Europe. Stud. Quat. 22, 27–33.

Święchowicz, J., 2016. Podatność na erozję wodną gleb wytworzonych z pyłowych utworów lessopodobnych (Przedgórze Brzeskie, Polska Południowa), in: Święchowicz, Jolanta;, Michno, A. (Eds.), Wybrane Zagadnienia Geomorfologii Eolicznej. Monografia Dedykowana Dr Hab. Bogdanie Izmaiłow w 44. Rocznicę Pracy Naukowej. Instytut Geografii i Gospodarki Przestrzennej Uniwersytetu Jagiellońskiego, Kraków, pp. 332–366.

Świtoniak, M., 2014. Use of soil profile truncation to estimate influence of accelerated erosion on soil cover transformation in young morainic landscapes, North-Eastern Poland. CATENA 116, 173–184. https://doi.org/10.1016/j.catena.2013.12.015

Świtoniak, M., Mroczek, P., Bednarek, R., 2016. Luvisols or Cambisols? Micromorphological study of soil truncation in young morainic landscapes - Case study: Brodnica and Chełmno Lake Districts (North Poland). Catena 137, 583–595. https://doi.org/10.1016/j.catena.2014.09.005

Turski, M., Witkowska-Walczak, B., 2004. Fizyczne właściwości gleb płowych wytworzonych z utworów pyłowych różnej genezy (in Polish). Acta Agrophysica 101.

Van Oost, K., Govers, G., Van Muysen, W., 2003. A process-based conversion model for caesium-137 derived erosion rates on agricultural land: an integrated spatial approach. Earth Surf. Process. Landforms 28, 187–207. https://doi.org/10.1002/esp.446

Van Rompaey, A.J.J., Verstraeten, G., Van Oost, K., Govers, G., Poesen, J., 2001. Modelling mean annual sediment yield using a distributed approach. Earth Surf. Process. Landforms 26, 1221–1236. https://doi.org/10.1002/esp.275

Verheijen, F.G.A., Jones, R.J.A., Rickson, R.J., Smith, C.J., 2009. Tolerable versus actual soil erosion rates in Europe. Earth-Science Rev. 94, 23–38. https://doi.org/10.1016/j.earscirev.2009.02.003

Verstraeten, G., Poesen, J., 2001. Factors controlling sediment yield from small

intensively cultivated catchments in a temperate humid climate. Geomorphology 40, 123–144. https://doi.org/10.1016/S0169-555X(01)00040-X

Vitharana, U.W.A., Van Meirvenne, M., Simpson, D., Cockx, L., De Baerdemaeker, J., 2008. Key soil and topographic properties to delineate potential management classes for precision agriculture in the European loess area. Geoderma 143, 206–215. https://doi.org/10.1016/j.geoderma.2007.11.003

von Blanckenburg, F., Belshaw, N.S., O'Nions, R.K., 1996. Separation of 9Be and cosmogenic 10Be from environmental materials and SIMS isotope dilution analysis. Chem. Geol. 129, 93–99. https://doi.org/https://doi.org/10.1016/0009-2541(95)00157-3

Waroszewski, J., Egli, M., Brandová, D., Christl, M., Kabala, C., Malkiewicz, M., Kierczak, J., Glina, B., Jezierski, P., 2018a. Identifying slope processes over time and their imprint in soils of medium-high mountains of Central Europe (the Karkonosze Mountains, Poland). Earth Surf. Process. Landforms 43, 1195–1212. https://doi.org/10.1002/esp.4305

Waroszewski, J., Pietranik, A., Sprafke, T., Kabała, C., Frechen, M., Jary, Z., Kot, A., Tsukamoto, S., Meyer-Heintze, S., Krawczyk, M., Łabaz, B., Schultz, B., Erban Kochergina, Y. V., 2021. Provenance and paleoenvironmental context of the Late Pleistocene thin aeolian silt mantles in south-west Poland – a widespread parent material for soils. Catena 204. https://doi.org/10.1016/j.catena.2021.105377

Waroszewski, J., Sprafke, T., Kabala, C., Musztyfaga, E., Łabaz, B., Woźniczka, P., 2018b. Aeolian silt contribution to soils on mountain slopes (Mt. Ślęza, southwest Poland). Quat. Res. (United States) 89, 702–717. https://doi.org/10.1017/qua.2017.76

Willenbring, J.K., von Blanckenburg, F., 2010. Meteoric cosmogenic Beryllium-10 adsorbed to river sediment and soil: Applications for Earth-surface dynamics. Earth-Science Rev. 98, 105–122. https://doi.org/10.1016/j.earscirev.2009.10.008

Wischmeier, W., Smith, D., 1978. Predicting rainfall erosiom losses - a guide to conservation planning.

Wyshnytzky, C.E., Ouimet, W.B., McCarthy, J., Dethier, D.P., Shroba, R.R., Bierman, P.R., Rood, D.H., 2015. Meteoric 10Be, clay, and extractable iron depth profiles in the Colorado Front Range: Implications for understanding soil mixing and erosion. CATENA 127, 32–45. https://doi.org/10.1016/j.catena.2014.12.008

Xu, Y., Qiao, J., Pan, S., Hou, X., Roos, P., Cao, L., 2015. Plutonium as a tracer for soil erosion assessment in northeast China. Sci. Total Environ. 511, 176–185. https://doi.org/10.1016/j.scitotenv.2014.12.006

Zádorová, T., Penížek, V., 2018. Formation, morphology and classification of colluvial soils: a review. Eur. J. Soil Sci. 69, 577–591. https://doi.org/10.1111/ejss.12673

Zádorová, T., Penížek, V., Šefrna, L., Rohošková, M., Borůvka, L., 2011. Spatial delineation of organic carbon-rich Colluvial soils in Chernozem regions by Terrain analysis and fuzzy classification. Catena 85, 22–33. https://doi.org/10.1016/j.catena.2010.11.006

Zhang, K., Pan, S., Liu, Z., Li, G., Xu, Y., Hao, Y., 2018. Vertical distributions and source

identification of the radionuclides 239Pu and 240Pu in the sediments of the Liao River estuary, China. J. Environ. Radioact. 181, 78–84. https://doi.org/10.1016/j.jenvrad.2017.10.016

Zhou, W., Xie, X., Beck, W., Kong, X., Xian, F., Du, Y., Wu, Z., 2015. Recent progress of 10Be tracer studies in Chinese loess. Nucl. Instruments Methods Phys. Res. Sect. B Beam Interact. with Mater. Atoms 361, 548–553. https://doi.org/10.1016/j.nimb.2015.02.061

Zmuda, R., Szewrański, S., Kowalczyk, T., Szarawarski, Łu., Kuriata, M., 2009. Landscape alteration in view of soil protection from water erosion - An example of the Mielnica watershed. J. Water L. Dev. 13, 161–175. https://doi.org/10.2478/v10025-010-0026-5

Zollinger, B., Alewell, C., Kneisel, C., Meusburger, K., Brandová, D., Kubik, P., Schaller, M., Ketterer, M., Egli, M., 2015. The effect of permafrost on time-split soil erosion using radionuclides (137Cs, 239 + 240Pu, meteoric 10Be) and stable isotopes (δ13C) in the eastern Swiss Alps. J. Soils Sediments 15, 1400–1419. https://doi.org/10.1007/s11368-014-0881-9

Załączniki

Aleksandra Loba, Jarosław Waroszewski, Marcin Sykuła, Cezary Kabała, Markus Egli, 2022. Meteoric 10Be, 137Cs and 239+240Pu as tracers of long- and medium-term soil erosion — A review. Minerals, 12, 359.
doi:10.3390/min12030359

Aleksandra Loba, Jarosław Waroszewski, Dmitry Tikhomirov, Francesca Calitri, Marcus Christl, Marcin Sykuła, Markus Egli, 2021. Tracing erosion rates in loess landscape of the Trzebnica Hills (Poland) over time using fallout and cosmogenic nuclides. Journal of Soils and Sediments 21, 2952 – 2968.
doi:10.1007/s11368-021-02996-x.

Aleksandra Loba, Junjie Zhang, Sumiko Tsukamoto, Marek Kasprzak, Joanna Beata Kowalska, Manfred Frechen, Jarosław Waroszewski, 2023. Multiproxy approach to the reconstruction of soil denudation events and the disappearance of Luvisols in the loess landscape of south-western Poland. CATENA 220, 106724.
doi:10.1016/ j.catena.2022.106724.

Aktywność naukowa

Staże naukowe i warsztaty:

- Staż naukowy na Uniwersytecie w Seulu, Korea Południowa, od 15 czerwca 2022 r. do 28 czerwca 2022 r.

- Staż naukowy w Leibniz Institute for Applied Geophysics (LIAG) w Hanowerze, Niemcy, od 19 lipca 2021 r. do 31 lipca 2021 r. oraz od 15 lipca 2020 r. do 12 sierpnia 2020 r.

- Staż naukowy na Uniwersytecie w Zurychu, Szwajcaria, od 17 lutego 2020 r. do 13 marca 2020 r. i od 23 września 2019 r. do 18 października 2019 r. oraz od 2 marca 2019 r. do 31 marca 2019 r.

- International Geochronology Summer School „Dating techniques in Environmental Research", Klosters Dorf, Szwajcaria, od 2 do 8 września 2018 r.

- International Course „Soils as an archive of natural and cultural change", Wurzburg, Niemcy, od 4 do 8 lipca 2018 r.

- Warsztaty glebowe w ramach The Freely Accessible Central European Soil (FACES), Kowno, Litwa, od 25 czerwca 2017 r. do 1 lipca 2017 r.

- IV edycja Akademii Menedżera Zrównoważonego Rozwoju organizowana przez Generalną Dyrekcję Ochrony Środowiska, Warszawa, Polska, od 18 lipca 2016 r. do 22 lipca 2016 r.

Publikacje:

- <u>Aleksandra Loba</u>, Junjie Zhang, Sumiko Tsukamoto, Marek Kasprzak, Joanna B. Kowalska, Manfred Frechen, Jarosław Waroszewski, 2023. Multiproxy approach to the reconstruction of soil denudation events and the disappearance of Luvisols in the loess landscape of south–western Poland, CATENA 220, 106724.

- <u>Aleksandra Loba</u>, Jarosław Waroszewski, Marcin Sykuła, Cezary Kabała, Markus Egli, 2022. Meteoric 10Be, 137Cs and 239+240Pu as tracers of long– and medium–term soil erosion – a review, Minerals 12, 359.

- <u>Aleksandra Loba,</u> Jarosław Waroszewski, Dmitry Tikhomirov, Francesca Calitri, Marcus Christl, Marcin Sykuła, Markus Egli, 2021. Tracing erosion rates in loess landscape of the Trzebnica Hills (Poland) over time using fallout and cosmogenic radionuclides. Journal of Soils and Sediments 21, 2952–2968.

- <u>Aleksandra Loba</u>, Marcin Sykuła, Jakub Kierczak, Beata Łabaz, Adam Bogacz, Jarosław Waroszewski, 2020. In-situ weathering of rocks or aeolian silt deposition: key parameters for verifying parent material and pedogenesis in the Opawskie Mountains – a case study from SW Poland, Journal of Soils and Sediments 20, 435-451.
- Jarosław Waroszewski, Tobias Sprafke, Cezary Kabała, Mirosław Kobierski, Jakub Kierczak, Elżbieta Musztyfaga, <u>Aleksandra Loba</u>, Ryszard Mazurek, Beata Łabaz, 2019. Tracking Textural, mineralogical and geochemical signatures in soils developed from basalt-derived materials covered with loess sediments (SW Poland), Geoderma 337, 983-997.

Udział w konferencjach

1. <u>Loba A.,</u> Waroszewski J., Egli M., Tikhomirov D., Calitri F. Short-term soil erosion rates in loess landscape of Trzebnica Hills reflected in $^{239+240}$Pu analysis. 4th International Conference of Young Scientists – Soil In The Environment. 29.05 – 01.06. 2022, Toruń, poster.
2. <u>Loba A.,</u> Waroszewski J., Egli M., Tikhomirov D., Calitri F. In-situ ^{10}Be i $^{239+240}$Pu jako znaczniki erozji gleb w krajobrazie lessowym Wzgórz Trzebnickich. Międzynarodowy Tydzień Geomorfologii, sesja geomorfologii glacjalnej organizowanej przez Stowarzyszenie Geomorfologów Polski i UMK w Toruniu. 1.03.2022, prezentacja.
3. <u>Loba A.,</u> Waroszewski J., Egli M., Tikhomirov D., Calitri F. $^{239+240}$Pu jako znacznik krótkoterminowej erozji osadów lessowych – wyniki badań ze Wzgórz Trzebnickich, SW Polska. Zjazd Geomorfologów Polskich, Gdańsk, 7 – 9.10.2021, poster.
4. <u>Loba A.,</u> Waroszewski J., Egli M., Tikhomirov D. Erozja gleby w krajobrazie lessowym w ujęciu badań izotopowych (in-situ ^{10}Be) – wstępne wyniki z Wzgórz Trzebnickich, SW Polska. 30 Kongres Polskiego Towarzystwa Gleboznawczego „Gleba źródłem życia", Lublin, 2 – 9.09.2019, poster.
5. <u>Loba A.,</u> Kabała C. Changes of soil quality in the vicinity of the Europe's largest copper ore tailings impoundment. International Conference CONTAMINATED SITES, Bańska Bystrzyca, 8 10.10.2018, poster.
6. <u>Loba A.,</u> Waroszewski J. Evidence of aeolian silt influence on soils in the Opawskie Mountains (SW Poland). 3rd International Conference of Young Scientists – Soil In the Environment, 16 19.09.2018, prezentacja.

7. <u>Loba A.,</u> Waroszewski J.Erosion rates and soil layering reflected in radionuclides analysis (^{137}Cs, ^{10}Be, $^{239+240}$Pu). 7th International Conference for Young Researchers, Kraków, 16 – 17.04.2018, poster.

8. <u>Loba A.,</u> Waroszewski J., Egli M. Meteoric ^{10}Be in soils – different approach for understanding erosion and layering. XXIV Session of the Petrology Group organized of the Mineralogical Society of Poland jointly with the Commission of Soil Mineralogy and micromorphology of the Soil Science Society of Poland, Pawłowice, 19 – 22.10.2017, poster.

9. <u>Loba A.</u> Właściwości poziomów placic występujących w glebach Parku Narodowego Gór Stołowych. VII Kopernikańskie Sympozjum Studentów Nauk Przyrodniczych, Toruń, 1 – 2.04.2017, poster.

10. <u>Loba A.,</u> Waroszewski J. Concept of loess – influenced soils in the Lower Silesia. 2nd International Conference of Young Scientists – Soil In The Environment, Ślesin, 11 – 14.09.2016, prezentacja.

11. <u>Loba A.,</u> Waroszewski J. Charakterystyka poziomów placic i ich rola w procesach pedogenicznych (Góry Stołowe). XLV Międzynarodowe Seminarium Kół Naukowych na Uniwersytecie Warmińsko – Mazurskim, Olsztyn, 25 – 26.04.2016, prezentacja.

12. <u>Loba A.,</u> Zagórski M., Łabuńska D. Torfowiska jako archiwa przemian szaty roślinnej i wpływu człowieka na środowisko – na przykładzie obiektu Białych Skał (Góry Stołowe, Polska). XX Międzynarodowa Konferencja Studenckich Kół Naukowych i XXXII Sejmik SKN, Wrocław, 14 – 15.05.2015, prezentacja.

13. <u>Loba A.,</u> Cuske M., Musztyfaga E. Wpływ aplikacji ekstraktu kompostu z odpadów zielonych na rozpuszczalność metali ciężkich w glebach zanieczyszczonych. IV Ogólnopolska Konferencja Młodych Naukowców w Poznaniu, „Nauka dla środowiska przyrodniczego", Poznań, 23 – 25.04. 2015, poster.

14. <u>Loba A.,</u> Musztyfaga E., Waroszewski J. Properties of soils developed from cretaceous sandstones in the Stołowe Mountains National Park. 9th International Conference of Young Naturalists – From Biotechnology to Environmental Protection – The Interdisciplinary Meeting of Young Naturalists. Zielona Góra, 6 – 8.11.2014.

Pozostała aktywność:

Organizacja:

- 4th International Conference of Young Scientists – Soil In The Environment, Toruń, 29.05 – 1.06.2022.

- Konferencja naukowa „Polskie gleboznawstwo na forum międzynarodowym" połączona z Jubileuszem 70-lecia Prof. dr. hab. J. Webera, Wrocław, 21 –23.10.2018.

- Konferencja naukowa „Przyrodnicze, Techniczne I Gospodarcze Aspekty Rozwoju Odrzańskiej Drogi Wodnej", Wrocław, 14 czerwca 2018.

Projekty:

- Kierownik i wykonawca zadania przeprowadzenia analiz izotopowych w grancie NCN OPUS 15 nr 2018/29/B/ST10/01282 pt. „Erosion rates and soil formation in loess landscape based on isotopic procedures (^{10}Be, $^{239+240}$Pu) and OSL datings, Trzebnickie Hills (SW, Poland)", Kierownik projektu: dr inż. Jarosław Waroszewski.

Stypendia:

- Stypendium projakościowe na rok akademicki 2021/2022.

- Stypendium w ramach projektu OPUS15 nr UMO-2018/29/B/ST10/01282. Stypendium przyznano na okres 18 miesięcy.

- Stypendium projakościowe na rok akademicki 2019/2020.

- Stypendium Prezesa Rady Ministrów na rok szkolny 2011/2012.

- Stypendium Starosty Wałbrzyskiego za osiągnięcia w nauce w latach: 2009/2010, 2010/2011, 2011/2012.

Wolontariat:

- Warsztaty dla dzieci z okazji dnia gleby, Wrocław, 4.12. 2018.
- Warsztaty edukacyjne Wydziału Przyrodniczo – Technologicznego, Wrocław, 13.04.2018.
- Wielki Test Wiedzy Geograficznej, Toruń, 9.04.2022.

Inne:

- Członek Polskiego Towarzystwa Geograficznego od 2021.

- Członek Międzynarodowej Unii Towarzystw Gleboznawczych od 2019.

- Członek Polskiego Towarzystwa Gleboznawczego od 2019.

- Przewodnicząca Koła Naukowego Gleboznawstwa i Ochrony Środowiska w latach 2015 –2017.

Meteoric ^{10}Be, ^{137}Cs and $^{239+240}$Pu as Tracers of Long- and Medium-Term Soil Erosion—A Review

Aleksandra Loba [1,2,*], Jarosław Waroszewski [1], Marcin Sykuła [2], Cezary Kabala [1] and Markus Egli [3]

1   Institute of Soil Science, Plant Nutrition and Environmental Protection, Wroclaw University of Environmental and Life Sciences, Grunwaldzka 53, 50-357 Wroclaw, Poland; jaroslaw.waroszewski@upwr.edu.pl (J.W.); cezary.kabala@upwr.edu.pl (C.K.)
2   Faculty of Earth Sciences and Spatial Management, Nicolaus Copernicus University in Toruń, Lwowska 1, 87-100 Toruń, Poland; sykula@umk.pl
3   Department of Geography, University of Zurich, CH-8057 Zurich, Switzerland; markus.egli@geo.uzh.ch
*   Correspondence: aleloba@umk.pl

Abstract: Isotopes of meteoric ^{10}Be, ^{137}Cs, $^{239+240}$Pu have been proposed as a soil redistribution tracer and applied worldwide as an alternative method to classical field-related techniques (e.g., sediment traps). Meteoric ^{10}Be provides information about long-term soil redistribution rates (millennia), while ^{137}Cs and $^{239+240}$Pu give medium-term rates (decades). A significant progress in developing new models and approaches for the calculation of erosion rates has been made; thus, we provide a global review (n = 59) of research articles to present these three isotopes (meteoric ^{10}Be, $^{239+240}$Pu and ^{137}Cs) as soil erosion markers in different environments and under different land-use types. Understanding the dynamics and behaviours of isotopes in the soil environment is crucial to determine their usefulness as soil erosion tracers; thus, we discuss the chemical–physical behaviour of meteoric ^{10}Be, ^{137}Cs and $^{239+240}$Pu in soils. The application of these isotopes sometimes has strong limitations, and we give suggestions on how to overcome them or how to adapt them to a given situation. This review also shows where these isotopic methods can potentially be applied in the future. A lack in knowledge about soil redistribution rates exists particularly in loess-dominated areas where the tillage system has changed or in areas with strong wind erosion.

Keywords: isotopes; $^{239+240}$Pu; ^{137}Cs; meteoric ^{10}Be; RUSLE; soil erosion

1. Introduction

The geochemical composition of soils reflects the chemical weathering of the parent material, atmospheric deposition, dust input and biological processes [1,2]. As a result, certain elements accumulate and are preserved over time in soils in stable landforms, such as plains and low-inclination slopes [2]. However, on slopes that experience mass wasting processes, including physical mixing, erosion and downslope sediment transport, the primary distribution of elements in the soil profile is disrupted, potentially resulting in selective elemental loss or accumulation over time [2,3].

Isotopes of beryllium (meteoric ^{10}Be), plutonium ($^{239+240}$Pu) and caesium (^{137}Cs) are widely used in Earth sciences to reconstruct, for example, Earth's palaeomagnetic field [4–6], snow palaeoaccumulation rates [7], seafloor sedimentation rates [8] and denudation rates [9] and to determine the age of fluvial terraces [10–12], evaluate seawater exchange cycles [13] and long-distance Asian dust transport [14], among several other processes. More recently, these isotopic tools have been used to investigate soil erosion processes in various environments, such as grasslands and forests of the European Alps or the Rocky Mountains [15–21], in arable lands, forests and grasslands of tropical and subtropical areas and the wet–dry tropics [22–26], in forested mountainous regions [21,27], forests and arable lands under continental Mediterranean climates [28–31], in moraine

landscapes used as farmlands and forests [2,32–35], in loess regions that are dominated by agriculture [36–40] or in post-fire forests and deserts areas [41,42].

The isotopes ^{10}Be, $^{239+240}$Pu and ^{137}Cs allow the tracing of sediment transport and erosion and deposition processes. Thus, they are essential for understanding the evolution of hillslopes and landscapes [2,43–47]. However, although they have a wide range of applications in environmental research, a comprehensive overview of meteoric ^{10}Be, $^{239+240}$Pu and ^{137}Cs, as soil erosion tracers, is lacking, which would facilitate identifying the most appropriate tools to study soil processes. Thus, the main aims of this review were: (1) to characterise ^{10}Be, $^{239+240}$Pu and ^{137}Cs as soil redistribution tracers and their chemical and physical behaviours in the soil environment; (2) to compile published worldwide articles from various environments with different types of land use where these isotopes were applied; (3) to compare erosion rates determined with isotopes with values obtained from the generally used RUSLE approach and (4) to show potential future applications.

2. Chemical Mechanisms and Behaviour Isotopes of ^{10}Be, $^{239+240}$Pu and ^{137}Cs

Understanding the dynamics and behaviours of isotopes in the soil environment is crucial to determining their usefulness as soil erosion tracers [48,49]. Therefore, in this section, we present the origin of meteoric ^{10}Be, ^{137}Cs and $^{239+240}$Pu and their chemistry and distribution in soils.

2.1. Formation of Meteoric ^{10}Be

Meteoric ^{10}Be is a cosmogenic radionuclide, produced constantly in the upper atmosphere and at the Earth's surface as a result of the spallation of ^{14}N and ^{16}O by high-energy cosmic rays to form ^{10}BeO or ^{10}Be(OH)$_2$ [50–52] (Figure 1 and Table 1). ^{10}Be formed in the atmosphere is adsorbed onto aerosols and is primarily delivered to the Earth's surface by wet and dry deposition [48,52,53]. The fluxes of ^{10}Be mainly depend on the precipitation rates and/or latitude [54,55]. At high latitudes, the precipitation rates are very low, which limit the meteoric ^{10}Be flux, whereas, at mid-latitudes, the precipitation tends to be higher; thus, ^{10}Be deposition is also higher [53,54]. Dry deposition is less important, because it represents <10% of the total ^{10}Be flux, except in areas with very low precipitation rates, such as deserts or the inner part of Antarctica [52–54,56].
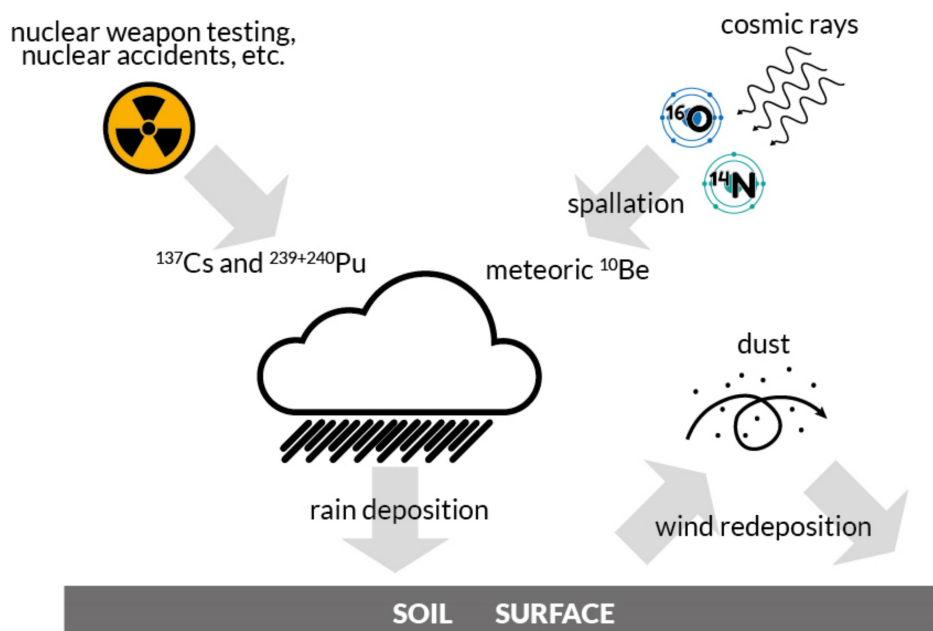

Figure 1. Origin of meteoric ^{10}Be, ^{137}Cs and $^{239+240}$Pu in soils.

Table 1. Comparison of ^{10}Be, ^{137}Cs and $^{239+240}$Pu characteristics.

	Meteoric ^{10}Be	$^{239+240}$Pu	^{137}Cs
Element category	alkaline earth metal	actinide metal	alkali metal
Oxidation state	II	III, IV, V and VI	I
Origin	cosmogenic radionuclide that is constantly produced by the spallation of oxygen and nitrogen by cosmic rays in the upper atmosphere and at the Earth's surface	distributed globally due to nuclear weapon fabrication and testing and nuclear power plants accidents, as well as nuclear fuel reprocessing	distributed globally due to nuclear weapon fabrication and testing, nuclear power plants accidents, as well as nuclear fuel reprocessing
Adsorption	on clay and fine particles, organic matter	associated with organic matter, sesquioxides and clay particles	mostly bound to the fine mineral (clay) fraction
Half-life	1.387 Myr	^{239}Pu 24 110 y and ^{240}Pu 6561 y	30.17 y
Time range in erosion studies	long-term erosion rates (millennia)	medium-term erosion rates (50–60 years)	medium-term erosion rates (50–60 years)
Measurement	AMS	ICP-MS and AMS	gamma-ray spectrometry (counting the 662 keV gamma line), ICP MS
Remarks	The depth distribution of meteoric ^{10}Be might be used to assess the occurrence of soil-mixing processes.	New tool which has been applied since more than one decade in a few countries. Proposed as an alternative to ^{137}Cs.	Difficulties in application in large part of Europe due to heterogeneous fallout caused by the Chernobyl accident. Moreover, due to short half-life over 70% of ^{137}Cs decayed.
		The depth distribution might be used to assess the occurrence of soil-mixing processes.	The depth distribution might be used to assess the occurrence of soil-mixing processes.

2.2. Meteoric ^{10}Be in Soils

After deposition, meteoric ^{10}Be is steadily adsorbed on clay and fine-particle surfaces having a diameter 0–2 µm (Figures 2 and 3) [37,52,57,58]. The Spearman's rank correlation coefficient based on data from various environments (n = 59) also confirms the strong correlation between ^{10}Be and the clay fraction (Figure 3). The magnitude of the adsorbed amount of beryllium is ultimately driven by the sorption capacity system [58]. The adsorption potential and, thus, the fixation of meteoric ^{10}Be in soils depends on pH, soil texture, organic matter, the oxyhydroxide content and its cation exchange capacity [2,48,59,60]. An increase in pH caused a net increase in the negative surface charge and related enhanced affinity for metal ions; thus, the cation exchange capacity also increased [61]. At a soil pH over 4, and in the absence of organic acids, ^{10}Be mostly occurs as hydrolysed species: $BeOH^+$, $Be(OH)_2$ and $Be(OH)_3{}^-$ (Figure 4) that are reactive and, thus, are readily adsorbed onto clay minerals.

Accumulation of meteoric ^{10}Be begins in the upper part of soil (because it reaches the surface with rainwater), from where it penetrates to greater depths until the whole soil column is saturated [53]. Willenbring and von Blackenburg [52], however, stated that concentrations of ^{9}Be and ^{10}Be in soils are too low to saturate the adsorption site; thus, a rather partial release of ^{10}Be occurs when pH < 4 and Be^{2+} competes with dissolved Al^{3+} for the exchange sites. In such acidic soils, ^{10}Be may be translocated to a greater soil or saprolite depth or lost through leaching [25]. Nevertheless, meteoric ^{10}Be still can be used for soil denudation research in acidic environments when its loss can be estimated [25,62]. Although some of the factors that influence the behaviour of meteoric ^{10}Be are described above, some of the mechanisms still need a better explanation.
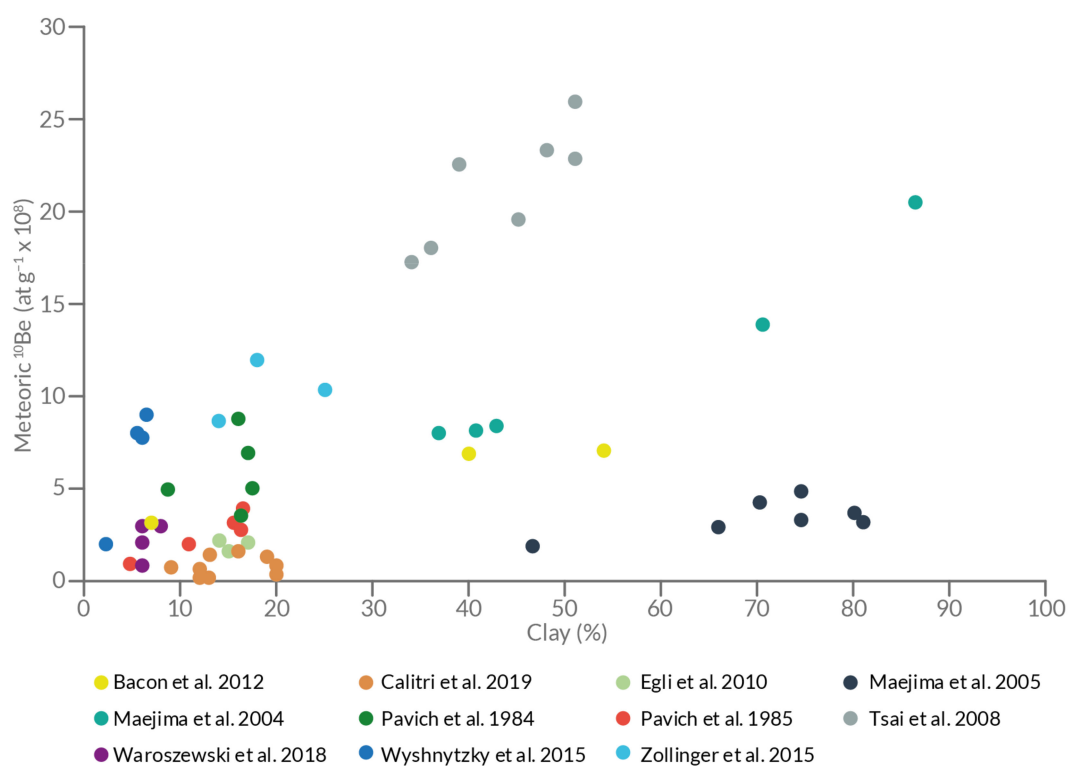
Figure 2. Meteoric ^{10}Be concentrations and clay contents in soils of various environments [2,10–12,15,18,27,33,57,62,63].
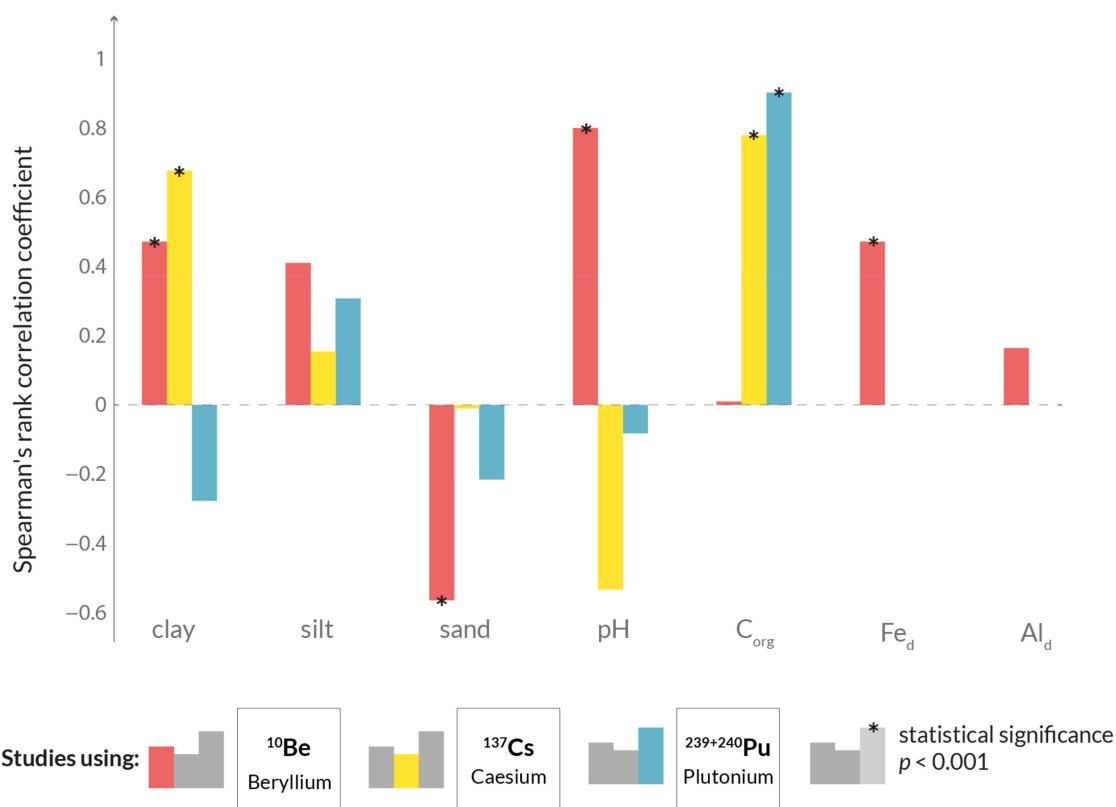

Figure 3. Spearman's rank correlation coefficients calculated using data from 27 publications (Table S1) between soil properties of the bulk samples.
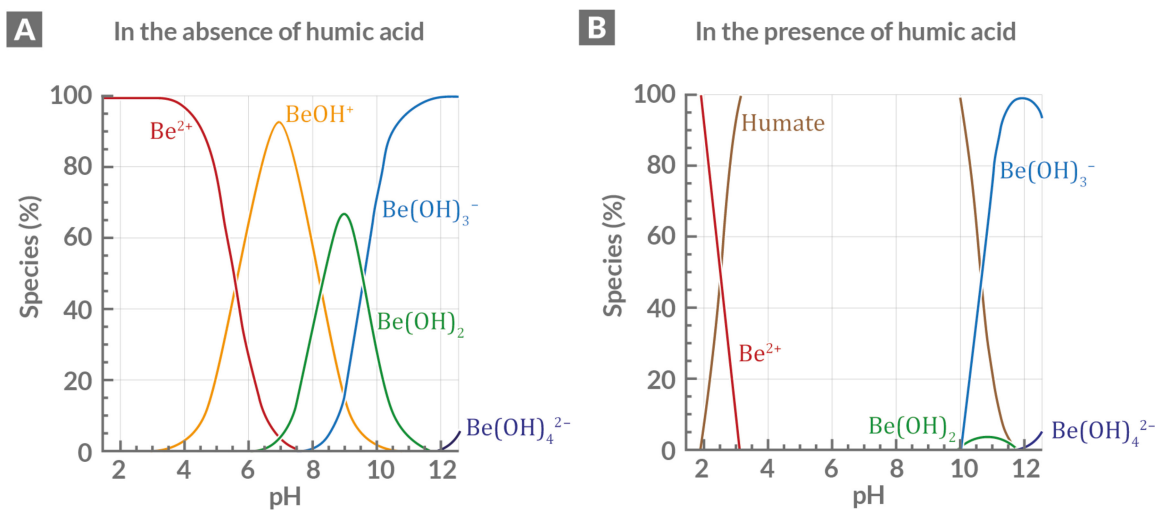
Figure 4. Beryllium speciation in aqueous solutions (total concentration of dissolved ^{10}Be is = 0.02 M) from Takahashi et al. [64]. (**A**) In the absence of organic ("humic") acid and (**B**) in the presence of organic acid (30 mg L^{-1}). Reprinted from Geochimica et Cosmochimica Acta, vol. 63, Y. Takahashi, Y. Minai, S. Ambe, Y. Makide, F. Ambe, Comparison of adsorption behavior of multiple inorganic ions on kaolinite and silica in the presence of humic acid using the multitracer technique, pp. 815–836, 1999, with permission from Elsevier.

2.3. Origin of Anthropogenic Radionuclides—^{137}Cs and $^{239+240}$Pu

Fallout radionuclides (FRNs), such as ^{137}Cs and $^{239+240}$Pu, are also called anthropogenic radionuclides. They have been distributed across the globe by nuclear weapons fabrication and testing, nuclear power plant accidents and nuclear fuel reprocessing (Figure 1 and Table 1) [17]. The Southern Hemisphere is characterised by a lower total fallout of radionuclides than the Northern Hemisphere, because more atmospheric nuclear testing occurred in the latter one [65]. ^{137}Cs is characterised by a short half-life of 30.17 y. About 70% of its global fallout has already disappeared through radioactive decay [66]. The plutonium isotopes, however, have a much longer half-life, namely 24,110 y for ^{239}Pu and 6561 y for ^{240}Pu. Therefore, they are becoming more popular as a replacement for ^{137}Cs [66].

2.4. Anthropogenic Nuclides in Soils

In soils, plutonium exists in four oxidation states: Pu(III), Pu(IV), Pu(V) and Pu(VI) [49,67]. $^{239+240}$Pu sorption depends on pH and redox conditions. In strongly acidic or anoxic soil conditions, organic compounds reduce Pu(VI) and Pu(V) to immobile Pu(III), which often occurs as an organic complex [49,67–69]. Therefore, $^{239+240}$Pu has a high affinity towards organic matter. Additionally, $^{239+240}$Pu is strongly bound to clay particles, which retain it in the soil [49,70–72]. Our data compilation from 25 soil profiles (Figure 3 and Table S1) showed a strongly positive correlation between $^{239+240}$Pu and organic carbon; however, a strong association with clay was not obvious. $^{239+240}$Pu is a relatively "new" soil erosion tracer. Thus, its sorption–desorption mechanisms in soil are not yet fully understood.

^{137}Cs shows a strong affinity towards clay minerals, whereas its affinity towards organic matter is rather low [71,73–75]. Based on data from various environments (*n* = 38 soil profiles), a significant positive correlation between the ^{137}Cs activity and clay content was found (Figure 3). Additionally, a positive correlation between the ^{137}Cs activity and organic carbon (*n* = 28) was calculated, but it might be caused by the relatively high SOC content in the samples considered. In general, ^{137}Cs components are readily soluble in water, although strong adsorption by the clay fraction in soils is highly likely [76]. Thus, the sorption of ^{137}Cs in the soil system mainly depends on the clay content but also on the pH or the redox conditions. In acidic environments, Cs$^+$ competes with H$^+$ for selective sorption sites, and due to the stronger dissolution of clay minerals in such

environments, the sorption of ^{137}Cs is lower, whilst under redox conditions, Cs$^+$ competes with NH$_4^+$ [74,77,78]. The binding of ^{137}Cs increases with the increasing pH (Figure 5), because under such conditions, a greater electrostatic attraction of the cation surface occurs; thus, more Cs$^+$ is sorbed onto the negatively charged clay minerals [74]. When the soil organic content is higher than 5%, it starts to outmatch the fixation of Cs$^+$ on clay minerals and becomes available for plant uptake or leaching into deeper soil layers [79,80]. Thus, in peaty or podzolic soils, ^{137}Cs is considerably more mobile than in other soils [81,82].
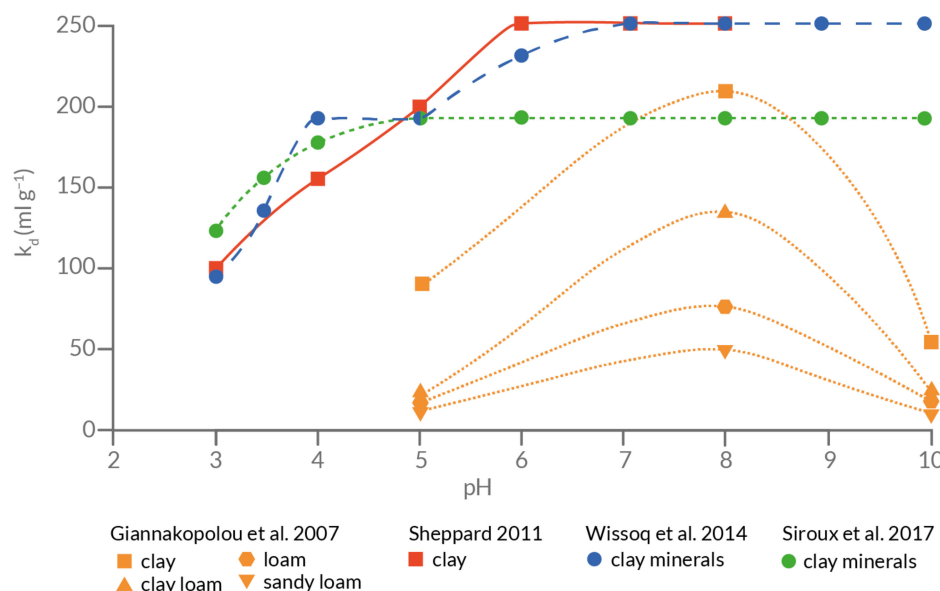
Figure 5. Sorption coefficient (k$_d$) of $_{137}$Cs in soils as a function of pH [74,83–85].

2.5. Profile Depth Distribution of Meteoric ^{10}Be, ^{137}Cs and $^{239+240}$Pu

^{10}Be is a useful geochronometer and long-term erosion tracer due to its long half-life (1.387 ± 0.012 Myr), worldwide occurrence and strong binding by fine soil particles [2,33,86]. Adsorbed meteoric ^{10}Be can be moved along the soil profile because of fine particles translocation via soil water and physical mixing and the percolation of water that may desorb ^{10}Be and transporting it [2]. In general, the highest content of meteoric ^{10}Be is measured in horizons having the highest clay contents (Figure 2) [2,10,11,27,37,52,57]. Thus, the distribution of ^{10}Be within a soil profile in nonacidic conditions as a declining, humped or uniform trend reflects soil evolutionary processes, the degree of surface erosion and soil mass movements [2,18,48,52]. Undisturbed soil profiles are characterised by a declining ^{10}Be content, with the highest value occurring in the topmost horizons (Figure 6(A1,B1)). Soils on actively eroding hillslopes are also characterised by declining ^{10}Be contents [48]. However, their highest content is up to one order of magnitude lower compared to noneroded soils (Figure 6(A3,B3)) [48,87]. The highest ^{10}Be content in subsurface horizons (Figure 6(A2,B2)) is typically found in soils where clay illuviation or intense podzolisation has occurred [11,15,37,57]. Soils that have undergone deep mixing by physical and paedogenic processes or colluvial soils where eroded material from the upper parts of a slope has been deposited (Figure 6 (A4,B4)) are, however, characterised by a uniform ^{10}Be content [38,48,88]. In cases where the topsoil has a different origin (e.g., due to the addition of aeolian silt) to the underlying horizons, significantly lower ^{10}Be concentrations occur in the upper part of the soil profile in contrast to the deeper horizons (Figure 6(A5,B5)) [27].
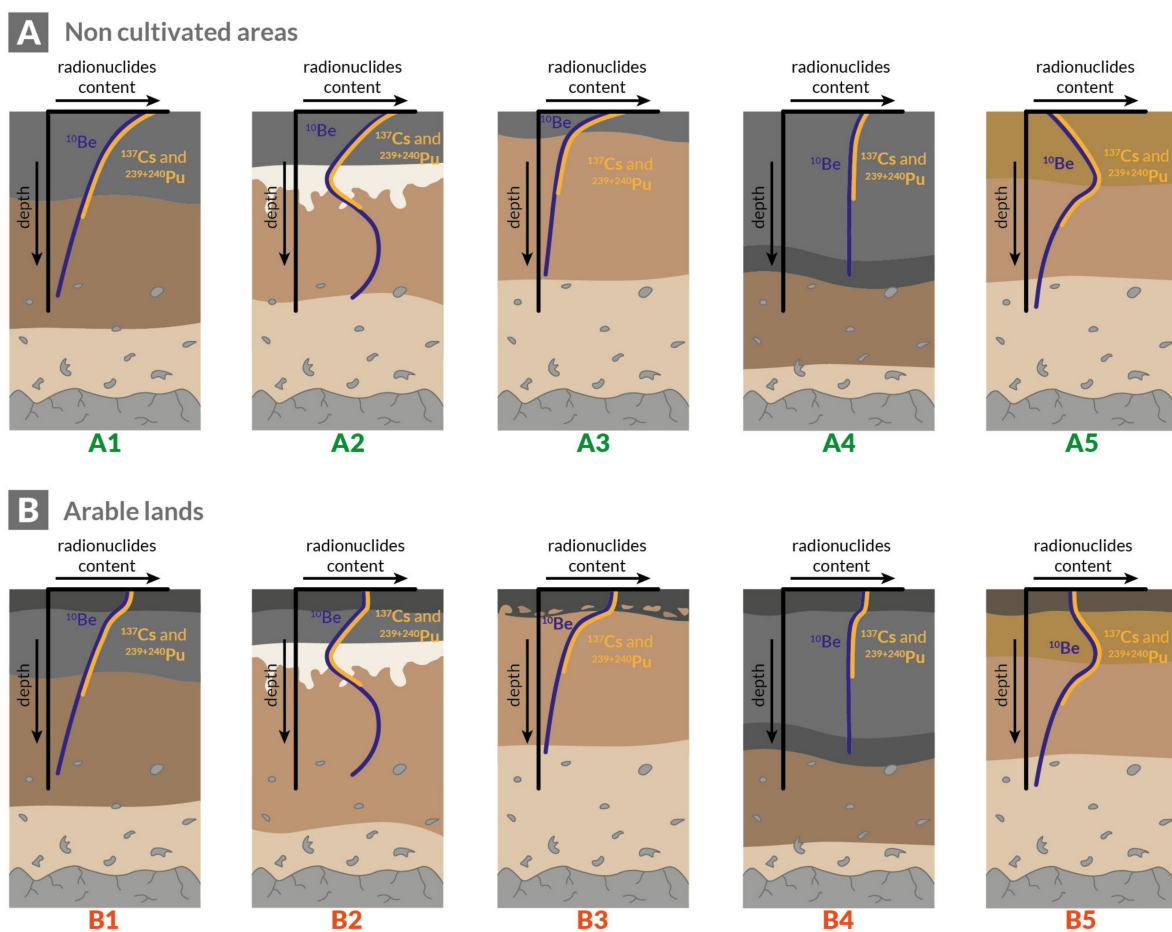
Figure 6. Examples of different profile depth distributions of the studied isotopes in ploughed (**A**) and unploughed (**B**) soils: (**A1**,**B1**)—typical distribution, (**A2**,**B2**)—distribution with clay illuviation, (**A3**,**B3**)—distribution under erosion processes, (**A4**,**B4**)—distribution forced by deep mixing and (**A5**,**B5**)—distribution in polygenetic soils.

Additionally, the FRNs from global fallout are strongly adsorbed onto the fine earth fraction in the topsoil [65,89], and their distribution occurs as a result of soil particle movements [65]. Consequently, the profile depth distributions of ^{137}Cs and $^{239+240}$Pu (Figure 6) are similar to meteoric ^{10}Be and provide information about soil erosion and accumulation, since they were introduced into the environment [49,90].

3. Calculation of Soil Erosion Rates Using Meteoric ^{10}Be

Most erosion calculations are based on the approaches defined by Lal [91], Egli et al. [15] and Zollinger et al. [19]. However, recently, a few advanced models were proposed to study the distribution of meteoric ^{10}Be. One of them is the soil–hillslope model (Be2D) that simulates vertical and lateral redistribution of soil and ^{10}Be along a hillslope and enables insight into processes that influence its transport [92]. The Be2D model considers soil formation, clay translocation, bioturbation and the chemical mobility of ^{10}Be [92]. Additionally, this model considers soil creep, tillage and water erosion reflecting lateral transport and is fully described in Campforts et al. [92].

Another one is the relatively new LODO (Loss Only, Diffusion Only) model presented by Jeliński et al. [32]. This model simulates ^{10}Be concentration profiles in soils over time. It considers vertical diffusion and the net soil flux. In the LODO model, the downward migration of ^{10}Be from the topsoil is modelled as a diffusive process with the depth dependent on diffusivity. It considers that, prior to diffusion, all ^{10}Be enter the surficial depth increment equally [32].

4. Reference Sites and Conversion Models for Anthropogenic Radionuclides

4.1. The Importance of Reference Sites

FRN techniques are used to calculate soil erosion or accumulation rates by comparing the total radionuclide inventory per unit area of a reference site with the FRN activity of a study site or by comparing the temporal evolution of the FRN stocks over time (i.e., by revisiting the sites) [49,93]. When the inventory of the study site is lower than that of reference site, this indicates erosion, whereas a higher stock indicates the deposition of soil material [49]. Thus, the choice of reference site plays a crucial role, because inaccurate values ascribed to the reference inventory will lead to underestimation or overestimation of erosion rates [93]. The undisturbed reference site where soil denudation is absent or negligible should be located, e.g., on a flat, well-vegetated, unploughed site [49]. According to Sutherland [94], the isotope content at a reference site can be used to calculate soil erosion if the variance coefficient is <30%. Recently, especially in the case of $^{239+240}$Pu, attention is paid to measure from five up to ten replicate cores per study site or to take a large amount of sample material (around 1–2 kg per sample) and homogenised them to overcome the large sampling number and measurements.

4.2. Soil Redistribution Rates

One usually assumes that the source of isotopes is just one, and if not, the percentage deposition from each source has to be known to use the calculation models properly [20,49,95]. This is especially the case with ^{137}Cs (see Section 4.3). Therefore, the separation of global and Chernobyl fallout may be done by estimating the initial inventory of ^{137}Cs related to atmospheric nuclear weapon tests. This estimation is based on the approach of Sarmiento and Gwinn [96] and precipitation data [95].

For the estimation of soil erosion and/or deposition rates using ^{137}Cs and $^{239+240}$Pu, various models like the Proportional Model (PM), Mass Balance Model (MBM), Profile Distribution Model (PDM) and Diffusion and Migration model (DDM) were widely applied [97–103]. Furthermore, a two-dimensional spatial integration of the MBM for ^{137}Cs was developed [104]. Van Oost et al. [104] described the crucial processes for ^{137}Cs redistribution that may be independently simulated in this complex approach. Soil mixing and tillage redistribution are modelled by the combination of the spatial distribution of ^{137}Cs with a displacement distribution, and water erosion is simulated using topographic equations [104]. Additionally, an approach exists that combines the MBM with models estimating the spatial soil redistribution, like WATEM/SEDEM (Water and Tillage Erosion Model/Sediment Delivery Model). Such a combination enables calibrating the parameters of spatial models and a detailed determination of the soil redistribution [31].

In 2016, a new algorithm was proposed—modelling deposition and erosion rates using radio nuclides (MODERN) [49,89]. MODERN is a new concept characterised by several noticeable advantages; it more accurately describes the measured FRN inventory in a soil profile. It does not make any distinct assumptions for the reference site and allows the conversion of isotope inventories into soil gain/loss rates, independent of the type of land use [49].

4.3. Radionuclide Ratios

The main assumption of using atmospheric isotopes is that their spatial distributions should be homogeneous [20,95]. However, in Western and Central Europe, the deposition of ^{137}Cs was rather heterogeneous [49]. Most of the fallout ^{137}Cs originates from the 1986 Chernobyl incident and not nuclear weapons tests. Additionally, on the East Coast of Honshu Island (Japan), the spatial distribution of ^{137}Cs fallout is heterogenous due to the Fukushima Daiichi Nuclear Power Plant (FDNPP) accident in 2011 [66]. Thus, the proportion of ^{137}Cs Chernobyl or FDNPP fallout at reference sites should be known [20]. $^{239+240}$Pu is not present in the volatile fraction of fuel debris from nuclear reactor accidents. Therefore, the Chernobyl $^{239+240}$Pu fallout is more limited to Russia, Ukraine, Belarus, Poland and the Baltic countries [105,106], and the FDNPP $^{239+240}$Pu fallout is mainly centred

around Fukushima Prefecture [107]. Other countries, however, have a homogeneous deposition of $^{239+240}$Pu that originated mainly from the atmospheric nuclear weapons tests conducted in the 1950s and 1960s [17,20]. Therefore, to determine the origin of radionuclides, their ratios are used, because the values of the ratio vary significantly depending on the source [66]. In the Northern Hemisphere, the ratio of ^{240}Pu/^{239}Pu for global fallout ranges from 0.14 to 0.24, with an average of 0.18; for the Chernobyl fallout, the ratios are between 0.37 and 0.41, and for FDNPP, the range is between 0.30 and 0.33 [66,108,109].

5. Application in Different Environments in Agricultural and Natural Landscapes

The use of isotopes for the study of soil erosion began in the late 1950s [110]. Since then, ^{10}Be, ^{137}Cs and $^{239+240}$Pu isotopes have been used for the estimation of erosion rates at the temporal and spatial scale. However, the rates can drastically differ as a response to land-use changes and modifications in land management. Thus, in this section, we briefly discuss the use of isotopes in different environments (Figures 7 and 8 and Table 2). Erosion rates determined with isotopes are compared with values from RUSLE. Potential problems in their application and how to avoid methodological problems are addressed (Table 3). Additionally, Mabit et al. [111] pointed out that FRNs should be used for studying soil redistribution within watersheds, the conversion models used should be improved and a conjunctive use of isotopes that cover different timescales provide more information about a study site. Below, we present whether these points are met in the current studies by analysing 83 soils from alpine sites, 35 from loess deposits, 28 from moraine landscapes, 35 from coral reef terraces and Mediterranean areas and 17 soils from the tropics (Figure 7).
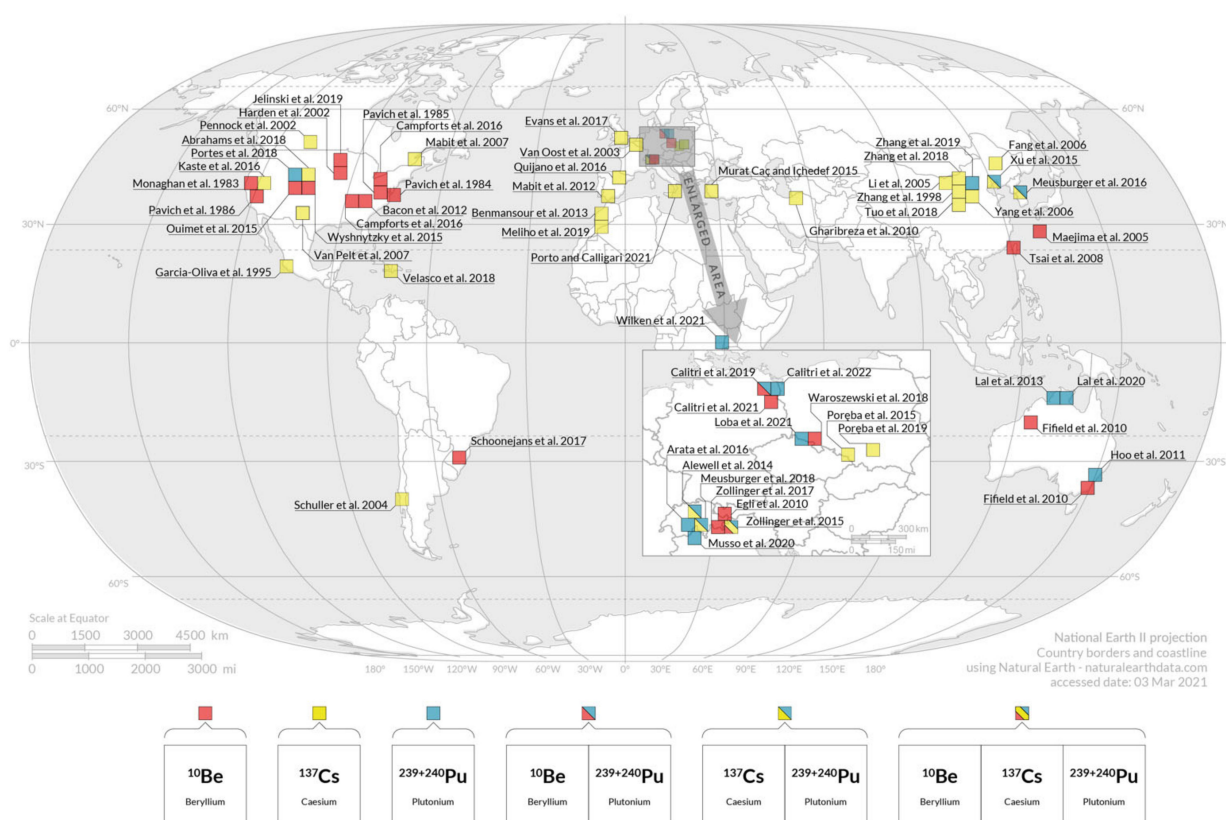
Figure 7. Worldwide isotopic studies (meteoric ^{10}Be, ^{137}Cs and $^{239+240}$Pu) dealing with the soil redistribution rates [2,11,12,15,17–30,32–36,38–42,57,60,62,63,66,79,87,89,92,95,104,112–130].
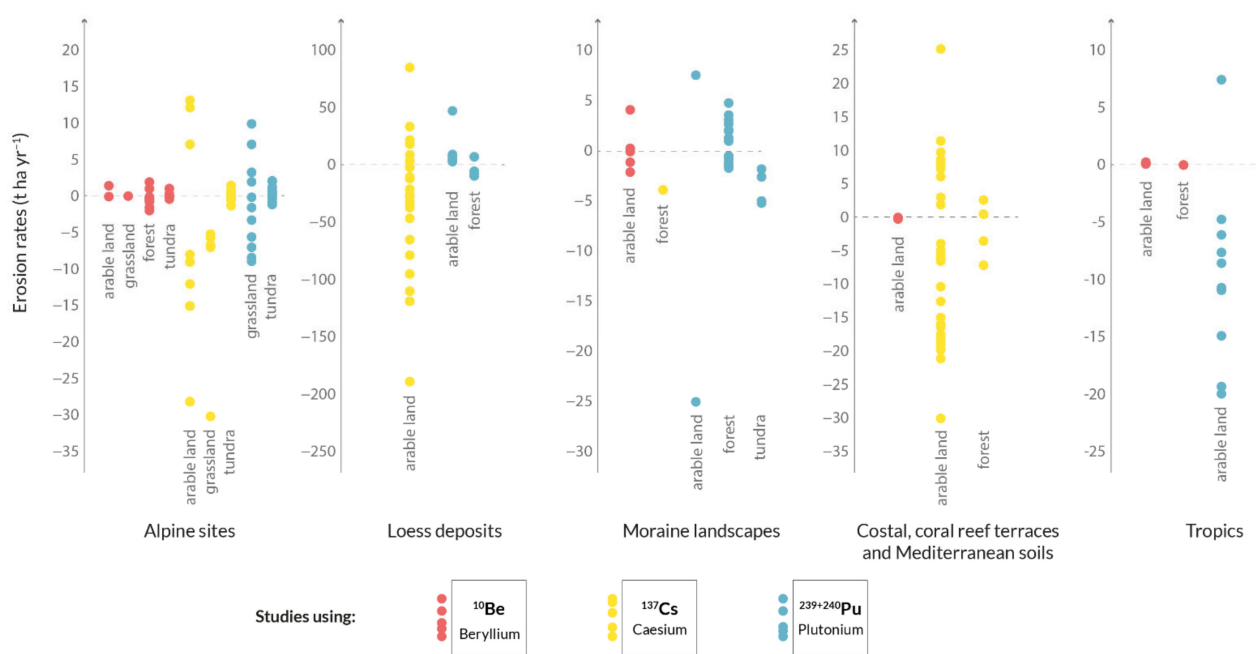
Figure 8. Compilation of published soil erosion rates determined with meteoric ^{10}Be, ^{137}Cs and $^{239+240}$Pu in different environments. Negative values = erosion and positive values = accumulation.

Table 2. Published soil erosion rates based on various isotopes and conversion models (only publications considered where both were available: isotope content and calculation of the soil redistribution rates).

No	Author	Location	Soil Texture	Number of Profiles	Land Use	Soil Erosion Rates (t ha^{-1} y^1)			
						Meteoric ^{10}Be	^{137}Cs	$^{239+240}$Pu	(R)USLE ***
1	Maejima et al. [11]	Coral reef terraces, Southwest Japan	C, SiC, CL	9	Arable land	−0.098 to −0.31 [a,*]	-	-	n.d. **
2	Tsai et al. [12]	Fluvial terraces, Taiwan	C, SiC, CL	3	n.d. **	−0.125 to −0.263 [a]	-	-	n.d. **
3	Egli et al. [15]	Swiss and Italian Alps	LS, SL	6	Mixed forest/alpine grassland	−0.6 to −2.50 [a] −0.03 to −0.6 [b]		-	−0.1 to −0.5 [131]
4	Fifield et al. [127]	Fingerpost Hill, Burra Creek, NW and SE Australia	n.d. **	13	Forest and Pasture	−0.03 to −0.19 [a]			−0.1 to −5.0 [132]
5	Campforts et al. [92]	Susquehanna Shale Hills Observatory, USA	n.d.	n.d. **	Arable land	−0.10 to 1.37 [c]			n.d.
6	Zollinger et al. [19]	Swiss Alps	LS, SL	18	Alpine grassland	−0.34 to −1.29 [a] −0.08 to 1.8 [b]		-	−1.0 to −0.3 [131]

Table 2. *Cont.*

No	Author	Location	Soil Texture	Number of Profiles	Land Use	Soil Erosion Rates (t ha^{-1} y^1)			
						Meteoric ^{10}Be	^{137}Cs	$^{239+240}$Pu	(R)USLE ***
7	Schoonejans et al. [25]	Critical Zone Observatory, Southern Brazil	n.d. **	3	Subtropical forest	−0.33 to −0.42 [d] −0.05 to −0.06 [e]	-	-	n.d.
8	Waroszewski et al. [27]	Karkonosze Mountains, Poland	SL, SiL	5	Mountain forest	−1.3 to −6.4 [f] −0.8 to −2.0 [g]	-	-	−2.0 to −5.0 [133]
9	Jelinski et al. [32]	West-Central Minnesota, USA	L	5	Arable land	−0.06 to 4.13 [h]	n.d.		n.d.
10	Zhang et al. [39]	Ansai, China	SiL	9	Arable land		−65.0 to 110.0 [i]	-	−50 to −80 [134]
11	Van Oost et al. [104]	Huldenberg, central Belgium	SiL	n.d. **	Arable land		−10.3 to 9.0 [j]	-	−0.5 to −1.0 [133]
12	Schuller et al. [115]	Coastal Mountain range of the 9th Region of Chile	n.d. **	6	Arable land		−28.0 to 12.0 [i]	-	n.d.
13	Fang et al. [125]	Jilin Province, China	CL	5	Arable land		−26.43 to 27.28 [k] −37.63 to 34.33 [i]	-	−45.0 to −4.0 [135]
14	Yang et al. [126]	Shaanxi Province, China	SiL	197	Forest and arable land		−25.0 to 150.0 [i,m]	-	−23.1 [135]
15	Mabit et al. [28]	Boyer River watershed, Canada	SL, SCL	412	Arable land	-	−9 to 6.4 [i]	-	−3.0 [28]
16	Mabit et al. [29]	Montefrio, Spain	CL	8	Arable land		−19.0 to 25.0 [i]	-	−10 to −20 [133]
17	Benmansour et al. [118]	Marchouch, Morocco	C	45	Arable land		−4.0 to −30.0 [i]	-	−4.0 to −56.0 [118]
18	Murat Sac and Ichedef [120]	Salihi Region, Western Turkey	n.d. **	4	Arable land	-	−21.1 to 11.3 [i] −9.6 to 19.4 [k]	-	n.d.
19	Poręba et al. [38]	Świerklany, South Poland	SiL	4	Arable land	-	−26.7 to 85.1 [i]	-	−10.0 to −20.0 [133]
20	Quijano et al. [117]	Ebro Basin, Spain	n.d.	156	Arable land		−19.8 to 7.4 [i]	-	−10.0 to −20.0 [133]
21	Velasco et al. [24]	Forêts des Pins, Haiti	C	12	Arable land	-	−23 to 71 [l]	-	−20 to −50 [136]
22	Tuo et al. [36]	Chinese Loess Plateau	SL	7	Arable land	-	−21.39 to −37.31 [i]	-	−23.1 [137]
23	Poręba et al. [95]	Biedrzykowice, South Poland	SiL	4	Arable land	-	−4.9 to 39.9 [i, k]	-	−10.0 to −20.0 [133]
24	Meliho et al. [30]	Ourika Watershed, High Atlas of Morocco	SL, L	33	Arable land and forest	-	−32.23 to −0.06 [i] −11.42 to 2.27 [m]	-	up to −45.0 [138]
25	Gharibreza et al. [124]	Golestan Province, Iran	SiL, SiC	93	Arable land and forest	-	−10 to −35.9 [i]	-	up to −70.0 [139]

Table 2. *Cont.*

No	Author	Location	Soil Texture	Number of Profiles	Land Use	Soil Erosion Rates (t ha^{-1} y^1)			
						Meteoric ^{10}Be	^{137}Cs	$^{239+240}$Pu	(R)USLE ***
26	Xu et al. [140]	Liaodong Bay, Northeast China	n.d.	6	Arable land and uncultivated land with low vegetation cover	-	−14.0 to −42.5 [i]	−20.3 to −72.0 [j]	n.d.
27	Meusburger et al. [89]	headwater catchment of Lake Soyang, South Korea	SL	25	Forest and arable land	-	−23.8 to 2.9 [m]	−17.5 to 3.6 [l]	−30.6 to −54.8 [141]
28	Meusburger et al. [20]	Swiss Central Alps	LS, SL	14	Alpine grassland	-	−5.2 to −6.7 [l]	−3.3 to −7.0 [o]	−2.0 to −12.0 [142]
29	Lal et al. [22]	Daly river basin, Northern Australia	n.d.	6	Arable land	-	-	−7.5 to −19.5 [k] −8.5 to −19.7 [i]	−10.0 to −50.0 [132]
30	Alewell et al. [17]	Swiss Central Alps	LS, SL	44	Alpine grassland	-	-	−8.9 to 8.3 [m] −1.9 to 7.0 [k] −0.2 to −16.4 [n]	−2.0 to −12.0 [142]
31	Arata et al. [129]	Swiss Central Alps	LS, SL	5	Mountain grassland	-	-	−8.4 to 9.8 [o]	−2.0 to −12.0 [142]
32	Portes et al. [21]	Central Rocky Mountains, USA	LS, SL	3	Alpine tundra/forest	-	-	−2.60 to −5.20 [k,m]	n.d.
33	Zhang et al. [121]	Gansu Province, China	SiL	6	Forest (before agriculture)		-	−9.4 to 7.2 [i]	−23.1 [137]
34	Lal et al. [23]	The Daily River Catchment, Northern Australia	L	3	Pasture, mahogany and peanut plantations	-	-	−8.4 to 7.2 [i]	−10 to −50 [132]
35	Loba et al. [40]	Trzebnica Hills, Southwest Poland	SiL, L		Arable land			−1.17 to 10.93 [o]	−5.0 to −10.0 [133]
36	Zollinger et al. [18]	Eastern Swiss Alps	LS, SL	19	Alpine tundra/natural forest	−0.40 to 0.04 [b]	−1.35 to 1.41 [m]	−1.20 to 2.04 [m]	−1.0 to −2.0 [131]
37	Calitri et al. [33]	Uckermark Region, Northeast Germany	SL, L	3	Arable land	−2.11 to 0.26 [b]	-	−0.25 to 7.6 [m]	up to −0.5 [133]

* Negative values mean erosion, positive deposition. ** No data. *** Authors are given in the brackets. Soil texture: SL—sandy loam, LS—loamy sand, L—loam, SiL—silt loam, SCL—sandy clay loam, SiC—silty clay, CL—clay loam and C—clay. Models: [a] Steady-state approach, [b] non-steady-state approach, [c] Be2D model, [d] not-corrected values, [e] corrected values, [f] assuming that the uppermost horizon has the same origin as the underlying soil, [g] the uppermost horizon is not considered due to its different origin, [h] integration of Be2D and LODO, [i] mass balance model, [j] integration of mass balance and spatial models, [k] proportional model, [l] diffusion and migration model, [m] profile distribution model, [n] inventory method and [o] MODERN.

Table 3. Summary of some main potential problems in applying isotopes as a soil tracer and possibilities for overcoming them.

Environment	Land Use	Difficulties	Solutions
Alpine sites, Loess areas	Grasslands, Forests, Arable lands	Heterogenous fallout of ^{137}Cs (Nuclear weapons tests and nuclear power plants fallout), which affects the calculation of soil erosion rates.	To overcome this limitation, both sources of ^{137}Cs have to be taken into account in the calculation model. The separation of global fallout from e.g., the Chernobyl fallout may be done by estimating the initial inventory of ^{137}Cs (described in Poręba et al. [95]) or by the determination of $^{239+240}$Pu/^{137}Cs activity ratios at reference sites (described in Meusburger et al. [20,143]).
Coral reef and fluvial terraces, Alpine sites	Grasslands, Forests, Arable lands	When meteoric ^{10}Be is used, the erosion/deposition rates obtained with the model of Lal [91], sometimes may raise doubts. Especially in soils exhibiting clay illuviation or podzolisation.	Application of different models, e.g., proposed by Egli et al. [15], Be2D model [92] and LODO [32]
Tropics	Arable lands	When soil is cultivated with traditional manual tillage practices, features of significant tillage mixing does not occur. Thus, conversion models for cultivated sites cannot be used.	A conversion model developed for undisturbed soils has to be applied [24].
Alpine sites	Forests	Cover beds or different overlaying parent materials for soil development exist. The topsoil, for example, may have aeolian silt admixture, whereas this is not the case for the subsoil. The interpretation of long-term erosion rates may be hampered.	Calculation of erosion rates with and without considering the topsoil may give indications about the range of results [27].
Acidic soils	Forests	In acidic soils, the considered isotopes may in part be solubilised and, thus, be leached.	Determination of a potential loss of meteoric ^{10}Be from the parent material, using chemical mass losses of stable ^{9}Be in a regolith profile [25,62]. The concepts and models for ^{137}Cs and $^{239+240}$Pu under acidic conditions still need to be improved.

5.1. Alpine Sites

Although, there are certain limitations in the application of the discussed isotopes at Alpine sites, they have been widely used to determine soil redistribution rates [15–19,27,92,129,130,144,145]. For example, Alewell et al. [17] employed $^{239+240}$Pu and ^{137}Cs as tools in measuring soil erosion in mountainous grasslands in the Swiss Alps. At such sites, the distribution of ^{137}Cs was chiefly due to the fallout from the Chernobyl accident. This incident occurred at a time when the mountains were still snow-covered. Following snowmelt, the spatial distribution of ^{137}Cs became very patchy, because part of it was lost due to the overland surface flow, whereas, at sites that had been snow-free, the ^{137}Cs remained and accumulated in the soil. The spatial distribution of $^{239+240}$Pu, however,

was not affected by the nuclear accident. Therefore, the erosion rates were determined using $^{239+240}$Pu (Table 2). The application of ^{137}Cs at such Chernobyl-affected sites is, however, still possible. To overcome this limitation, Meusburger et al. [20] determined the $^{239+240}$Pu/^{137}Cs activity ratios at the reference sites. The calculation of this ratio provided information about the relative influence of the global versus Chernobyl deposition and allowed the consideration of two ^{137}Cs sources by a using conversion model. The values of the $^{239+240}$Pu/^{137}Cs activity ratios increased with the soil depth, indicating the predominant origin of the ^{137}Cs in the topsoil being Chernobyl, while the deeper layers were characterised by a higher proportion of the ^{137}Cs from global fallout. Therefore, the average Chernobyl contribution was estimated to be 75%, which was used to convert the ^{137}Cs inventories (Table 2), and the obtained results were in the range of those determined with RUSLE [131] (Table 2).

The soil erosion rates using ^{137}Cs and $^{239+240}$Pu were also determined in the Lake Soyang catchment, which has a total area of 65 km^2 [89]. The rates agree well with data from RUSLE [141]. The calculation model is crucial for the interpretation of long-term erosion rates based on meteoric ^{10}Be at Alpine sites. As discussed by Zollinger et al. [19] and Egli et al. [15], an approach using steady-state conditions gives unreliable results and does not detect deposition processes. In addition, the interpretation of meteoric ^{10}Be data becomes difficult in soils developed from heterogenous parent materials. This problem was addressed by Waroszewski et al. [27], where a thin aeolian silt drape overlayed periglacial mica schist deposits; thus, two calculations were used and compared to estimate the erosion rates in mountainous forests. The first based on the assumption that the uppermost horizon had the same origin as the underlying layers, and the second did not consider the uppermost horizon due to its different origin. Version 1 overestimated the erosion rates, while version 2 produced erosion values (Table 2) that seemed more plausible for this mountainous region. The better suitability of the second version was also supported by RUSLE data (Table 2).

Recently, using a combination of isotopes that cover different intervals of time (e.g., $^{239+240}$Pu and ^{10}Be) has been applied. This can help in deciphering processes over different timescales. It may shed light onto changes of soil redistribution caused by evolving environmental settings or anthropogenic forcing and allow for the comparison of different time ranges. For instance, Zollinger et al. [19] showed that the short- to mid-term soil redistribution rates in the alpine tundra are dramatically higher than the long-term rates (covering a period of ~15 kyr). This has been mainly caused by climate warming and melting of the permafrost, which has distinctly increased soil redistribution over the last few decades.

5.2. Loess Deposits

Loess deposits are very susceptible to erosion processes [124,139,146–149]. Thus, isotopic techniques were widely applied in such landscapes [36,38,39,95,104,121,126,150]. Poręba et al. [38,95] applied ^{137}Cs measurements to a loess colluvium to interpret soil erosion in a Polish loess area under agriculture use (arable lands). In this case, about 45–90% of ^{137}Cs derived from the Chernobyl accident. When taking this into account, the erosion rates were in a typical range for loess environments, as shown by RUSLE (Table 2). Other results showed, by using $^{239+240}$Pu, that the soil erosion rates of loess landscapes of Southwestern Poland are often much higher than tolerable rates but still in the range of values from RUSLE [40]. For the Chinese Loess Plateau, Zhang et al. [39] showed that soil erosion determined using ^{137}Cs is considerably lower than the modelled rates using the RUSLE model or sediment yields. This issue was explained by the simulation errors and the effect of the topography. Additionally, in arable areas of the Chinese Loess Plateau, ^{137}Cs was involved to determine wind erosion by subtracting the water erosion from the total erosion calculated using ^{137}Cs [36,123,151]. However, such an approach can cause some uncertainty. The RUSLE model, which is used to calculate water erosion, may underestimate or overestimate erosion rates [36,151]. Thus, the issue of determining wind erosion

with isotopes definitely requires more research. In loess landscapes, the methodological combination of soil redistribution rates based on ^{137}Cs measurements with spatial soil erosion models was applied in forests and arable lands [104,126]. Recently, [239+240]Pu and ^{137}Cs were used for the assessment of rehabilitation effectiveness at sites that were used in the past for agriculture and now are afforested or are grasslands [121,124,127,134]. Examples showing the effect of changes in a tillage system on erosion rates in loess landscapes are still scarce.

5.3. Moraine Landscapes

In moraine landscapes, radioisotopes may help to decipher the evolution of soil erosion rates with soil development. Portes et al. [21], by using [239+240]Pu, showed that soil erosion rates in forests and the tundra on moraine hillslopes have strongly decreased over time. Both applied models—the profile distribution model [98,100] and the inventory model [22]—detected the same trend. The application of [239+240]Pu in forests of such landscapes may provide information if the erosion in a studied area is recent or ancient, as presented by Calitri et al. [34]. The combination of [239+240]Pu (last few decades) and meteoric [10]Be (integration over millennia) in arable lands often confirms that the intensification of agriculture in recent decades has strongly influenced soil redistribution rates [33]. Moreover, recent investigations of Jelinski et al. [32] exhibited that natural and anthropogenic soil redistribution rates can be discerned when meteoric [10]Be is combined with the LODO, Be2D and WaTEM models.

Some investigations, however, did not focus on the calculation of soil erosion and considered only isotope inventories [2,35]. Ouimet et al. [35] presented the spatial and temporal variations of meteoric [10]Be inventories in moraines and fluvial terraces, which allowed to identify specific slope processes. Soil erosion seemed to have occurred even at the older sites (>90 ka), whereas the younger sites (15–21 ka) exhibited higher [10]Be inventories, indicating the dynamic aspects of [10]Be deposition, like snow drift that caused spatial variations in measured inventories at individual sites.

5.4. Coastal and Coral Reef Terraces and Mediterranean Soils

Isotopes were also applied in soils on coral reef, coastal and fluvial terraces [11,12,35,60,113,120] and Mediterranean landscapes [29–31,118]. Maejima et al. [11] and Tsai et al. [12] applied (meteoric) [10]Be to the soils of uplifted coral reef terraces in Southwestern Japan and in fluvial terraces in Taiwan, respectively. These cases showed the importance of the calculation model for the determination of soil erosion rates. In both publications, the mathematical model of Lal [91] was used. Therefore, processes such as eluviation/illuviation or vertical mixing were not considered in the model, which resulted in an overestimation of the soil erosion rates.

Radioisotopes are suitable tracers of soil erosion rates in such environments [35,60]. For instance, Meliho et al. [30] applied ^{137}Cs to determine the erosion on terraces with different land uses (forestry and agriculture) in the High Atlas (Ourika watershed) of Morocco, whereas Mabit et al. [29] and Quijano et al. [31] applied radioisotopes to study soil erosion alone or in combination with spatial models in Mediterranean landscapes. The obtained results were reliable, because they lie in the range of data provided by RUSLE (Table 2; Panagos et al. [133,138]).

5.5. Tropics

Radioisotopes have been widely used in the tropics [22,23,79,127,128] and comparable with results from USLE model [132,136]. Lal et al. [23] applied [239+240]Pu to analyse soil losses and gains in the wet–dry tropics of Northern Australia on three major land-use types (grazing fields, mahogany and peanut plantation). Wilken et al. [26] demonstrated that pristine forests show no indication of soil redistribution based on [239+240]Pu along topographical gradients. They, however, have measured tremendously high soil erosion and sedimentation rates up 87 t ha^{-1} y^{-1} during the last 55 years. Hoo et al. [128] also

used ^{239}Pu to determine the recent soil erosion rates at the scale of a Canberra water supply catchment of a few hundred km^2 in a fire-ravaged area. Here, erosion and water quality are tightly interconnected. Fifield et al. [127] combined meteoric ^{10}Be and ^{137}Cs to compare the long- and medium-term soil erosion and production rates. The authors showed that modern soil loss is considerably higher than soil production. ^{137}Cs also traced erosion processes on hillslopes in Haiti, where tillage is performed with traditional manual tools. Thus, cultivated sites did not exhibit any evidence of significant tillage mixing, and it was not possible to apply a standard conversion model for cultivated soils. Consequently, a conversion model developed for undisturbed sites had to be used to calculate the soil erosion rates, which seemingly provided reliable results [24].

5.6. Acidic Soils

Under acidic conditions, the discussed isotopes may occur in mobile forms, and they may be transported to the saprolite and/or lost through leaching [52,59,62,74,152]. To overcome this limitation for meteoric ^{10}Be, Bacon et al. [62] proposed to use the stable isotope ^{9}Be that is mobilised from the parent material through weathering to determine the potential loss of meteoric ^{10}Be [25]. This approach is based on the chemical mass losses of ^{9}Be in a regolith profile being used to constrain the chemical depletion of ^{10}Be. Adding chemical losses of ^{9}Be to the measured ^{9}Be inventory and assuming that ^{9}Be and meteoric ^{10}Be behave similarly in the regolith, the reactive ^{9}Be fractions are positively related to the ^{10}Be concentrations. Therefore, the ratio between the corrected and measured ^{9}Be concentrations enables a correction of the ^{10}Be concentrations, so that erosion rates can be calculated. Additionally, in acidic environments such as forests, the Be2D model, which considers meteoric ^{10}Be translocation within a soil profile, was applied, and the results seemed reasonable [92].

6. Conclusions and Outlook

Meteoric ^{10}Be, ^{137}Cs and $^{239+240}$Pu are useful tracers of soil redistribution. They have been applied in different environments, such as moraines, loess landscapes, alpine sites, coastal and coral reef terraces, Mediterranean soils, tropics, acidic soils and forest soils and used as forests, grasslands and arable lands. The results determined with isotopes were in a good agreement with the values from RUSLE, which proves their usefulness as soil erosion tracers. Meteoric ^{10}Be allows the calculation of long-term redistribution rates (often since the start of soil formation), while ^{137}Cs and $^{239+240}$Pu give possibility to calculating the medium-term (decades) rates. The application of ^{137}Cs, however, has increasing limitations caused by its short half-life and its heterogeneous distribution in European soils owing to the Chernobyl nuclear accident. Thus, $^{239+240}$Pu has been suggested as a promising alternative. Its high precision and increasing application have indicated its success.

When using these isotopes, a crucial issue is selecting the most suitable conversion model for calculating the soil redistribution rates. For meteoric ^{10}Be, the most popular models are those proposed by Lal [91] and Egli et al. [15]; however, the latter appears to work better, because it assumes that soils are an open system. New models such as LODO with Be2D provide insights into the natural and anthropogenic soil redistribution rates. For ^{137}Cs and $^{239+240}$Pu, the mass balance, diffusion and migration, profile distribution models and inventory method are often used, whereas MODERN is a recently developed model that stimulates the stock and the FRN profile distribution.

When using $^{239+240}$Pu and ^{137}Cs, the choice of a reference profile is crucial, as the results of sites exhibiting soil redistribution are referenced. Choosing an unrepresentative (disturbed and eroded) reference profile will lead to under- or overestimation of these rates.

Many examples have proved the usefulness of these isotopes in estimating the soil redistribution rates. There are, however, also several limitations with these isotopic methods, although solutions exist for some of them. For example, the distribution of ^{137}Cs may not be homogeneous. In such cases, $^{239+240}$Pu may be helpful in correcting any bias. Likewise,

in deeply weathered and acidic soils, losses of the inventory of [10]Be may be corrected by using [9]Be.

Moreover, the simultaneous application of [10]Be and ^{137}Cs and/or [239+240]Pu enables tracing back changes in the soil erosion rates over time. It has been shown that global warming has accelerated the soil redistribution rates in Alpine regions and on agriculture land. Using a combination of several isotopes at the same study sites enables cross-checking whether the obtained results are comparable and, therefore, reliable. This kind of approach was presented by Mabit et al. [111] as a challenge and necessity in the use of isotopes.

Isotopic tools are still underexplored in soils, but they could be increasingly applied under different agroecological conditions, with soil redistribution rates being quantified over decades to millennia. Still, several gaps in the knowledge about soil redistribution exists, e.g., in loess areas under different tillage systems or applying isotopes in larger scales like watersheds. The determination of wind erosion and the application of new calculation models are additional challenges.

References

1. Dethier, D.P.; Birkeland, P.W.; McCarthy, J.A. Using the accumulation of CBD-extractable iron and clay content to estimate soil age on stable surfaces and nearby slopes, Front Range, Colorado. *Geomorphology* **2012**, *173–174*, 17–29. [CrossRef]
2. Wyshnytzky, C.E.; Ouimet, W.B.; McCarthy, J.; Dethier, D.P.; Shroba, R.R.; Bierman, P.R.; Rood, D.H. Meteoric [10]Be, clay, and extractable iron depth profiles in the Colorado Front Range: Implications for understanding soil mixing and erosion. *Catena* **2015**, *127*, 32–45. [CrossRef]
3. Dixon, J.L.; von Blanckenburg, F. Soils as pacemakers and limiters of global silicate weathering. *C. R. Geosci.* **2012**, *344*, 597–609. [CrossRef]
4. Frank, M.; Schwarz, B.; Baumann, S.; Kubik, P.W.; Suter, M.; Mangini, A. A 200 kyr record of cosmogenic radionuclide production rate and geomagnetic field intensity from [10]Be in globally stacked deep-sea sediments1. *Earth Planet. Sci. Lett.* **1997**, *149*, 121–129. [CrossRef]
5. Simon, Q.; Suganuma, Y.; Okada, M.; Haneda, Y. High-resolution [10]Be and paleomagnetic recording of the last polarity reversal in the Chiba composite section: Age and dynamics of the Matuyama–Brunhes transition. *Earth Planet. Sci. Lett.* **2019**, *519*, 92–100. [CrossRef]
6. Wagner, G.; Beer, J.; Masarik, J.; Muscheler, R.; Kubik, P.W.; Mende, W.; Laj, C.; Raisbeck, G.M.; Yiou, F. Presence of the Solar de Vries Cycle (~205 years) during the Last Ice Age. *Geophys. Res. Lett.* **2001**, *28*, 303–306. [CrossRef]
7. Wagner, G.; Laj, C.; Beer, J.; Kissel, C.; Muscheler, R.; Masarik, J.; Synal, H.-A. Reconstruction of the paleoaccumulation rate of central Greenland during the last 75 kyr using the cosmogenic radionuclides [36]Cl and [10]Be and geomagnetic field intensity data. *Earth Planet. Sci. Lett.* **2001**, *193*, 515–521. [CrossRef]
8. Frank, M.; Backman, J.; Jakobsson, M.; Moran, K.; O'Regan, M.; King, J.; Haley, B.A.; Kubik, P.W.; Garbe-Schönberg, D. Beryllium isotopes in central Arctic Ocean sediments over the past 12.3 million years: Stratigraphic and paleoclimatic implications. *Paleoceanography* **2008**, *23*, 1–12. [CrossRef]
9. Dannhaus, N.; Wittmann, H.; Krám, P.; Christl, M.; von Blanckenburg, F. Catchment-wide weathering and erosion rates of mafic, ultramafic, and granitic rock from cosmogenic meteoric [10]Be/[9]Be ratios. *Geochim. Cosmochim. Acta* **2018**, *222*, 618–641. [CrossRef]
10. Maejima, Y.; Matsuzaki, H.; Nakano, C. [10]Be concentrations of Red soils in Southwest Japan and its possibility of dating. *Nucl. Instrum. Methods Phys. Res. Sect. B Beam Interact. Mater. At.* **2004**, *223–224*, 596–600. [CrossRef]

11. Maejima, Y.; Matsuzaki, H.; Higashi, T. Application of cosmogenic [10]Be to dating soils on the raised coral reef terraces of Kikai Island, southwest Japan. *Geoderma* **2005**, *126*, 389–399. [CrossRef]

12. Tsai, H.; Maejima, Y.; Hseu, Z.Y. Meteoric [10]Be dating of highly weathered soils from fluvial terraces in Taiwan. *Quat. Int.* **2008**, *188*, 185–196. [CrossRef]

13. Hao, Y.; Xu, Y.; Pan, S.; Song, X.; Zhang, K.; Guo, H.; Gu, Z. Sources of plutonium isotopes and ^{137}Cs in coastal seawaters of Liaodong Bay and Bohai Strait, China and its environmental implications. *Mar. Pollut. Bull.* **2018**, *130*, 240–248. [CrossRef]

14. Dong, W.; Zheng, J.; Guo, Q. Particle-size speciation of Pu isotopes in surface soils from Inner Mongolia (China) and its implications for Asian Dust monitoring. *Appl. Radiat. Isot.* **2017**, *120*, 133–136. [CrossRef] [PubMed]

15. Egli, M.; Brandová, D.; Böhlert, R.; Favilli, F.; Kubik, P.W. [10]Be inventories in Alpine soils and their potential for dating land surfaces. *Geomorphology* **2010**, *119*, 62–73. [CrossRef]

16. Konz, N.; Prasuhn, V.; Alewell, C. On the measurement of alpine soil erosion. *Catena* **2012**, *91*, 63–71. [CrossRef]

17. Alewell, C.; Meusburger, K.; Juretzko, G.; Mabit, L.; Ketterer, M.E. Suitability of [239+240]Pu and ^{137}Cs as tracers for soil erosion assessment in mountain grasslands. *Chemosphere* **2014**, *103*, 274–280. [CrossRef]

18. Zollinger, B.; Alewell, C.; Kneisel, C.; Meusburger, K.; Brandová, D.; Kubik, P.; Schaller, M.; Ketterer, M.; Egli, M. The effect of permafrost on time-split soil erosion using radionuclides (^{137}Cs, [239+240]Pu, meteoric [10]Be) and stable isotopes (δ^{13}C) in the eastern Swiss Alps. *J. Soils Sediments* **2015**, *15*, 1400–1419. [CrossRef]

19. Zollinger, B.; Alewell, C.; Kneisel, C.; Brandová, D.; Petrillo, M.; Plötze, M.; Christl, M.; Egli, M. Soil formation and weathering in a permafrost environment of the Swiss Alps: A multi-parameter and non-steady-state approach. *Earth Surf. Process. Landf.* **2017**, *42*, 814–835. [CrossRef]

20. Meusburger, K.; Porto, P.; Mabit, L.; La Spada, C.; Arata, L.; Alewell, C. Excess Lead-210 and Plutonium-239+240: Two suitable radiogenic soil erosion tracers for mountain grassland sites. *Environ. Res.* **2018**, *160*, 195–202. [CrossRef]

21. Portes, R.; Dahms, D.; Brandová, D.; Raab, G.; Christl, M.; Kühn, P.; Ketterer, M.; Egli, M. Evolution of soil erosion rates in alpine soils of the Central Rocky Mountains using fallout Pu and δ^{13}C. *Earth Planet. Sci. Lett.* **2018**, *496*, 257–269. [CrossRef]

22. Lal, R.; Tims, S.G.; Fifield, L.K.; Wasson, R.J.; Howe, D. Applicability of [239]Pu as a tracer for soil erosion in the wet-dry tropics of northern Australia. *Nucl. Instrum. Methods Phys. Res. Sect. B Beam Interact. Mater. At.* **2013**, *294*, 577–583. [CrossRef]

23. Lal, R.; Fifield, L.K.; Tims, S.G.; Wasson, R.J.; Howe, D. A study of soil erosion rates using [239]Pu, in the wet-dry tropics of Northern Australia. *J. Environ. Radioact.* **2020**, *211*, 106085. [CrossRef] [PubMed]

24. Velasco, H.; Astorga, R.T.; Joseph, D.; Antoine, J.S.; Mabit, L.; Toloza, A.; Dercon, G.; Walling, D.E. Adapting the Caesium-137 technique to document soil redistribution rates associated with traditional cultivation practices in Haiti. *J. Environ. Radioact.* **2018**, *183*, 7–16. [CrossRef]

25. Schoonejans, J.; Vanacker, V.; Opfergelt, S.; Christl, M. Long-term soil erosion derived from in-situ [10]Be and inventories of meteoric [10]Be in deeply weathered soils in southern Brazil. *Chem. Geol.* **2017**, *466*, 380–388. [CrossRef]

26. Wilken, F.; Fiener, P.; Ketterer, M.; Meusburger, K.; Muhindo, D.I.; van Oost, K.; Doetterl, S. Assessing soil redistribution of forest and cropland sites in wet tropical Africa using [239+240]Pu fallout radionuclides. *Soil* **2021**, *7*, 399–414. [CrossRef]

27. Waroszewski, J.; Egli, M.; Brandová, D.; Christl, M.; Kabala, C.; Malkiewicz, M.; Kierczak, J.; Glina, B.; Jezierski, P. Identifying slope processes over time and their imprint in soils of medium-high mountains of Central Europe (the Karkonosze Mountains, Poland). *Earth Surf. Process. Landf.* **2018**, *43*, 1195–1212. [CrossRef]

28. Mabit, L.; Bernard, C.; Laverdière, M.R. Assessment of erosion in the Boyer River watershed (Canada) using a GIS oriented sampling strategy and ^{137}Cs measurements. *Catena* **2007**, *71*, 242–249. [CrossRef]

29. Mabit, L.; Chhem-Kieth, S.; Toloza, A.; Vanwalleghem, T.; Bernard, C.; Amate, J.I.; González de Molina, M.; Gómez, J.A. Radioisotopic and physicochemical background indicators to assess soil degradation affecting olive orchards in southern Spain. *Agric. Ecosyst. Environ.* **2012**, *159*, 70–80. [CrossRef]

30. Meliho, M.; Nouira, A.; Benmansour, M.; Boulmane, M.; Khattabi, A.; Mhammdi, N.; Benkdad, A. Assessment of soil erosion rates in a Mediterranean cultivated and uncultivated soils using fallout [137]Cs. *J. Environ. Radioact.* **2019**, *208–209*, 106021. [CrossRef]

31. Quijano, L.; Beguería, S.; Gaspar, L.; Navas, A. Estimating erosion rates using ^{137}Cs measurements and WATEM/SEDEM in a Mediterranean cultivated field. *Catena* **2016**, *138*, 38–51. [CrossRef]

32. Jelinski, N.A.; Campforts, B.; Willenbring, J.K.; Schumacher, T.E.; Li, S.; Lobb, D.A.; Papiernik, S.K.; Yoo, K. Meteoric Beryllium-10 as a Tracer of Erosion Due to Postsettlement Land Use in West-Central Minnesota, USA. *J. Geophys. Res. Earth Surf.* **2019**, *124*, 874–901. [CrossRef]

33. Calitri, F.; Sommer, M.; Norton, K.; Temme, A.; Brandová, D.; Portes, R.; Christl, M.; Ketterer, M.E.; Egli, M. Tracing the temporal evolution of soil redistribution rates in an agricultural landscape using [239+240]Pu and [10]Be. *Earth Surf. Process. Landf.* **2019**, *44*, 1783–1789. [CrossRef]

34. Calitri, F.; Sommer, M.; van der Meij, M.W.; Egli, M. Soil erosion along a transect in a forested catchment: Recent or ancient processes? *Catena* **2020**, *194*, 104683. [CrossRef]

35. Ouimet, W.; Dethier, D.; Bierman, P.; Wyshnytzky, C.; Shea, N.; Rood, D.H. Spatial and temporal variations in meteoric [10]Be inventories and long-term deposition rates, Colorado Front Range. *Quat. Sci. Rev.* **2015**, *109*, 1–12. [CrossRef]

36. Tuo, D.; Xu, M.; Gao, G. Relative contributions of wind and water erosion to total soil loss and its effect on soil properties in sloping croplands of the Chinese Loess Plateau. *Sci. Total Environ.* **2018**, *633*, 1032–1040. [CrossRef]

37. Jagercikova, M.; Cornu, S.; Bourlès, D.; Antoine, P.; Mayor, M.; Guillou, V. Understanding long-term soil processes using meteoric [10]Be: A first attempt on loessic deposits. *Quat. Geochronol.* **2015**, *27*, 11–21. [CrossRef]

38. Poręba, G.J.; Śnieszko, Z.; Moska, P. Application of OSL dating and ^{137}Cs measurements to reconstruct the history of water erosion: A case study of a Holocene colluvium in Świerklany, south Poland. *Quat. Int.* **2015**, *374*, 189–197. [CrossRef]

39. Zhang, X.; Quine, T.A.; Walling, D.E. Soil erosion rates on sloping cultivated land on the Loess Plateau near Ansai, Shaanxi Province, China: An investigation using ^{137}Cs and rill measurements. *Hydrol. Process.* **1998**, *12*, 171–189. [CrossRef]

40. Loba, A.; Waroszewski, J.; Tikhomirov, D.; Calitri, F.; Christl, M.; Sykuła, M.; Egli, M. Tracing erosion rates in loess landscape of the Trzebnica Hills (Poland) over time using fallout and cosmogenic nuclides. *J. Soils Sediments* **2021**, *21*, 2952–2968. [CrossRef]

41. Kaste, J.M.; Elmore, A.J.; Vest, K.R.; Okin, G.S. Groundwater controls on episodic soil erosion and dust emissions in a desert ecosystem. *Geology* **2016**, *44*, 771–774. [CrossRef]

42. Abrahams, E.R.; Kaste, J.M.; Ouimet, W.; Dethier, D.P. Asymmetric hillslope erosion following wildfire in Fourmile Canyon, Colorado. *Earth Surf. Process. Landf.* **2018**, *43*, 2009–2021. [CrossRef]

43. McKean, J.A.; Dietrich, W.E.; Finkel, R.C.; Southon, J.R.; Caffee, M.W. Quantification of soil production and downslope creep rates from cosmogenic [10]Be accumulations on a hillslope profile. *Geology* **1993**, *21*, 343–346. [CrossRef]

44. Small, E.E.; Anderson, R.S.; Hancock, G.S. Estimates of the rate of regolith production using [10]Be and [26]Al from an alpine hillslope. *Geomorphology* **1999**, *27*, 131–150. [CrossRef]

45. Jungers, M.C.; Bierman, P.R.; Matmon, A.; Nichols, K.; Larsen, J.; Finkel, R. Tracing hillslope sediment production and transport with in situ and meteoric [10]Be. *J. Geophys. Res. Earth Surf.* **2009**, *114*, 1–16. [CrossRef]

46. West, N.; Kirby, E.; Bierman, P.; Slingerland, R.; Ma, L.; Rood, D.; Brantley, S. Regolith production and transport at the Susquehanna Shale Hills Critical Zone Observatory, Part 2: Insights from meteoric [10]Be. *J. Geophys. Res. Earth Surf.* **2013**, *118*, 1877–1896. [CrossRef]

47. West, N.; Kirby, E.; Bierman, P.; Clarke, B.A. Aspect-dependent variations in regolith creep revealed by meteoric [10]Be. *Geology* **2014**, *42*, 507–510. [CrossRef]

48. Graly, J.A.; Bierman, P.R.; Reusser, L.J.; Pavich, M.J. Meteoric [10]Be in soil profiles—A global meta-analysis. *Geochim. Cosmochim. Acta* **2010**, *74*, 6814–6829. [CrossRef]

49. Alewell, C.; Pitois, A.; Meusburger, K.; Ketterer, M.; Mabit, L. [239+240]Pu from "contaminant" to soil erosion tracer: Where do we stand? *Earth-Sci. Rev.* **2017**, *172*, 107–123. [CrossRef]

50. McHargue, L.R.; Damon, P.E. The global beryllium 10 cycle. *Rev. Geophys.* **1991**, *29*, 141. [CrossRef]

51. Monaghan, M.C.; Krishnaswami, S.; Turekian, K.K. The global-average production rate of [10]Be. *Earth Planet. Sci. Lett.* **1986**, *76*, 279–287. [CrossRef]

52. Willenbring, J.K.; von Blanckenburg, F. Meteoric cosmogenic Beryllium-10 adsorbed to river sediment and soil: Applications for Earth-surface dynamics. *Earth-Sci. Rev.* **2010**, *98*, 105–122. [CrossRef]

53. Beer, J.; McCracken, K.; von Steiger, R. *Cosmogenic Radionuclides. Theory and Applications in the Terrestial and Space Environments*; Physics of Earth and Space Environments; Springer: Berlin/Heidelberg, Germany, 2012; Volume 53, ISBN 978-3-642-14650-3.

54. Kaste, J.M.; Baskaran, M. Meteoric [7]Be and [10]Be as Process Tracers in the Environment. In *Handbook of Environmental Isotope Geochemistry*; Baskaran, M., Ed.; Advances in Isotope Geochemistry; Springer: Berlin/Heidelberg, Germany, 2012; Volume 1, pp. 61–85, ISBN 978-3-642-10636-1.

55. Graly, J.A.; Reusser, L.J.; Bierman, P.R. Short and long-term delivery rates of meteoric [10]Be to terrestrial soils. *Earth Planet. Sci. Lett.* **2011**, *302*, 329–336. [CrossRef]

56. Kaste, J.M.; Norton, S.A.; Hess, C.T. Environmental Chemistry of Beryllium-7. *Rev. Mineral. Geochem.* **2002**, *50*, 271–289. [CrossRef]

57. Pavich, M.J.; Brown, L.; Valette-Silver, J.N.; Klein, J.; Middleton, R. [10]Be analysis of a Quaternary weathering profile in the Virginia Piedmont. *Geology* **1985**, *13*, 39. [CrossRef]

58. Boschi, V.; Willenbring, J.K. Chemical and physical drivers of beryllium retention in two soil endmembers. *Sci. Total Environ.* **2021**, *754*, 141591. [CrossRef] [PubMed]

59. You, C.-F.; Lee, T.; Li, Y.-H. The partition of Be between soil and water. *Chem. Geol.* **1989**, *77*, 105–118. [CrossRef]

60. Pavich, M.J.; Brown, L.; Harden, J.; Klein, J.; Middleton, R. [10]Be distribution in soils from Merced River terraces, California. *Geochim. Cosmochim. Acta* **1986**, *50*, 1727–1735. [CrossRef]

61. Vesely, J.; Norton, S.A.; Skrivan, P.; Majer, V.; Kram, P.; Navratil, T.; Kaste, J.M. Environmental Chemistry of Beryllium. *Rev. Mineral. Geochem.* **2002**, *50*, 291–317. [CrossRef]

62. Bacon, A.R.; Richter, D.D.B.; Bierman, P.R.; Rood, D.H. Coupling meteoric [10]Be with pedogenic losses of [9]Be to improve soil residence time estimates on an ancient North American interfluve. *Geology* **2012**, *40*, 847–850. [CrossRef]

63. Pavich, M.J.; Brown, L.; Klein, J.; Middleton, R. [10]Be accumulation in a soil chronosequence. *Earth Planet. Sci. Lett.* **1984**, *68*, 198–204. [CrossRef]

64. Takahashi, Y.; Minai, Y.; Ambe, S.; Makide, Y.; Ambe, F. Comparison of adsorption behavior of multiple inorganic ions on kaolinite and silica in the presence of humic acid using the multitracer technique. *Geochim. Cosmochim. Acta* **1999**, *63*, 815–836. [CrossRef]

65. Ritchie, J.C.; McHenry, J.R. Application of Radioactive Fallout Cesium-137 for Measuring Soil Erosion and Sediment Accumulation Rates and Patterns: A Review. *J. Environ. Qual.* **1990**, *19*, 215–233. [CrossRef]

66. Xu, Y.; Qiao, J.; Pan, S.; Hou, X.; Roos, P.; Cao, L. Plutonium as a tracer for soil erosion assessment in northeast China. *Sci. Total Environ.* **2015**, *511*, 176–185. [CrossRef]

67. Nelson, D.M.; Lovett, M.B. Oxidation state of plutonium in the Irish Sea. *Nature* **1978**, *276*, 599–601. [CrossRef]
68. Penrose, W.R.; Metta, D.N.; Hylko, J.M.; Rinckel, L.A. The reduction of plutonium(V) by aquatic sediments. *J. Environ. Radioact.* **1987**, *5*, 169–184. [CrossRef]
69. Choppin, G.R. Actinide speciation in aquatic systems. *Mar. Chem.* **2006**, *99*, 83–92. [CrossRef]
70. Eakins, J.D.; Morgan, A.; Baston, G.M.N.; Pratley, F.W.; Strange, L.P.; Burton, P.J. Measurements of α-emitting plutonium and americium in the intertidal sands of West Cumbria, UK. *J. Environ. Radioact.* **1990**, *11*, 37–54. [CrossRef]
71. Iurian, A.-R.; Phaneuf, M.O.; Mabit, L. Mobility and Bioavailability of Radionuclides in Soils. In *Radionuclides in the Environment. Influence of Chemical Speciation and Plant Uptake on Radionuclide Migration*; Springer: Cham, Switzerland, 2015; pp. 38–59.
72. Kim, C.S.; Lee, M.H.; Kim, C.K.; Kim, K.H. ^{90}Sr, ^{137}Cs, $^{239+240}$Pu and ^{238}Pu concentrations in surface soils of Korea. *J. Environ. Radioact.* **1998**, *40*, 75–88. [CrossRef]
73. Chibowski, S.; Zygmunt, J. The influence of the sorptive properties of organic soils on the migration rate of ^{137}Cs. *J. Environ. Radioact.* **2002**, *61*, 213–223. [CrossRef]
74. Giannakopoulou, F.; Haidouti, C.; Chronopoulou, A.; Gasparatos, D. Sorption behavior of cesium on various soils under different pH levels. *J. Hazard. Mater.* **2007**, *149*, 553–556. [CrossRef] [PubMed]
75. Livens, F.R.; Loveland, P.J. The influence of soil properties on the environmental mobility of caesium in Cumbria. *Soil Use Manag.* **1988**, *4*, 69–75. [CrossRef]
76. Kabata-Pendias, A.; Mukherjee, A.B. (Eds.) *Trace Elements of Group 1 (Previously Group Ia) BT—Trace Elements from Soil to Human*; Springer: Berlin/Heidelberg, Germany, 2007; pp. 87–104, ISBN 978-3-540-32714-1.
77. Tamura, T.; Jacobs, D.G. Structural implications in cesium sorption. *Health Phys.* **1960**, *2*, 391—398. [CrossRef] [PubMed]
78. Bertsch, P.M. Cesium-137 in floodplain sediments of the Lower Three Runs Creek on the DOE Savannah River Site. *J. Radioanal. Nucl. Chem.* **2005**, *264*, 481–488. [CrossRef]
79. García-Oliva, F.; Lugo, R.M.; Maass, J.M. Soil ^{137}Cs activity in a tropical deciduous ecosystem under pasture conversion in Mexico. *J. Environ. Radioact.* **1995**, *26*, 37–49. [CrossRef]
80. Van Bergeijk, K.E.; Noordijk, H.; Lembrechts, J.; Frissel, M.J. Influence of pH, soil type and soil organic matter content on soil-to-plant transfer of radiocesium and -strontium as analyzed by a nonparametric method. *J. Environ. Radioact.* **1992**, *15*, 265–276. [CrossRef]
81. Matisoff, G.; Whiting, P.J. Measuring Soil Erosion Rates Using Natural (^{7}Be, ^{210}Pb) and Anthropogenic (^{137}Cs, ^{239,240}Pu) Radionuclides. In *Handbook of Environmental Isotope Geochemistry*; Springer: Berlin/Heidelberg, Germany, 2012; Volume 1–2, pp. 487–519, ISBN 9783642106378.
82. Sanchez, A.L.; Wright, S.M.; Smolders, E.; Naylor, C.; Stevens, P.A.; Kennedy, V.H.; Dodd, B.A.; Singleton, D.L.; Barnett, C.L. High Plant Uptake of Radiocesium from Organic Soils Due to Cs Mobility and Low Soil K Content. *Environ. Sci. Technol.* **1999**, *33*, 2752–2757. [CrossRef]
83. Sheppard, S.C. Robust Prediction of Kd from Soil Properties for Environmental Assessment. *Hum. Ecol. Risk Assess. Int. J.* **2011**, *17*, 263–279. [CrossRef]
84. Wissocq, A.; Beaucaire, C.; Latrille, C. Application of the multi-site ion exchanger model to the sorption of Sr and Cs on natural clayey sandstone. *Appl. Geochem.* **2018**, *93*, 167–177. [CrossRef]
85. Siroux, B.; Beaucaire, C.; Tabarant, M.; Benedetti, M.F.; Reiller, P.E.; Wissocq, A.; Beaucaire, C.; Latrille, C. Adsorption of strontium and caesium onto an Na-MX80 bentonite: Experiments and building of a coherent thermodynamic modelling. *Appl. Geochem.* **2018**, *93*, 167–175. [CrossRef]
86. Nishiizumi, K.; Imamura, M.; Caffee, M.W.; Southon, J.R.; Finkel, R.C.; McAninch, J. Absolute calibration of ^{10}Be AMS standards. *Nucl. Instrum. Methods Phys. Res. Sect. B Beam Interact. Mater. At.* **2007**, *258*, 403–413. [CrossRef]
87. Harden, J.W.; Fries, T.L.; Pavich, M.J. Cycling of beryllium and carbon through hillslope soils in Iowa. *Biogeochemistry* **2002**, *60*, 317–336. [CrossRef]
88. Knudsen, M.F.; Egholm, D.L.; Jansen, J.D. Time-integrating cosmogenic nuclide inventories under the influence of variable erosion, exposure, and sediment mixing. *Quat. Geochronol.* **2019**, *51*, 110–119. [CrossRef]
89. Meusburger, K.; Mabit, L.; Ketterer, M.; Park, J.H.; Sandor, T.; Porto, P.; Alewell, C. A multi-radionuclide approach to evaluate the suitability of $^{239+240}$Pu as soil erosion tracer. *Sci. Total Environ.* **2016**, *566–567*, 1489–1499. [CrossRef]
90. Mabit, L.; Martin, P.; Jankong, P.; Toloza, A.; Padilla-Alvarez, R.; Zupanc, V. Establishment of control site baseline data for erosion studies using radionuclides: A case study in East Slovenia. *J. Environ. Radioact.* **2010**, *101*, 854–863. [CrossRef]
91. Lal, D. New Nuclear Methods for Studies of Soil Dynamics Utilizing Cosmic Ray Produced Radionuclides. In *Sustaining the Global Farm-10th International Soil Conservation Organization Meeting*; Stott, D.E., Mohtar, R.H., Steinhardt, G.C., Eds.; Purdue University: West Lafayette, IN, USA; USDA-ARS National Soil Erosion Research Laboratory: Washington, DC, USA, 2001; pp. 1044–1052.
92. Campforts, B.; Vanacker, V.; Vanderborght, J.; Baken, S.; Smolders, E.; Govers, G. Simulating the mobility of meteoric ^{10}Be in the landscape through a coupled soil-hillslope model (Be2D). *Earth Planet. Sci. Lett.* **2016**, *439*, 143–157. [CrossRef]
93. Owens, P.N.; Walling, D.E. Spatial variability of caesium-137 inventories at reference sites: An example from two contrasting sites in England and Zimbabwe. *Appl. Radiat. Isot.* **1996**, *47*, 699–707. [CrossRef]
94. Sutherland, R.A. Examination of caesium-137 areal activities in control (uneroded) locations. *Soil Technol.* **1991**, *4*, 33–50. [CrossRef]

95. Poręba, G.; Śnieszko, Z.; Moska, P.; Mroczek, P.; Malik, I. Interpretation of soil erosion in a Polish loess area using OSL, ^{137}Cs, [210]Pbex, dendrochronology and micromorphology—Case study: Biedrzykowice site (s Poland). *Geochronometria* **2019**, *46*, 57–78. [CrossRef]

96. Sarmiento, J.L.; Gwinn, E. Strontium 90 fallout prediction. *J. Geophys. Res.* **1986**, *91*, 7631. [CrossRef]

97. Poreba, G.J. Caesium-137 as a soil erosion tracer: A review. *Geochronometria* **2006**, *25*, 37–46.

98. Walling, D.E.; Quine, T.A. Calibration of caesium-137 measurements to provide quantitative erosion rate data. *Land Degrad. Dev.* **1990**, *2*, 161–175. [CrossRef]

99. Kachanoski, R.G.; de Jong, E. Predicting the Temporal Relationship between Soil Cesium-137 and Erosion Rate. *J. Environ. Qual.* **1984**, *13*, 301–304. [CrossRef]

100. Zhang, X.; Higgit, D.L.; Walling, D.E. A preliminary assessment of the potential for using caesium-137 to estimate rates of soil erosion in the Loess Plateau of China. *Hydrol. Sci. J.* **1990**, *35*, 243–252. [CrossRef]

101. Walling, D.E.; He, Q. Improved Models for Estimating Soil Erosion Rates from Cesium-137 Measurements. *J. Environ. Qual.* **1999**, *28*, 611–622. [CrossRef]

102. He, Q.; Walling, D.E. The distribution of fallout ^{137}Cs and ^{210}Pb in undisturbed and cultivated soils. *Appl. Radiat. Isot.* **1997**, *48*, 677–690. [CrossRef]

103. Owens, P.N.; Walling, D.E. The use of a numerical mass-balance model to estimate rates of soil redistribution on uncultivated land from ^{137}Cs measurements. *J. Environ. Radioact.* **1998**, *40*, 185–203. [CrossRef]

104. Van Oost, K.; Govers, G.; Van Muysen, W. A process-based conversion model for caesium-137 derived erosion rates on agricultural land: An integrated spatial approach. *Earth Surf. Process. Landf.* **2003**, *28*, 187–207. [CrossRef]

105. Mietelski, J.W.; Was, B. Plutonium from Chernobyl in Poland. *Appl. Radiat. Isot.* **1995**, *46*, 1203–1211. [CrossRef]

106. Ketterer, M.E.; Zheng, J.; Yamada, M. Applications of Transuranics as Tracers and Chronometers in the Environment. In *Handbook of Environmental Isotope Geochemistry*; Springer: Berlin/Heidelberg, Germany, 2012; Volume 1–2, pp. 395–417, ISBN 9783642106378.

107. Zheng, J.; Tagami, K.; Watanabe, Y.; Uchida, S.; Aono, T.; Ishii, N.; Yoshida, S.; Kubota, Y.; Fuma, S.; Ihara, S. Isotopic evidence of plutonium release into the environment from the Fukushima DNPP accident. *Sci. Rep.* **2012**, *2*, 304. [CrossRef]

108. Kelley, J.M.; Bond, L.A.; Beasley, T.M. Global distribution of Pu isotopes and [237]Np. *Sci. Total Environ.* **1999**, *237–238*, 483–500. [CrossRef]

109. Ketterer, M.E.; Hafer, K.M.; Link, C.L.; Kolwaite, D.; Wilson, J.; Mietelski, J.W. Resolving global versus local/regional Pu sources in the environment using sector ICP-MS. *J. Anal. At. Spectrom.* **2004**, *19*, 241–245. [CrossRef]

110. Mabit, L.; Benmansour, M.; Walling, D.E. Comparative advantages and limitations of the fallout radionuclides ^{137}Cs, [210]Pbex and [7]Be for assessing soil erosion and sedimentation. *J. Environ. Radioact.* **2008**, *99*, 1799–1807. [CrossRef] [PubMed]

111. Mabit, L.; Dercon, G.; Benmansour, M.; Walling, D.E. Use of ^{137}Cs,[210]Pbex and [7]Be for documenting soil redistribution: The future. In *Guidelines for Using Fallout Radionuclides to Assess Erosion and Effectiveness of Soil Conservation Strategies*; IAEA-TECDOC-1741; IAEA: Vienna, Austria, 2014; pp. 203–208, ISBN 978–92–0–105414–2.

112. Pennock, D.J.; Lemmen, D.S.; De Jong, E. Cesium-137-measured erosion rates for soils of five parent-material groups in southwestern Saskatchewan. *Can. J. Soil Sci.* **1995**, *75*, 205–210. [CrossRef]

113. Monaghan, M.C.; Krishnaswami, S.; Thomas, J.H. [10]Be concentrations and the long-term fate of particle-reactive nuclides in five soil profiles from California. *Earth Planet. Sci. Lett.* **1983**, *65*, 51–60. [CrossRef]

114. Van Pelt, R.S.; Zobeck, T.M.; Ritchie, J.C.; Gill, T.E. Validating the use of ^{137}Cs measurements to estimate rates of soil redistribution by wind. *Catena* **2007**, *70*, 455–464. [CrossRef]

115. Schuller, P.; Walling, D.; Sepúlveda, A.; Trumper, R.; Rouanet, J.; Pino, I.; Castillo, A. Use of ^{137}Cs measurements to estimate changes in soil erosion rates associated with changes in soil management practices on cultivated land. *Appl. Radiat. Isot.* **2004**, *60*, 759–766. [CrossRef]

116. Evans, R.; Collins, A.L.; Zhang, Y.; Foster, I.D.L.; Boardman, J.; Sint, H.; Lee, M.R.F.; Griffith, B.A. A comparison of conventional and ^{137}Cs-based estimates of soil erosion rates on arable and grassland across lowland England and Wales. *Earth-Sci. Rev.* **2017**, *173*, 49–64. [CrossRef]

117. Quijano, L.; Gaspar, L.; Navas, A. Spatial patterns of SOC, SON, ^{137}Cs and soil properties as affected by redistribution processes in a Mediterranean cultivated field (Central Ebro Basin). *Soil Tillage Res.* **2016**, *155*, 318–328. [CrossRef]

118. Benmansour, M.; Mabit, L.; Nouira, A.; Moussadek, R.; Bouksirate, H.; Duchemin, M.; Benkdad, A. Assessment of soil erosion and deposition rates in a Moroccan agricultural field using fallout ^{137}Cs and [210]Pbex. *J. Environ. Radioact.* **2013**, *115*, 97–106. [CrossRef]

119. Porto, P.; Callegari, G. Using ^{137}Cs measurements to estimate soil erosion rates in forest stands affected by wildfires. Results from plot experiments. *Appl. Radiat. Isot.* **2021**, *172*, 109668. [CrossRef]

120. Saç, M.M.; İçhedef, M. Application of ^{137}Cs technique for evaluation of erosion and deposition rates within cultivated fields of Salihli region, Western Turkey. *J. Radiat. Res. Appl. Sci.* **2015**, *8*, 477–482. [CrossRef]

121. Zhang, W.; Xing, S.; Hou, X. Evaluation of soil erosion and ecological rehabilitation in Loess Plateau region in Northwest China using plutonium isotopes. *Soil Tillage Res.* **2019**, *191*, 162–170. [CrossRef]

122. Zhang, K.; Pan, S.; Liu, Z.; Li, G.; Xu, Y.; Hao, Y. Vertical distributions and source identification of the radionuclides [239]Pu and [240]Pu in the sediments of the Liao River estuary, China. *J. Environ. Radioact.* **2018**, *181*, 78–84. [CrossRef]

123. Li, M.; Li, Z.; Liu, P.; Yao, W. Using Cesium-137 technique to study the characteristics of different aspect of soil erosion in the Wind-water Erosion Crisscross Region on Loess Plateau of China. *Appl. Radiat. Isot.* **2005**, *62*, 109–113. [CrossRef] [PubMed]
124. Gharibreza, M.; Zaman, M.; Porto, P.; Fulajtar, E.; Parsaei, L.; Eisaei, H. Assessment of deforestation impact on soil erosion in loess formation using ^{137}Cs method (case study: Golestan Province, Iran). *Int. Soil Water Conserv. Res.* **2020**, *8*, 393–405. [CrossRef]
125. Hua-juni, F.; Xue-ming, Y.; Xiao-ping, Z.; Ai-zhenl, L. Using [137]Cs Tracer Technique to Evaluate Erosion and Deposition of Black Soil in Northeast China. *Pedosphere* **2006**, *16*, 201–209.
126. Yang, M.-Y.; Tian, J.-L.; Liu, P.-L. Investigating the spatial distribution of soil erosion and deposition in a small catchment on the Loess Plateau of China, using [137]Cs. *Soil Tillage Res.* **2006**, *87*, 186–193. [CrossRef]
127. Fifield, L.K.; Wasson, R.J.; Pillans, B.; Stone, J.O.H. The longevity of hillslope soil in SE and NW Australia. *Catena* **2010**, *81*, 32–42. [CrossRef]
128. Hoo, W.T.; Fifield, L.K.; Tims, S.G.; Fujioka, T.; Mueller, N. Using fallout plutonium as a probe for erosion assessment. *J. Environ. Radioact.* **2011**, *102*, 937–942. [CrossRef]
129. Arata, L.; Alewell, C.; Frenkel, E.; A'Campo-Neuen, A.; Iurian, A.R.; Ketterer, M.E.; Mabit, L.; Meusburger, K. Modelling Deposition and Erosion rates with RadioNuclides (MODERN)—Part 2: A comparison of different models to convert [239+240]Pu inventories into soil redistribution rates at unploughed sites. *J. Environ. Radioact.* **2016**, *162–163*, 97–106. [CrossRef] [PubMed]
130. Musso, A.; Ketterer, M.E.; Greinwald, K.; Geitner, C.; Egli, M. Rapid decrease of soil erosion rates with soil formation and vegetation development in periglacial areas. *Earth Surf. Process. Landforms* **2020**, *45*, 2824–2839. [CrossRef]
131. Schmidt, S.; Alewell, C.; Meusburger, K. Monthly RUSLE soil erosion risk of Swiss grasslands. *J. Maps* **2019**, *15*, 247–256. [CrossRef]
132. Lu, H.; Prosser, I.P.; Moran, C.J.; Gallant, J.C.; Priestley, G.; Stevenson, J.G. Predicting sheetwash and rill erosion over the Australian continent. *Soil Res.* **2003**, *41*, 1037. [CrossRef]
133. Panagos, P.; Borrelli, P.; Poesen, J.; Ballabio, C.; Lugato, E.; Meusburger, K.; Montanarella, L.; Alewell, C. The new assessment of soil loss by water erosion in Europe. *Environ. Sci. Policy* **2015**, *54*, 438–447. [CrossRef]
134. Fu, B.; Liu, Y.; Lü, Y.; He, C.; Zeng, Y.; Wu, B. Assessing the soil erosion control service of ecosystems change in the Loess Plateau of China. *Ecol. Complex.* **2011**, *8*, 284–293. [CrossRef]
135. Yang, X.M.; Zhang, X.P.; Deng, W.; Fang, H.J. Black soil degradation by rainfall erosion in Jilin, China. *Land Degrad. Dev.* **2003**, *14*, 409–420. [CrossRef]
136. Borrelli, P.; Robinson, D.A.; Fleischer, L.R.; Lugato, E.; Ballabio, C.; Alewell, C.; Meusburger, K.; Modugno, S.; Schütt, B.; Ferro, V.; et al. An assessment of the global impact of 21st century land use change on soil erosion. *Nat. Commun.* **2017**, *8*, 2013. [CrossRef]
137. Sun, W.; Shao, Q.; Liu, J.; Zhai, J. Assessing the effects of land use and topography on soil erosion on the Loess Plateau in China. *Catena* **2014**, *121*, 151–163. [CrossRef]
138. Ayt Ougougdal, H.; Khebiza, M.Y.; Messouli, M.; Bounoua, L.; Karmaoui, A. Delineation of vulnerable areas to water erosion in a mountain region using SDR-InVEST model: A case study of the Ourika watershed, Morocco. *Sci. Afr.* **2020**, *10*, e00646. [CrossRef]
139. Sheikh, V.; Kornejady, A.; Ownegh, M. Application of the coupled TOPSIS–Mahalanobis distance for multi-hazard-based management of the target districts of the Golestan Province, Iran. *Nat. Hazards* **2019**, *96*, 1335–1365. [CrossRef]
140. Fülöp, R.H.; Bishop, P.; Fabel, D.; Cook, G.T.; Everest, J.; Schnabel, C.; Codilean, A.T.; Xu, S. Quantifying soil loss with in-situ cosmogenic[10]Be and ^{14}C depth-profiles. *Quat. Geochronol.* **2015**, *27*, 78–93. [CrossRef]
141. Arnhold, S.; Lindner, S.; Lee, B.; Martin, E.; Kettering, J.; Nguyen, T.T.; Koellner, T.; Ok, Y.S.; Huwe, B. Conventional and organic farming: Soil erosion and conservation potential for row crop cultivation. *Geoderma* **2014**, *219–220*, 89–105. [CrossRef]
142. Meusburger, K.; Konz, N.; Schaub, M.; Alewell, C. Soil erosion modelled with USLE and PESERA using QuickBird derived vegetation parameters in an alpine catchment. *Int. J. Appl. Earth Obs. Geoinf.* **2010**, *12*, 208–215. [CrossRef]
143. Meusburger, K.; Evrard, O.; Alewell, C.; Borrelli, P.; Cinelli, G.; Ketterer, M.; Mabit, L.; Panagos, P.; van Oost, K.; Ballabio, C. Plutonium aided reconstruction of caesium atmospheric fallout in European topsoils. *Sci. Rep.* **2020**, *10*, 11858. [CrossRef]
144. Arata, L.; Meusburger, K.; Frenkel, E.; A'Campo-Neuen, A.; Iurian, A.R.; Ketterer, M.E.; Mabit, L.; Alewell, C. Modelling Deposition and Erosion rates with RadioNuclides (MODERN)—Part 1: A new conversion model to derive soil redistribution rates from inventories of fallout radionuclides. *J. Environ. Radioact.* **2016**, *162–163*, 45–55. [CrossRef]
145. Schaub, M.; Konz, N.; Meusburger, K.; Alewell, C. Application of in-situ measurement to determine ^{137}Cs in the Swiss Alps. *J. Environ. Radioact.* **2010**, *101*, 369–376. [CrossRef]
146. Evrard, O.; Vandaele, K.; van Wesemael, B.; Bielders, C.L. A grassed waterway and earthen dams to control muddy floods from a cultivated catchment of the Belgian loess belt. *Geomorphology* **2008**, *100*, 419–428. [CrossRef]
147. Haase, D.; Fink, J.; Haase, G.; Ruske, R.; Pécsi, M.; Richter, H.; Altermann, M.; Jäger, K.D. Loess in Europe-its spatial distribution based on a European Loess Map, scale 1:2,500,000. *Quat. Sci. Rev.* **2007**, *26*, 1301–1312. [CrossRef]
148. Šimanský, V.; Juriga, M.; Mendyk, Ł. Slope position and management practices as factors influencing selected properties of topsoil. *Soil Sci. Annu.* **2019**, *70*, 137–146. [CrossRef]
149. Licznar, M.; Kowaliński, S.; Drozd, J. Changes of some physical properties of soils of the głubczyce plateau under the water erosion effect. *Rocz. Glebozn.* **1981**, *XXXII*, 45–52.
150. Poręba, G.; Śnieszko, Z.; Moska, P. Some aspects of age assessment of Holocene loess colluvium: OSL and ^{137}Cs dating of sediment from Biała agricultural area, South Poland. *Quat. Int.* **2011**, *240*, 44–51. [CrossRef]

151. Zhang, J.; Yang, M.; Sun, X.; Zhang, F. Estimation of wind and water erosion based on slope aspects in the crisscross region of the Chinese Loess Plateau. *J. Soils Sediments* **2018**, *18*, 1620–1631. [CrossRef]
152. Aldahan, A.; Haiping, Y.; Possnert, G. Distribution of beryllium between solution and minerals (biotite and albite) under atmospheric conditions and variable pH. *Chem. Geol.* **1999**, *156*, 209–229. [CrossRef]

UNIWERSYTET
PRZYRODNICZY
WE WROCŁAWIU

Wrocław, 13.10.2022

Mgr inż. Aleksandra Loba
Instytut Nauk o Glebie, Żywienia Roślin
i Ochrony Środowiska
Uniwersytet Przyrodniczy we Wrocławiu

Oświadczenie

Oświadczam, że w pracy: Loba A., Waroszewski J., Sykuła M., Kabała C., Egli M., 2021. *Meteoric ^{10}Be, ^{137}Cs and $^{239+240}Pu$ as tracers of long- and medium-term soil erosion — A review*. Minerals, 12, 359 (doi:10.3390/min12030359) mój udział polegał na wyborze analizowanych prac naukowych, opracowaniu merytorycznym uzyskanych danych oraz przygotowaniu treści manuskryptu.

....
(podpis)

Wrocław, 20.10.2022

Dr hab. inż. Jarosław Waroszewski, prof. UPWr
Instytut Nauk o Glebie, Żywienia Roślin
i Ochrony Środowiska
Uniwersytet Przyrodniczy we Wrocławiu

Oświadczenie

Oświadczam, że w pracy: Loba A., Waroszewski J., Sykuła M., Kabała C., Egli M., 2021. *Meteoric ^{10}Be, ^{137}Cs and $^{239+240}Pu$ as tracers of long- and medium-term soil erosion — A review*. Minerals, 12, 359 (doi:10.3390/min12030359) mój udział polegał na nadzorowaniu przy opracowaniu założeń prowadzonych badań literaturowych. Nadzór merytoryczny obejmował także poprawność interpretacji wyników oraz przygotowanie treści manuskryptu.

…………………………………..
(podpis)

UNIWERSYTET
MIKOŁAJA KOPERNIKA
W TORUNIU

Toruń, 18.10.2022

Dr Marcin Sykuła
Katedra Gleboznawstwa
i Kształtowania Krajobrazu
Uniwersytet Mikołaja Kopernika
w Toruniu

Oświadczenie

Oświadczam, że w pracy: Loba A., Waroszewski J., Sykuła M., Kabała C., Egli M., 2021. *Meteoric* ^{10}Be, ^{137}Cs *and* $^{239+240}Pu$ *as tracers of long- and medium-term soil erosion — A review*. Minerals, 12, 359 (doi:10.3390/min12030359) mój udział polegał na graficznym opracowaniu wyników badań i sprawdzeniu finalnej wersji manuskryptu.
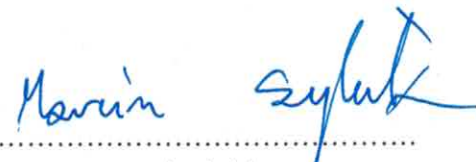
(podpis)

Wrocław, 24.10.2022

Prof. dr hab. inż. Cezary Kabała
Instytut Nauk o Glebie, Żywienia Roślin
i Ochrony Środowiska
Uniwersytet Przyrodniczy we Wrocławiu

Oświadczenie

Oświadczam, że w pracy: Loba A., Waroszewski J., Sykuła M., Kabała C., Egli M., 2021. *Meteoric ^{10}Be, ^{137}Cs and $^{239+240}Pu$ as tracers of long- and medium-term soil erosion — A review*. Minerals, 12, 359 (doi:10.3390/min12030359) mój udział polegał na nadzorowaniu poprawności interpretacji wyników oraz przygotowania treści manuskryptu.

....
(podpis)

Zürich, 24th of October 2022

Prof. Dr. Markus Egli
Department of Geography
University of Zurich

Oświadczenie/Statement

Oświadczam, że w pracy: Loba A., Waroszewski J., Sykuła M., Kabała C., Egli M., 2021. *Meteoric ^{10}Be, ^{137}Cs and $^{239+240}Pu$ as tracers of long- and medium-term soil erosion — A review*. Minerals, 12, 359 (doi:10.3390/min12030359) mój udział polegał na nadzorowaniu przy opracowaniu założeń prowadzonych badań literaturowych. Nadzór merytoryczny obejmował także poprawność interpretacji wyników oraz przygotowanie treści manuskryptu.

I declare that in the paper: Loba A., Waroszewski J., Sykuła M., Kabała C., Egli M., 2021. *Meteoric ^{10}Be, ^{137}Cs and $^{239+240}Pu$ as tracers of long- and medium-term soil erosion — A review*. Minerals, 12, 359 (doi:10.3390/min12030359) my participation consisted in the supervision and guidance of the literature study. This supervision also included the correctness of the interpretation of the results and the preparation of content of the manuscript.

……………………………………
(podpis/signature)

SOILS, SEC 5 · SOIL AND LANDSCAPE ECOLOGY · RESEARCH ARTICLE

Tracing erosion rates in loess landscape of the Trzebnica Hills (Poland) over time using fallout and cosmogenic nuclides

Aleksandra Loba[1] · Jarosław Waroszewski[1] · Dmitry Tikhomirov[2] · Fancesca Calitri[2,3] · Marcus Christl[4] · Marcin Sykuła[5] · Markus Egli[2]

Abstract

Purpose Loess landscapes are highly susceptible to soil erosion, which affects soil stability and productivity. Erosion is non-linear in time and space and determines whether soils form or degrade. While the spatial variability of erosion is often assessed by either modelling or on-site measurements, temporal trends over decades to millennia are very often lacking. In this study, we determined long- and short-term erosion rates to trace the dynamics of loess deposits in south-western Poland.
Materials and methods We quantified long-term (millennial) erosion rates using cosmogenic (in situ ^{10}Be) and short-term (decadal) rates with fallout radionuclides ($^{239+240}$Pu). Erosion processes were studied in two slope-soil transects (12 soil pits) with variable erosion features. As a reference site, an undisturbed soil profile under natural forest was sampled.
Results and discussion The long-term erosion rates ranged between 0.44 and 0.85 t ha^{-1} year^{-1}, whereas the short-term erosion rates varied from 1.2 to 10.9 t ha^{-1} year^{-1} and seem to be reliable. The short-term erosion rates are up to 10 times higher than the long-term rates. The soil erosion rates are quite consistent with the terrain relief, with erosion increasing in the steeper slope sections and decreasing in the lower parts of the slope, while still maintaining high values.
Conclusions Soil erosion rates have increased during the last few decades owing to agriculture intensification and probably climate change. The measured values lie far above tolerable erosion rates, and the soils were found to be strongly imbalanced and exhibit a drastic shallowing of the productive soils horizons.

Keywords Soil erosion · In situ ^{10}Be · $^{239+240}$Pu · Loess landscape · Radionuclides

✉ Aleksandra Loba
aleksandra.loba@upwr.edu.pl

[1] Institute of Soil Science and Environmental Protection, Wroclaw University of Environmental and Life Sciences, Grunwaldzka 53, 50-357 Wroclaw, Poland

[2] Department of Geography, University of Zurich, 8057 Zurich, Switzerland

[3] Leibniz-Centre for Agricultural Landscape Research (ZALF), Eberswalder Straße 84, 15374 Muncheberg, Germany

[4] Laboratory of Ion Beam Physics, ETH-Zurich, 8093 Zurich, Switzerland

[5] Department of Soil Science and Landscape Management, Nicolaus Copernicus University in Toruń, Lwowska Str. 1, 87-100 Torun, Poland

1 Introduction

The increase in soil erosion is a direct consequence of agricultural exploitation and threatens soil stability, quality and its productivity (Rickson 2014; Guzmán et al. 2015; Alewell et al. 2017; Golosov et al. 2021). Long-term and intense erosion removes topsoil from the upper part of a slope and deposits the eroded material at the toe of the slope, thus leading to irreversible changes in the natural structure of those soils and their corresponding horizons (Świtoniak et al. 2016; Zádorová and Penížek 2018; Golosov et al. 2021). One of the materials most susceptible to erosion are loess deposits (Licznar et al. 1981; Yang et al. 2006; Zhang et al. 2018; Poręba et al. 2019). Loess materials are widely distributed across the world (Muhs 2013; Schaetzl and Attig 2013; Pasquini et al. 2017). In Europe, the most extensive deposits on Earth cover an area from France to Russia, having developed during the Last Glacial period (Haase et al. 2007; Lehmkuhl et al. 2020). Productive soils have

developed on the loess, including Chernozems, Pheozems and Luvisols (Altermann et al. 2005; Gerlach et al. 2012; Labaz et al. 2018; Kabała et al. 2019; Loba et al. 2020). As a consequence, since the Neolithic period, loess areas have been deforested and transformed into arable lands, which has given rise to intense soil erosion processes (Altermann et al. 2005; Gerlach et al. 2012; Poręba et al. 2019).

So far, ^{137}Cs has predominantly been used as the isotope tracer for soil erosion in loess landscapes (Yang et al. 2006; Poręba et al. 2011, 2015, 2019). ^{137}Cs is a fallout radionuclide (FRN) that is distributed globally as a result of, for example, nuclear weapons testing in the 1960s and nuclear power plant accidents, and so it enables the investigation of erosion rates over the last few decades (Alewell et al. 2014, 2017; Zollinger et al. 2015; Meusburger et al. 2016). However, it is characterised by a short half-life of 30.17 year, and recent estimations have indicated that more than 70% of the global ^{137}Cs has disappeared due to its radioactive decay (Xu et al. 2015). At sites exhibiting erosion and a subsequent additional loss of ^{137}Cs, its detectability becomes increasingly difficult. Moreover, the Chernobyl accident in 1986 caused a spatially inhomogeneous distribution of ^{137}Cs in Central and Western Europe, which has caused some limitations in its application (Arata et al. 2016a; Alewell et al. 2017). As a result, $^{239+240}$Pu isotopes are currently more often used due to their longer half-lives (24,110 and 6561 years, respectively) and because Pu is absent from the volatile fraction released by the reactor accident of Chernobyl (Arata et al. 2016a).

Long-term erosion rates (over several millennia) can be determined using cosmogenic nuclides, such as ^{10}Be (Hidy et al. 2010; Zollinger et al. 2015; Calitri et al. 2019). Based on their origin, two types of ^{10}Be are distinguished: (1) meteoric ^{10}Be, which is constantly produced in the upper atmosphere by the spallation of nitrogen and oxygen by cosmic rays and is deposited at the Earth's surface by rainfall (Graly et al. 2010; Willenbring and von Blanckenburg 2010; Wyshnytzky et al. 2015), and (2) in situ ^{10}Be, which is directly produced in the crystal lattice of quartz by the interaction of cosmogenic rays (Hidy et al. 2010). For loess landscapes, there is a lack of studies using meteoric or in situ ^{10}Be to determine denudation rates. Meteoric ^{10}Be has been applied to studying palaeoclimatic variations (Gu et al. 1997; Zhou et al. 2015), estimating palaeoprecipitation (Sartori et al. 2005), establishing time scales for loess deposition (Chengde et al. 1992) and in tracking the translocation of ^{10}Be in Luvisols (Jagercikova et al. 2015). In most cases, ^{10}Be and $^{239+240}$Pu or ^{137}Cs have been used separately for calculating erosion rates (Arata et al. 2016a; Waroszewski et al. 2018; Musso et al. 2020). Recent studies, however, have combined these two types of isotopes to compare medium- and long-term erosion rates.

For instance, Zollinger et al. (2015), Calitri et al. (2019) and Jelinski et al. (2019) applied both types of isotopes to compare erosion processes for the last 50–60 years with long-term rates in order to crystallise the effects of anthropogenic pressures and climate change on soil processes.

In this study, we made a first attempt to apply in situ ^{10}Be and $^{239+240}$Pu to quantify soil erosion in a loess landscape, with special focus on (1) documenting long- and short-term erosion rates, (2) cross-checking recent and past erosion rates to determine how much erosive processes have intensified in recent decades and (3) verifying whether isotopic methods are suitable tools for studying erosion processes in the south-western Polish loess belt.

2 Study area

The investigation area was located in the Trzebnica Hills, south-western Poland (Fig. 1). The subglacial glaciotectonic disturbances in this region are estimated to have come from the Odra Glaciation (Saalian–Drenthe, marine isotope stage [MIS] 8/6) (Krzyszkowski 1993; Jary 1996). In general, the local geology is dominated by Quaternary deposits (loess, glacial till, fluvioglacial sediments), but Neogene deposits (clays, sands and gravels) occur locally in small areas (Pachucki 1952; Dyjor 1970; Dyjor and Kościówko 1982; Jary 1996). Loess, which is the youngest deposit, is distributed across the Trzebnica Hills as a layer with varying thickness (Jary 1996). The outcrop in Zaprężyn provides a record of loess dynamics and pedogenesis from the Last Interglacial (Eemian, MIS 5e) to the Upper Pleniweichselian (MIS2) (Jary and Ciszek 2013).

The soils in this region, mostly developed from the loess deposits, are characterised by subsoil clay illuviation (Luvisols) or the presence of a dark humic topsoil (Chernozems and Pheozems) (Licznar et al. 1988; Licznar and Licznar 2002; Zmuda et al. 2009; Kabała and Marzec 2010; Glina et al. 2014) and have been affected by denudation processes due to agricultural use since the Neolithic period (Poręba et al. 2011).

The native vegetation is represented by oak-hornbeam forest, although most of the land is used for agriculture due to the productivity of the soils (Anioł-Kwiatkowska 1998). The main crops cultivated are wheat, beetroot and corn. According to the Köppen–Geiger climate classification, the Trzebnica Hills experience warm summers and a humid, continental climate. The mean annual temperature is 8 °C, with average temperatures in the coldest and warmest months being − 3 °C (January) and 17 °C (July), respectively (Bac and Rojek 2012). The annual average precipitation is ca. 600 mm (Bac and Rojek 2012).

Fig. 1 Map of the study sites in the Trzebnica Hills
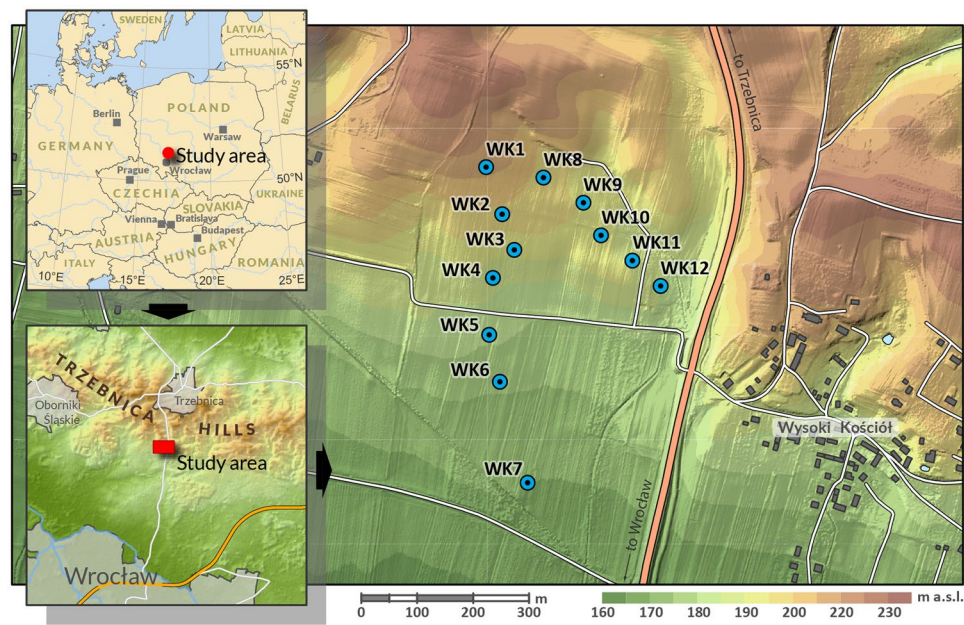
3 Materials and methods

3.1 Field sampling

The sites sampled were in the southern part of the Trzebnica Hills, close to the village of Wysoki Kościół. Two transects along two slopes with pronounced erosion features were samples in order to track the multidirectional character of soil erosion (Table 1, Fig. 1). The two slope catenas started at the top of the local hill, sharing sample WK1 as the starting profile for both transects, and with the first transect (WK1, WK2–WK7) trending to the south and the second (WK1, WK8–WK12) to the north-east. The range of slope inclination was similar for both transects and reached the highest values with 12–13° at the shoulder position (Table 1). The altitudinal differences along the first catena (WK1–WK7) are about 36 m and along the second catena (WK1–WK12) 20 m. For each transect, the soil profiles were described according to the guidelines for soil description (Food and Agriculture Organization [FAO] 2006) and classified according to the FAO-World Reference Base (WRB) system (International Union of Soil Sciences Working Group WRB 2015). Undisturbed soil samples were taken, using stainless steel rings (100 cm^3), from all the soil horizons for bulk density analysis. About 1 kg of bulk soil material was sampled for physicochemical and geochemical analyses. To obtain enough quartz (0.25–0.60 mm fraction) for in situ ^{10}Be analysis, 8–9 kg of soil material were taken at depths of 20 cm from the surface to 100 cm. For the $^{239+240}$Pu analyses, samples were taken every 5 cm from the surface to a depth of 40 cm. However, the Ap horizon (0–20/0–25 cm) was mostly homogenous due to ploughing, so only one

sample was taken from the first 20/25 cm. In addition, a reference soil profile was sampled in a nearby forested area. To overcome the large sampling number, a large amount of sample material (about 1 kg) was taken per depth increment and homogenised. Prior to the measurements, the soil samples were dried, crushed and sieved (2 mm mesh).

3.2 Soil properties

The particle-size distribution was measured using a sieving (sand fraction) and hydrometer method to determine the silt and clay fractions (van Reeuwijk 2002). The pH of the samples was measured potentiometrically (in deionised water) in a 1:2.5 suspension (Kabała et al. 2016). The hydrolytic acidity was extracted using a 1-M sodium acetate (CH$_3$COONa) solution and potentiometric titration, while the exchangeable ions (Ca^{2+}, Mg^{2+}, K$^+$, Na$^+$) were extracted using a 1-M ammonium acetate (CH$_3$COONH$_4$) solution at pH 7(van Reeuwijk 2002). Calcium carbonate (CaCO$_3$) was measured conductometrically using a Scheibler apparatus. The soil organic carbon (SOC) content was determined by dry combustion at 550 °C and the non-dispersive infrared absorption of CO$_2$, using a Ströhlein CS-mat 5500 analyser (prior to the analysis, the calcium carbonates were removed, if present). The bulk density was measured using the dry weight method (van Reeuwijk 2002).

The geochemical composition was determined using X-ray fluorescence (XRF). Approximately 5 g of soil was milled to 50 μm in a tungsten carbide disc swing mill (Retsch® RS1, Germany). The milled samples were then weighed into plastic cups using a Prolen® foil and measured using an energy-dispersive, helium-flushed XRF

Table 1 Main characteristics of studied sites

Soil profile	Latitude and longitude	Elevation (m asl)	Inclination (°)	Slope position	Land use	Classification according to WRB (IUSS, 2015)
WK1	51° 16′ 09.0″ N 17° 02′ 36.7″ E	206.8	4	Top slope	Arable land	Albic Luvisol (Aric, Cutanic, Densic, Ochric, Siltic)
WK2	51° 16′ 06.3″ N 17° 02′ 38.3″ E	198.2	10	Shoulder	Arable land	Haplic Luvisol (Aric, Cutanic, Endodensic, Endoloamic, Ochric, Episiltic, Raptic)
WK3	51° 16′ 02.6″ N 17° 02′ 37.6″ E	191.8	13	Shoulder	Arable land	Lamellic Luvisol (Aric, Cutanic, Ochric, Siltic)
WK4	51° 15′ 59.3″ N 17° 02′ 37.4″ E	187.1	10	Back slope	Arable land	Stagnic Albic Luvisol (Aric, Cutanic, Ochric, Siltic)
WK5	51° 15′ 56.6″ N 17° 02′ 38.5″ E	181.1	5	Back slope	Arable land	Albic Luvisol (Aric, Cutanic, Ochric, Siltic)
WK6	51° 15′ 50.8″ N 17° 02′ 41.3″ E	176.1	3	Foot slope	Arable land	Haplic Luvisol (Aric, Colluvic, Cutanic, Endoloamic, Ochric, Episiltic)
WK7	51° 16′ 04.3″ N 17° 02′ 39.5″ E	170.2	2	Toe slope	Arable land	Eutric Colluvic Regosol (Aric, Ochric, Raptic, Episiltic)
WK8	51° 16′ 08.5″ N 17° 02′ 42.0″ E	198.1	7	Shoulder	Arable land	Calcic Luvisol (Aric, Cutanic, Densic, Endoloamic, Ochric, Episiltic, Raptic)
WK9	51° 16′ 07.1″ N 17° 02′ 45.8″ E	193.7	12	Shoulder	Arable land	Regosol (Aric, Densic, Endoloamic, Ochric, Episiltic)
WK10	51° 16′ 05.2″ N 17° 02′ 47.5″ E	191.4	7	Back slope	Arable land	Haplic Luvisol (Aric, Cutanic, Endoloamic, Ochric, Episiltic, Raptic)
WK11	51° 16′ 03.8″ N 17° 02′ 50.4″ E	188.9	3	Back slope	Arable land	Haplic Luvisol (Aric, Cutanic, Ochric, Siltic)
WK12	51° 16′ 02.4″ N 17° 02′ 53.1″ E	185.6	2	Foot slope	Arable land	Endostagnic Luvisol (Colluvic, Ochric, Siltic)
WK0[*]	51°16′ 49.28″ 17°04′ 15.01″	225.9	0	Plateau	Forest	Albic Luvisol (Ochric, Siltic)

[*]Reference profile

spectrometer (ED-XRF, SPECTRO X-LAB 2000). The accuracy of the measurements was checked using soil reference material (Reference Soil Sample CCRMP SO-4, Canada Centre for Mineral and Energy Technology) with certified total element contents.

To estimate the degree of weathering of the soil layers, the Chemical Index of Alternation (CIA) (Nesbitt and Young 1982) was used (molar ratios):

$$CIA \times \left[\frac{Al_2O_3}{Al_2O_3 + CaO + Na_2O + K_2O} \right] \tag{1}$$

3.3 Determination of cosmogenic, in situ ^{10}Be

^{10}Be was extracted from pre-cleaned quartz grains from the 0.25–0.60 mm fraction using an isotope dilution method that followed the modified protocol of von Blanckenburg (Kohl and Nishiizumi 1992; von Blanckenburg et al. 1996) at the University of Zurich. The ^{10}Be/^{9}Be ratios were measured using a Tandy accelerator mass spectrometer (AMS) at ETH Zurich (Christl et al. 2013), normalised to the ETH AMS standard S2007 N (^{10}Be/^{9}Be = 28.1 × 10^{-12} nominal) and calibrated to ICN 01–5-1 (^{10}Be/^{9}Be = 2.709 × 10^{-11} nominal) (Nishiizumi et al. 2007), both associated with a ^{10}Be half-life of 1.387 ± 0.012 Myr.

3.4 Determination of the $^{239+240}$Pu activity in soils

The soil samples were prepared and measured for plutonium isotope analysis according to the method of Ketterer et al. (2004). Concentrations of ^{239}Pu and ^{240}Pu were measured relative to the ^{242}Pu spike using an Agilent 8800 Triple quad ICP-MS spectrometer equipped with an ICA Apex-IR nebuliser, which allows the detection of ultra-trace-elemental concentrations down to the parts-per-quadrillion level. The resulting concentrations were converted into the combined activity of $^{239+240}$Pu, corrected to the preparation blanks and normalised to the standard reference material IAEA-447 (IAEA-CU-2009–03 2012). The reproducibility of the laboratory preparation was checked using randomly-picked duplicates of the samples.

3.5 Calculation of soil redistribution rates

The long-term erosion rate was determined based on the assumption of the secular equilibrium of ^{10}Be production and decay in the upper 80 cm of the soil. We used the CRONUS online calculator to convert ^{10}Be concentrations into an erosion rate (Balco et al. 2008; https://hess.ess.washington.edu). The calculator includes all production channels of ^{10}Be by secondary cosmic rays through the specified soil depth. For the short-term denudation rates, two conversion models were applied:

1. The profile distribution model (PDM) of Walling and Quine (1990) and Zhang et al. (1990), which was developed to convert FRN inventories into soil redistribution rates for undisturbed sites. A recent study by Calitri et al. (2019), however, showed that it can also be used for agricultural soils:

$$E = \frac{10}{t - t_0} \times \ln\left(1 - \frac{X}{100}\right) \times h_0 \tag{2}$$

where E is the erosion rate (t ha^{-1} year^{-1}), t is the year of sampling, t_0 is 1963 (year of thermonuclear weapons testing), X is the % reduction in total inventory with regard to the local reference value and h_0 is a profile shape factor; and.

2. Modelling Deposition and Erosion rates with Radio-Nuclides (MODERN) (Arata et al. 2016a, b), which models the FRN depth profile using a stepwise function. For each increment, *inc* returns a value Inv_{inc}, which is the total inventory of the sampling site, measured for the whole depth profile, d (cm). MODERN provides results in centimetres (cm) of soil loss or gain and can be calculated in t ha^{-1} year^{-1} using the equation:

$$Y = 10 \times \frac{x^* xm}{d \cdot t_1 - t_0} \tag{3}$$

where Y is the soil erosion or deposition rate (t ha^{-1} year^{-1}), x^* is the soil loss or gain returned in centimetres from MODERN, xm is the mass depth (kg m^{-2}), d is the total depth increment considered at the sampling site, t_1 is the sampling year and t_0 is the reference year.

3.6 Statistical analysis

To test the statistical association between the chosen soils and relief characteristics, the Pearson's correlation coefficients were calculated using Statistica 13 software.

4 Results

4.1 Morphology and soil properties

The soils along the two studied transects predominantly developed from loess deposits that had a thickness of up to 1.5 m (Table 2). In some cases, the thin loess mantle (shallowed by erosion) was found to be underlain by a glaciofluvial substrate (WK2) and/or a calcareous glacial till (WK7, WK8, WK9). These lithic discontinuities were clearly recognisable in the grain size distribution and in part in the bulk density (Table 2). The loess deposits had a silt loam texture with a dominance of coarse silt, while the glaciofluvial and glacial sediments had a sandy loam, loam or clay loam texture. In general, the loess mantle was completely decalcified along the first transect (except for the glacial till in WK7), while the profiles WK8 and WK9 of the second transect contained some small amounts of calcium carbonate (0.02–5.80%). As a result, the presence of calcium carbonate is linked to a high base saturation and relatively high pH (Table 2). All soils were characterised by a low SOC content, oscillating between 0.09 and 0.88%, and by a very low nitrogen content (0.02–0.08%).f

Almost all the soils revealed a clear morphological differentiation related to clay illuviation. Complete Luvisols, with E and Bt horizons, were only found at the top of the studied hill (WK1) and in the mid-slope section (WK4–WK6), however. The other soil profiles had strong features related to erosion, such as the absence of an E horizon and the incorporation of the Bt into the Ap horizon (WK2, WK3, WK10, WK11), or the deposition of eroded fine-grained material covering the remnants of an older A horizon (WK6; Ab horizon at a depth of 45 cm) and the formation of a thick colluvium (nearly 60 cm in depth) in the toe slope (WK12). In profile WK7, a clear stratification of sand and silt was detected over the glacial till. The sandy material revealed a diagonal lineation. The morphology of the soils suggests a strong differentiation caused by significant geomophodynamic processes acting on the slopes. This led to the shallowing of the loess deposits and exhumation of glaciofluvial and glacial sediments.

4.2 Geochemical composition of the soils

The content of major oxides in the soils was relatively similar in both transects (Table S1), oscillating in the range of 61.1–87.0% for SiO_2, 5.6–11.8% for Al_2O_3, 1.0–3.7% for Fe_2O_3 and 1.7–2.8% for K_2O. The CaO content mainly ranged from 0.4 to 0.7%, whereas the Ca content was significantly higher in horizons bearing carbonate nodules.

Table 2 Morphology and basic chemical and physical properties of investigated soils

Soil profile	Horizon	Depth (cm)	Colour (moist)	Structure	Boundary	pH (H$_2$O)	C$_{org}$ (%)	CaCO$_3$ (%)	Bulk density (g cm^3)	Sand (%)	Silt	Clay	Texture group
WK1	Ap	0–23	10 YR 4/3	AS	G	6.4	0.88	0.05	1.51	15	71	14	SiL
	AE	23–31	10 YR 6/4	AB	G,W	6.4	0.61	0.05	1.45	14	69	17	SiL
	E	31–41	10 YR 5/4, 7.5 YR 4/6	AB	G,W	6.9	0.32	0.07	1.46	16	65	19	SiL
	EBtg	41–56	10 YR 7/3, 10 YR 5/4	AB	G	7.2	0.19	0	1.26	15	63	22	SiL
	Btg1	56–80	10 YR 6/6, 10 YR 7/3	AB	G	7.5	0.15	0	1.40	14	61	25	SiL
	Btg2	80–92	10 YR 6/6	AB, PL		7.5	0.13	0	1.46	19	57	24	SiL
WK2	Ap	0–18	10 YR 4/4	SB	G	7.2	0.69	0.07	1.46	21	62	17	SiL
	A/Bt	18–27	10 YR 4/3	AS	C	6.0	0.69	0.02	1.45	20	61	19	SiL
	Bt/BC	27–38	10 YR 6/6	AB	G	6.3	0.33	0.02	1.46	19	63	18	SiL
	BC1	38–60	10 YR 7/6, 2.5 Y 7/3	AB	G	6.7	0.17	0	1.37	22	60	18	SiL
	BC2	60–70	10 YR 7/4	AS,PL	C	6.9	0.15	0	1.35	37	46	17	L
	2Btb	70–85	10 YR 6/4	AB	G	7.1	0.10	0	1.72	57	30	13	SL
	2Bt/2BCb	85–105	10 YR 7/6, 7.5 YR 5/8	PL	C	7.0	0.05	0	1.68	64	26	10	SL
	2BCb	105–134	10 YR 6/6, 2.5 YR 8/4	PL		7.0	0.09	0	1.70	62	26	12	SL
WK3	Ap	0–23	10 YR 4/4	SB	C	6.3	0.82	0.02	1.50	20	64	16	SiL
	AE	23–30	10 YR 6/4	AS	A	6.0	0.77	0.02	1.45	19	65	16	SiL
	Bt1	30–54	10 YR 6/6	AB,PL	G	6.6	0.22	0	1.46	16	63	21	SiL
	Bt2	54–85	10 YR 7/4, 10 YR 8/2	AB,PL	G	7.1	0.20	0	1.26	19	62	19	SiL
	BC	85–105	10 YR 6/6, 10 YR 7/4	AB,PL	G	7.3	0.12	0	1.32	22	60	18	SiL
	BC	105–132	10 YR 7/6	PL		7.3	0.21	0	1.38	27	57	16	SiL
WK4	Ap	0–23	10 YR 5/4	AS	G	5.3	0.59	0.02	1.50	35	57	8	SiL
	AE	23–40	10 YR 5/4	AB	G	6.1	0.46	0	1.45	27	64	9	SiL
	E	40–58	10 YR 7/4	AB	G	7.0	0.28	0	1.46	21	69	10	SiL
	EBt	58–78	10 YR 8/1, 10 YR 7/4	AB	G,W	7.3	0.13	0	1.26	22	66	12	SiL
	Bt/E	78–100	10 YR 5/6, 10 YR 8/2	AB	G	7.3	0.13	0	1.40	20	64	16	SiL
	Bt	100–121	10 YR 7/4, 10 YR 5/4	AB,PL	G	7.1	0.18	0	1.46	21	60	19	SiL
	BC	121–142	10 YR 5/6	AB,PL		7.1	0.18	0	1.28	23	59	18	SiL
WK5	Ap	0–30	10 YR 4/3	AS	G	6.3	0.80	0.05	1.39	24	64	12	SiL
	AEg	30–42	10 YR 4/2	AB	C	5.8	0.62	0.02	1.41	26	63	11	SiL
	Eg	42–60	10 YR 8/2	AB	C	6.7	0.27	0	1.26	25	65	10	SiL
	EBtg	60–80	10 YR 7/4, 7.5 YR 5/6	AB,PL	G	7.0	0.22	0	1.46	20	60	20	SiL
	Btg	80–106	10 YR 6/6, 7.5 5/6	AB,PL	G	7.0	0.20	0	1.55	26	56	18	SiL
	BC	106–122	10 YR 6/2, 7.5 YR 6/6	PL		6.9	0.14	0	1.51	25	53	22	SiL
WK6	Ap	0–25	10 YR 5/4	GR	G	7.5	0.91	0.07	1.42	34	55	11	SiL
	AE	25–31	10 YR 4/2	SB	G	7.1	0.80	0	1.54	36	54	10	SiL
	Eg	31–45	10 YR 5/3	AB	G	7.4	0.75	0	1.50	34	54	12	SiL

Table 2 (continued)

Soil profile	Horizon	Depth (cm)	Colour (moist)	Structure	Boundary	pH (H$_2$O)	C$_{org}$ (%)	CaCO$_3$ (%)	Bulk density (g cm^3)	Sand (%)	Silt	Clay	Texture group
	Ab	45–81	10 YR 4/3	SB	G	7.4	0.57	0	1.45	48	40	12	L
	AEb	81–93	10 YR 5/4	AB	G	7.2	0.43	0	1.50	38	48	14	L
	EBgb1	93–129	10 YR 6/3, 7.5 YR 4/6	AB,PL	G	7.1	0.16	0	1.64	39	45	16	L
	EBgb2	129–141	10 YR 6/3, 10 YR 8/1	AB,PL	G	7.2	0.09	0	1.61	47	36	17	L
	BCg	141–156	10 YR 6/6, 2.5 Y 7/1	PL		7.3	0.09	0	1.50	48	34	18	L
WK7	Ap	0–25	10 YR 4/3	GR	C	6.8	0.95	0.05	1.44	25	60	15	SiL
	AE	25–36	10 YR 5/4	AB	C,W	7.0	0.64	0	1.52	29	59	12	SiL
	Eg	36–66	10 YR 7/3	AB,PL	G,W	7.5	0.33	0	1.59	36	53	11	SiL
	2EBg1	66–84	10 YR 6/4, 2.5 YR 7/4	AB	G	7.5	0.15	0	1.53	64	28	8	SL
	2EBg2	84–102	10 YR 5/4, 2.5 YR 7/3	SB	G	7.6	0.20	0	1.49	61	31	8	SL
	3C	102–116	10 YR 6/4	SB	A	7.7	0.20	0	1.48	62	28	10	SL
	4Cgk	116–145	7.5 YR 5/6, 5 Y 6/2	AB,PL		8.3	0.11	8.50	1.51	35	33	32	CL
WK8	Ap	0–23	10 YR 4/4	SB	C,W	6.8	0.59	0.14	1.5	20	64	16	SiL
	Bt	23–34	10 YR 5/4	AB	G	6.9	0.12	0.14	1.6	22	60	18	SiL
	Bt/BC	34–61	10 YR 6/4, 10 YR 5/6	AB	G,W	6.9	0.12	0.14	1.5	25	56	19	SiL
	2BCk1	61–82	10 YR 6/4, 10 YR 4/4	AB	G	7.7	0.12	3.36	1.7	39	35	26	L
	2BCk2	82+	10 YR 5/6	AB,PL		7.6	0.11	3.29	1.7	40	36	24	L
WK9	Ap	0–29	10 YR 4/3	SB	C	7.5	0.60	2.36	1.6	36	44	20	SiL
	BCk1	29–35	10 YR 5/4, 7.5 YR 4/6	AB	A,W	7.8	0.14	5.65	1.6	28	42	30	CL
	BCk2	35–70	10 YR 6/4	AB		7.9	0.12	5.82	1.7	32	43	25	L
WK10	Ap1/Bt	0–22	10 YR 5/4, 10 YR 5/8	SB	G	7.0	0.75	0.04	1.6	19	64	17	SiL
	A2/Bt	22–28	10 YR 6/4, 10 YR 5/8	AB	A	7.2	0.70	0.02	1.4	23	61	16	SiL
	Bt	28–68	2.5 Y 7/4	AB	G	7.2	0.10	0.02	1.4	26	60	14	SiL
	BC1	68–93	2.5 Y 7/4	AB,PL	G	7.1	0.06	0.02	1.6	46	40	14	L
	BC2	93–130	2.5 Y 7/4	AB,PL		7.3	0.04	0.02	1.4	47	38	15	L
WK11	Ap/Bt	0–23	10 YR 4/2	AS	C	6.9	1.05	0.04	1.5	26	59	15	SiL
	Bt/Ap	23–37	10 YR 6/6	AS	G	7.2	0.42	0.02	1.4	28	58	14	SiL
	BC	37–65	10 YR 6/4, 7.5 YR 4/6	SB	G	7.3	0.17	0.02	1.4	29	58	13	SiL
	BC1	65–101	2.5 Y 7/4	AB,PL	G	7.2	0.16	0.02	1.4	25	61	14	SiL
	BC2	101–120	2.5 Y 7/3, 2.5 Y 8/2	PL		7.2	0.16	0.02	1.4	25	62	13	SiL
WK12	A/C	0–14	10 YR 6/4	SB	C,W	7.0	1.22	0.02	1.4	13	74	13	SiL
	A	14–57	10 YR 4/4	SB	C,W	6.7	0.56	0.02	1.4	19	68	13	SiL
	BC1g	57–97	10 YR 5/6, 10 YR 5/3	SB	G,W	6.6	0.35	0.04	1.5	20	65	15	SiL
	BC2g	97–127	10YR 5/6, 10 YR 5/3	AB,PL		6.7	0.30	0.02	1.5	21	60	19	SiL
WK0	AE	0–11	10 YR 5/3	SB	G,W	6.8	2.35	0.02	1.1	16	70	14	SiL

Table 2 (continued)

Soil profile	Horizon	Depth (cm)	Colour (moist)	Structure	Boundary	pH (H₂O)	C_{org} (%)	$CaCO_3$ (%)	Bulk density (g cm³)	Sand (%)	Silt	Clay	Texture group
	E	11–32	10 YR 6/4	AB	G,W	6.5	0.65	0.04	1.3	14	68	18	SiL
	E/Bt	32–65	10 YR 5/8, 2.5 Y 8/1	AB		4.2	0.32	0.02	1.3	14	62	24	SiL

Types of structure: *AB* angular blocky, *AS* angular and subangular blocky, *SB* subangular blocky, *PL* platy, *GR* granular

Horizon boundary (distinctness, topography): *A* abrupt, *C* clear, *G* gradual, *S* smooth, *W* wavy

The Zr and Hf content often indicates the presence of aeolian material (De Vos and Tarvainen 2006), and they were used to discriminate these from glacial sediments. The average Zr and Hf contents in the loess layer were 302 and 8.9 mg kg⁻¹, respectively (McLennan 2001). The lowermost horizons of WK2, WK7, WK8 and WK9 had lower Zr and Hf contents, with a maximum of 256 and 6.9 mg kg⁻¹, respectively. This reflects the lithological discontinuity observed in the field. The relatively high variability of Hf and Zr in soil profiles WK5 and WK6 highlights the dynamics of slope processes and/or loess sorting along the slope (Table S1). The reference soil profile (WK0) situated in the forested area was characterised by similar values for the major oxides, Zr and Hf as in the studied soils, which confirm their origin as loess deposits.

The majority of the soils revealed CIA values above 50 (Table S1), corresponding to a low degree of weathering. Only the samples from profiles WK8 and WK9 and the lowermost horizon of WK7 had CIA value of below 50, representing less-weathered material (Nesbitt and Young 1982).

4.3 In situ ¹⁰Be and erosion rates

The average content of in situ ¹⁰Be in the soils ranged from 0.9 to 1.5 (× 10⁵) atoms g⁻¹ (Table 3). In both transects, the soils situated on the upper part of the slope had slightly lower concentrations than the soils in lower/toe slope positions. The calculated long-term erosion rates were similar for both transects. In profile WK1 (the starting point for both transects), the long-term erosion rate was 0.46 t ha⁻¹ year⁻¹. In the mid-slope position, the erosion rate increased, oscillating between 0.56 and 0.85 t ha⁻¹ year⁻¹, while in the toe slope, it decreased again down to 0.44–0.50 t ha⁻¹ year⁻¹. The site with the highest erosion rate was WK9, with the lowest erosion rate measured in WK6 (Fig. 2).

4.4 Activity of ²³⁹⁺²⁴⁰Pu and erosion rates

The plutonium activity in the soils was generally low, ranging from 0.002 to 0.520 Bq kg⁻¹ (Table 4, Fig. 3). The isotopic ratio of ²⁴⁰Pu/²³⁹Pu (Table 4) can be used to determine the origin of the plutonium in soils (Alewell et al. 2014, 2017). The ratio refers to Northern Hemisphere mid-latitude weapons testing fallout (Alewell et al. 2017) when its value ranges between 0.14 and 24 (typically around 0.18), whereas ratios of 0.37 to 0.41 indicate influence from the Chernobyl accident (Alewell et al. 2017). The mean ratio of ²⁴⁰Pu/²³⁹Pu in the investigated soils was 0.18, indicating no influence from the Chernobyl fallout. The erosion rates varied considerably depending on the model applied (Fig. 2, Table S2). The PDM gave higher erosion rates, ranging from 1.4 to 16.9 t ha⁻¹ year⁻¹, whereas MODERN gave lower rates of between 1.2 and 10.9 t ha⁻¹ year⁻¹. In general, the soils of the second transect experienced higher erosion rates

Table 3 Content of in situ [10]Be in the soil samples

Soil profile	[10]Be/[9]Be (10^{-12})	Err[10]Be/[9]Be (%)	[10]Be (at g^{-1})	Err [10]Be (%)
WK1	0.189	4.0%	130,486	5.2%
WK2	0.150	4.8%	104,168	6.3%
WK3	0.143	4.9%	105,154	6.5%
WK4	0.200	4.3%	143,742	5.6%
WK5	0.191	4.7%	137,108	5.8%
WK6	0.207	4.9%	149,627	5.8%
WK7	0.166	4.6%	120,430	5.7%
WK8	0.160	4.2%	97,816	5.3%
WK9	0.146	3.4%	89,510	4.6%
WK10	0.163	3.3%	102,658	4.5%
WK11	0.214	4.0%	137,282	5.1%
WK12	0.197	3.4%	119,454	5.7%

than the first. Both models pointed to high erosion rates at the toe of the first transect (WK7), which is rather unusual for such a topographical position.

4.5 Correlation analysis

A positive correlation was detectable between the soil erosion rates (obtained from [10]Be and [239+240]Pu) and the slope gradient (Table 5), indicating, not surprisingly, higher erosion with a steeper slope. The negative correlation between the CIA values and erosion rates suggested that slope processes led to the removal of the topsoil and exposed substrates in deeper horizons that were less weathered or even had a different lithology.

5 Discussion

5.1 Long- and short-term erosion rates in loess deposits

The calculated long-term erosion rates were consistent with the terrain relief. In both transects, erosion increased in the mid-slope position, which was steeper (WK2, WK3, WK8, WK9), and mostly decreased in the lower, flatter parts of the slope. Erosion processes still occurred in the toe slope positions. However, the erosion rate was lower than in the upper parts of the slope (Fig. 2). This cross-check and agreement with independent data (Table 6) indicated that the assumption of secular equilibrium is plausible.

To determine the short-term erosion rates based on [239+240]Pu, two conversion models were applied. The PDM showed considerably higher values (from 1.4 to 16.9 t ha^{-1} year^{-1}) than the MODERN (1.2 to 10.9 t ha^{-1} year^{-1}). The PDM assumed that the activity of [239+240]Pu had an exponential decay function within the soil profile (Arata et al. 2016b; Calitri et al. 2020). The MODERN, however, did not make any assumptions about the [239+240]Pu distribution along

the profile (Arata et al. 2016b) and thus may more precisely simulate the behaviour of FRN (e.g., under ploughing activities) (Alewell et al. 2017). Therefore, the results obtained using this model were deemed to be more reliable. Similar to the long-term rates determined by [10]Be, the mid-slope positions (WK3, 4, 5, 8, 9 and 10) exhibited, in general, the highest erosion rates. Although site WK4 exhibits a relatively thick soil profile, the present-day erosion rates are high. This indicates that such high erosion rates must be a recent process, as otherwise such a thick profile could not persist. This mid-slope position has a relatively steep slope and is, therefore, particularly susceptible to erosion. In general, the measured erosion rates are high but are frequently measured or modelled for arable land in Europe (Cerdan et al. 2010).

While in situ [10]Be does not form any inorganic or organo-mineral complexes nor colloids (because this nuclide is directly produced in the crystal lattice of quartz by the interaction of cosmogenic rays), it also does not move along the soil profile. Pu, however, accumulates in soils and sediments through atmospheric deposition. Consequently, part of Pu might be lost with time through pedogenetic processes or leaching. Pu has, however, an extremely low solubility and a high affinity to organic matter (Alewell et al. 2017) or is strongly adsorbed onto clay particles. In undisturbed soils, essentially, the entire inventory is concentrated in the top 30 cm (Ketterer et al. 2011; Iurian et al. 2015). Because the isotopes of [239+240]Pu are strongly adsorbed, the redistribution of these isotopes has occurred as a result of physical particle movements such as erosion (Alewell et al. 2017). Luvisols are encountered in the investigation. These soils are characterised by clay illuviation. It might be that a small part of Pu migrated along the soil profile due to the translocation of clay particles. This seems rather unlikely, given the fact that the content of Pu strongly decreases with soil depth, except in profile WK12. In this soil, however, no clay translocation was observed. Therefore, the Pu content is primarily affected by soil redistribution.
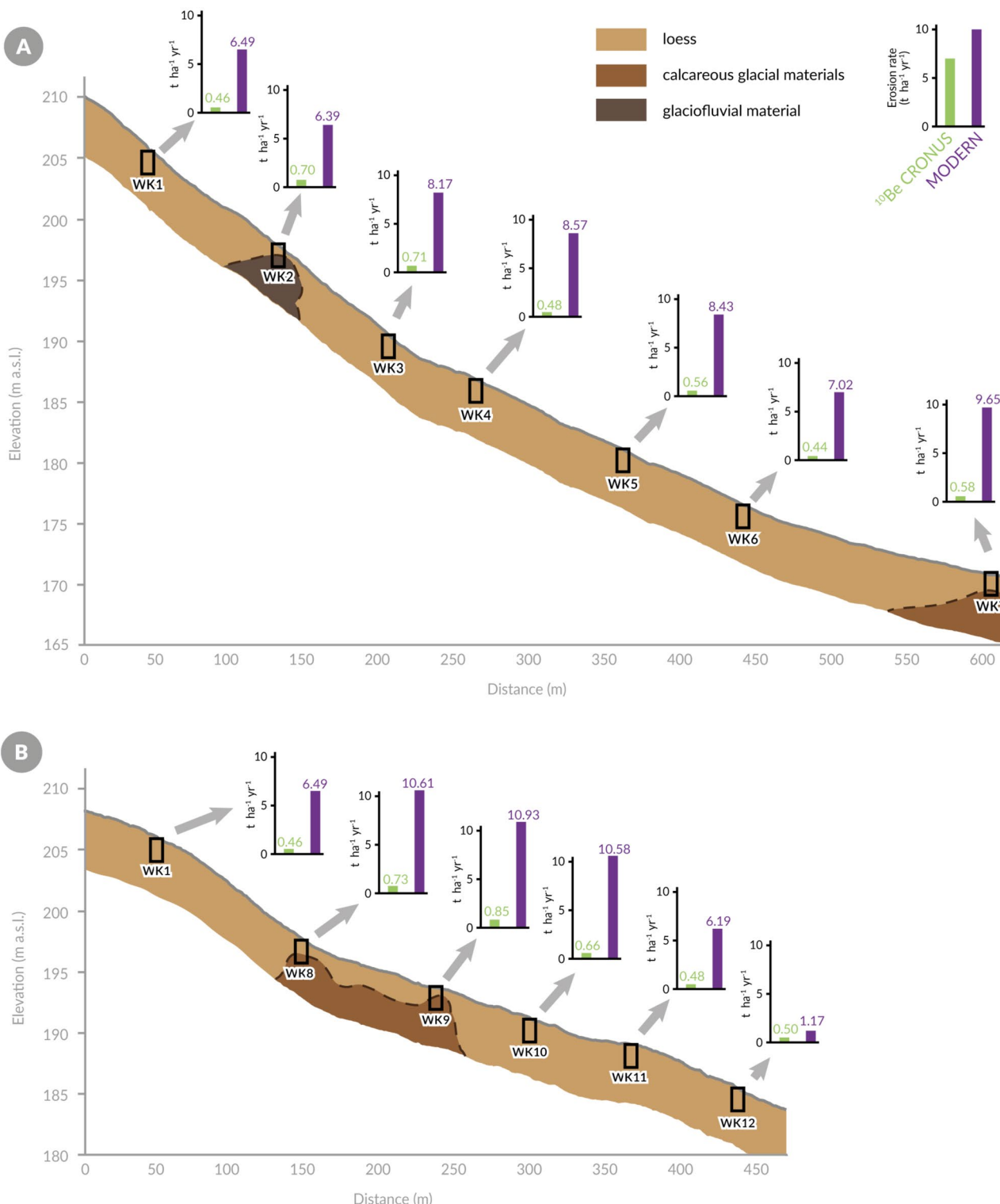
Fig. 2 Short- and long-term soil erosion rates along the studied toposequences. The thickness of the loess mantle is not to scale. Drillings were made down to 2 m

6 Soil erosion rates in loess landscapes

The long-term erosion rates of the studied pedons (0.44–0.85 t ha^{-1} year^{-1}), calculated using in situ ^{10}Be,

were in a good agreement with values from other studies of loess landscapes using different methods (Table 6). In Germany, Dreibrodt et al. (2010, 2013) determined the erosion in the Early Bronze Age (0.3–0.6 t ha^{-1} year^{-1}) and of

Table 4 $^{239+240}$Pu activity in studied soils

Soil profile	Depth (cm)	$^{239+240}$Pu (Bq kg^{-1})	SD (Bq kg^{-1})	^{240}Pu/^{239}Pu ratio
WK1	0–25	0.0802	0.0086	0.19
	25–30	0.0668	0.0065	0.16
	30–35	0.0069	0.0019	0.18
	35–40	0.0151	0.0018	0.13
WK2	0–20	0.0515	0.0070	0.19
	20–25	0.0622	0.0067	0.19
	25–30	0.0515	0.0050	0.17
	30–35	0.0024	0.0011	N/A
	35–40	0.0073	0.0033	0.18
WK3	0–25	0.0664	0.0068	0.19
	25–30	0.0070	0.0027	N/A
	30–35	0.0044	0.0016	0.20
	35–40	0.0353	0.0057	0.18
WK4	0–25	0.0497	0.0094	0.14
	25–30	0.0044	0.0019	0.24
	30–35	0.0011	N/A	N/A
	35–40	0.0009	0.0007	0.28
WK5	0–25	0.0740	0.0051	0.21
	25–30	0.0062	0.0024	0.14
	30–35	0.0078	0.0030	0.31
	35–40	0.0137	0.0040	0.28
WK6	0–25	0.0694	0.0061	0.16
	25–30	0.0696	0.0079	0.18
	30–35	0.0041	0.0017	0.15
	35–40	0.0041	0.0020	0.25
WK7	0–25	0.0666	0.0039	0.20
	25–30	0.0118	0.0025	0.20
	30–35	0.0043	0.0015	0.14
	35–40	0.0010	0.0006	0.09
WK8	0–20	0.0531	0.0065	0.20
	20–25	0.0064	0.0020	0.15
	25–30	0.0024	0.0013	0.05
	30–35	0.0012	0.0008	N/A
	35–40	0.0006	0.0007	N/A
WK9	0–25	0.0571	0.0054	0.20
	25–30	0.0007	N/A	N/A
	30–35	0.0000	0.0001	N/A
WK10	0–25	0.0616	0.0093	0.18
	25–30	0.0047	0.0021	N/A
	30–35	0.0013	0.0007	0.18
WK11	0–20	0.0835	0.0058	0.18
	20–25	0.0189	0.0032	0.17
	25–30	0.0527	0.0042	0.21
	30–35	0.0106	0.0032	0.19
	35–40	0.0034	0.0011	0.12

Table 4 (continued)

Soil profile	Depth (cm)	$^{239+240}$Pu (Bq kg^{-1})	SD (Bq kg^{-1})	^{240}Pu/^{239}Pu ratio
WK12	0–5	0.0804	0.0081	0.16
	5–10	0.0671	0.0051	0.21
	10–15	0.0815	0.0090	0.20
	15–20	0.0875	0.0082	0.18
	20–25	0.0944	0.0086	0.21
	25–30	0.0986	0.0111	0.19
	30–35	0.0937	0.0112	0.21
	35–40	0.0932	0.0098	0.20
WK0	0–5	0.5290	0.0197	0.21
	5–10	0.3492	0.0147	0.21
	10–15	0.1018	0.0116	0.20
	15–20	0.0338	0.0062	0.24
	20–25	0.0371	0.0050	0.21
	25–30	0.0080	0.0034	0.15
	30–35	0.0026	0.0012	0.13
	35–40	0.0012	0.0005	N/A

SD standard deviation, *N/A* not applicable

the Late Neolithic to Bronze Age (0.4–0.5 t ha^{-1} year^{-1}) by relating the mass of the deposited sediments to the that of the catchment area and/or by reconstructing slope cross sections. Gillijns et al. (2005) and Kołodyńska-Gawrysiak et al. (2018) analysed closed depression catchments in Belgium and Poland, respectively. The obtained erosion rate from 430 AD to today was estimated to be 2.1 t ha^{-1} year^{-1} for sites in Belgium (Gillijns et al. 2005), whereas those of the selected sites in Poland varied between 0.24 and 0.27 t ha^{-1} year^{-1} from the Late Vistulian (Weichselian) up to today (Kołodyńska-Gawrysiak et al. 2018).

The short-term erosion rates of the studied soils (1.2–10.9 t ha^{-1} year^{-1}), using $^{239+240}$Pu as a tracer, differed from the data presented so far (Table 6). Erosion rates were also calculated for the Trzebnica Hills using USLE (Licznar and Licznar 2002; Licznar et al. 2002). These calculated rates ranged between 2.5 and 4.3 t ha^{-1} year^{-1} — although these values lie within the range determined by $^{239+240}$Pu, they were in general a factor of 2 lower. Other studies on erosion rates in Polish loess landscapes have shown a wide variability. Poręba et al. (2019, 2015) determined soil erosion rates of 4.9 to 39.9 t ha^{-1} year^{-1} using ^{137}Cs and 2.2 to 30.7 t ha^{-1} year^{-1} using ^{210}Pb$_{ex}$. Rejman et al. (2008) used sediment yields over a 10-year period, obtaining erosion rates from 0.4 to 95.0 t ha^{-1} year^{-1}, whereas Święchowicz (2016) and Rejman and Brodowski (2010) determined with sediment yields soil losses of 47.3 t ha^{-1} year^{-1} and 98.2 t ha^{-1} year^{-1}, respectively. Rafalska-Przysucha and Rejman (2015) assessed erosion rates of 24.3 t ha^{-1} year^{-1} using
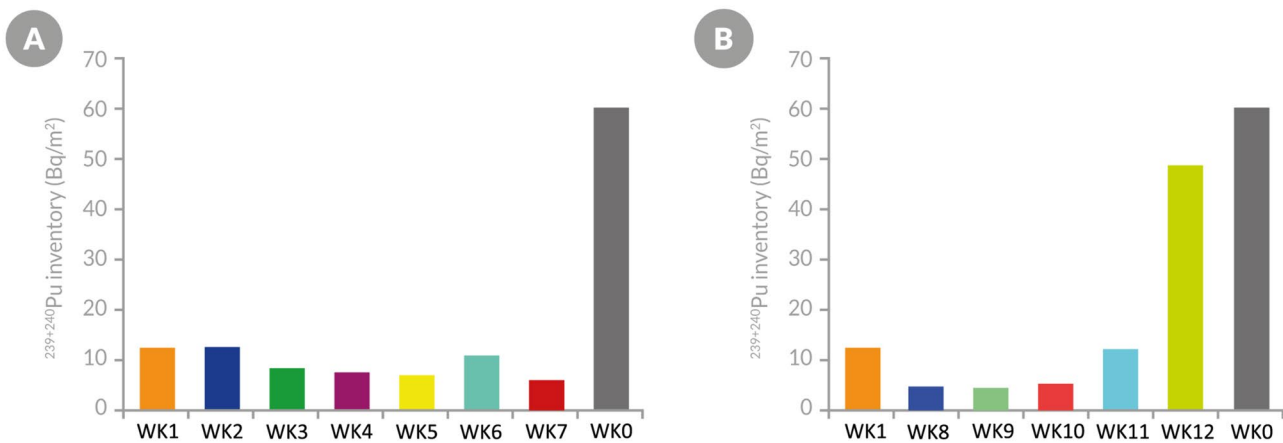
Fig. 3 $^{239+240}$Pu inventories in transects A and B

sedimentary archives from closed depressions. The discrepancies between these results might be explained by the different methods used and/or by the landscape relief. USLE involves mathematical modelling only and includes parameters that depend on precipitation and crop rotation, which change over time (Kaszubkiewicz. et al. 2011). Therefore, a direct comparison with FRN-derived erosion rates may not be practicable. The determination of erosion rates using ^{137}Cs in Central and Western Europe may be difficult because two different sources exist (nuclear weapons testing in the 1950s and 1960s and the Chernobyl accident). When using this approach, the proportions of these two sources must be determined (Alewell et al. 2017; Poręba et al. 2019). These conditions were met by the investigation of Poręba et al. (2019, 2015). The erosion rates determined with ^{210}Pb$_{ex}$ were much higher than in our study (Poręba et al. 2019). This apparent discrepancy to our erosion rates is related to a different terrain relief and land-use intensity. Rejman et al. (2008), Rejman and Brodowski (2010) and Święchowicz (2016) measured very high erosion rates, which was likely predominantly due to an almost complete absence of vegetation on their plots. Closed depressions as an archive of soil erosion refer to Modern Times; however, in research presented by Rafalska-Przysucha and Rejman (2015), this covers a longer time span (188 year) than $^{239+240}$Pu analysis.

Our data lie within the range of those from other loess areas in Europe. In Germany, the erosion rates range mostly between 2 and 10 t ha^{-1} year^{-1} when using the CORINE database (Cerdan et al. 2010). When using other methods such as the reconstruction of the slope cross section or by relating the mass of the deposited sediments to the catchment area, then the erosion rates are normally in the range of 3.2 and 13.3 t ha^{-1} year^{-1} (Dreibrodt et al. 2010, 2013). In Belgium, analysis of the sediments in a closed depression catchment showed erosion rates from 5.5 to 9.8 t ha^{-1} year^{-1} (Gillijns et al. 2005), the erosion rates from sediment yields ranged from 0.5 to 7.9 t ha^{-1} year^{-1} (Verstraeten and Poesen 2001; Evrard et al. 2008), whereas with the SEDEM model (sediment delivery model) and ^{137}Cs, soil losses ranging from 2.0 to 5.0 t ha^{-1} year^{-1} and 3.0 t ha^{-1} year^{-1} were determined, respectively (Van Rompaey et al. 2001; Van Oost et al. 2003). The relatively narrow range of erosion rates for soils on loess (Europe) may indicate the starting point of their agricultural use.

6.1 Cross-check of long- and short-term erosion rates

Applying isotopes that cover different time ranges along two transects has enabled a cross-check of the long- and medium-term erosion rates (Zollinger et al. 2015; Jelinski et al. 2019) but has also provided an insight into the multidirectional course and intensity of erosional processes.

The short-term erosion rates are distinctly higher (up to 10 times) than the long-term rates. This finding fits very well with the results presented in Kołodyńska-Gawrysiak et al. (2018), proving that, since prehistoric times, soil erosion rates (0.39–0.57 t ha^{-1} year^{-1}) have increased by a factor of almost 10 compared to the time span between the Middle Ages and Modern Times (3.7–5.9 t ha^{-1} year^{-1}).

Moreover, the results from in situ ^{10}Be and $^{239+240}$Pu analyses show the intensity of erosion processes along hillslopes. The pedons located in mid-slope positions experienced

Table 5 Correlation between chosen characteristics of studied soils and terrain relief

	Slope gradient	$^{239+240}$Pu erosion rates	^{10}Be erosion rates
CIA mean	− 0.39*	− 0.53*	− 0.44*
Slope gradient	-	0.59*	0.75*

*Pearson correlation coefficient

Table 6 Long- and medium-term soil erosion rates from loess regions

No	Location	Time scale	Method	Soil erosion rate (t ha⁻¹ year⁻¹)	References
1.	Germany, Salzmünde	Early bronze age Modern times	Relating mass of deposited sediments to superficial catchment area;	0.4–0.6 4.4–13.3	Dreibrodt et al. (2013)
		Early bronze age Modern times	Reconstruction of the slope cross section	0.3–0.4 3.2–9.5	
2.	Germany, Kleiner Tornowsee	Late Neolith–Bronze Age Modern times	Reconstruction of slope cross section	0.4–0.5 3.2–10.4	Dreibrodt et al. (2010)
3.	Germany, Lower Saxony	Modern times	Mapping erosion events	1.7	Steinhoff-Knopp and Burkhard (2018)
4.	Germany, Chemnitz	Modern times	CORINE database, based on sediment plots	5–10	Cerdan et al. (2010)
5.	Belgium, Leuven	Modern times	CORINE database, based on sediment plots	2–5	
6.	Belgium, Zaventem	Modern times	Sediment yields	7.9	Verstraeten and Poesen (2001)
7.	Belgium, Bertem	Modern times Since 430AD–until today	Closed depression catchment	5.5–9.8 2.1	Gillijns et al. (2005)
8.	Belgium, Dijle	Modern times	SEDEM	2.0–5.0	Van Rompaey et al (2001)
9.	Belgium, Huldenberg	Modern times	¹³⁷Cs	3.0	Van Oost et al. (2003)
10.	Belgium, Velm	Modern times	Sediment yield	0.5–3.5	Evrard et al. (2008)
11.	France, Austreberthe	Modern times	Water erosion map	3.3	Delmas et al. (2012)
12.	Poland, Trzebnica Hills	Modern times	USLE	2.5–4.3	Licznar and Licznar (2002)
13.	Poland, Bogucin	Modern times	Runoff plots	0.4–10.8	Rejman et al. (2008)
14.	Poland, Czesławice	Modern times	Runoff plots	10.8–96.1	
15.	Poland, Brzesko Foreland	Modern times	Runoff plots	47.3	Święchowicz (2016)
16.	Poland, Bogucin	Modern times	Runoff plots	98.2	Rejman and Brodowski (2010)
17.	Poland, Świerklany	Modern times	¹³⁷Cs	26.7	Poręba et al. (2015)
18.	Poland, Biedrzykowice	Modern times	¹³⁷Cs	4.9–39.9	Poręba et al. (2019)
19.	Poland, Biedrzykowice	Modern times	²¹⁰Pb$_{ex}$	2.2–30.7	
20.	Poland, Tomaszowice	Late Vistulian–until today	Closed depressions catchment	0.24–0.27	Kołodyńska-Gawrysiak et al. (2018)
21.	Poland, Rąblów	Prehistoric times Early Neolithic–Middle Bronze Age	Closed depressions catchment	0.39–0.57 0.3–0.5	
		Early Middle Ages–until today		3.8–4.1	
		Middle Ages–Modern Times		3.7–5.9	
22.	Poland, Bogucin	Modern times	Closed depression catchment	24.3	Rafalska-Przysucha and Rejman (2015)

SEDEM sediment delivery model

generally higher erosion rates. This is especially evident in the second transect where the soil morphology exhibits features that are strongly linked to erosion, such as the absence of an E horizon and the incorporation of the Bt into the Ap horizon. Although the soil WK1 apparently looks disturbed, the CIA values (Table S1) indicate that the profile is disturbed (the CIA value should decrease with increasing soil depth which is, however, not the case here).

Usually, in the toe slope position, eroded material is deposited and, consequently, accumulation is expected (Henkner et al. 2017). At our sites, however, erosion was still measurable here. This highlights that intense erosion occurred along the studied slopes. During heavy rain, the material was eroded from the entire length of the slope, even from sites where the slope gradient was decreased (Fig. 4). The erosion rates have increased during the last few decades
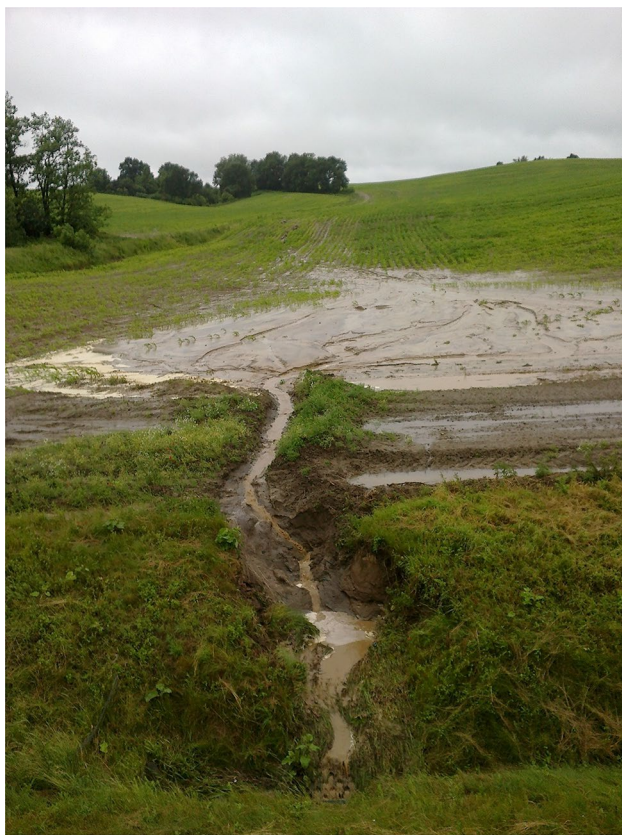
Fig. 4 Effects of soil erosion in the study area after intensive rainfall. Silt fine particles are visible as a wide yellowish-brown "plate" at the toe slope section and small erosion channels caused by concentrated runoff

even at sites with a low slope gradient, such as WK7 and WK12 (Table 1). The morphology of site WK12 indicated the accumulation of colluvial material, but the recent erosion rates were 2.5 times higher than the long-term rates. At site WK7, this increase was almost by a factor of 20. The fact that the soil at WK7 experienced higher erosion rates than at WK12 may be due to the protective effect of redcurrants (*Ribes spicatum* Robson) for a few years at the latter site, which may have improved soil resilience. A further explanation is that the position of profile WK7 is in the marginal zone of the hill. There, periodic surface runoff may have increased the erosion rates. In general, the high rates of short-term erosion are related to the intensification and mechanisation of agriculture (Foucher et al. 2014; Kopittke et al. 2019; Poręba et al. 2019), although agricultural activities alone may be responsible for the increase erosion rates. Climate change might be an additional factor causing higher erosion rates because it is giving rise to drier soils, fewer rainfall events, but increasing event intensity (Routschek et al. 2014; Zollinger et al. 2015; Zádorová and Penížek 2018). Kundzewicz and Matczak (2012) also noted an increase in rainfall intensity in Poland. The effect of climate change on soil erosion can, however, not be further quantified.

Alewell et al. (2015) posited that tolerable soil erosion rates must be less than or equal to the soil production rates, otherwise the soil would start to degrade. Because soil production rates strongly decrease with the age of a soil, also the tolerable erosion rates (as a soil destructive process) decrease with time. Most of the European soils in the lowlands have an age of > 10 kyr. Tolerable erosion rates for soils in alpine climates and having a surface age of > 10 kyr are between 0.5 and 1 t ha^{-1} year^{-1} (Alewell et al. 2015). Also, Verheijen et al. (2009) showed that tolerable erosion rates for European soils should be less than 1 t ha^{-1} year^{-1}. Mediterranean to alpine soils show all after 10 kyr strongly reduced formation rates (< 1 t ha^{-1} year^{-1}; Egli et al. 2014). Consequently, tolerable erosion rates in the range of 0.5 to 1 t ha^{-1} year^{-1} are also applicable to our investigation area. Only the long-term erosion rates in our investigated area were in this range or below. However, the short-term erosion rates were 10–22 times higher and thus far beyond any tolerable rates. Therefore, the present-day soil loss considerably exceeds soil production and will lead to significant soil thinning and reduce its productivity (Alewell et al. 2015).

7 Conclusions

The long-term erosion rates of loess landscapes calculated using in situ ^{10}Be were in agreement with the results from sedimentary archives of closed depressions and slope cross-section reconstructions. The short-term erosion rates determined using $^{239+240}$Pu differed from previously published results in Poland that used other approaches (^{137}Cs, USLE, sediment yields, closed depressions). The main reasons for these discrepancies are the differences in conceptual approach and local terrain variability, such as topography, land-use modifications over time, etc. The recent erosion rates determined for the investigated sites using $^{239+240}$Pu are comparable to those from loess sites in Germany, Belgium and France. The short-term erosion rates are up to more than one order of magnitude higher than the long-term rates. This indicates the strong recent impact of agriculture and probably also climate change. The current soil erosion values are far above any tolerable erosion rate. Therefore, the soil is strongly imbalanced, resulting in drastic soil thinning. From a methodological point of view, the use of in situ ^{10}Be and $^{239+240}$Pu can provide insights into the temporal evolution of soil erosion rates, although loess soils have problematic characteristics, such as clay migration, that may affect their determination.

References

Alewell C, Egli M, Meusburger K (2015) An attempt to estimate tolerable soil erosion rates by matching soil formation with denudation in Alpine grasslands. J Soils Sediments 15:1383–1399. https://doi.org/10.1007/s11368-014-0920-6

Alewell C, Meusburger K, Juretzko G et al (2014) Suitability of 239+240Pu and 137Cs as tracers for soil erosion assessment in mountain grasslands. Chemosphere 103:274–280. https://doi.org/10.1016/j.chemosphere.2013.12.016

Alewell C, Pitois A, Meusburger K et al (2017) 239+240 Pu from "contaminant" to soil erosion tracer: where do we stand? Earth-Science Rev 172:107–123. https://doi.org/10.1016/j.earscirev.2017.07.009

Altermann M, Rinklebe J, Merbach I et al (2005) Chernozem - soil of the year 2005. J Plant Nutr Soil Sci 168:725–740. https://doi.org/10.1002/jpln.200521814

Anioł-Kwiatkowska J (1998) Endangered and rare segetal species in the microregion Trzebnica Hills. Acta Univ Lodz 13:169–176

Arata L, Alewell C, Frenkel E et al (2016a) Modelling deposition and erosion rates with radioNuclides (MODERN) - part 2: a comparison of different models to convert 239+240Pu inventories into soil redistribution rates at unploughed sites. J Environ Radioact 162–163:97–106. https://doi.org/10.1016/j.jenvrad.2016.05.009

Arata L, Meusburger K, Frenkel E et al (2016b) Modelling deposition and erosion rates with radionuclides (MODERN) - part 1: a new conversion model to derive soil redistribution rates from inventories of fallout radionuclides. J Environ Radioact 162–163:45–55. https://doi.org/10.1016/j.jenvrad.2016.05.008

Bac S, Rojek M (2012) Meteorologia i klimatologia w inżynierii środowiska. Wydawnictwo Uniwersytetu Przyrodniczego we Wrocławiu, Wrocław

Balco G, Stone JO, Lifton NA, Dunai TJ (2008) A complete and easily accessible means of calculating surface exposure ages or erosion rates from 10Be and 26Al measurements. Quat Geochronol 3:174–195. https://doi.org/10.1016/j.quageo.2007.12.001

Calitri F, Sommer M, Norton K et al (2019) Tracing the temporal evolution of soil redistribution rates in an agricultural landscape using 239+240 Pu and 10 Be. Earth Surf Process Landforms esp.4612. https://doi.org/10.1002/esp.4612

Calitri F, Sommer M, van der Meij MW, Egli M (2020) Soil erosion along a transect in a forested catchment: Recent or ancient processes? CATENA 194:104683. https://doi.org/10.1016/j.catena.2020.104683

Cerdan O, Govers G, Le Bissonais Y et al (2010) Rates and spatial variation of soil erosion in Europe: a study based on erosion plot data. Geomorphology 122:167–177. https://doi.org/10.1016/j.geomorph.2010.06.011

Chengde S, Beer J, Tungsheng L et al (1992) 10Be in Chinese loess. Earth Planet Sci Lett 109:169–177. https://doi.org/10.1016/0012-821X(92)90081-6

Christl M, Vockenhuber C, Kubik PW et al (2013) The ETH Zurich AMS facilities: performance parameters and reference materials. Nucl Instruments Methods Phys Res Sect B Beam Interact with Mater Atoms 294:29–38. https://doi.org/10.1016/j.nimb.2012.03.004

De Vos W, Tarvainen T (2006) Interpretation of Geochemical Maps, Additional Tables, Figures, Maps and Related Publications. In: De Vos W, Tarvainen T (ed) Geochemical Atlas of Europe. Part 2, Otamedia Oy, Espoo, pp. 690

Delmas M, Pak LT, Cerdan O et al (2012) Erosion and sediment budget across scale: A case study in a catchment of the European loess belt. J Hydrol 420–421:255–263. https://doi.org/10.1016/j.jhydrol.2011.12.008

Dreibrodt S, Jarecki H, Lubos C et al (2013) Holocene soil formation and soil erosion at a slope beneath the Neolithic earthwork Salzmünde (Saxony-Anhalt, Germany). CATENA 107:1–14. https://doi.org/10.1016/j.catena.2013.03.002

Dreibrodt S, Lomax J, Nelle O et al (2010) Are mid-latitude slopes sensitive to climatic oscillations? Implications from an Early Holocene sequence of slope deposits and buried soils from eastern Germany. Geomorphology 122:351–369. https://doi.org/10.1016/j.geomorph.2010.05.015

Dyjor S (1970) Seria poznańska w Polsce Zachodniej. Kwart Geol 14:819–834

Dyjor S, Kościówko H (1982) Formacja trzeciorzędowa południowozachodniej Polski i związane z nią perspektywy wybranych surowców. Biul Inst Geol 341

Egli M, Norton K, Dahms D (2014) Soil formation rates on silicate parent material in alpine environments: different approaches, different results? Geoderma 213:320–333

Evrard O, Vandaele K, van Wesemael B, Bielders CL (2008) A grassed waterway and earthen dams to control muddy floods from a cultivated catchment of the Belgian loess belt. Geomorphology 100:419–428. https://doi.org/10.1016/j.geomorph.2008.01.010

FAO (ed) (2006) Guidelines for soil description, 4th edn. FAO, Rome

Foucher A, Salvador-Blanes S, Evrard O et al (2014) Increase in soil erosion after agricultural intensification: evidence from a lowland basin in France. Anthropocene 7:30–41. https://doi.org/10.1016/j.ancene.2015.02.001

Gerlach R, Fischer P, Eckmeier E, Hilgers A (2012) Buried dark soil horizons and archaeological features in the Neolithic settlement region of the Lower Rhine area, NW Germany: Formation, geochemistry and chronostratigraphy. Quat Int 265:191–204. https://doi.org/10.1016/j.quaint.2011.10.007

Gillijns K, Poesen J, Deckers J (2005) On the characteristics and origin of closed depressions in loess-derived soils in Europe—a case study from central Belgium. CATENA 60:43–58. https://doi.org/10.1016/j.catena.2004.10.001

Glina B, Waroszewski J, Kabal C (2014) Water retention of the loess-derived Luvisols with lamellic illuvial horizon in the Trzebnica Hills (SW Poland). Soil Sci Annu 65:18–24. https://doi.org/10.2478/ssa-2014-0003

Golosov VN, Collins AL, Dobrovolskaya NG et al (2021) Soil loss on the arable lands of the forest-steppe and steppe zones of European Russia and Siberia during the period of intensive agriculture. Geoderma 381:114678. https://doi.org/10.1016/j.geoderma.2020.114678

Graly JA, Bierman PR, Reusser LJ, Pavich MJ (2010) Meteoric 10Be in soil profiles - a global meta-analysis. Geochim Cosmochim Acta 74:6814–6829. https://doi.org/10.1016/j.gca.2010.08.036

Gu ZY, Lal D, Liu TS et al (1997) Weathering histories of Chinese loess deposits based on uranium and thorium series nuclides and cosmogenic 10 Be. Geochim Cosmochim Acta 61:5221–5231. https://doi.org/10.1016/S0016-7037(97)00313-X

Guzmán G, Laguna A, Cañasveras JC et al (2015) Study of sediment movement in an irrigated maize–cotton system combining rainfall simulations, sediment tracers and soil erosion models. J Hydrol 524:227–242. https://doi.org/10.1016/j.jhydrol.2015.02.033

Haase D, Fink J, Haase G et al (2007) Loess in Europe-its spatial distribution based on a European Loess Map, scale 1:2,500,000. Quat Sci Rev 26:1301–1312. https://doi.org/10.1016/j.quascirev.2007.02.003

Henkner J, Ahlrichs JJ, Downey S et al (2017) Archaeopedology and chronostratigraphy of colluvial deposits as a proxy for regional land use history (Baar, southwest Germany). CATENA 155:93–113. https://doi.org/10.1016/j.catena.2017.03.005

Hidy AJ, Gosse JC, Pederson JL et al (2010) A geologically constrained Monte Carlo approach to modeling exposure ages from profiles of cosmogenic nuclides: an example from Lees Ferry, Arizona. Geochemistry Geophys Geosystems 11:Q0AA10. https://doi.org/10.1029/2010GC003084

Iurian A-R, Phaneuf MO, Mabit L (2015) Mobility and bioavailability of radionuclides in soils. In: Walther C, Gupta DK (ed) Radionuclides in the environment: influence of chemical speciation and plant uptake on radionuclide migration. Springer, pp 37–59

IUSS Working Group WRB (2015) World Reference Base for soil 721 resources 2014, update 2015 international soil classification 722 system for naming soils and creating legends for soil maps. World 723 soil resources reports no. 106. FAO, Rome

Jagercikova M, Cornu S, Bourlès D et al (2015) Understanding long-term soil processes using meteoric 10Be: A first attempt on loessic deposits. Quat Geochronol 27:11–21. https://doi.org/10.1016/j.quageo.2014.12.003

Jary Z (1996) Chronostratygrafia oraz warunki sedymentacji lessów południowo-zachodniej Polski na przykładzie Płaskowyżu Głubczyckiego i Wzgórz Trzebnickich. Studia Geograficzne LXIII Uniwersytetu Wrocławskiego, Wrocław.pdf

Jary Z, Ciszek D (2013) Late Pleistocene loess-palaeosol sequences in Poland and western Ukraine. Quat Int 296:37–50. https://doi.org/10.1016/j.quaint.2012.07.009

Jelinski NA, Campforts B, Willenbring JK et al (2019) Meteoric beryllium-10 as a tracer of erosion due to postsettlement land use in West-Central Minnesota, USA. J Geophys Res Earth Surf 124:874–901. https://doi.org/10.1029/2018JF004720

Kabała C, Marzec M (2010) Vertical and spatial diversity of grain-size distribution in Luvisols developed from loess in south-western Poland. Rocz Glebozn LXI:52–64

Kabała C, Musztyfaga E, Gałka B, et al (2016) Conversion of soil pH 1:2.5 KCl and 1:2.5 H2O to 1:5 H2O: conclusions for soil management, environmental monitoring, and international soil databases. Polish J Environ Stud 25:647–653. https://doi.org/10.15244/pjoes/61549

Kabała C, Przybył A, Krupski M et al (2019) Origin, age and transformation of Chernozems in northern Central Europe – new data from Neolithic earthen barrows in SW Poland. CATENA 180:83–102. https://doi.org/10.1016/j.catena.2019.04.014

Kaszubkiewicz. J, Tasz W, Kawałko D, Serafin R (2011) USLE model simplification proposal for application in a small agricultural catchment area. Rocz Glebozn LXII:75–81

Ketterer ME, Hafer KM, Link CL et al (2004) Resolving global versus local/regional Pu sources in the environment using sector ICP-MS. J Anal at Spectrom 19:241–245. https://doi.org/10.1039/B302903D

Ketterer ME, Zheng J, Yamada M (2011) Applications of transuranics as tracers and chronometers in the environment. In: Baskaran M (ed.) Handbook of environmental isotope geochemistry, Advances in Isotope Geochemistry. Springer, pp. 395–417. https://doi.org/10.1007/978-3-642-10637-8_20

Kohl CP, Nishiizumi K (1992) Chemical isolation of quartz for measurement of in-situ-produced cosmogenic nuclides. Geochim Cosmochim Acta 56:3583–3587. https://doi.org/10.1016/0016-7037(92)90401-4

Kołodyńska-Gawrysiak R, Poesen J, Gawrysiak L (2018) Assessment of long-term Holocene soil erosion rates in Polish loess areas using sedimentary archives from closed depressions. Earth Surf Process Landforms 43:978–1000. https://doi.org/10.1002/esp.4296

Kopittke PM, Menzies NW, Wang P et al (2019) Soil and the intensification of agriculture for global food security. Environ Int 132:105078. https://doi.org/10.1016/j.envint.2019.105078

Krzyszkowski D (1993) Pleistocene stratigraphy near Trzebnica, Silesian Rampart, Southwestern Poland. Bull Pol Acad Sci

Kundzewicz ZW, Matczak P (2012) Climate change regional review: Poland. Wiley Interdiscip Rev Clim Chang 3:297–311. https://doi.org/10.1002/wcc.175

Labaz B, Musztyfaga E, Waroszewski J et al (2018) Landscape-related transformation and differentiation of Chernozems – catenary approach in the Silesian Lowland, SW Poland. CATENA 161:63–76. https://doi.org/10.1016/j.catena.2017.10.003

Lehmkuhl F, Nett JJ, Pötter S et al (2020) Loess landscapes of Europe – mapping, geomorphology, and zonal differentiation Earth-Science Rev 103496 https://doi.org/10.1016/j.earscirev.2020.103496

Licznar M, Kowaliński S, Drozd J (1981) Changes of some physical properties of soils of the głubczyce plateau under the water erosion effect. Rocz Glebozn XXXII:45–52

Licznar M, Licznar P (2002) Erodibility of Trzebnica Hills loessive soils. Zesz Probl Postępów Nauk Rol 487:129–136

Licznar P, Sasik J, Żmuda R (2002) Prognozowanie erozji wodnej w małych zlewniach rolniczych Wzgórz Trzebnickich. Zesz Probl Postępów Nauk Rol 487:137–146

Licznar S, Kowaliński S, Licznar M (1988) Zastosowanie metod mikromorfologicznych i submikromorfologicznych w badaniu gleb erodowanych. Rocz Glebozn 39:21–34

Loba A, Sykuła M, Kierczak J et al (2020) In situ weathering of rocks or aeolian silt deposition: key parameters for verifying parent material and pedogenesis in the Opawskie Mountains—a case study from SW Poland. J Soils Sediments 20:435–451. https://doi.org/10.1007/s11368-019-02377-5

McLennan SM (2001) Relationships between the trace element composition of sedimentary rocks and upper continental crust. Geochemistry, Geophys Geosystems 2:n/a-n/a. https://doi.org/10.1029/2000GC000109

Meusburger K, Mabit L, Ketterer M et al (2016) A multi-radionuclide approach to evaluate the suitability of 239 + 240Pu as soil erosion tracer. Sci Total Environ 566–567:1489–1499. https://doi.org/10.1016/j.scitotenv.2016.06.035

Muhs DR (2013) The geologic records of dust in the quaternary. Aeolian Res 9:3–48. https://doi.org/10.1016/j.aeolia.2012.08.001

Musso A, Ketterer ME, Greinwald K et al (2020) Rapid decrease of soil erosion rates with soil formation and vegetation development in periglacial areas. Earth Surf Process Landforms 45:2824–2839. https://doi.org/10.1002/esp.4932

Nesbitt HW, Young GM (1982) Early Proterozoic climates and plate motions inferred from major element chemistry of lutites. Nature 299:715–717. https://doi.org/10.1038/299715a0

Nishiizumi K, Imamura M, Caffee MW et al (2007) Absolute calibration of 10Be AMS standards. Nucl Instruments Methods Phys Res Sect B Beam Interact with Mater Atoms 258:403–413. https://doi.org/10.1016/j.nimb.2007.01.297

Pachucki C (1952) Badania geologiczne na arkuszach 1:100 000 Trzebnica i Syców. Biul Inst Geol, 66:355–294

Pasquini AI, Campodonico VA, Rouzaut S, Giampaoli V (2017) Geochemistry of a soil catena developed from loess deposits in a semiarid environment, Sierra Chica de Córdoba, central Argentina. Geoderma 295:53–68. https://doi.org/10.1016/j.geoderma.2017.01.033

Poręba G, Śnieszko Z, Moska P et al (2019) Interpretation of soil erosion in a Polish loess area using OSL, 137Cs, 210Pbex, dendrochronology and micromorphology – case study: Biedrzykowice site (s Poland). Geochronometria 46:57–78. https://doi.org/10.1515/geochr-2015-0109

Poręba G, Śnieszko Z, Moska P (2011) Some aspects of age assessment of Holocene loess colluvium: OSL and 137Cs dating of sediment from Biała agricultural area, South Poland. Quat Int 240:44–51. https://doi.org/10.1016/j.quaint.2011.02.005

Poręba GJ, Śnieszko Z, Moska P (2015) Application of OSL dating and 137Cs measurements to reconstruct the history of water erosion: a case study of a Holocene colluvium in Świerklany, south Poland. Quat Int 374:189–197. https://doi.org/10.1016/j.quaint.2015.04.004

Rafalska-Przysucha A, Rejman J (2015) Assessment of soil erosion in the catchment of two combined closed depressions in the Naleczow Plateau (Lublin Upland). Acta Agrophysica 22:91–101.

Rejman J, Brodowski R (2010) Evaluation of water erosion under sugar beet and spri wheat on loess soil on runoff plots. Prace i Studia Geograficzne 45:215–228

Rejman J, Brodowski R, Iglik I (2008) Annual variations of soil erodibility of silt loam developed from loess based on 10-years runoff plot studies. Ann Warsaw Univ Life Sci - SGGW L Reclam 39:77–83. https://doi.org/10.2478/v10060-008-0007-4

Rickson RJ (2014) Can control of soil erosion mitigate water pollution by sediments? Sci Total Environ 468–469:1187–1197. https://doi.org/10.1016/j.scitotenv.2013.05.057

Routschek A, Schmidt J, Kreienkamp F (2014) Impact of climate change on soil erosion - a high-resolution projection on catchment scale until 2100 in Saxony/Germany. CATENA 121:99–109. https://doi.org/10.1016/j.catena.2014.04.019

Sartori M, Evans ME, Heller F et al (2005) The last glacial/interglacial cycle at two sites in the Chinese Loess Plateau: mineral magnetic, grain-size and 10Be measurements and estimates of palaeoprecipitation. Palaeogeogr Palaeoclimatol Palaeoecol 222:145–160. https://doi.org/10.1016/j.palaeo.2005.03.013

Schaetzl RJ, Attig JW (2013) The loess cover of northeastern Wisconsin. Quat Res 79:199–214. https://doi.org/10.1016/j.yqres.2012.12.004

Steinhoff-Knopp B, Burkhard B (2018) Soil erosion by water in Northern Germany: long-term monitoring results from Lower Saxony. Catena 165:299–309. https://doi.org/10.1016/j.catena.2018.02.017

Święchowicz J (2016) Susceptibility to water erosion soils derived from loess-like deposits (Brzesko Foreland, Southern Poland). In: Święchowicz J, Michno A (ed) Wybrane zagadnienia geomorfologii eolicznej. Monografia dedykowana dr hab. Bogdanie Izmaiłow w 44. rocznicę pracy naukowej. IGiGP UJ, Kraków, pp. 332–366

Świtoniak M, Mroczek P, Bednarek R (2016) Luvisols or Cambisols? Micromorphological study of soil truncation in young morainic landscapes - case study: Brodnica and Chełmno Lake Districts (North Poland). CATENA 137:583–595. https://doi.org/10.1016/j.catena.2014.09.005

Van Oost K, Govers G, Van Muysen W (2003) A process-based conversion model for caesium-137 derived erosion rates on agricultural land: an integrated spatial approach. Earth Surf Process Landforms 28:187–207. https://doi.org/10.1002/esp.446

van Reeuwijk L (2002) Procedures for soil analysis, 6th edn. Wageningen, ISRIC

Van Rompaey AJJ, Verstraeten G, Van Oost K et al (2001) Modelling mean annual sediment yield using a distributed approach. Earth Surf Process Landforms 26:1221–1236. https://doi.org/10.1002/esp.275

Verheijen FGA, Jones RJA, Rickson RJ, Smith CJ (2009) Tolerable versus actual soil erosion rates in Europe. Earth-Science Rev 94:23–38

Verstraeten G, Poesen J (2001) Factors controlling sediment yield from small intensively cultivated catchments in a temperate humid climate. Geomorphology 40:123–144. https://doi.org/10.1016/S0169-555X(01)00040-X

von Blanckenburg F, Belshaw NS, O'Nions RK (1996) Separation of 9Be and cosmogenic 10Be from environmental materials and SIMS isotope dilution analysis. Chem Geol 129:93–99. https://doi.org/10.1016/0009-2541(95)00157-3

Walling DE, Quine TA (1990) Calibration of caesium-137 measurements to provide quantitative erosion rate data. L Degrad Dev 2:161–175. https://doi.org/10.1002/ldr.3400020302

Waroszewski J, Egli M, Brandová D et al (2018) Identifying slope processes over time and their imprint in soils of medium-high mountains of Central Europe (the Karkonosze Mountains, Poland). Earth Surf Process Landforms 43:1195–1212. https://doi.org/10.1002/esp.4305

Willenbring JK, von Blanckenburg F (2010) Meteoric cosmogenic beryllium-10 adsorbed to river sediment and soil: applications for Earth-surface dynamics. Earth-Science Rev 98:105–122. https://doi.org/10.1016/j.earscirev.2009.10.008

Wyshnytzky CE, Ouimet WB, McCarthy J et al (2015) Meteoric 10Be, clay, and extractable iron depth profiles in the Colorado Front Range: implications for understanding soil mixing and erosion. CATENA 127:32–45. https://doi.org/10.1016/j.catena.2014.12.008

Xu Y, Qiao J, Pan S et al (2015) Plutonium as a tracer for soil erosion assessment in northeast China. Sci Total Environ 511:176–185. https://doi.org/10.1016/j.scitotenv.2014.12.006

Yang MY, Tian JL, Liu PL (2006) Investigating the spatial distribution of soil erosion and deposition in a small catchment on the Loess Plateau of China, using 137Cs. Soil Tillage Res 87:186–193. https://doi.org/10.1016/j.still.2005.03.010

Zádorová T, Penížek V (2018) Formation, morphology and classification of colluvial soils: a review. Eur J Soil Sci 69:577–591. https://doi.org/10.1111/ejss.12673

Zhang K, Pan S, Liu Z et al (2018) Vertical distributions and source identification of the radionuclides 239Pu and 240Pu in the sediments of the Liao River estuary, China. J Environ Radioact 181:78–84. https://doi.org/10.1016/j.jenvrad.2017.10.016

Zhang X, Higgit DL, Walling DE (1990) A preliminary assessment of the potential for using caesium-137 to estimate rates of soil erosion in the Loess Plateau of China. Hydrol Sci J 35:243–252. https://doi.org/10.1080/02626669009492427

Zhou W, Xie X, Beck W et al (2015) Recent progress of 10Be tracer studies in Chinese loess. Nucl Instruments Methods Phys Res Sect B Beam Interact with Mater Atoms 361:548–553. https://doi.org/10.1016/j.nimb.2015.02.061

Zmuda R, Szewrański S, Kowalczyk T et al (2009) Landscape alteration in view of soil protection from water erosion - an example of the Mielnica watershed. J Water L Dev 13:161–175. https://doi.org/10.2478/v10025-010-0026-5

Zollinger B, Alewell C, Kneisel C et al (2015) The effect of permafrost on time-split soil erosion using radionuclides (137Cs, 239 + 240Pu, meteoric 10Be) and stable isotopes (δ13C) in the eastern Swiss Alps. J Soils Sediments 15:1400–1419. https://doi.org/10.1007/s11368-014-0881-9

Wrocław, 1.11.2022

Mgr inż. Aleksandra Loba
Instytut Nauk o Glebie, Żywienia Roślin
i Ochrony Środowiska
Uniwersytet Przyrodniczy we Wrocławiu

Oświadczenie

Oświadczam, że w pracy: Loba A., Waroszewski J., Tikhomirov D., Calitri F[*]., Christl M., Sykuła M., Egli M., 2021. *Tracing erosion rates in loess landscape of the Trzebnica Hills (Poland) over time using fallout and cosmogenic nuclides*. Journal of Soils and Sediments 21, 2952 – 2968, doi:10.1007/s11368-021-02996-x, mój udział polegał na opracowaniu założeń prowadzonych badań, wyborze powierzchni badawczych oraz doborze metodyki prac terenowych i laboratoryjnych, wykonaniu analiz laboratoryjnych, przygotowaniu próbek glebowych do pomiaru zawartości ^{10}Be in-situ i $^{239+240}$Pu, kalkulacji tempa erozji, opracowaniu merytorycznym uzyskanych wyników oraz przygotowaniu treści niniejszego manuskryptu.

....
(podpis)

Wrocław, 20.10.2022

Dr hab. inż. Jarosław Waroszewski, prof. UPWr
Instytut Nauk o Glebie, Żywienia Roślin
i Ochrony Środowiska
Uniwersytet Przyrodniczy we Wrocławiu

Oświadczenie

Oświadczam, że w pracy: Loba A., Waroszewski J., Tikhomirov D., Calitri F., Christl M., Sykuła M., Egli M., 2021. *Tracing erosion rates in loess landscape of the Trzebnica Hills (Poland) over time using fallout and cosmogenic nuclides*. Journal of Soils and Sediments 21, 2952 – 2968, doi:10.1007/s11368-021-02996-x, mój udział polegał na nadzorowaniu przy opracowaniu założeń prowadzonych badań, wyborze powierzchni badawczych oraz doborze metodyki prac terenowych i laboratoryjnych. Nadzór merytoryczny obejmował także poprawność interpretacji wyników oraz przygotowanie treści manuskryptu.

…………………………………..
(podpis)

Universität Zürich [UZH]

Dr Dmitry Tikhomirov
Department of Geography
University of Zurich

Oświadczenie/Statement

Oświadczam, że w pracy: Loba A., Waroszewski J., Tikhomirov D., Calitri F., Christl M., Sykuła M., Egli M., 2021. *Tracing erosion rates in loess landscape of the Trzebnica Hills (Poland) over time using fallout and cosmogenic nuclides.* Journal of Soils and Sediments 21, 2952 – 2968, doi:10.1007/s11368-021-02996-x, mój udział polegał na nadzorowaniu przygotowania próbek do analizy spektrometrii masowej 10Be i 239+240Pu, a także na pomiarze zawartości 239+240Pu za pomocą ICP-MS w badanych próbkach. Jako współautor pracowałem nad przygotowaniem manuskryptu oraz nadzorowałem prawidłową interpretacją wyników pomiarów.

I declare that in the paper: Loba A., Waroszewski J., Tikhomirov D., Calitri F., Christl M., Sykuła M., Egli M., 2021. *Tracing erosion rates in loess landscape of the Trzebnica Hills (Poland) over time using fallout and cosmogenic nuclides.* Journal of Soils and Sediments 21, 2952 – 2968, doi:10.1007/s11368-021-02996-x, my participation consisted of supervision of sample preparation for mass spectrometry analysis of ^{10}Be and $^{239+240}$Pu, as well as measurement $^{239+240}$Pu content with ICP-MS in the studied samples. I worked as a co-author on preparation of the manuscript including supervision of correct interpretation of the measurement results.

(podpis/signature)

ETH *zürich*

Zurich, 29.10.2022

Dr Marcus Christl
Laboratory of Ion Beam Physics
Institute for Particle Physics and Astrophysics
ETH Zurich

Oświadczenie/Statement

Oświadczam, że w pracy: Loba A., Waroszewski J., Tikhomirov D., Calitri F., Christl M., Sykuła M., Egli M., 2021. *Tracing erosion rates in loess landscape of the Trzebnica Hills (Poland) over time using fallout and cosmogenic nuclides*. Journal of Soils and Sediments 21, 2952 – 2968, doi:10.1007/s11368-021-02996-x, mój udział polegał na nadzorowaniu wykonania analiz ^{10}Be in-situ i kalkulacji tempa erozji. Nadzór merytoryczny obejmował poprawność interpretacji wyników oraz przygotowanie treści manuskryptu.

I declare that in the paper: Loba A., Waroszewski J., Tikhomirov D., Calitri F., Christl M., Sykuła M., Egli M., 2021. *Tracing erosion rates in loess landscape of the Trzebnica Hills (Poland) over time using fallout and cosmogenic nuclides*. Journal of Soils and Sediments 21, 2952 – 2968, doi:10.1007/s11368-021-02996-x, my participation consisted of supervising performance of ^{10}Be in-situ analyses and calculation of erosion rates. Substantive supervision also included the correctness of the interpretation of the results and preparation of the content of manuscript.

....
(podpis/signature)

Toruń, 18. 10. 2022

Dr Marcin Sykuła
Katedra Gleboznawstwa
i Kształtowania Krajobrazu
Uniwersytet Mikołaja Kopernika
w Toruniu

Oświadczenie

Oświadczam, że w pracy: Loba A., Waroszewski J., Tikhomirov D., Calitri F., Christl M., Sykuła M., Egli M., 2021. *Tracing erosion rates in loess landscape of the Trzebnica Hills (Poland) over time using fallout and cosmogenic nuclides*. Journal of Soils and Sediments 21, 2952 – 2968, doi:10.1007/s11368-021-02996-x, mój udział polegał na graficznym opracowaniu wyników badań i sprawdzeniu finałowej wersji manuskryptu.

....
(podpis)

Zürich, 24th of October 2022

Prof. Dr. Markus Egli
Department of Geography
University of Zurich

Oświadczenie/Statement

Oświadczam, że w pracy: Loba A., Waroszewski J., Tikhomirov D., Calitri F., Christl M., Sykuła M., Egli M., 2021. *Tracing erosion rates in loess landscape of the Trzebnica Hills (Poland) over time using fallout and cosmogenic nuclides*. Journal of Soils and Sediments 21, 2952 – 2968, doi:10.1007/s11368-021-02996-x, mój udział polegał na nadzorowaniu przy opracowaniu założeń prowadzonych badań, wyborze powierzchni badawczych oraz doborze metodyki prac terenowych i laboratoryjnych. Nadzór merytoryczny obejmował także pomoc w kalkulacji tempa erozji, poprawność interpretacji wyników oraz przygotowanie treści manuskryptu.

I declare that in the paper: Loba A., Waroszewski J., Tikhomirov D., Calitri F., Christl M., Sykuła M., Egli M., 2021. *Tracing erosion rates in loess landscape of the Trzebnica Hills (Poland) over time using fallout and cosmogenic nuclides*. Journal of Soils and Sediments 21, 2952 – 2968, doi:10.1007/s11368-021-02996-x, my participation consisted in the supervision and guidance of the research and methodology in the field and laboratory. The supervision also included assistance in calculating soil erosion rates, the correctness of the interpretation of the results and the preparation of the manuscript.

………………………………….
(podpis/signature)

Wrocław, 1.11.2022

Mgr inż. Aleksandra Loba
Instytut Nauk o Glebie, Żywienia Roślin
i Ochrony Środowiska
Uniwersytet Przyrodniczy we Wrocławiu

Oświadczenie

Oświadczam, że w pracy: Loba A., Waroszewski J., Tikhomirov D., Calitri F[*]., Christl M., Sykuła M., Egli M., 2021. *Tracing erosion rates in loess landscape of the Trzebnica Hills (Poland) over time using fallout and cosmogenic nuclides*. Journal of Soils and Sediments 21, 2952 – 2968, doi:10.1007/s11368-021-02996-x, udział **Francesci Calitri** polegał na kalkulacji tempa erozji za pomocą modelu konwersji MODERN i sprawdzenia gotowej wersji manuskryptu.

Obecnie mgr Francesca Calitri nie jest już doktorantką na Uniwersytecie w Zurychu i nie mam z nią kontaktu.
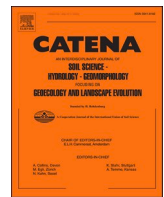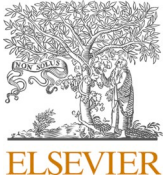
………………………………….
(podpis)

Multiproxy approach to the reconstruction of soil denudation events and the disappearance of Luvisols in the loess landscape of south-western Poland

Aleksandra Loba [a,b,*], Junjie Zhang [c], Sumiko Tsukamoto [c], Marek Kasprzak [d], Joanna Beata Kowalska [b], Manfred Frechen [c], Jarosław Waroszewski [b]

[a] *Nicolaus Copernicus University in Toruń, Faculty of Earth Sciences and Spatial Management, Lwowska 1, 87-100, Toruń, Poland*
[b] *Wrocław University of Environmental and Life Sciences, Institute of Soil Science, Plant Nutrition and Environmental Protection, Grunwaldzka 53, 50-357 Wrocław, Poland*
[c] *Leibniz Institute for Applied Geophysics (LIAG), Stilleweg 2, 30655 Hannover, Germany*
[d] *University of Wrocław, Institute of Geography and Regional Development, Plac Uniwersytecki 1, 50-137 Wrocław, Poland*

ABSTRACT

Loess landscapes are highly susceptible to soil redeposition processes and thus may provide detailed insights into the record of denudation processes. Using optically stimulated luminescence dating and the soil micromorphology of 12 soil profiles, we reconstructed a complete record of denudation processes in south-western Poland. The first episode of soil redeposition took place around 9.1 ka. The denudation events that followed were attributed to the Neolithic (6.4 ± 0.3 ka), early Bronze Age (3.8 ± 0.2 ka), early and late Middle Ages (1.5 ± 0.1 ka and 0.7 ± 0.03 ka, respectively) and early Modern (0.4 ± 0.02 ka). As a consequence of the denudation processes, the soil cover in the studied area had been strongly reshaped. The predominant Luvisols had experienced progressive erosion processes that led first to a significant shallowing of the eluvial and argic horizons (truncated Luvisol) and, after some time, to their complete removal. Further thinning of the loess mantles had exposed geological substrates with very weak pedogenic alternations, thus pushing their transformation towards Regosol types. Similarly, Regosols occurred in toeslopes where freshly eroded material had been deposited, and where diagnostic horizons had not yet developed. Modern soil erosion rates in the studied loess area have considerably increased, and it is estimated that the Luvisol status may be completely transformed within approximately 80–300 years, if not sooner, due to progressive climate change.

1. Introduction

Denudation processes understood as a surface lowering of the land by erosion and near-surface processes, lead to a significant landscape modifications (Karasiewicz et al., 2014; Raab et al., 2021). In agricultural landscapes and hill county, the soil erosion is essential for denudation (Meij et al., 2019; Raab et al., 2018). Erosion processes disintegrate and remove topsoil from the upslope and deposit the transported material in the toe slope, where it forms colluvial soils. Thus, as a consequence irreversible changes occur in the natural structure, physical, chemical and morphological features of these soils and their corresponding horizons as well as their distribution in the landscape (Kaiser et al., 2021; Matecka and Świtoniak, 2020; Pindral and

Świtoniak, 2017; Zádorová et al., 2014; Zádorová and Penížek, 2018).

One of the materials most susceptible to denudation processes is loess (Poręba et al., 2019; Šimanský et al., 2019; Zhang et al., 2018b), sediment that is widespread on a global scale (Muhs, 2013). In Europe, loess deposits occur from France to Ukraine and Russia (Haase et al., 2007; Lehmkuhl et al., 2021; Scheib et al., 2014) with their most intense accumulation having occurred during the Last Glacial Maximum (LGM) in Marine Isotope Stage (MIS) 2 (Frechen, 2003; Jary, 1996). Since the Neolithic, soil erosion/deposition processes have been accelerated in the loess-covered areas due to deforestation and the use of that land for arable (Altermann et al., 2005; Gerlach et al., 2012; Kołodyńska-Gawrysiak et al., 2017). These changes in land use occurred because most fertile soils, such as Chernozems and Pheozems, characterised by a

---

thick, dark humus (chernic/mollic) horizon, have developed in loess belts (Altermann et al., 2005; Drewnik et al., 2014; Gerlach et al., 2012; Labaz et al., 2018; Smetanová et al., 2017).

Much has been written about erosion and redeposition processes in soils bearing chernic (and mollic) horizons developed in loess-dominated landscapes in the Czech Republic (Smetanová et al., 2017; Zádorová et al., 2011), Germany (Altermann et al., 2005; Gerlach et al., 2012), Poland (Drewnik and Żyła, 2019; Kabała et al., 2019), Ukraine (Dreibrodt et al., 2022; Łanczont et al., 2021) and Russia (Khokhlova et al., 2015). Erosion processes thin humus-rich horizons and, as a result, their colour is greatly lightened (Drewnik and Żyła, 2019). Consequently, the criteria for chernic/mollic horizons are not met and the soils are transformed into Luvisols (Kabała et al., 2019; Labaz et al., 2018). These are still fertile soils because of their high saturation with alkaline cations and favourable hydro-physical properties (Glina et al., 2014; Rejman et al., 2014a; Turski and Witkowska-Walczak, 2004; Vitharana et al., 2008). However, they are intensively used in agriculture and thus exposed to further degradation (Klimowicz and Uziak, 2001). Erosion and soil degradation are issues specifically highlighted in the European Parliament's resolution on soil protection from 2021 (European Parliament, 2021) and the Food and Agriculture Organization's (FAO) statement of 2019 (FAO, 2019). Thus, detailed actual research on this topic is still needed.

Using knowledge on soil erosion rates, soil conservation practices can be optimised (Alewell et al., 2017). Erosion processes have been widely studied in loess landscapes using isotope techniques, such as beryllium-10, cesium-137, plutonium-239/240, excess lead-210, δ^{13}C, δ^{15}N, and classical methods, including closed depressions and the Universal Soil Loss Equation, in France, Germany, Belgium, Poland, China and the USA (Baumgart et al., 2017; Dreibrodt et al., 2013, 2010b; Gillijns et al., 2005; Jagercikova et al., 2015, 2014; Jakab et al., 2018; Kołodyńska-Gawrysiak et al., 2018; Li et al., 2005; Liu et al., 2018; Loba et al., 2022, 2021; Poręba et al., 2019, 2015; Tuo et al., 2018; Van Oost et al., 2003; Yu et al., 2017; Zhang et al., 2018a; Zhang et al., 2019). The data obtained on soil erosion may be supported by dating techniques, such as radiocarbon (^{14}C) dating of soil organic matter, charcoals from colluvial sediments or optically stimulated luminescence (OSL), which can provide information concerning when the constituent mineral grains were last exposed to sunlight, thus providing an age for the sediment (re) deposition (Fuchs et al., 2010; Kołodyńska-Gawrysiak et al., 2017; Novák et al., 2018; Poręba et al., 2011; Rahimzadeh et al., 2019; Zgłobicki and Rodzik, 2007). Such approaches enable the reconstruction of erosion–deposition events, an analysis of the evolution of relief in the Pleistocene and Holocene, and the modelling of past environmental dynamics (Döhler et al., 2018; Kołodyńska-Gawrysiak et al., 2018; Malik et al., 2021; Poręba et al., 2019; Rahimzadeh et al., 2019; Scherer et al., 2021).

Recent studies have shown that progressive climate change and agricultural intensification accelerate erosion processes (Kopittke et al., 2019; Kundzewicz and Matczak, 2012; Loba et al., 2021; Radziuk and Świtoniak, 2021; Routschek et al., 2014; Zollinger et al., 2015), and therefore the status of Luvisols occurring in the loess landscapes is uncertain. In order to track past and present changes in Luvisols we aimed to: i) reconstruct time-intervals of denudation processes using OSL dating; ii) outline the soil development trajectories forced by denudation processes; and iii) calculate the approximate timing of the disappearance of the Luvisols.
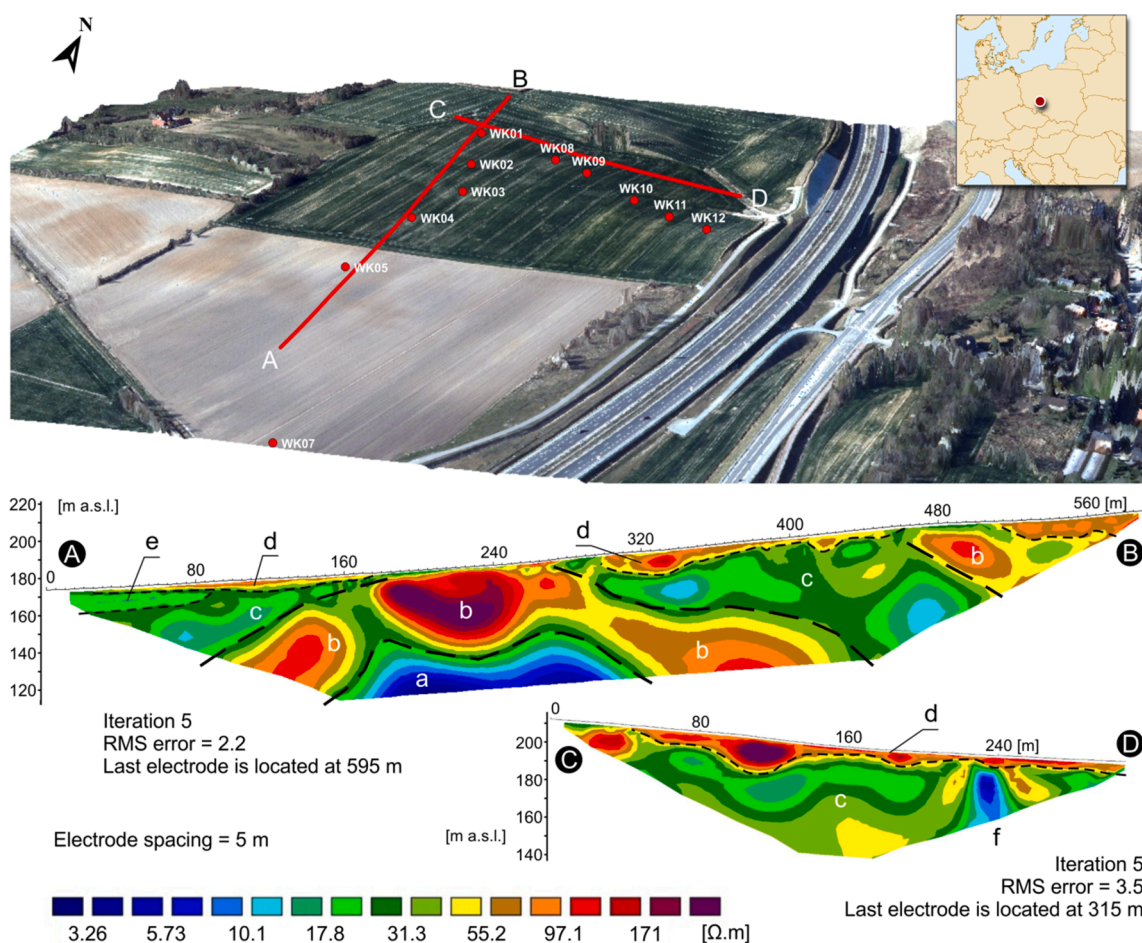

Fig. 1. Study sites in the Trzebnica Hills and inversion models for two Electrical Resistivity Tomography sections.

2. Methods

2.1. Study area and sampling strategy

The study area was situated in south-western Poland, around the edges of the Trzebnica Hills, north of Wrocław (Fig. 1, Table 1). The local lithology is dominated by Quaternary deposits, including glacial tills, fluvioglacial sediments and loess, the latter being the youngest (late Pleistocene) deposit, which is spread over the hills, forming a mantle with varying thickness (Glina et al., 2014; Jary, 1996). Most of the land is used for agriculture due to the presence of productive soils (Luvisols, Pheozems, Chernozems) (Anioł-Kwiatkowska, 1998). The study area is characterised by warm summers and a humid, continental climate. The mean annual temperature is 9.5 °C, while the mean annual precipitation ranges from 500 to 620 mm (Bac and Rojek, 2012).

Two soil transects were arranged along slopes that bore visible features of erosion and accumulation processes. Profile WK1 was a common point for both transects (Fig. 1), with the first transect including Profiles WK1–WK7, and the second WK1 and WK8–WK12. Drilling down to 70 cm between the soil profiles was done in order to assess the thickness of the loess mantle and the disappearance of the E and Bt horizons. All soil profiles were described according to the Guidelines for Soil Description (FAO, 2006) and classified according to the FAO–World Reference Base (WRB) system (IUSS Working Group WRB, 2022). From all designated soil horizons, about 1 kg of bulk material was sampled for chemical and physical analysis. Additionally, 15 samples were taken for OSL dating from selected horizons by hammering steel tubes into the freshly cleaned outcrop walls, with 12 undisturbed samples being taken for micromorphological investigation using Kubiena boxes (6 × 4 cm).

2.2. Electrical resistivity tomography

The ERT measurements allow for a visualisation of the variability of the geological structure of the shallow ground and distinction of the main lithological units (Fig. 1). Electrical resistivity tomography (ERT) was carried out as part of the fieldwork (Kasprzak and Traczyk, 2014), and included zones of previously made soil profiles and drillings. The survey campaign took place in rain-free weather conditions and on moist, vegetation-free soil. An ARES II device, with a set of cables enabling the simultaneous connection of 80 electrodes distributed along

the measured section, was used to perform the measurements. The measurements were taken in two sections, one 595 m long (Section AB), using rolling cables, and the other 315 m long (Section CD), and reached a maximum depth of about 75 m. In both cases, the distance between the electrodes was 5 m. This was also the resolution of the data obtained from the near-surface layer, whereas, in the deeper part of the profile, the resolution decreased. The measurements were made using the Schlumberger method—regarded as relatively universal for recognizing both vertical and horizontal structures in the subsurface—which also offers a relatively large number of combinations of electrodes and thus measurement points (Reynolds, 2011). The data were subjected to a smooth type of inversion (L2) using RES2DINV software (Geotomo, Malaysia), which included a topographic correction. Results are presented for the fifth iteration, with the colour scale unified for both inversion models. The interpretation of the obtained models was based on data from available geological sources (Krzyszkowski and Łabno, 2002; Winnicki, 1997), including a geological map with explanatory notes (Winnicki, 1990, 1985) and nearby boreholes data (Central Geological Database).

2.3. Soil micromorphology

Sampled soil blocks were left to air-dry. They were then embedded in polyester resin (T.R.A., Finress) and left to cure for 2–4 weeks at room temperature, after which, 1–2-cm-thick slabs were cut from the blocks and trimmed to match the dimensions of a glass slide. The cut side of the embedded block was polished using diamond paste. The grinding and polishing on a diamond wheel were performed manually and checked regularly under the microscope until quartz interference colours matching a 30-μm-thick thin section were obtained. The thin sections were prepared at the University of Ghent (Laboratory for Mineralogy and Petrology). The thin sections were observed in both plane and polarised light using a Zeiss Axio Lab A1 transmitting-light microscope and were described according to the terminology of Stoops (Stoops, 2003).

2.4. Particle size distribution

The particle size distributions between 0.4 and 2000 μm were measured following sample dispersion for 12 h on a rotator using 1%

Table 1
Main characteristics of studied sites.

Soil profile	Latitude and longitude	Elevation (m asl)	Inclination (°)	Slope position	Land use	Classification according to WRB (IUSS, 2022)	Horizons layout
WK1	51° 16′ 09.0″ N 17° 02′ 36.7″ E	206.8	4	Top slope	Arable land	Albic Luvisol (Aric, Cutanic, Ochric, Siltic)	Ap – AE – E – EBtg – Btg1 – Btg2
WK2	51° 16′ 06.3″ N 17° 02′ 38.3″ E	198.2	10	Shoulder	Arable land	Haplic Luvisol (Aric, Cutanic, Endodensic, Endoloamic, Ochric, Episiltic, Raptic)	Ap – A/Bt – Bt/BC – BC1 – BC2 – 2Btb – 2Bt/2BCb
WK3	51° 16′ 02.6″ N 17° 02′ 37.6″ E	191.8	13	Shoulder	Arable land	Lamellic Luvisol (Aric, Cutanic, Ochric, Siltic)	Ap – AE – Bt1 -Bt2 – BC
WK4	51° 15′ 59.3″ N 17° 02′ 37.4″ E	187.1	10	Back slope	Arable land	Stagnic Albic Luvisol (Aric, Cutanic, Ochric, Siltic)	Ap – AE – E – Ebt – Bt/E – Bt -BC
WK5	51° 15′ 56.6″ N 17° 02′ 38.5″ E	181.1	5	Back slope	Arable land	Albic Luvisol (Aric, Cutanic, Ochric, Siltic)	Ap -AEg – Eg – EBtg – Btg - BC
WK6	51° 15′ 50.8″ N 17° 02′ 41.3″ E	176.1	3	Foot slope	Arable land	Haplic Luvisol (Aric, Cutanic, Endoloamic, Ochric, Episiltic, Solimovic)	Ap – AE – Eg – Ab – AEb – EBgb1 – EBgb2 - BCg
WK7	51° 15′ 51.0″ N 17° 02′ 41.0″ E	170.2	2	Toe slope	Arable land	Eutric Solimovic Regosol (Aric, Ochric, Episiltic)	Ap – AE – Eg – 2EBg1 – 2EBg2 – 3C – 4C
WK8	51° 16′ 08.5″ N 17° 02′ 42.0″ E	198.1	7	Shoulder	Arable land	Haplic Luvisol (Aric, Cutanic, Endoloamic, Ochric, Episiltic, Raptic)	Ap – Bt – Bt/BC – 2BCk1 – 2BCk2
WK9	51° 16′ 07.1″ N 17° 02′ 45.8″ E	193.7	12	Shoulder	Arable land	Eutric Regosol (Aric, Endoloamic, Ochric, Episiltic)	Ap – BCk1 – BCk2
WK10	51° 16′ 05.2″ N 17° 02′ 47.5″ E	191.4	7	Back slope	Arable land	Haplic Luvisol (Aric, Cutanic, Endoloamic, Ochric, Episiltic, Raptic)	Ap1/Bt – A2/Bt – Bt -BC1 – BC2
WK11	51° 16′ 03.8″ N 17° 02′ 50.4″ E	188.9	3	Back slope	Arable land	Haplic Luvisol (Aric, Cutanic, Ochric, Siltic)	Ap/Bt – Bt/Ap – BC – BC1 – BC2
WK12	51° 16′ 03.0″ N 17° 02′ 50.0″ E	185.6	2	Foot slope	Arable land	Endostagnic Solimovic Eutric Regosol (Pantosiltic, Ochric)	A/C – A – BC1g – BC2g

ammonium hydroxide and a Beckman–Coulter LS 13 320 laser diffraction analyser at the Leibniz-Institut für Angewandte Geophysik in Hannover, Germany

2.5. OSL dating

Samples for OSL dating were prepared under subdued red-light conditions. The soil material from the outer ~ 2 cm of both sides of the sampling tubes was removed and used for dose-rate determination. Material from the inner part of the tubes was treated with 10% HCl to dissolve the carbonates, 3% sodium oxalate to separate the aggregates and 30% H_2O_2 to remove the organic matter. The fine silt size fraction (4–11 μ m) was separated by sedimentation based on Stoke's law. To obtain a pure quartz fraction for measurement, the sample was treated with 40% H_2SiF_6 acid for 5 days in order to dissolve any remaining feldspars. Fine silt polymineral and quartz extracts were deposited on Al discs (2 mg/disc). All measurements were performed using an automated luminescence reader (Risø TL/OSL-DA-15) equipped with a $^{90}Sr/^{90}Y$ beta source for irradiation. For the polymineral fraction, infrared (870 ± 40 nm) LEDs were used for stimulation, and luminescence signals were detected through a combined filter pack with blue transmission (Schott BG-39 and Corning 7–59). For the quartz fraction blue LEDs (470 ± 30 nm) were applied for stimulation, and the luminescence signals were detected through a 7.5 -mm Hoya U-340 filter with UV transmission. The single-aliquot regenerative (SAR) dose protocols used for dating are shown in Table 2. A low-temperature post-IR IRSL (pIRIR) dating protocol was applied to the polymineral fraction, preheat to 200 °C for 60 s and then with a first IR stimulation at 50 °C (IR_{50}) for 100 s and a second IR stimulation at 170 °C ($pIRIR_{170}$) for 100 s' (Li et al., 2015; Reimann et al., 2011). The first 10 s signal of the decay curve was integrated for equivalent dose (De) estimation with the last 10 s subtracted as background. Six aliquots were measured for each sample. All the aliquots showed good luminescence characteristics, including high signal intensity ($T_n > BG + 3\sigma$), a recycling ratio within 10% of unity, and a recuperation ratio of less than 5%. No aliquot was rejected in D_e estimation. Fading rates (g-values) of the IR_{50} and $pIRIR_{170}$ signals were measured using the SAR protocol (Auclair et al., 2003). Fading correction was performed following the method of Huntley and Lamothe (2001), using the 'calc_FadingCorr' function in the 'Luminescence' R package (Kreutzer et al., 2012). To test the reliability of the SAR protocol for the D_e measurements, samples LUM4248, LUM4253 and LUM4259 were used for dose recovery tests. Five aliquots from each sample were bleached using a Hönle solar simulator (SOL2) for 2 h to remove the natural signal. Two aliquots were used to measure the residual dose and three aliquots were given doses of 50.0, 28.5 and 10.7 Gy for LUM4248, LUM4253 and LUM4259, respectively. Then the aliquots were treated as natural aliquots in order to measure the D_e. The recovered doses (residual dose subtracted) were within 5% of the given

doses for both the IR_{50} and $pIRIR_{170}$ signals (Fig. 2).

For the quartz fraction, the preheating treatment involved 220 °C for 10 s, with the OSL signal measured at 125 °C for 40 s. The first 0.5-s signal of the decay curve was used for D_e estimation, with the last 3.2-s signal subtracted as background. For each sample, 10–12 aliquots were measured. Similarly, to the polymineral analysis, the OSL characteristics of the quartz samples were very good and all aliquots passed the rejection criteria. An IR depletion ratio test was performed on each sample and no feldspar contamination was identified (Duller, 2003). A high preheating temperature can induce a thermally transferred OSL signal and result in D_e overestimation, whereas a low preheating temperature may not be able to remove the unstable signals of the regenerative doses, thereby resulting in D_e underestimation (Wintle and Murray, 2006). To test whether the preheating temperature of 220 °C was suitable for the quartz D_e measurements, the D_e values of two samples (LUM4253 and LUM4259) were measured using different preheating temperatures, ranging from 160 to 280 °C, with an interval of 20 °C. This demonstrated that a D_e plateau could be reached using preheating temperatures between 180 and 220 °C (Fig. 3a, b). A dose recovery using different preheating temperatures was performed on LUM4249. A group of aliquots from LUM4249 were bleached in natural sunlight for 30 min in April 2021, in Hannover, Germany. A fixed dose of 14.3 Gy was given to the bleached aliquots. The aliquots were divided into seven groups (with three aliquots in each group) and measured using the SAR protocol and different preheating temperatures. Another group of aliquots were used to measure the residual doses under different preheating temperatures. The residual doses were less than 0.1 Gy for all the aliquots. The recovered doses (residual dose subtracted) were divided by the given dose to obtain the dose recovery ratios. This showed that the recovery ratios were within 2% of unity when the preheating temperature was between 160 and 240 °C (Fig. 3c). Similar dose recovery tests were performed on five more quartz samples, with different given doses from 1.4 to 61 Gy, but with a fixed preheating temperature of 220 °C. All the recovered doses were within 5% of the given doses (Fig. 3d). These results indicate that the measured D_e values were reliable.

The uranium (U), thorium (Th), and potassium (K) concentrations were measured, using gamma spectrometry to calculate the dose rates (Table 3). A 20% radon loss from the ^{238}U series was assumed (Olley

Table 2
Protocols used for dating.

| Step	pIRIR protocol for polymineral	Observed	Blue OSL protocol for quartz	Observed
1	Given dose Di		Given dose Di	
2	Preheat at 200 °C for 60 s		Preheat at 220 °C for 10 s	
3	IRSL at 50 °C for 100 s	L_{x1}	OSL at 125 °C for 40 s	L_x
4	IRSL at 170 °C for 100 s	L_{x2}	Test dose	
5	Test dose		Cutheat to 200 °C	
6	Preheat at 200 °C for 60 s		OSL at 125 °C for 40 s	T_x
7	IRSL at 50 °C for 100 s	T_{x1}	OSL bleaching 240 °C for 40 s	
8	IRSL at 170 °C for 100 s	T_{x2}	Return to step 1	
9	IR bleaching at 220 °C for 40 s			
10	Return to step 1			

Fig. 2. Dose recovery tests with the $pIRIR_{50, 170}$ SAR protocol. Each data point is an average of 3 aliquots. Samples LUM4248, LUM4253, LUM4259 were bleached by the SOL2 for 2 h and given doses of 50.0 Gy, 28.5 Gy, and 10.7 Gy respectively. The recovered doses were within 5% of the given doses.
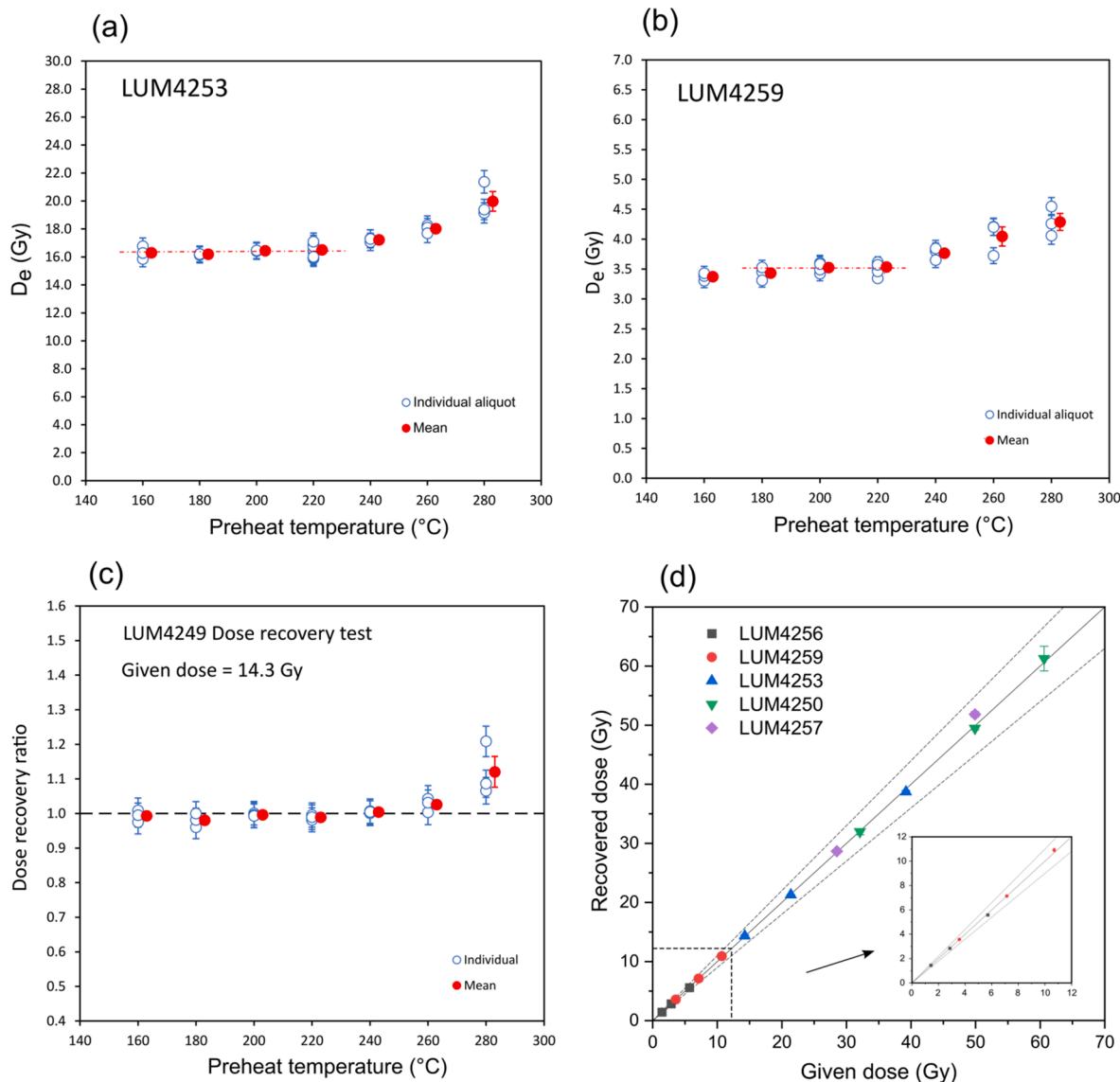
Fig. 3. a) De vs. preheat temperature of LUM4253, b) De vs. preheat temperature of LUM4259, c) Dose recovery ratio vs. preheat temperature of LUM4249, d) Recovered doses vs. given doses with a fixed preheat temperature at 220 °C.

et al., 1997). Conversion factors from Liritzis et al. (Liritzis et al., 2013) were applied. The *a*-value was taken as 0.04 ± 0.02 (Rees-Jones and Tite, 1997). The cosmic dose rate was estimated based on the sample depth, altitude, and geographical coordinates of each sample (Prescott and Hutton, 1994). Water content of $20 \pm 5\%$ was used for all samples.

2.6. Verification of the reliability of OSL ages

The dose rates are summarised in Table 4. It is well known that the quartz OSL signal is much easier to be bleached than the feldspar IRSL signal (Godfrey-Smith et al., 1988; Thomsen et al., 2008; Wallinga, 2002), and that the pIRIR signal is even harder to be bleached than the IR_{50} signal (Buylaert et al., 2011; Chen et al., 2013). Because the fading-corrected $pIRIR_{170}$ ages are always greater than the fading-corrected IR_{50} ages (Table 4), we assumed that the $pIRIR_{170}$ signal of the samples was not fully bleached before deposition and that the corresponding ages were overestimated. For most of the samples, the fading-corrected IR_{50} ages were consistent with the quartz OSL ages (age ratios within 10% of unity, considering the error), indicating that both the IR_{50} and OSL signals were fully reset before deposition. However, for several samples, the fading-corrected IR_{50} ages were still greater than the quartz

OSL ages, with an overestimation of up to 140% (e.g. LUM4255, LUM4262), indicating incomplete resetting of the IR_{50} signal before deposition. Thus, to check whether the OSL signal for these samples was fully reset, we applied the method proposed by Murray et al. (2012), by comparing the D_e values between the IR_{50} and quartz OSL signals. For a sample with an OSL signal that had been fully reset before deposition, the difference between the measured and predicted D_e values of IR_{50} should have been less than the acceptance limit, termed as ΔF in Murray et al. (2012). The ΔF is dependent on the size of the measured De of the quartz OSL, and it can be determined based on the different bleaching rates of quartz OSL and feldspar IR_{50} signals (Murray et al., 2012). In Fig. 4, example data for ΔF at several different quartz D_e values are given, taken from Murray et al. (2012), and the dashed line was fitted using these example data. It should be noted that the expected D_e values of IR_{50} were calculated by multiplying the dose rates of the polymineral fine-grained material with the quartz OSL ages and a fading factor. Murray et al. (2012) applied a fading factor of 0.55, based on the study of Buylaert et al. (2012) which showed that the fading uncorrected IR_{50} ages made up about 0.55 of the independent ages. In our study, the ratios of fading-uncorrected IR_{50} ages to fading-corrected IR_{50} ages were between 0.80 and 0.91 for all samples, with a mean ratio of 0.84. Thus, we

Table 3
Dose rates of quartz and polymineral fine grains.

Sample ID	Profile	Horizon	Depth (m)	U (ppm)	Th (ppm)	K (%)	Water (%)	Dose rate (Gy/ka) Quartz	Polymineral
LUM4245	WK2	BC1	0.52	2.55 ± 0.13	8.32 ± 0.42	1.79 ± 0.09	20 ± 5	3.00 ± 0.13	3.44 ± 0.17
LUM4247	WK3	Bt1	0.45	2.50 ± 0.13	9.05 ± 0.46	1.88 ± 0.10	20 ± 5	3.12 ± 0.14	3.58 ± 0.18
LUM4249	WK4	E	0.54	2.44 ± 0.13	7.20 ± 0.37	1.71 ± 0.09	20 ± 5	2.81 ± 0.12	3.25 ± 0.16
LUM4250	WK5	Eg	0.58	2.21 ± 0.11	7.81 ± 0.40	1.79 ± 0.09	20 ± 5	2.87 ± 0.13	3.22 ± 0.16
LUM4251	WK5	BC	1.17	2.11 ± 0.11	8.14 ± 0.41	1.63 ± 0.08	20 ± 5	2.72 ± 0.12	3.28 ± 0.16
LUM4252	WK6	Eg	0.36	1.95 ± 0.10	7.11 ± 0.36	1.61 ± 0.08	20 ± 5	2.62 ± 0.11	3.12 ± 0.16
LUM4253	WK6	EBgb1	1.02	2.07 ± 0.11	6.60 ± 0.34	1.60 ± 0.08	20 ± 5	2.56 ± 0.11	2.99 ± 0.15
LUM4255	WK7	2EBg2	0.90	1.56 ± 0.11	5.64 ± 0.33	1.37 ± 0.07	20 ± 5	2.17 ± 0.09	2.74 ± 0.14
LUM4257	WK8	Bt/BC	0.52	2.08 ± 0.11	7.82 ± 0.40	1.73 ± 0.09	20 ± 5	2.79 ± 0.12	2.93 ± 0.15
LUM4259	WK10	BC2	1.04	2.20 ± 0.11	7.73 ± 0.39	1.70 ± 0.09	20 ± 5	2.77 ± 0.12	3.19 ± 0.16
LUM4260	WK11	BC2	1.05	1.69 ± 0.09	6.31 ± 0.33	1.39 ± 0.07	20 ± 5	2.27 ± 0.10	3.17 ± 0.16
LUM4261	WK12	BC1g	0.62	2.31 ± 0.12	8.09 ± 0.41	1.67 ± 0.09	20 ± 5	2.81 ± 0.12	2.60 ± 0.13
LUM4262	WK12	BC2g	1.24	2.47 ± 0.13	8.19 ± 0.42	1.72 ± 0.09	20 ± 5	2.88 ± 0.13	3.23 ± 0.16

applied a fading factor of 0.84 to calculate the predicted D_e of IR_{50}. Consequently, we also adjusted the ΔF data from Murray et al. (2012), multiplying it by a factor of 1.53 (i.e. 0.84/0.55). It can be seen from Fig. 4 that all samples, except for two from profile WK7 (LUM4254, LUM4256), plotted below the acceptance limit, indicating that the quartz OSL of these samples was fully reset before deposition and that the quartz OSL ages were reliable. For sample LUM4260, the measured IR_{50} D_e was even smaller than the predicted IR_{50} D_e. The reason for this might be that the measured fading rate for LUM4260 was underestimated. It should also be noted that, even when applying a fading factor of 0.55, as used in Murray et al. (2012), all the samples still plotted below the acceptance limit line. It was reasonable for Murray et al. (2012) to use a higher fading factor than in this study because, in their study, the IR_{50} signal was measured after a preheating treatment of 320 °C. It has been widely reported that when a high preheating temperature (e.g. > 250 °C) is used, the dose recovery ratio of the IR_{50} using the SAR protocol is always underestimated due to failure of the sensitivity correction in the first cycle (Kars et al., 2014; Qin et al., 2018; Wallinga et al., 2000; Zhang, 2018). The IR_{50} D_e underestimation resulting from the failure of the sensitivity correction was also incorporated into the fading factor in Murray et al. (2012). In our study, the preheating temperature was set at just 200 °C. The D_e was not further underestimated by failure of a sensitivity correction, and the fading factor was thus larger.

2.7. Radiocarbon dating.

Three samples of secondary carbonate nodules were measured by accelerator mass spectrometry using 1.5 SDH Compact Pelletron (National Electrostatics Corporation, Middleton, USA) at the Poznan Radiocarbon Laboratory. Calendar ages were obtained using the OxCal 4.4 calibration program (Bronk Ramsey, 2009, 2001) based on the IntCal 13 calibration curve (Reimer et al., 2013). The calibrated ages are given in the 2σ range (minimum and maximum value for each) (Table 5).

3. Results

3.1. Visualisation of lithology using the ERT tool

The ERT measurements allowed visualisation of the variability of the geological structure of the shallow ground and distinction of the main lithological units (Fig. 1). All investigated rock formations had relatively low electrical resistivity (Fig. 1). It was difficult to relate them directly to existing geological data because there were no boreholes through the Quaternary sediments in the vicinity of the surveyed sections. There are boreholes ~ 4 km to the south-east through the footslope of the studied hills (Pierwoszów 1) and 6 km to the north (Trzebnica IG-1), but both penetrate a different, higher morphological position (Winnicki, 1997, 1990, 1985).

Nevertheless, based on interpretations from those boreholes, it was assumed that the AB inversion model also represented pre-Quaternary sediments. These might be glacigenically deformed Miocene clays (Section a in Fig. 1) overlain by two or three generations of Quaternary sediments (Subdivisions b and c), which were interpreted as sequences of glacial deposits. Two thin layers of slope sediments (d) were visible in the ground surface zone, including thicker colluvium at the base of the slope (e).

3.2. Soil classification and morphology

The field soil survey, including the profiles (Fig. 5) and drillings, confirmed loess thicknesses that varied between 1 and 1.2 m in stable landscape positions (top slope with 4° inclination), where relatively complete Luvisols with preserved E and Bt horizons had developed (WK1). The rest of the studied soils revealed morphologies shaped by

Table 4

The De values and OSL ages.

| Sample ID	Profile	Horizon	Signal	D_e (Gy)			Apparent age (ka)			g_{2d} (%/decade)			Fading corrected age (ka)			Age ratio IR_{50}/quartz		
LUM 4245	WK2	BC1	OSL	49.6	±	1.1	16.6	±	0.8							1.01	±	0.08
			IR_{50}	46.5	±	0.4	13.5	±	0.7	3.24	±	0.00	16.8	±	0.9			
			$pIRIR_{170}$	66.0	±	0.4	19.2	±	1.0	1.27	±	0.27	20.8	±	1.1			
LUM 4247	WK3	Bt1	OSL	45.2	±	1.1	14.5	±	0.7							0.92	±	0.07
			IR_{50}	39.4	±	0.2	11.0	±	0.6	2.96	±	0.06	13.3	±	0.7			
			$pIRIR_{170}$	52.3	±	0.2	14.6	±	0.7	1.14	±	0.06	15.7	±	0.8			
LUM 4249	WK4	E	OSL	10.7	±	0.1	3.8	±	0.2							1.16	±	0.08
			IR_{50}	12.0	±	0.1	3.7	±	0.2	2.87	±	0.04	4.4	±	0.2			
			$pIRIR_{170}$	16.9	±	0.4	5.2	±	0.3	1.11	±	0.08	5.6	±	0.3			
LUM 4250	WK5	Eg	OSL	26.2	±	0.2	9.1	±	0.4							1.39	±	0.10
			IR_{50}	34.1	±	0.3	10.4	±	0.5	3.06	±	0.03	12.7	±	0.7			
			$pIRIR_{170}$	44.6	±	0.5	13.6	±	0.7	1.15	±	0.05	14.6	±	0.8			
LUM 4251	WK5	BC	OSL	40.9	±	0.8	15.1	±	0.7							1.00	±	0.07
			IR_{50}	38.2	±	0.2	12.2	±	0.6	3.17	±	0.09	15.1	±	0.8			
			$pIRIR_{170}$	51.7	±	0.3	16.5	±	0.8	1.27	±	0.14	17.9	±	0.9			
LUM 4252	WK6	Eg	OSL	1.8	±	0.0	0.7	±	0.03							1.17	±	0.08
			IR_{50}	2.2	±	0.1	0.73	±	0.04	2.28	±	0.07	0.82	±	0.05			
			$pIRIR_{170}$	3.9	±	0.1	1.30	±	0.08	0.61	±	0.25	1.34	±	0.08			
LUM 4253	WK6	EBgb1	OSL	16.5	±	0.1	6.4	±	0.3							1.33	±	0.09
			IR_{50}	20.8	±	0.2	7.1	±	0.4	2.94	±	0.07	8.6	±	0.5			
			$pIRIR_{170}$	28.3	±	0.3	9.7	±	0.5	1.53	±	0.09	10.6	±	0.6			
LUM4255	WK7	2EBg2	OSL	3.3	±	0.1	1.5	±	0.1							2.43	±	0.17
			IR_{50}	7.5	±	0.1	3.0	±	0.2	3.31	±	0.19	3.68	±	0.2			
			$pIRIR_{170}$	20.2	±	0.9	8.2	±	0.5	1.11	±	0.19	8.72	±	0.6			
LUM 4257	WK8	Bt/BC	OSL	48.0	±	1.8	17.2	±	1.0							0.93	±	0.07
			IR_{50}	41.1	±	0.2	12.9	±	0.6	3.25	±	0.12	16.0	±	0.8			
			$pIRIR_{170}$	62.1	±	0.9	19.5	±	1.0	0.68	±	0.21	20.3	±	1.1			
LUM 4259	WK10	BC2	OSL	3.5	±	0.0	1.3	±	0.1							1.75	±	0.12
			IR_{50}	6.1	±	0.1	1.9	±	0.1	2.67	±	0.08	2.2	±	0.1			
			$pIRIR_{170}$	11.4	±	0.2	3.6	±	0.2	0.78	±	0.11	3.7	±	0.2			
LUM 4260	WK11	BC2	OSL	60.3	±	3.1	26.6	±	1.8							0.78	±	0.07
			IR_{50}	43.7	±	0.2	16.8	±	0.8	3.07	±	0.13	20.7	±	1.1			
			$pIRIR_{170}$	88.0	±	0.4	33.9	±	1.7	1.28	±	0.23	36.9	±	2.0			
LUM 4261	WK12	BC1g	OSL	1.2	±	0.0	0.4	±	0.02							1.35	±	0.10
			IR_{50}	1.7	±	0.0	0.5	±	0.03	2.08	±	0.04	0.57	±	0.03			
			$pIRIR_{170}$	4.7	±	0.1	1.5	±	0.08	0.09	±	0.16	1.47	±	0.09			
LUM 4262	WK12	BC2g	OSL	4.4	±	0.0	1.5	±	0.1							1.88	±	0.13
			IR_{50}	8.2	±	0.1	2.5	±	0.1	2.79	±	0.17	2.9	±	0.2			
			$pIRIR_{170}$	17.7	±	0.2	5.3	±	0.3	1.04	±	0.14	5.7	±	0.3			
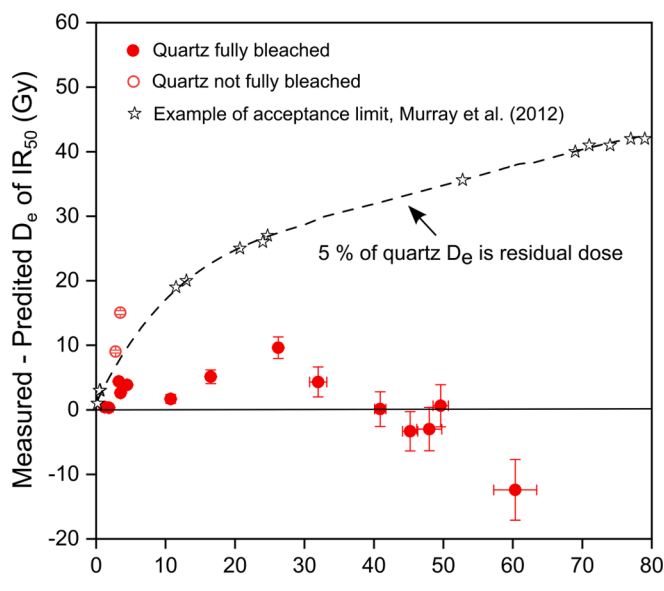
Fig. 4. The differences between measured and predicted D_e values of IR_{50} plotted against the measured quartz D_e. The dashed line indicates the acceptance limit. If a sample is plotted under the dashed line, it indicates that the quartz OSL signal of this sample has been fully bleached before deposition.

Table 5

Radiocarbon ages of carbonate hard nodules.

Soil profile/ soil horizon	Depth (cm)	Lab code	Uncalibrated ^{14}C age (yr BP)	Calibrated age (2-sigma range (95.4%)) cal BC
WK7/4Cgk	120	Poz-112868	6860 ± 50	5843–5640
WK8/ 2Bck2	82	Poz-120446	1700 ± 60	11718–11501
WK9/BCk1	35	Poz-120447	16020 ± 80	17587–17181

denudation processes. Erosion processes led to a thinning of the loess mantle that had substantial morphological consequences, resulting in the removal of the E horizon and further incorporation of the Bt horizon into the Ap horizon due to ploughing (WK2, WK3, WK8, WK10, WK11). In extreme cases, the Bt horizon was not a master horizon but a part of a transitional horizon (Table 1) with a thickness of only 14 cm. Progressive erosion, causing a shallowing loess mantle, may have also resulted in the exhumation of underlying coarse-grained materials (e.g., in WK9). The deposition of eroded material from the upslope was recorded in the mid-and foot-slope positions of both transects. In the south-trending transect, its presence was observed in profiles WK4 and WK5, expressed as much thicker topsoil (A, AE and E, EB horizons), while in WK6, we detected a buried A horizon covered with 45 cm of slopewash sediment. Profile WK7 represented the stratification of fine- and coarse-grained (with diagonal lineation) colluvium over glacial till. In the eastern transect, clear morphological features of accumulation were
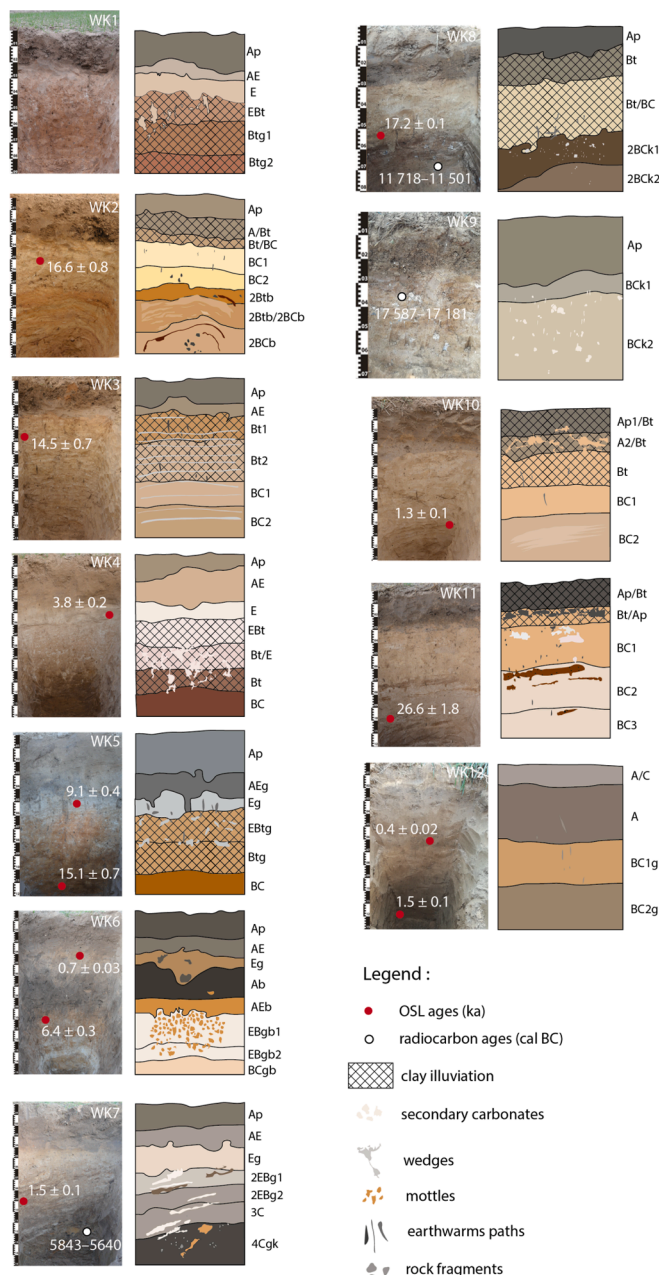
Fig. 5. Photos and sketches presenting morphology of studied soil profiles and sampling positions for OSL dating with obtained ages.

detected only in WK12, which had 60 cm of colluvium. Loess mantles are carbonate free; however, hard carbonate nodules and coatings were found in the glacial materials of the WK7, WK8 and WK9 sites.

Although most of the soils had experienced erosion processes, almost all were classified as Luvisols (Table 1). Because the topsoil horizons did not meet the criteria for being mollic or chernic (too high values and chromas), they still (in the case of strongly eroded pedons, e.g., WK2/WK3) had argic horizons. Profiles WK7, WK9 and WK12 fell into the Regosol reference group because no diagnostic horizons were recognised in these. Detailed information on the physicochemical properties is available in Loba et al. (2021)

3.3. Grain size distribution

In the profiles, the most dominant fraction was coarse silt (45–50 μ m) (Fig. S1), which is typical of loess deposits. However, the grain size

distribution also indicated certain differences. Materials deposited during MIS 2 have a narrow peak range between 44 and 48 μ m, whereas younger sediments are bimodal (Fig. 6A), with dominant coarse silt (35–58 μ m) and medium sand (210–550 μ m) fractions. In the soils characterised by lithic discontinuities, the most pronounced fractions in the lower horizons tended to be in the medium sand range (102–104 μ m), as in WK2, or were multimodal, with their highest peaks at 8, 50 and 120 μ m (WK8) or 7, 49 and 230 μ m (WK9). In WK6 and WK10, the fractions were bimodal, the highest peak being within the range of coarse silt (45–49 μ m) and the smaller peaks within the range of medium sand (370 μ m) (Fig. 6B).

3.4. Soil micromorphology

The thin sections revealed mostly a subangular and crumby type of microstructure (e.g. WK6, WK12), with vugs and plane types of voids. Sometimes, a void chamber type was recognised (e.g. in WK2, WK3, WK6). The groundmass was characterised by enaulic and porphyric coarse:fine (c:f) related distribution patterns, albeit with various coarse and fine size limits (Table S1). The b-fabric of the horizons varied from porostriated, to granostriated and randomly striated, with rare mono-striated to speckled or stipple-speckled patterns. The soils from the toe slope mostly had undifferentiated b-fabric patterns (Table S1).

The most common pedofeatures were typic and, rarely, concentric or aggregate Fe-hydroxide nodules with weak and moderately
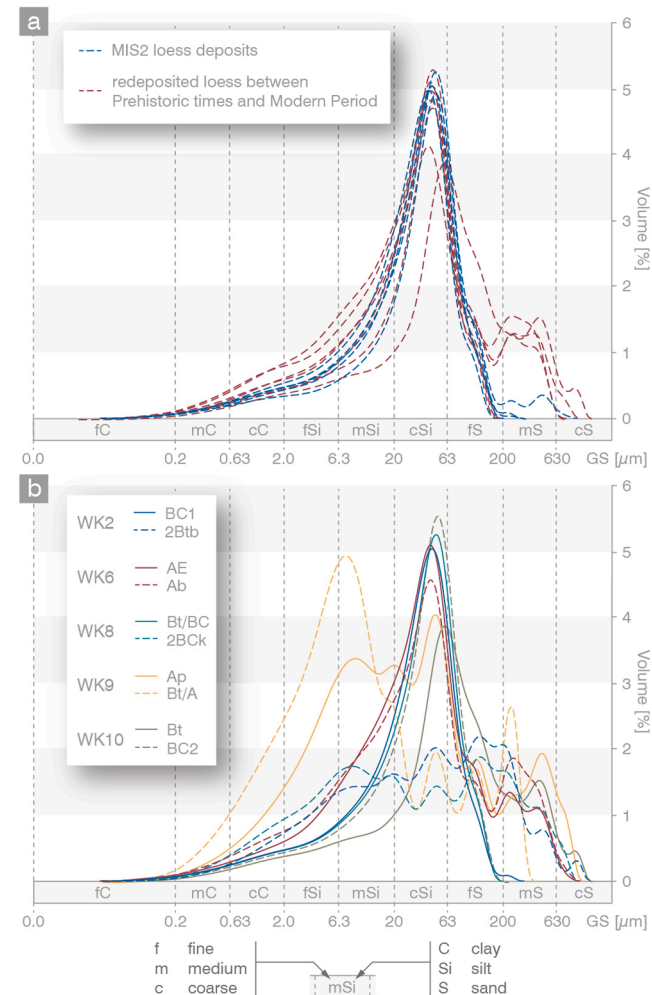

Fig. 6. Grain-size curves illustrating main modes in a) loess sediments deposited during MIS2 and redeposited between Prehistoric times to Modern Period, and b) soils with the textural contrast.

impregnation, and having orthic and/or anorthic character (e.g., Fig. 7A: c, e, h and Fig. 7B: c, d).

The expression of clay pedofeatures differed in the soils along the transects. The best-developed illuviation features were recognised in WK2 (Bt/BC), which exhibited mostly fragmented, dense, incomplete and loose, continuous dusty clay infillings (Table S1), but also fine yellowish-brown clay coatings were found in that profile (Fig. 7A: a). Horizon 2Bt/2BCg of WK2 revealed more definite features related to clay illuviation; however, the typical coatings or infillings were not always formed, with the clay occurring mostly around grains and as yellowish-brown, elongated, limpid aggregations of fine clays (with no laminations), often broken and heterogeneously distributed in the groundmass (Fig. 7A: b).

The soil profiles from the middle section of the slopes (WK3, WK4, WK8, WK9) showed weak clay illuviation characteristics, but their abundance and typology differed. The Ap horizon of WK3 had a very
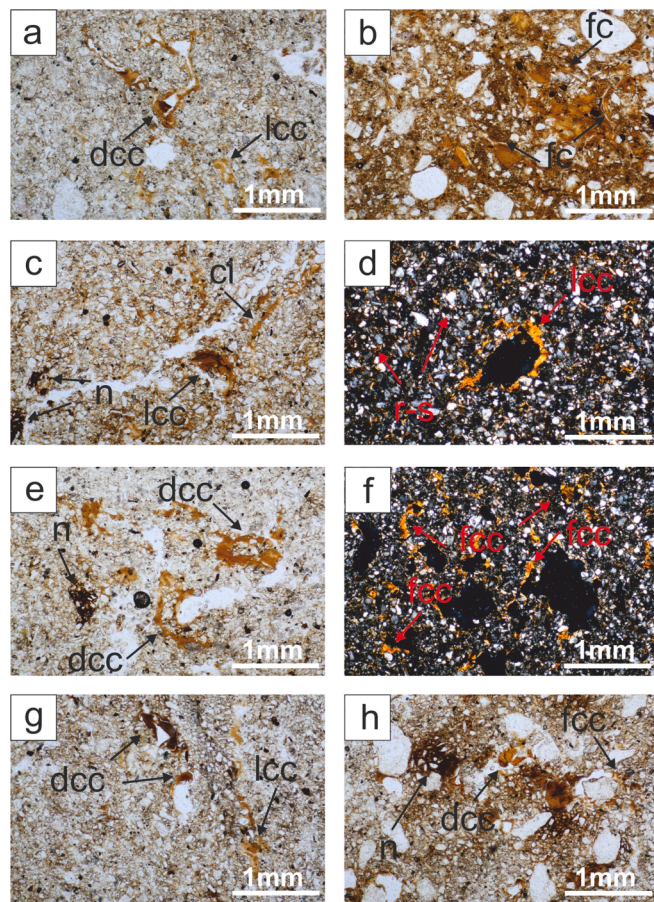
Fig. 7A. Microphotographs of soil thin sections showing alternating clay illuvial pedofeatures relative to location on the slopes. (a) profile WK2, horizon Bt/BC: dcc – dusty layered clay illuvial coatings, lcc – limpid layered clay illuvial coatings, PPL; (b) profile WK2, horizon 2Bt/2BCg: fc – yellowish-brown elongated fine clay aggregations, PPL; (c) profile WK3, horizon Ap: dcc – displaced and fragmented microlaminated limpid clay illuvial coatings, ci – dense incomplete, loose discontinuous clay infillings, n – weakly impregnated anorthic Fe hydroxide nodules, PPL; (d) profile WK3, horizon Ap: llc – fragmented layered limpid clay illuvial coatings, r-s – random-striated b-fabric pattern, XPL; (e) profile WK3, horizon Bt1: dcc – fragmented layered dusty clay illuvial coatings, n –moderately impregnated anorthic Fe hydroxide nodules, PPL; (f) profile WK3, horizon Bt1: fcc – fragmented microlaminated clay illuvial coatings, XPL; (g) profile WK4, horizon Bt/E: dcc – fragmented microlaminated dusty clay illuvial coatings, lcc – microlaminated limpid clay illuvial coatings, PPL; (h) profile WK6, horizon EBgb1: dcc – dusty microlaminated clay illuvial coatings, fcc – fragmented microlaminated clay illuvial coatings, n – moderately impregnated anorthic Fe hydroxide nodules, PPL. Bar length = 1 mm.
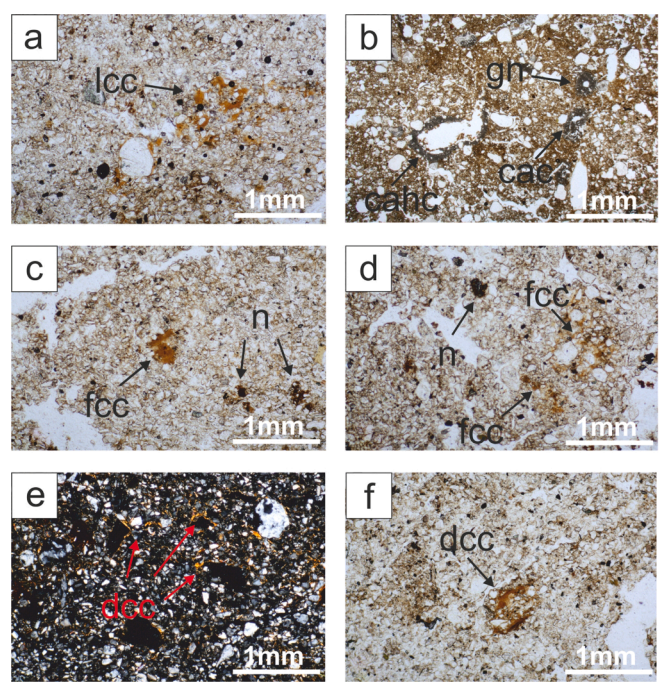

Fig. 7B. Microphotographs of soil thin sections showing alternating clay illuvial pedofeatures relative to location on the slopes. (a) profile WK8, horizon Bt: lcc – fragmented microlaminated limpid clay illuvial coatings, PPL; (b) profile WK8, horizon Bt/BC: gn – geodic calcitic nodules, cac – calcitic coatings, cahc – calcitic hypocoatings, PPL; (c) profile WK11, horizon Ap/Bt–Bt/Ap: fcc – displaced and fragmented microlaminated clay illuvial coatings, n – weakly impregnated anorthic Fe hydroxide nodules, PPL; (d) profile WK11, horizon Bt/Ap: fcc – strongly fragmented and microlaminated clay illuvial coatings, n – moderately impregnated anorthic Fe hydroxide nodules, PPL; (e) profile WK12, horizon BC1g: dcc – fragmented dusty clay illuvial coatings, XPL; (f) profile WK12, horizon BC1g: dcc – fragmented and microlaminated dusty clay illuvial coatings, PPL. Bar length = 1 mm.

high content of microlaminated coatings of limpid yellowish-brown clay, often disrupted and fragmented (Fig. 7A: c, d). However, some well-developed laminated yellowish-brown clay coatings also occurred (Fig. 7A: d). Moreover, a lot of fine, dense, incomplete fragmented clay infillings were found (Fig. 7A: c). The lower horizons (Bt1, Bt2, Bt/E) similarly showed microlaminated, but very small and strongly fragmented, yellowish-brown clay coatings and single, weakly and moderately developed laminated clay coatings (Fig. 7A: e–g), as well as fragmented and small, dense, incomplete and loose continuous clay infillings. The illuvial clay features indicated disturbance of the illuviation process, mainly due to mass wasting. We observed many illuvial features in the Ap horizon, as the Bt horizon was partially incorporated into that. Apart from occasional occurrences of non-laminated, very fragmented yellowish-brown coatings of illuvial clay in the Bt horizon of WK8 (Fig. 7B: a), there were no other signs of clay illuviation in the soils. Furthermore, a large quantity of geodic calcite nodules, along with calcitic coatings/hypocoatings, were found in the Bt/BC horizon of WK8 (Fig. 7B: b). Profiles from the backslope and toe slopee (WK6, WK11, WK12), apart from very residual and fragmentary clay coatings (Fig. 7B: c, d), generally exhibited no pedofeatures typical of clay illuviation. Only the Eg and EBgb1 horizons of WK6 and BC1g of WK12 contained fragments of disrupted, microlaminated, illuvial reddish-brown clay coatings (Fig. 7A: h and 7B: e, f, respectively). Their morphology and size suggested an ex-situ origin, probably an effect of the slopewash.

3.5. OSL and ^{14}C dating

The luminescence ages from the soil profiles represent a wide

timespan. Most of the ages correlated to MIS 2 (LUM 4245, LUM 4247, LUM 4251, LUM 4257, LUM 4260), but also to the Prehistoric times (9.1 ± 0.4 ka; LUM4250), the Neolithic (6.4 ± 0.3 ka; LUM 4253) and the Bronze Age (1.5 ± 0.1 ka; LUM 4249). The youngest dates relate to the Middle Ages and the early Modern, with a minimum age of ~ 0.4 ka (Table 4). Moreover, two samples (LUM4258, LUM4246) from the bottom parts of WK2 and WK9, respectively, were saturated with luminescence signals from both quartz and feldspar because they were much older than the last glaciation. Radiocarbon ages for the hard carbonate nodules covered a broad spectrum, from 17.5 to 5.4 cal ka BP (Table 5).

4. Discussion

4.1. Record of denudation events

The OSL dating suggested that the loess deposits in their lowermost horizons (BC and C) were LGM or late glacial in age (Table 4), which is typical for the thin aeolian-silt mantle in the southwestern Poland (Moska et al., 2019; Waroszewski et al., 2021). In the toe slopes, however, the ages for the uppermost eluvial horizons indicated sediment redeposition along the slope due to erosional processes and their termination as colluvial deposits (Table 4). Based on our OSL ages, we assumed that the first phase of redeposition occurred ~ 9.1 ka (profile WK5), at the transition from the Preboreal to the Boreal. This could be related to cold and dry climatic oscillations that triggered natural forest fires and, as a consequence, soil erosion and colluviation (Dreibrodt et al., 2010a, 2010b; Kołodyńska-Gawrysiak et al., 2018). It seems that, following this event, slope-washing processes were intensified no earlier than the Neolithic. A record of this colluviation was detected in WK6 (6.4 ± 0.3 ka). The acceleration of soil erosion was probably related to the Linear Pottery culture that settled the area of the Central European loess belt at that time, after which vast forested areas were gradually transformed into farmland (Dreibrodt and Bork, 2021; Gerlach et al., 2012; Poręba et al., 2011; Starkel et al., 2013). Also, the burning (slash and burn) practices to prepare arable lands and obtain high crop yields that were typical during the Neolithic may have increased soil erosion rates (Gerlach et al., 2012). However, we did not find pyrogenic features in the studied soils. Later, another phase of redeposition occurred that was recorded in WK4 (LUM 4249). This particular phase was attributed to the transition from the Early to Middle Bronze Age (3.8 ± 0.2 ka), when the climate was cold and humid (Dotterweich, 2008) and there was an expansion of the human population and farming activities (Kołodyńska-Gawrysiak et al., 2017; Rejman and Rodzik, 2006). However, colluvial sediments corresponding to this period have been found in Germany and other parts of Poland (Döhler et al., 2015; Kołodyńska-Gawrysiak et al., 2018, 2017; Poręba et al., 2011), whereas, in southwest Poland, there is a lack of such data. The ages from WK6, WK7 and WK10 correspond to the early (1.5 ± 0.1 ka to1.3 ± 0.1 ka) and late (0.7 ± 0.03 ka) Middle Ages. At the beginning of the Middle Ages, the climate was warm and temporarily dry, however, in the later period, the summers were wet and rainy, leading to flooding (Dotterweich, 2008; Dreibrodt and Bork, 2021). The signal for the last episode of soil erosion (WK12) came from the early Modern (0.4 ± 0.02 ka) and corresponded to the Little Ice Age, when the temperature decreased and precipitation rates increased, and mass processes on slopes were consequently accelerated (Starkel, 2005).

The progressive denudation led to the exhumation of deposits older than the loess that is not suitable for dating due to their saturated luminescence signals. These deposits include the lowermost horizons of WK2 (LUM4246) and WK9 (LUM4258). Denudation intensity is also expressed in grain size composition. Soil has a limited infiltration capacity, so, during intensive rainfall, surface runoff occurs and sediment is transported in the flow (Morgan, 2005; Wacha et al., 2018). The redeposited sediments (Fig. 6A) had dominant coarse silt fractions but also exhibited peaks in medium sand. The climate during this time was humid/wet (Starkel, 2005), and thus favourable to erosion processes

because the highest detachment of soil particles is at the beginning of a storm and the transport capacity is reached very quickly (Morgan, 2005). Such conditions enabled the transport of medium-sand-sized particles that could have originated from coarser loess deposits or older substrates, such as glaciofluvial materials, that occurred in the upper/middle slope positions.

The broad time over which the sediments were redeposited is in agreement with the findings from other studies on Central Europe. For instance, Dotterweich et al. (2012), Kołodyńska-Gawrysiak et al. (2018), Dreibrodt et al. (2013) and Scherer et al. (2021) reported colluvial deposits from eastern Poland and Germany as corresponding to the Neolithic and Bronze Age, respectively. The erosion/deposition processes were intensified in the Middle Ages due to the development of new tools for agriculture, which enabled the expansion of arable land, as presented by Dreibrodt and Bork (2021), Dreibrodt et al. (2013), Poręba et al. (2011), Döhler et al. (2015), Dotterweich (2008) and Dotterweich et al. (2013, 2012). In the late Middle Ages, climatic anomalies, such as long, cold winters and wet rainy summers, probably also affected the intensity of soil erosion (Dreibrodt and Bork, 2021; Starkel, 2005). Furthermore, the increase in land-use intensity continued into the beginning of the Modern Times (Dreibrodt and Bork, 2021), then becoming amplified in the 20th century due to agricultural mechanization (Kopittke et al., 2019).

The denudation processes, however, were nonlinear on the convex (first transect) and concave (second transit) slopes of the study site. The age of the colluvium materials varied considerably in a catenary arrangement. For example, the colluvium making up the topsoil in WK4 and WK5 had a wide age range of deposition—3.8 ± 0.2 ka and 9.1 ± 0.4 ka, respectively. In the second transect, young colluvium (1.3 ± 0.1 ka) in WK10 was followed by a much older bed (~26.6 ± 1.8 ka) in nearby WK11. This diversity in the OSL ages supports a dynamic denudation system and reveals the presence of multiple erosion/accumulation events that occurred in the Holocene. This illustrates their utility in the reconstruction of environmental change because they enable the tracing of denudation events and can identify which layer/horizon was redeposited/truncated.

4.2. Disappearance of Luvisols

In loess areas, soils with or without erosion features create a mosaic pattern along sloping regions that are shaped by denudation processes. The loess was deposited as thick sediments around the LGM in Lower Silesia and, according to the radiocarbon ages of hard carbonate nodules, they were decalcified during two older phases ~ 17 and 11 ka, while the youngest decalcification took place around 5 ka (Table 5). At the end of the Pleistocene/early Holocene, Chernozems (Altermann et al., 2005; Eckmeier et al., 2007; Kabała et al., 2019; Kołodyńska-Gawrysiak et al., 2017; Labaz et al., 2018) most likely developed in the loess. We can hypothesise that they were preserved until the Neolithic (Kabała et al., 2019), at which point they began to degrade into Luvic Chernozems/Pheozems and finally into Luvisols (Drewnik and Żyła, 2019; Zádorová et al., 2014). This last step in their transformation was evidenced in our study site, with Luvisols being the dominant soil group, revealing varied morphologies as a result of multiple erosion/accumulation events, dependant on the dynamics of slope processes. In the middle slope and toe slope sections (WK4, WK6, WK7), colluvial materials (Neolithic/Bronze Age/Medieval) served as a substrate for the development of thick eluvial horizons. In the slope zones where soil erosion reached its peak, a progressive shallowing of the loess mantle was observed, and consequently, a significant modification of the soil morphology took place. Thus, truncated Luvisols developed as a direct effect of eluvial horizon mixing due to ploughing into the Ap horizon (WK3). However, more extreme cases existed, where argic horizons (Bt) were incorporated into surface humus horizons (WK2, WK10, WK11). In such situations, the A horizons contained clay coatings (Fig. 7) originating from the aggregates of the Bt horizon being dragged up during

agricultural activities. With time, there was a progressive shallowing of the Bt horizons, leading to their complete disappearance. Further thinning of the loess mantle resulted in the exhumation of older sediments, such as glacial tills and glaciofluvial substrates, with no, or very weak, pedogenic alternations (WK9), which led to transformation of the soil into Regosols (Fig. 8). Eroded material was transported downslope and was usually deposited in toeslope positions, forming colluvial soils. The relatively deep colluvium (WK12), being a fresh substrate, may have contained some clay coatings inherited from the eroded Bt horizons (Fig. 7B), but did not have any diagnostic horizons, meaning that it also fell into the Regosol soil reference group. In the young morainic landscape of northern Poland, this kind of direct exposure of the Bt horizon at the soil surface resulted in the formation of Calcisols or Regosols (Radziuk and Świtoniak, 2021; Świtoniak et al., 2016) and led to severe modifications of organic matter and nutrient pools. In Central Europe a transformation of Luvisols due to shallowing of Bt horizons as a consequence of intense soil erosion processes and formation of colluvial soils in the lower parts of slopes is also observed in catenary research of loess areas of Czechia (Strouhalová et al., 2020; Zádorová et al., 2014, 2013; Zádorová and Penížek, 2018), southwestern Germany (Leopold et al., 2011; Scherer et al., 2021; Terhorst, 2000), eastern Poland (Klimowicz and Uziak, 2001; Paluszek, 2013; Rejman et al., 2014b, 2014a; Rejman and Iglik, 2010), southern Poland (Dudek et al., 2022; Glina et al., 2014; Labaz et al., 2022, 2018; Poręba et al., 2015), Belgium (Nachtergaele and Poesen, 2002; Rommens et al., 2005), France (Jagercikova et al., 2015, 2014; Krekelbergh et al., 2020) and in young morainic landscape of western Lithuania (Jarašiūnas et al., 2020).

Recent research on short-term erosion rates conducted on soils developed from loess deposits, by Loba et al. (2021), clearly showed that modern soil erosion rates have considerably increased and considerably exceed soil production rate, and therefore soil transformation will move towards the disappearance of productive Luvisols in arable landscapes. The soil degradation resulting from erosion events causes a shallowing of the loess solum, depletion in organic matter and nutrients and a reduction in crop productivity, mostly due to a decrease in the retention capacity for plant-available water (Glina et al., 2014; Paluszek, 2010; Rejman and Iglik, 2010) that is usually stored in the Bt horizons that are being actively eroded.

Short-term erosion rates, quantified using $^{239+240}$Pu fallout radionuclides (Loba et al., 2021), present an opportunity to speculate about the approximate timing of the disappearance of the Bt horizons (Table S2). Soil degradation seems to have been the most intense in WK2, WK8 and WK10, where the soil class may have significantly changed within ~ 200, 130 and 80 years, respectively. In these profiles, soil erosion was at its peak, already has led to a distinct shallowing of the loess mantle. In the other profiles, the prognosis seems to be slightly better, with the Bt horizon possibly having disappeared after 300 years. However, it needs to be borne in mind that these calculations are based on values calculated in the present day. Progressive climate change, causing soil drying and less frequent, but more intense, rainfall events, may lead to an increase in erosive events (Routschek et al., 2014; Zádorová and Penížek, 2018; Zollinger et al., 2015). Therefore, the disappearance of Luvisols may be even more accelerated. Thus, the effective application of anti-erosive treatments and sustainable land use is crucial to the protection of vital soil resources.

5. Conclusions

The luminescence (OSL) dating enabled to reconstruction time intervals of denudation processes in the studied loess area. In total, five soil redeposition phases took place starting from 9.1 ka. Other phases occurred ca. 6.4 ka, 3.8 ka, 1.5–0.7 ka and 0.4 ka. Due to the progressive denudation processes, the soil cover in the study area was very dynamic. Most likely, at the beginning of the Holocene, soils bearing chernic/mollic horizons developed in the loess mantle, which later, as a result of erosional/depositional processes, transformed into Luvisols. Modern soil erosion rates increased considerably, causing the removal of the eluvial and argic horizons, thus transforming the Luvisols into Regosols. This soil degradation causes a shallowing of the loess mantle, depletion in organic matter and nutrients and a reduction in crop productivity. Based on soil erosion rates, we calculate that the soil class may significantly change within ~ 80–300 years, although progressive climate change may intensify the erosion events, thus further accelerating the disappearance of the fertile loess mantle and Luvisols. Therefore, it is necessary to apply effective anti-erosion treatments, making landowners aware of the risks caused by erosion and thus implementing the European Parliament resolution on soil protection.
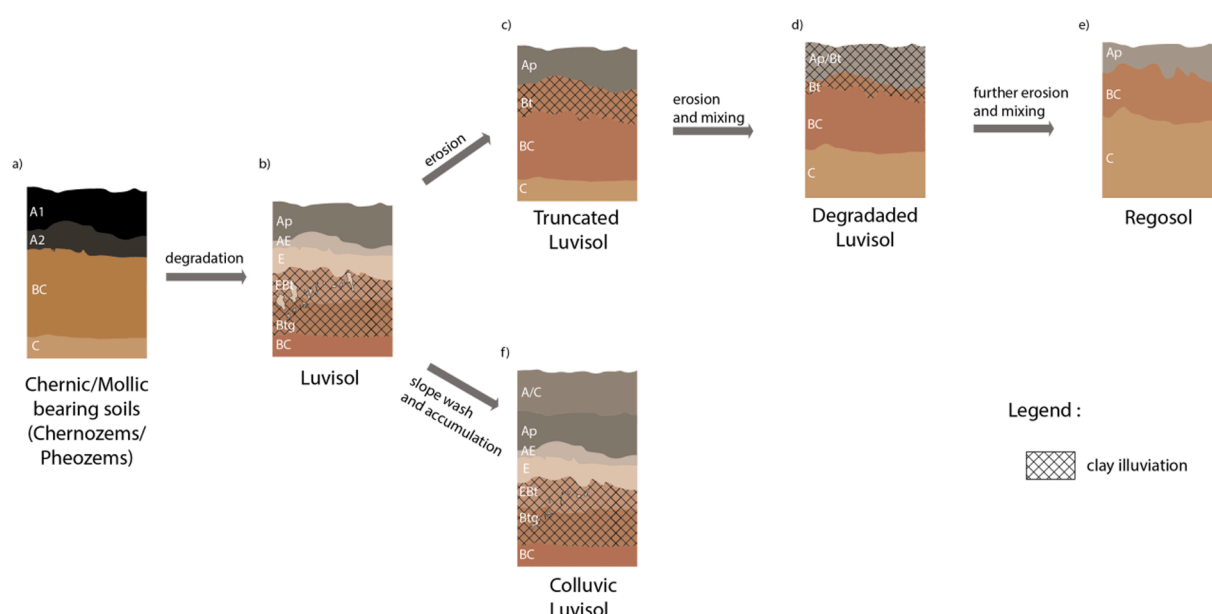

Fig. 8. Hypothetical pathways of soil evolution resulting from denudation processes in loess areas in Central Europe. (The model starts from the Chernozem/Pheozem predominating in the European loess belt during Late Glacial/early Holocene as showed by Labaz et al. (2018) and Kabała et al. (2019).

Uncited references

CRediT authorship contribution statement

Aleksandra Loba: Formal analysis, Visualization, Writing – original draft. **Junjie Zhang:** Writing – review & editing. **Sumiko Tsukamoto:** Writing – review & editing. **Marek Kasprzak:** Writing – review & editing. **Joanna Beata Kowalska:** Writing – review & editing. **Manfred Frechen:** Writing – review & editing. **Jarosław Waroszewski:** Conceptualization, Visualization, Writing – original draft, Project administration, Funding acquisition.

Declaration of Competing Interest

The authors declare that they have no known competing financial interests or personal relationships that could have appeared to influence the work reported in this paper.

Data availability

Data will be made available on request.

Appendix A. Supplementary data

Supplementary data to this article can be found online at https://doi. org/10.1016/j.catena.2022.106724.

References

Alewell, C., Pitois, A., Meusburger, K., Ketterer, M., Mabit, L., 2017. 239+240 Pu from "contaminant" to soil erosion tracer: Where do we stand? Earth-Science Rev. 172, 107–123. https://doi.org/10.1016/j.earscirev.2017.07.009.

Altermann, M., Rinklebe, J., Merbach, I., Körschens, M., Langer, U., Hofmann, B., 2005. Chernozem - Soil of the Year 2005. J. Plant Nutr. Soil Sci. 168, 725–740. https://doi.org/10.1002/jpln.200521814.

Anioł-Kwiatkowska, J., 1998. Endangered and rare segetal species in the microregion Trzebnica Hills. Acta Univ. Lodz. 13, 169–176.

Auclair, M., Lamothe, M., Huot, S., 2003. Measurement of anomalous fading for feldspar IRSL using SAR. Radiat. Meas. 37, 487–492. https://doi.org/10.1016/S1350-4487 (03)00018-0.

Bac, S., Rojek, M., 2012. Meteorologia i klimatologia w inżynierii środowiska. Wydawnictwo Uniwersytetu Przyrodniczego we Wrocławiu, Wrocław.

Baumgart, P., Eltner, A., Domula, A.R., Barkleit, A., Faust, D., 2017. Scale dependent soil erosion dynamics in a fragile loess landscape. Zeitschrift für Geomorphol. 61 (3), 191–206.

Bronk Ramsey, C., 2009. Dealing with Outliers and Offsets in Radiocarbon Dating. Radiocarbon 51, 1023–1045. https://doi.org/10.1017/S0033822200034093.

Bronk Ramsey, C., 2001. Development of the Radiocarbon Calibration Program. Radiocarbon 43, 355–363. https://doi.org/10.1017/S0033822200038212.

Buylaert, J.-P., Jain, M., Murray, A.S., Thomsen, K.J., Thiel, C., Sohbati, R., 2012. A robust feldspar luminescence dating method for Middle and Late Pleistocene sediments. Boreas 41, 435–451. https://doi.org/10.1111/j.1502-3885.2012.00248. x.

Buylaert, J.-P., Thiel, C., Murray, A., Vandenberghe, D., Yi, S., Lu, H., 2011. IRSL and post-IR IRSL residual doses recorded in modern dust samples from the Chinese Loess Plateau. Geochronometria 38, 432–440. https://doi.org/10.2478/s13386-011-0047-0.

Chen, Y., Li, S.-H., Li, B., 2013. Residual doses and sensitivity change of post IR IRSL signals from potassium feldspar under different bleaching conditions. Geochronometria 40, 229–238. https://doi.org/10.2478/s13386-013-0128-3.

Döhler, S., Damm, B., Terhorst, B., Thiel, C., Frechen, M., 2015. Late Pleistocene and Holocene landscape formation in a gully catchment area in Northern Hesse. Germany. Quat. Int. 365, 42–59. https://doi.org/10.1016/j.quaint.2014.08.001.

Döhler, S., Terhorst, B., Frechen, M., Zhang, J., Damm, B., 2018. Chronostratigraphic interpretation of intermediate layer formation cycles based on OSL-dates from intercalated slope wash sediments. Catena 162, 278–290. https://doi.org/10.1016/j. catena.2017.11.003.

Dotterweich, M., 2008. The history of soil erosion and fluvial deposits in small catchments of central Europe: Deciphering the long-term interaction between humans and the environment — A review. Geomorphology 101, 192–208. https://doi.org/10.1016/j.geomorph.2008.05.023.

Dotterweich, M., Rodzik, J., Zgłobicki, W., Schmitt, A., Schmidtchen, G., Bork, H.-R., 2012. High resolution gully erosion and sedimentation processes, and land use changes since the Bronze Age and future trajectories in the Kazimierz Dolny area (Nałęczów Plateau, SE-Poland). CATENA 95, 50–62. https://doi.org/10.1016/j. catena.2012.03.001.

Dotterweich, M., Stankoviansky, M., Minár, J., Koco, Š., Papčo, P., 2013. Human induced soil erosion and gully system development in the Late Holocene and future perspectives on landscape evolution: The Myjava Hill Land, Slovakia. Geomorphology 201, 227–245. https://doi.org/10.1016/j.geomorph.2013.06.023.

Dreibrodt, S., Bork, H., 2021. Soil Erosion and Sedimentation in Central Europe From the Neolithic to the Industrial Revolution-The German and Polish Records. In: Reference Module in Earth Systems and Environmental Sciences. Elsevier, pp. 1–15. https://doi.org/10.1016/B978-0-12-818234-5.00061-4.

Dreibrodt, S., Hofmann, R., Dal Corso, M., Bork, H.-R., Duttmann, R., Martini, S., Saggau, P., Schwark, L., Shatilo, L., Videiko, M., Nadeau, M.-J., Grootes, P.M., Kirleis, W., Müller, J., 2022. Earthworms, Darwin and prehistoric agriculture-Chernozem genesis reconsidered. Geoderma 409, 115607. https://doi.org/10.1016/j.geoderma.2021.115607.

Dreibrodt, S., Jarecki, H., Lubos, C., Khamnueva, S.V., Klamm, M., Bork, H.-R., 2013. Holocene soil formation and soil erosion at a slope beneath the Neolithic earthwork Salzmünde (Saxony-Anhalt, Germany). CATENA 107, 1–14. https://doi.org/10.1016/j.catena.2013.03.002.

Dreibrodt, S., Lomax, J., Nelle, O., Lubos, C., Fischer, P., Mitusov, A., Reiss, S., Radtke, U., Nadeau, M., Grootes, P.M., Bork, H.-R., 2010a. Are mid-latitude slopes sensitive to climatic oscillations? Implications from an Early Holocene sequence of slope deposits and buried soils from eastern Germany. Geomorphology 122, 351–369. https://doi.org/10.1016/j.geomorph.2010.05.015.

Dreibrodt, S., Lubos, C., Terhorst, B., Damm, B., Bork, H.-R., 2010b. Historical soil erosion by water in Germany: Scales and archives, chronology, research perspectives. Quat. Int. 222, 80–95. https://doi.org/10.1016/j.quaint.2009.06.014.

Drewnik, M., Skiba, M., Szymański, W., Żyła, M., 2014. Mineral composition vs. soil forming processes in loess soils - A case study from Kraków (Southern Poland). Catena 119, 166–173. https://doi.org/10.1016/j.catena.2014.02.012.

Drewnik, M., Żyła, M., 2019. Properties and classification of heavily eroded post-chernozem soils in Proszowice Plateau (southern Poland). Soil Sci. Annu. 70, 225–233. https://doi.org/10.2478/ssa-2019-0020.

Dudek, M., Łabaz, B., Bednik, M., Medyńska-Juraszek, A., 2022. Humic Substances as Indicator of Degradation Rate of Chernozems in South-Eastern Poland. Agronomy 12, 733. https://doi.org/10.3390/agronomy12030733.

Duller, G.A.T., 2003. Distinguishing quartz and feldspar in single grain luminescence measurements. Radiat. Meas. 37, 161–165. https://doi.org/10.1016/S1350-4487 (02)00170-1.

Eckmeier, E., Gerlach, R., Gehrt, E., Schmidt, M.W.I., 2007. Pedogenesis of Chernozems in Central Europe — A review. Geoderma 139, 288–299. https://doi.org/10.1016/j.geoderma.2007.01.009.

European Parliament, 2021. Resolution on soil protection (2021/2548(RSP)) [WWW Document]. URL https://www.europarl.europa.eu/doceo/document/TA-9-2021-0143_EN.html.

FAO, 2019. Soil erosion: the greatest challenge to sustainble soil management. Rome. https://doi.org/10.1080/00050326.1941.10437468.

FAO, 2006. Guidlines for soil description, 4th ed. Rome. https://doi.org/10.1007/978-3-030-33443-7_3.

Frechen, M., 2003. Loess in Europe—mass accumulation rates during the Last Glacial Period. Quat. Sci. Rev. 22, 1835–1857. https://doi.org/10.1016/S0277-3791(03) 00183-5.

Fuchs, M., Fischer, M., Reverman, R., 2010. Colluvial and alluvial sediment archives temporally resolved by OSL dating: Implications for reconstructing soil erosion. Quat. Geochronol. 5, 269–273. https://doi.org/10.1016/j.quageo.2009.01.006.

Gerlach, R., Fischer, P., Eckmeier, E., Hilgers, A., 2012. Buried dark soil horizons and archaeological features in the Neolithic settlement region of the Lower Rhine area, NW Germany: Formation, geochemistry and chronostratigraphy. Quat. Int. 265, 191–204. https://doi.org/10.1016/j.quaint.2011.10.007.

Gillijns, K., Poesen, J., Deckers, J., 2005. On the characteristics and origin of closed depressions in loess-derived soils in Europe—a case study from central Belgium. CATENA 60, 43–58. https://doi.org/10.1016/j.catena.2004.10.001.

Glina, B., Waroszewski, J., Kabal, C., 2014. Water retention of the loess-derived Luvisols with lamellic illuvial horizon in the Trzebnica Hills (SW Poland). Soil Sci. Annu. 65, 18–24. https://doi.org/10.2478/ssa-2014-0003.

Godfrey-Smith, D.I., Huntley, D.J., Chen, W.-H., 1988. Optical dating studies of quartz and feldspar sediment extracts. Quat. Sci. Rev. 7, 373–380. https://doi.org/10.1016/0277-3791(88)90032-7.

Haase, D., Fink, J., Haase, G., Ruske, R., Pécsi, M., Richter, H., Altermann, M., Jäger, K. D., 2007. Loess in Europe-its spatial distribution based on a European Loess Map, scale 1:2,500,000. Quat. Sci. Rev. 26, 1301–1312. https://doi.org/10.1016/j.quascirev.2007.02.003.

Huntley, D.J., Lamothe, M., 2001. Ubiquity of anomalous fading in K-feldspars and the measurement and correction for it in optical dating. Can. J. Earth Sci. 38, 1093–1106. https://doi.org/10.1139/e01-013.

IUSS Working Group WRB, 2022. World Reference Base for Soil Resources. International soil classification system for naming soils and creating legends for maps, 4th edition. FAO, Rome, Vienna, Austria.

Jagercikova, M., Cornu, S., Bourlès, D., Antoine, P., Mayor, M., Guillou, V., 2015. Understanding long-term soil processes using meteoric 10Be: A first attempt on loessic deposits. Quat. Geochronol. 27, 11–21. https://doi.org/10.1016/j.quageo.2014.12.003.

Jagercikova, M., Evrard, O., Balesdent, J., Lefèvre, I., Cornu, S., 2014. Modeling the migration of fallout radionuclides to quantify the contemporary transfer of fine particles in Luvisol profiles under different land uses and farming practices. Soil Tillage Res. 140, 82–97. https://doi.org/10.1016/j.still.2014.02.013.

Jakab, G., Hegyi, I., Fullen, M., Szabó, J., Zacháry, D., Szalai, Z., 2018. A 300-year record of sedimentation in a small tilled catena in Hungary based on δ13C, δ15N, and C/N distribution. J. Soils Sediments 18, 1767–1779. https://doi.org/10.1007/s11368-017-1908-9.

Jarašiūnas, G., Świtoniak, M., Kinderienė, I., 2020. Dynamics of slope processes under changing land use conditions in young morainic landscapes. Western Lithuania. Int. Agrophysics 1, 43–55. https://doi.org/10.31545/intagr/116404.

Jary, Z., 1996. Chronostratigrafia oraz warunki sedymentacji lessów południowo-zachodniej Polski na przykładzie Płaskowyżu Głubczyckiego i Wzgórz Trzebnickich. Studia Geograficzne LXIII Uniwersytetu Wrocławskiego, Wrocław.pdf.

Kabała, C., Przybył, A., Krupski, M., Łabaz, B., Waroszewski, J., 2019. Origin, age and transformation of Chernozems in northern Central Europe – New data from Neolithic earthen barrows in SW Poland. Catena 180, 83–102. https://doi.org/10.1016/j.catena.2019.04.014.

Kaiser, K., Tolksdorf, J.F., de Boer, A.M., Herbig, C., Hieke, F., Kasprzak, M., Koćár, P., Petr, L., Schubert, M., Schröder, F., Fülling, A., Hemker, C., 2021. Colluvial sediments originating from past land-use activities in the Erzgebirge Mountains, Central Europe: occurrence, properties, and historic environmental implications. Archaeol. Anthropol. Sci. 13, 220. https://doi.org/10.1007/s12520-021-01469-z.

Karasiewicz, M.T., Hulisz, P., Świtoniak, M., 2014. Wpływ procesów denudacji na właściwości osadów wypełniających zagłębienia między krętymi wałami z erozji wód subglacjalnych w okolicy Zbójna (Pojezierze Dobrzyńskie). Landf. Anal. 25, 29–42. https://doi.org/10.12657/landfana.025.004.

Kars, R.H., Reimann, T., Wallinga, J., 2014. Are feldspar SAR protocols appropriate for post-IR IRSL dating? Quat. Geochronol. 22, 126–136. https://doi.org/10.1016/j.quageo.2014.04.001.

Kasprzak, M., Traczyk, A., 2014. LiDAR and 2D Electrical Resistivity Tomography as a Supplement of Geomorphological Investigations in Urban Areas: A Case Study from the City of Wrocław (SW Poland). Pure Appl. Geophys. 171, 835–855. https://doi.org/10.1007/s00024-013-0693-7.

Khokhlova, O.S., Chendev, Y.G., Myakshina, T.N., Alexandrovskiy, A.L., Khokhlov, A.A., 2015. Evolution of Chernozems in the southern forest-steppe of the Central Russian upland under long-term cultivation examined in the agro-chronosequences. Quat. Int. 365, 175–189. https://doi.org/10.1016/j.quaint.2014.10.012.

Klimowicz, Z., Uziak, S., 2001. The influence of long-term cultivation on soil properties and patterns in an undulating terrain in Poland. Catena 43, 177–189. https://doi.org/10.1016/S0341-8162(00)00162-4.

Kołodyńska-Gawrysiak, R., Chodorowski, J., Mroczek, P., Plak, A., Zgłobicki, W., Kiebała, A., Trzciński, J., Standzikowski, K., 2017. The impact of natural and anthropogenic processes on the evolution of closed depressions in loess areas. A multi-proxy case study from Nałęczów Plateau. Eastern Poland. CATENA 149, 1–18. https://doi.org/10.1016/j.catena.2016.07.029.

Kołodyńska-Gawrysiak, R., Poesen, J., Gawrysiak, L., 2018. Assessment of long-term Holocene soil erosion rates in Polish loess areas using sedimentary archives from closed depressions. Earth Surf. Process. Landforms 43, 978–1000. https://doi.org/10.1002/esp.4296.

Kopittke, P.M., Menzies, N.W., Wang, P., McKenna, B.A., Lombi, E., 2019. Soil and the intensification of agriculture for global food security. Environ. Int. 132, 105078 https://doi.org/10.1016/j.envint.2019.105078.

Krekelbergh, N., Frankl, A., Dondeyne, S., 2020. Understanding soil profiles and sediment redistribution over long time scales in an agrarian setting : the case of Lauwerdal (Northern France). EGU Gen. Assem. 2020. https://doi.org/10.5194/egusphere-egu2020-14026.

Kreutzer, S., Schmidt, C., Fuchs, M.C., Dietze, M., Fischer, M., Fuchs, M., 2012. Introducing an R package for luminescence dating analysis. Anc. TL 30, 1–8.

Krzyszkowski, D., Łabno, A., 2002. Late Saalian (Wartanian) glacial palaeogeography and formation of end moraines at the northern slope of Silesian Rampart, Southwestern Poland. Ann. Soc. Geol. Pol. 72, 67–87.

Kundzewicz, Z.W., Matczak, P., 2012. Climate change regional review: Poland. Wiley Interdiscip. Rev. Clim. Chang. 3, 297–311. https://doi.org/10.1002/wcc.175.

Labaz, B., Musztyfaga, E., Waroszewski, J., Bogacz, A., Jezierski, P., Kabala, C., 2018. Landscape-related transformation and differentiation of Chernozems – Catenary approach in the Silesian Lowland, SW Poland. Catena 161, 63–76. https://doi.org/10.1016/j.catena.2017.10.003.

Labaz, B., Waroszewski, J., Dudek, M., Bogacz, A., Kabala, C., 2022. Persistence of arable Chernozems and Chernic Rendzic Phaeozems in the eroded undulating loess plateau in Central Europe. CATENA 216, 106417. https://doi.org/10.1016/j.catena.2022.106417.

Łanczont, M., Komar, M., Madeyska, T., Mroczek, P., Standzikowski, K., Hołub, B., Fedorowicz, S., Sytnyk, O., Bogucki, A., Dmytruk, R., Yatsyshyn, A., Koropetskyi, R., Tomeniuk, O., 2021. Spatio-temporal variability of topoclimates and local palaeoenvironments in the Upper Dniester River Valley: Insights from the Middle and Upper Palaeolithic key-sites of the Halych region (western Ukraine). Quat. Int. 632, 112–131.

Lehmkuhl, F., Nett, J.J., Pötter, S., Schulte, P., Sprafke, T., Jary, Z., Antoine, P., Wacha, L., Wolf, D., Zerboni, A., Hošek, J., Marković, S.B., Obreht, I., Sümegi, P., Veres, D., Zeeden, C., Boemke, B., Schaubert, V., Viehweger, J., Hambach, U., 2021. Loess landscapes of Europe – Mapping, geomorphology, and zonal differentiation. Earth-Science Rev. 215, 103496 https://doi.org/10.1016/j.earscirev.2020.103496.

Leopold, M., Hürkamp, K., Völkel, J., Schmotz, K., 2011. Black soils, sediments and brown calcic luvisols: A pedological description of a newly discovered neolithic ring ditch system at Stephansposching, Eastern Bavaria. Germany. Quat. Int. 243, 293–304. https://doi.org/10.1016/j.quaint.2010.11.021.

Li, G., Wen, L., Xia, D., Duan, Y., Rao, Z., Madsen, D.B., Wei, H., Li, F., Jia, J., Chen, F., 2015. Quartz OSL and K-feldspar pIRIR dating of a loess/paleosol sequence from arid central Asia, Tianshan Mountains, NW China. Quat. Geochronol. 28, 40–53. https://doi.org/10.1016/j.quageo.2015.03.011.

Li, M., Li, Z., Liu, P., Yao, W., 2005. Using Cesium-137 technique to study the characteristics of different aspect of soil erosion in the Wind-water Erosion Crisscross Region on Loess Plateau of China. Appl. Radiat. Isot. 62, 109–113. https://doi.org/10.1016/j.apradiso.2004.06.005.

Liritzis, I., Stamoulis, K., Papachristodoulou, C., Ioannides, K., 2013. A re-evaluation of radiation dose-rate conversion factors. Mediterr. Archaeol. Archaeom. 13, 1–15.

Liu, C., Li, Z., Chang, X., He, J., Nie, X., Liu, L., Xiao, H., Wang, D., Peng, H., Zeng, G., 2018. Soil carbon and nitrogen sources and redistribution as affected by erosion and deposition processes: A case study in a loess hilly-gully catchment. China. Agric. Ecosyst. Environ. 253, 11–22. https://doi.org/10.1016/j.agee.2017.10.028.

Loba, A., Waroszewski, J., Sykuła, M., Kabala, C., Egli, M., 2022. Meteoric 10Be, 137Cs and 239+240Pu as Tracers of Long- and Medium-Term Soil Erosion—A Review. Minerals 12, 359. https://doi.org/10.3390/min12030359.

Loba, A., Waroszewski, J., Tikhomirov, D., Calitri, F., Christl, M., Sykuła, M., Egli, M., 2021. Tracing erosion rates in loess landscape of the Trzebnica Hills (Poland) over time using fallout and cosmogenic nuclides. J. Soils Sediments 21, 2952–2968. https://doi.org/10.1007/s11368-021-02996-x.

Malik, I., Poręba, G., Wistuba, M., Woskowicz-Ślęzak, B., 2021. Combining 137Cs, 210Pb and dendrochronology for improved reconstruction of erosion–sedimentation events in a loess gully system (southern Poland). L. Degrad. Dev. 32, 2336–2350. https://doi.org/10.1002/ldr.3903.

Matecka, P., Świtoniak, M., 2020. Delineation, characteristic and classification of soils containing carbonates in plow horizons within young moraine areas. Soil Sci. Annu. 71, 23–36. https://doi.org/10.37501/soilsa/121489.

Meij, W.M., Reimann, T., Vornehm, V.K., Temme, A.J.A.M., Wallinga, J., Beek, R., Sommer, M., 2019. Reconstructing rates and patterns of colluvial soil redistribution in agrarian (hummocky) landscapes. Earth Surf. Process. Landforms 44, 2408–2422. https://doi.org/10.1002/esp.4671.

Morgan, R.P., 2005. Soil erosion and conservation. Blackwell Science Ltd.

Moska, P., Jary, Z., Adamiec, G., Bluszcz, A., 2019. Chronostratigraphy of a loess-palaeosol sequence in Biały Kościół, Poland using OSL and radiocarbon dating. Quat. Int. 502, 4–17. https://doi.org/10.1016/j.quaint.2018.05.024.

Muhs, D.R., 2013. The geologic records of dust in the quaternary. Aeolian Res. 9, 3–48. https://doi.org/10.1016/j.aeolia.2012.08.001.

Murray, A.S., Thomsen, K.J., Masuda, N., Buylaert, J.P., Jain, M., 2012. Identifying well-bleached quartz using the different bleaching rates of quartz and feldspar luminescence signals. Radiat. Meas. 47, 688–695. https://doi.org/10.1016/j.radmeas.2012.05.006.

Nachtergaele, J., Poesen, J., 2002. Spatial and temporal variations in resistance of loess-derived soils to ephemeral gully erosion. Eur. J. Soil Sci. 53, 449–463. https://doi.org/10.1046/j.1365-2389.2002.00443.x.

Novák, T.J., Molnár, M., Buró, J., 2018. Reconstruction of Soil Carbon Redistribution Processes along a Hillslope Section in a Forested Area. Radiocarbon 60, 1413–1424. https://doi.org/10.1017/RDC.2018.94.

Olley, J.M., Roberts, R.G., Murray, A.S., 1997. Disequilibria in the uranium decay series in sedimentary deposits at Allen's cave, nullarbor plain, Australia: Implications for dose rate determinations. Radiat. Meas. 27, 433–443. https://doi.org/10.1016/S1350-4487(96)00114-X.

Paluszek, J., 2013. Assessment of soil structure of Luvisols developed from loess classified in various complexes of agricultural suitability. Soil Sci. Annu. 64, 41–48. https://doi.org/10.2478/ssa-2013-0008.

Paluszek, J., 2010. Zmiany pokrywy glebowej pod wpływem erozji. Pr. i Stud. Geogr. 45, 279–294.

Pindral, S., Świtoniak, M., 2017. The usefulness of soil-agricultural maps to identify classes of soil truncation. Soil Sci. Annu. 68, 2–10. https://doi.org/10.1515/ssa-2017-0001.

Poręba, G., Śnieszko, Z., Moska, P., 2011. Some aspects of age assessment of Holocene loess colluvium: OSL and 137Cs dating of sediment from Biała agricultural area, South Poland. Quat. Int. 240, 44–51. https://doi.org/10.1016/j.quaint.2011.02.005.

Poręba, G., Śnieszko, Z., Moska, P., Mroczek, P., Malik, I., 2019. Interpretation of soil erosion in a Polish loess area using OSL, 137Cs, 210Pbex, dendrochronology and micromorphology – case study: Biedrzykowice site (s Poland). Geochronometria 46, 57–78. https://doi.org/10.1515/geochr-2015-0109.

Poręba, G.J., Śnieszko, Z., Moska, P., 2015. Application of OSL dating and 137Cs measurements to reconstruct the history of water erosion: A case study of a Holocene colluvium in Świerklany, south Poland. Quat. Int. 374, 189–197. https://doi.org/10.1016/j.quaint.2015.04.004.

Prescott, J.R., Hutton, J.T., 1994. Cosmic ray contributions to dose rates for luminescence and ESR dating: Large depths and long-term time variations. Radiat. Meas. 23, 497–500. https://doi.org/10.1016/1350-4487(94)90086-8.

Qin, J., Chen, J., Li, Y., Zhou, L., 2018. Initial sensitivity change of K-feldspar pIRIR signals due to uncompensated decrease in electron trapping probability: Evidence from radiofluorescence measurements. Radiat. Meas. 120, 131–136. https://doi.org/10.1016/j.radmeas.2018.06.017.

Raab, G., Martin, A.P., Norton, K.P., Christl, M., Scarciglia, F., Egli, M., 2021. Complex patterns of schist tor exposure and surface uplift, Otago (New Zealand). Geomorphology 389, 107849. https://doi.org/10.1016/j.geomorph.2021.107849.

Raab, G., Scarciglia, F., Norton, K., Dahms, D., Brandová, D., Castro Portes, R., Christl, M., Ketterer, M.E., Ruppli, A., Egli, M., 2018. Denudation variability of the Sila Massif upland (Italy) from decades to millennia using 10Be and 239+240Pu. L. Degrad. Dev. 29, 3736–3752. https://doi.org/10.1002/ldr.3120.

Radziuk, H., Świtoniak, M., 2021. Soil erodibility factor (K) in soils under varying stages of truncation. Soil Sci. Annu. 72, 1–8. https://doi.org/10.37501/soilsa/134621.

Rahimzadeh, N., Khormali, F., Gribenski, N., Tsukamoto, S., Kehl, M., Pint, A., Kiani, F., Frechen, M., 2019. Timing and development of sand dunes in the Golestan Province, northern Iran—Implications for the Late-Pleistocene history of the Caspian Sea. Aeolian Res. 41, 100538 https://doi.org/10.1016/j.aeolia.2019.07.004.

Rees-Jones, J., Tite, M.S., 1997. Optical dating results for British archaeological sediments. Archaeometry 39, 177–187. https://doi.org/10.1111/j.1475-4754.1997.tb00797.x.

Reimann, T., Tsukamoto, S., Naumann, M., Frechen, M., 2011. The potential of using K-rich feldspars for optical dating of young coastal sediments – A test case from Darss-Zingst peninsula (southern Baltic Sea coast). Quat. Geochronol. 6, 207–222. https://doi.org/10.1016/j.quageo.2010.10.001.

Reimer, P.J., Bard, E., Bayliss, A., Beck, J.W., Blackwell, P.G., Ramsey, C.B., Buck, C.E., Cheng, H., Edwards, R.L., Friedrich, M., Grootes, P.M., Guilderson, T.P., Haflidason, H., Hajdas, I., Hatté, C., Heaton, T.J., Hoffmann, D.L., Hogg, A.G., Hughen, K.A., Kaiser, K.F., Kromer, B., Manning, S.W., Niu, M., Reimer, R.W., Richards, D.A., Scott, E.M., Southon, J.R., Staff, R.A., Turney, C.S.M., van der Plicht, J., 2013. IntCal13 and Marine13 Radiocarbon Age Calibration Curves 0–50,000 Years cal BP. Radiocarbon 55, 1869–1887. https://doi.org/10.2458/azu_js_rc.55.16947.

Rejman, J., Iglik, I., 2010. Topsoil reduction and cereal yields on loess soils of southeast Poland. L. Degrad. Dev. 21, 401–405. https://doi.org/10.1002/ldr.963.

Rejman, J., Iglik, I., Paluszek, J., Rodzik, J., 2014a. Soil redistribution and crop productivity in loess areas (Lublin Upland, Poland). Soil Tillage Res. 143, 77–84. https://doi.org/10.1016/j.still.2014.05.011.

Rejman, J., Rafalska-Przysucha, A., Rodzik, J., 2014b. The Effect of Land Use Change on Transformation of Relief and Modification of Soils in Undulating Loess Area of East Poland. Sci. World J. 2014, 1–11. https://doi.org/10.1155/2014/341804.

Rejman, J., Rodzik, J., 2006. Soil erosion in Europe -. In: Boardman, J., Poesen, J. (Eds.), Soil Erosion in Europe. John Wiley & Sons Ltd, Poland, pp. 95–106.

Reynolds, J.M., 2011. Electrical Resistivity Method, in: An Introduction to Applied and Environmental Geophysics. Willey, pp. 289–372.

Rommens, T., Verstraeten, G., Lang, A., Poesen, J., Govers, G., Van Rompaey, A., Lang, A., Peeters, I., 2005. Soil erosion and sediment deposition in the Belgian oess belt during the Holocene: establishing a sediment budget for a small agricultural catchment. The Holocene 15, 1032–1043. https://doi.org/10.1191/0959683605hl876ra.

Routschek, A., Schmidt, J., Kreienkamp, F., 2014. Impact of climate change on soil erosion - A high-resolution projection on catchment scale until 2100 in Saxony/Germany. Catena 121, 99–109. https://doi.org/10.1016/j.catena.2014.04.019.

Scheib, A.J., Birke, M., Dinelli, E., 2014. Geochemical evidence of aeolian deposits in European soils. Boreas 43 (1), 175–192.

Scherer, S., Deckers, K., Dietel, J., Fuchs, M., Henkner, J., Höpfer, B., Junge, A., Kandeler, E., Lehndorff, E., Leinweber, P., Lomax, J., Miera, J., Poll, C., Toffolo, M. B., Knopf, T., Scholten, T., Kühn, P., 2021. What's in a colluvial deposit? Perspectives from archaeopedology. Catena 198, 105040.

Šimanský, V., Juriga, M., Mendyk, Ł., 2019. Slope position and management practices as factors influencing selected properties of topsoil. Soil Sci. Annu. 70, 137–146. https://doi.org/10.2478/ssa-2019-0012.

Smetanová, A., Verstraeten, G., Notebaert, B., Dotterweich, M., Létal, A., 2017. Landform transformation and long-term sediment budget for a Chernozem-dominated lowland agricultural catchment. CATENA 157, 24–34. https://doi.org/10.1016/j.catena.2017.05.007.

Starkel, L., 2005. Role of climatic and anthropogenic factors accelerating soil erosion and fluvial activity in Central Europe. Stud. Quat. 22, 27–33.

Starkel, L., Michczyńska, D.J., Krapiec, M., Margielewski, W., Nalepka, D., Pazdur, A., 2013. Progress in the holocene chrono-climatostratigraphy of Polish territory. Geochronometria 40, 1–21. https://doi.org/10.2478/s13386-012-0024-2.

Stoops, G., 2003. Guidlines for analysis and description of soil and regolith thin section/. Soil Science Society of America Inc, Madison, Wisconsin, USA.

Strouhalová, B., Gebhardt, A., Ertlen, D., Šefrna, L., Flašarová, K., Kolařík, P., Schwartz, D., 2020. From Chernozem to Luvisol or from Luvisol to Chernozem? A discussion about the relationships and limits of the two types of soils. A case study of the soil catena of Hrušov. Czechia. Geografie 125, 473–500. https://doi.org/10.37040/geografie2020125040473.

Świtoniak, M., Mroczek, P., Bednarek, R., 2016. Luvisols or Cambisols? Micromorphological study of soil truncation in young morainic landscapes - Case study: Brodnica and Chełmno Lake Districts (North Poland). Catena 137, 583–595. https://doi.org/10.1016/j.catena.2014.09.005.

Terhorst, B., 2000. The influence of Pleistocene landforms on soil-forming processes and soil distribution in a loess landscape of Baden-Württemberg (south-west Germany). CATENA 41, 165–179. https://doi.org/10.1016/S0341-8162(00)00098-9.

Thomsen, K.J., Murray, A.S., Jain, M., Bøtter-Jensen, L., 2008. Laboratory fading rates of various luminescence signals from feldspar-rich sediment extracts. Radiat. Meas. 43, 1474–1486. https://doi.org/10.1016/j.radmeas.2008.06.002.

Tuo, D., Xu, M., Gao, G., 2018. Relative contributions of wind and water erosion to total soil loss and its effect on soil properties in sloping croplands of the Chinese Loess Plateau. Sci. Total Environ. 633, 1032–1040. https://doi.org/10.1016/j.scitotenv.2018.03.237.

Turski, M., Witkowska-Walczak, B., 2004. Fizyczne właściwości gleb płowych wytworzonych z utworów pyłowych różnej genezy (in Polish). Acta Agrophysica 101.

Van Oost, K., Govers, G., Van Muysen, W., 2003. A process-based conversion model for caesium-137 derived erosion rates on agricultural land: an integrated spatial approach. Earth Surf. Process. Landforms 28, 187–207. https://doi.org/10.1002/esp.446.

Vitharana, U.W.A., Van Meirvenne, M., Simpson, D., Cockx, L., De Baerdemaeker, J., 2008. Key soil and topographic properties to delineate potential management classes for precision agriculture in the European loess area. Geoderma 143, 206–215. https://doi.org/10.1016/j.geoderma.2007.11.003.

Wacha, K.M., Thanos Papanicolaou, A.N., Giannopoulos, C.P., Abban, B.K., Wilson, C.G., Zhou, S., Hatfield, J.L., Filley, T.R., Hou, T., 2018. The role of hydraulic connectivity and management on soil aggregate size and stability in the clear creek watershed. Iowa. Geosci. 8, 1–18. https://doi.org/10.3390/geosciences8120470.

Wallinga, J., 2002. Optically stimulated luminescence dating of fluvial deposits: a review. Boreas 31, 303–322. https://doi.org/10.1080/030094802320942536.

Wallinga, J., Murray, A., Duller, G., 2000. Underestimation of equivalent dose in single-aliquot optical dating of feldspars caused by preheating. Radiat. Meas. 32, 691–695. https://doi.org/10.1016/S1350-4487(00)00127-X.

Waroszewski, J., Pietranik, A., Sprafke, T., Kabała, C., Frechen, M., Jary, Z., Kot, A., Tsukamoto, S., Meyer-Heintze, S., Krawczyk, M., Łabaz, B., Schultz, B., Erban Kochergina, Y.V., 2021. Provenance and paleoenvironmental context of the Late Pleistocene thin aeolian silt mantles in south-west Poland – a widespread parent material for soils. Catena 204. https://doi.org/10.1016/j.catena.2021.105377.

Winnicki, J., 1997. Geological structure of the Trzebnica Hills in the light of new investigation. Geol. Q. 41, 365–380.

Winnicki, J., 1990. Objaśnienia do Szczegółowej Mapy Geologicznej Polski 1:50 000, Arkusz Trzebnica (727).

Winnicki, J., 1985. Szczegółowa Mapa Geologiczna Polski 1:50 000, Arkusz Trzebnica (727).

Wintle, A.G., Murray, A.S., 2006. A review of quartz optically stimulated luminescence characteristics and their relevance in single-aliquot regeneration dating protocols. Radiat. Meas. 41, 369–391. https://doi.org/10.1016/j.radmeas.2005.11.001.

Yu, K., Xu, H., Lan, J., Sheng, E., Liu, B., Wu, H., Tan, L., Yeager, K.M., 2017. Climate change and soil erosion in a small alpine lake basin on the Loess Plateau. China. Earth Surf. Process. Landforms 42, 1238–1247. https://doi.org/10.1002/esp.4071.

Zádorová, T., Penížek, V., 2018. Formation, morphology and classification of colluvial soils: a review. Eur. J. Soil Sci. 69, 577–591. https://doi.org/10.1111/ejss.12673.

Zádorová, T., Penížek, V., Šefrna, L., Drábek, O., Mihaljevič, M., Volf, Š., Chuman, T., 2013. Identification of Neolithic to Modern erosion–sedimentation phases using geochemical approach in a loess covered sub-catchment of South Moravia, Czech Republic. Geoderma 195–196, 56–69. https://doi.org/10.1016/j.geoderma.2012.11.012.

Zádorová, T., Penížek, V., Šefrna, L., Rohošková, M., Borůvka, L., 2011. Spatial delineation of organic carbon-rich Colluvial soils in Chernozem regions by Terrain analysis and fuzzy classification. Catena 85, 22–33. https://doi.org/10.1016/j.catena.2010.11.006.

Zádorová, T., Žížala, D., Penížek, V., Čejková, Š., 2014. Relating extent of colluvial soils to topographic derivatives and soil variables in a luvisol sub-catchment, Central Bohemia. Czech Republic. Soil Water Res. 9, 47–57. https://doi.org/10.17221/57/2013-swr.

Zgłobicki, W., Rodzik, J., 2007. Heavy metals in the slope deposits of loess areas of the Lublin Upland (E Poland). Catena 71, 84–95. https://doi.org/10.1016/j.catena.2006.10.008.

Zhang, J., 2018. Behavior of the electron trapping probability change in IRSL dating of K-feldspar: A dose recovery study. Quat. Geochronol. 44, 38–46. https://doi.org/10.1016/j.quageo.2017.12.001.

Zhang, J., Yang, M., Sun, X., Zhang, F., 2018a. Estimation of wind and water erosion based on slope aspects in the crisscross region of the Chinese Loess Plateau. J. Soils Sediments 18, 1620–1631. https://doi.org/10.1007/s11368-017-1855-5.

Zhang, K., Pan, S., Liu, Z., Li, G., Xu, Y., Hao, Y., 2018b. Vertical distributions and source identification of the radionuclides 239Pu and 240Pu in the sediments of the Liao River estuary. China. J. Environ. Radioact. 181, 78–84. https://doi.org/10.1016/j.jenvrad.2017.10.016.

Zhang, W., Xing, S., Hou, X., 2019. Evaluation of soil erosion and ecological rehabilitation in Loess Plateau region in Northwest China using plutonium isotopes. Soil Tillage Res. 191, 162–170. https://doi.org/10.1016/j.still.2019.04.004.

Zollinger, B., Alewell, C., Kneisel, C., Meusburger, K., Brandová, D., Kubik, P., Schaller, M., Ketterer, M., Egli, M., 2015. The effect of permafrost on time-split soil erosion using radionuclides (137Cs, 239 + 240Pu, meteoric 10Be) and stable isotopes (δ13C) in the eastern Swiss Alps. J. Soils Sediments 15, 1400–1419. https://doi.org/10.1007/s11368-014-0881-9.

UNIWERSYTET
PRZYRODNICZY
WE WROCŁAWIU

Wrocław, 17.10.2022

Mgr inż. Aleksandra Loba
Instytut Nauk o Glebie, Żywienia Roślin
i Ochrony Środowiska
Uniwersytet Przyrodniczy we Wrocławiu

Oświadczenie

Oświadczam, że w pracy: Loba A., Zhang J., Tsukamoto S., Kasprzak M., Kowalska J. B., Frechen M., Waroszewski J., 2022. *Multiproxy approach to the reconstruction of soil denudation events and the disappearance of Luvisols in the loess landscape of south-western Poland*. CATENA, mój udział polegał na opracowaniu założeń prowadzonych badań, wyborze powierzchni badawczych oraz doborze metodyki prac terenowych i laboratoryjnych, wykonaniu analiz laboratoryjnych, przygotowaniu próbek glebowych do datowań OSL, opracowaniu merytorycznym uzyskanych wyników oraz przygotowaniu treści niniejszego manuskryptu.

....
(podpis)

Leibniz Institute for Applied Geophysics

Hannover, 24.10.2022

Dr Junjie Zhang
Department of Geochronology
Leibniz Institute for Applied Geophysics

Oświadczenie/Statement

Oświadczam, że w pracy: Loba A., Zhang J., Tsukamoto S., Kasprzak M., Kowalska J. B., Frechen M., Waroszewski J., 2022. *Multiproxy approach to the reconstruction of soil denudation events and the disappearance of Luvisols in the loess landscape of south-western Poland*. CATENA, mój udział polegał na wyborze protokołów, przeprowadzeniu pomiarów i kalkulacji datowań OSL. Nadzór merytoryczny obejmował także poprawność interpretacji wyników oraz przygotowanie treści manuskryptu.

I declare that in the paper: Loba A., Zhang J., Tsukamoto S., Kasprzak M., Kowalska J. B., Frechen M., Waroszewski J., 2022. *Multiproxy approach to the reconstruction of soil denudation events and the disappearance of Luvisols in the loess landscape of south-western Poland*. CATENA, my participation consisted selecting protocols, conducting measurements and calculating OSL ages. Substantive supervision also included the correctness of the interpretation of the results and preparation of the content of manuscript.

………………………………….
(podpis/signature)

Hannover, 24.10.2022

Dr Sumiko Tsukamoto
Department of Geochronology
Leibniz Institute for Applied Geophysics

Oświadczenie/Statement

Oświadczam, że w pracy: Loba A., Zhang J., Tsukamoto S., Kasprzak M., Kowalska J. B., Frechen M., Waroszewski J., 2022. *Multiproxy approach to the reconstruction of soil denudation events and the disappearance of Luvisols in the loess landscape of south-western Poland.* CATENA, mój udział polegał na nadzorowaniu przy doborze metodyki prac związanych z datowaniami OSL. Nadzór merytoryczny obejmował także poprawność interpretacji wyników oraz przygotowanie treści manuskryptu.

I declare that in the paper: Loba A., Zhang J., Tsukamoto S., Kasprzak M., Kowalska J. B., Frechen M., Waroszewski J., 2022. *Multiproxy approach to the reconstruction of soil denudation events and the disappearance of Luvisols in the loess landscape of south-western Poland.* CATENA, my participation consisted of supervision in the selection of methodology for OSL dating. Substantive supervision also included the correctness of the interpretation of the results and preparation of the content of manuscript.

(podpis/signature)

Wrocław, 24.10.2022 r.

Dr hab. Marek Kasprzak
Instytut Geografii i Rozwoju Regionalnego
Uniwersytet Wrocławski

Oświadczenie

Oświadczam, że w pracy: Loba A., Zhang J., Tsukamoto S., Kasprzak M., Kowalska J. B., Frechen M., Waroszewski J., 2022. *Multiproxy approach to the reconstruction of soil denudation events and the disappearance of Luvisols in the loess landscape of south-western Poland*. CATENA, mój udział polegał na wykonaniu pomiarów elektrooporowych na badanym terenie, stworzeniu modelu inwersyjnego wykonanych pomiarów i jego interpretacji oraz przygotowaniu treści niniejszego manuskryptu odnoszących się do badań elektrooporowych.

Signed by /
Podpisano przez:

Marek Marcin
Kasprzak
Uniwersytet
Wrocławski

Date / Data:
2022.10.24.09:36

(podpis)

Wrocław, 24.10.2022

Dr inż. Joanna Beata Kowalska
Instytut Nauk o Glebie, Żywienia Roślin
i Ochrony Środowiska
Uniwersytet Przyrodniczy we Wrocławiu

Oświadczenie

Oświadczam, że w pracy: Loba A., Zhang J., Tsukamoto S., Kasprzak M., Kowalska J. B., Frechen M., Waroszewski J., 2022. *Multiproxy approach to the reconstruction of soil denudation events and the disappearance of Luvisols in the loess landscape of south-western Poland*. CATENA, mój udział polegał na wykonaniu zdjęć szlifów mikromorfologicznych oraz ich opisie i analizie.

Joanna Beata Kowalska
(podpis)

Prof. Dr Manfred Frechen
Department of Geochronology
Leibniz Institute for Applied Geophysics

Oświadczenie/Statement

Oświadczam, że w pracy: Loba A., Zhang J., Tsukamoto S., Kasprzak M., Kowalska J. B., Frechen M., Waroszewski J., 2022. *Multiproxy approach to the reconstruction of soil denudation events and the disappearance of Luvisols in the loess landscape of south-western Poland*. CATENA, mój udział polegał na nadzorowaniu poprawności interpretacji wyników oraz przygotowanie treści manuskryptu.

I declare that in the paper: Loba A., Zhang J., Tsukamoto S., Kasprzak M., Kowalska J. B., Frechen M., Waroszewski J., 2022. *Multiproxy approach to the reconstruction of soil denudation events and the disappearance of Luvisols in the loess landscape of south-western Poland*. CATENA, my participation consisted supervising the correctness of the interpretation of results and preparation of the content of manuscript.

……………………………….
(podpis/signature)

Wrocław, 20.10.2022

Dr hab. inż. Jarosław Waroszewski, prof. UPWr
Instytut Nauk o Glebie, Żywienia Roślin
i Ochrony Środowiska
Uniwersytet Przyrodniczy we Wrocławiu

Oświadczenie

Oświadczam, że w pracy: Loba A., Zhang J., Tsukamoto S., Kasprzak M., Kowalska J. B., Frechen M., Waroszewski J., 2022. *Multiproxy approach to the reconstruction of soil denudation events and the disappearance of Luvisols in the loess landscape of south-western Poland*. CATENA, mój udział polegał na nadzorowaniu przy opracowaniu założeń prowadzonych badań, wyborze powierzchni badawczych oraz doborze metodyki prac terenowych i laboratoryjnych. Nadzór merytoryczny obejmował także poprawność interpretacji wyników oraz przygotowanie treści manuskryptu.

…………………………………..
(podpis)